Trinity College Dublin
Coláiste na Tríonóide, Baile Átha Cliath
The University of Dublin

Preparation of cocrystal-in-excipient systems by advanced pharmaceutical methods

A thesis submitted for the degree of

Dodoctor of Philosophy

at the

School of Pharmacy and Pharmaceutical Sciences

Trinity College Dublin, The University of Dublin

Ireland

by

David Walsh

BPharm, MPharm, M.P.S.I.

under the direction and supervision of

Professor Anne Marie Healy

B.Sc. (Pharm), PhD, M.P.S.I., F.T.C.D.

March 2019

Declaration

I declare that this thesis has not been submitted as an exercise for a degree at this or any other university. A small proportion of the work presented in this thesis was carried out by others, and is duly acknowledged where relevant. I declare that all other work is entirely my own.

I agree to deposit this thesis in the University's open access institutional repository or allow the Library to do so on my behalf, subject to Irish Copyright Legislation and Trinity College Library conditions of use and acknowledgement.

_____

David Walsh

Table of contents

Summary

This thesis has focused on the study of pharmaceutical cocrystal production, and the impact of introducing an excipient into the manufacturing process. Cocrystals of sulfadimidine (SDM) and 4-aminosalicylic acid (4ASA) were formed in the presence of an excipient by spray drying and spray coating, while cocrystals of ibuprofen (IBU) and isonicotinamide (INA) were formed by spray drying and hot melt extrusion.

Cocrystals of SDM and 4ASA were formed in the presence of a number of excipients. The Hansen Solubility Parameter (HSP) of the cocrystal and excipients was calculated. Cocrystal formation was preserved when the API and coformer was co-spray dried in the presence of four excipients at excipient loadings of 50 %. These excipients (inulin, microcrystalline cellulose (MCC), dextran and mannitol), were determined to be immiscible with the cocrystal, based on HSP values, with the difference between the HSP of cocrystal and excipient being at least 9.6 $MPa^{0.5}$ in all cases. Excipients which were miscible with the cocrystal, based on the differences in HSP values (Soluplus, PVP K15 and HPMC), resulted in the formation of an amorphous solid dispersion at excipient loadings of 50 %. However, it was determined that cocrystal-in-excipient matrix systems could be formed with two of these excipients when the excipient loading was decreased. Excipients that showed partial miscibility with the cocrystal (polyvinyl alcohol, glycine) resulted in a cocrystal-in-excipient matrix, with single component crystals of API and conformer also present. The experimental solubility of the cocrystal in amorphous excipients was determined, and a simple equation was proposed to predict whether cocrystal formation would be retained in the presence of an excipient, based on the difference in HSP between the cocrystal and excipient, the experimental solubility, and the percentage of excipient to be incorporated into the spray drying process.

Co-spray drying the API and coformer in the presence of two excipients (inulin, MCC) was also investigated. Different excipient loadings and ratios of inulin:MCC were incorporated into the spray drying process. In all cases, cocrystal formation was preserved. The co-spray dried powders were found to be poorly flowable, with a Carr's index > 25 for all formulations investigated. The powders were subsequently tabletted, with higher excipient loadings resulting in a higher tensile strength of the tablets formed.

Spray drying was compared to hot melt extrusion in the formation of cocrystal-in-excipient matrix systems. Due to the thermal instability of 4ASA, the model cocrystal

chosen was IBU:INA, which was processed by spray drying and hot melt extrusion in the presence of a number of excipients. Mannitol, Soluplus and PVP K15 were chosen as excipients which were processed with the API and coformer by spray drying. Xylitol, Soluplus and PVP K15 were chosen as excipients for the extrusion studies. Cocrystal formation was seen in the presence of mannitol by spray drying with up to 50 % excipient loadings, while cocrystal formation was only seen when no more than 10 % PVP K15 and Soluplus were incorporated into the process. This can be explained by the differences in HSP between the cocrystal and excipients. Mannitol is immiscible with the cocrystal with a difference in HSP of 18.3 $MPa^{0.5}$, while the difference in HSP between the cocrystal and excipient is 2.1 and 1.6 $MPa^{0.5}$ for Soluplus and PVP K15 respectively.

Different results were observed for the hot melt extruded formulations. Cocrystal formation was seen only at low xylitol loading (10 %), despite a large difference in HSP between the cocrystal and excipient (20.7 $MPa^{0.5}$). Cocrystal formation, as well as the presence of individual API and coformer, was observed when PVP K15 and Soluplus were incorporated into the extrusion process at 10 % excipient loading. Therefore, spray drying may be considered a more feasible method to produce cocrystal-in-excipient systems. The greater molecular mobility of the API and coformer in solution during the spray drying process, relative to the presumed lower molecular mobility during hot melt extrusion, may allow higher excipient loads to be incorporated into the process while still retaining cocrystal structure.

Spray coating was successfully employed as a method to produce a layer of cocrystals on the surface of inert beads. Both formulation and process parameters were optimised to produce cocrystal coated beads. The spray rate of the solution onto the beads and the total amount of mass sprayed had a positive effect on the degree of crystallinity and the loading efficiency, while the nitrogen airflow and atomisation pressure had a negative impact on the loading efficiency. In addition, the atomisation pressure promoted attrition of the beads.

Flow studies of the coated and uncoated beads were performed. The cocrystal coated beads demonstrated improved flow properties, suggesting that the cocrystal beads may be amenable to downstream processes such as capsule filling. In addition, a faster release of SDM from the cocrystal coated beads compared to the spray dried cocrystal was observed. In previous studies, during dissolution, the spray dried cocrystal was observed

to agglomerate, reducing the dissolution rate of the spray dried cocrystal compared to the cocrystal produced by different crystallisation methods. However, due to the large particle size of the sugar beads, agglomeration does not occur, thereby increasing the surface area available from which dissolution can occur.

Based on the results from the studies in this thesis, it appears that cocrystallisation can occur in the presence of an excipient when the method of cocrystal formation is mediated by the amorphous state. The process itself (spray drying, hot melt extrusion, spray coating) and associated process and formulation parameters may dictate the excipient loading that can be incorporated into the process without impeding cocrystal formation.

Acknowledgements

First of all, I would like to thank my supervisor Professor Anne Marie Healy for her help and guidance throughout my PhD. I very much appreciate the opportunity to become part of her research group, and for her continued support throughout these years. I would also like the thank Science Foundation Ireland and the Synthesis and Solid State Pharmaceutical Centre for providing the funding which made this research possible, and to everyone in the SSPC for taking the time to listen to my presentations and providing helpful discussions about my research.

I would like to thank everyone who contributed to my work and guided me along the way. A special thanks to Loli and Zelalem for taking the time to discuss my results with me, and help to make sense of them. This work would not have been possible without your help. Thanks also to Peter for all his help with the HPLC, and general troubleshooting in the lab. I would like to thank all the PhD students who I shared the lab with for their company: Kate, Karl, Emer, Jer, Alan, James, Ricardo, Svenja, Kieran, Hannah, Agnieszka and Claire. I am very grateful for your support. Thanks also to the postdocs who guided me in the lab, and were never too busy when I asked for help: Loli, Zelalem, Atif, May, Valerio, Dinesh and Stefano. I would also like to thank my final year student Emily for all her help during her project.

Many thanks to Dr. Brendan Twamley in the School of Chemistry for his advice and help with the SCXRD studies. Thanks also to the technicians in the pharmaceutics lab: Brian Talbot, Conan Murphy and Trevor Woods for their technical help in the lab.

I would like to thank my family for their unconditional support, my parents, Margaret and David, my brother Robert and my sisters Siobhan and Mary.

Finally, I would like to thank my girlfriend Sadhbh, who supported me through both the good times and the not so good times. I am deeply grateful for your encouragement throughout these years.

Publications and presentations

Publications associated with the thesis:

- Walsh, D., Serrano, D.R., Worku, Z.A., Madi, A.M., O'Connell, P., Twamley, B. and Healy, A.M., 2018. Engineering of pharmaceutical cocrystals in an excipient matrix: spray drying versus hot melt extrusion. *International Journal of Pharmaceutics* 551, 241-256.
- Walsh, D., Serrano, D.R., Worku, Z.A., Norris, B.A., Healy, A.M., 2018. Production of cocrystals in an excipient matrix by spray drying. *International Journal of Pharmaceutics* 536, 467-477.
- Serrano, D.R., Walsh, D., O'Connell, P., Mugheirbi, N.A., Worku Z.A., Bolas-Fernandez, F., Galiana, C., Dea-Ayuela, M.A., Healy, A.M., 2017. Optimising the in vitro and in vivo performance of oral cocrystal formulations via spray coating. *European Journal of Pharmaceutics and Biopharmaceutics* 124, 13-27.

Other publications:

- Serrano, D.R., Paluch, K.J., O'Connell, P., Walsh D., Healy A.M., 2016. Cocrystal habit engineering to improve drug dissolution and alter derived powder properties. *Journal of Pharmacy and Pharmacology* 68(5), 665-677.

Poster presentations:

- Walsh D, Serrano DR, Worku ZA, Healy AM. Production of Ibuprofen-Isonicotinamide Cocrystal-in-Carrier-Excipient-Suspensions via a One-Step Spray Drying Process. Association of Pharmaceutical Scientists Annual Meeting, November 2017, San Diego, California, USA.
- Walsh D, Serrano DR, Worku ZA, Healy AM. Production of Ibuprofen-Isonicotinamide Cocrystal-in-Carrier-Excipient-Suspensions via a One-Step Spray Drying Process. Synthesis and Solid State Pharmaceutical Centre International Review, November 2017, Limerick, Ireland.
- Walsh D, Serrano DR, Worku ZA, Norris BA, Healy AM. Process Integration – The Production of Cocrystals in an Excipient Matrix by Spray Drying.

American Association of Pharmaceutical Scientists Annual Meeting, November 2016, Denver, Colorado, USA.

- Walsh D, Serrano DR, Smyth K, Norris BA, Healy AM. Production of cocrystals in an amorphous matrix via spray drying. Controlled Release Society Annual Meeting, July 2015, Edinburgh, Scotland.
- Walsh D, Serrano DR, Smyth K, Norris BA, Healy AM. Use of Hansen Solubility Parameter to predict cocrystal formation in an amorphous matrix by spray drying. All Ireland Schools of Pharmacy annual conference, March 2015, Belfast, Ireland.

Abbreviations and symbols

^Exo	Exothermic direction
2θ	2 theta (diffraction angle)
4ASA	4-Aminosalicylic acid
ANOVA	Analysis of variance
API	Active pharmaceutical ingredient
arb. units	Arbitrary units
ASD	Amorphous solid dispersion
ATR-FTIR	Attenuated total reflectance fourier transform infrared spectroscopy
AUC	Area under the curve
BCS	Biopharmaceutics Classification System
BET	Brunauer, Emmett, Teller
BFE	Basic flow energy
CC	Cocrystal
CCDC	Cambridge Crystallographic Data Centre
CFP	Cocrystal formation prediction
cGMP	Current good manufacturing practice
CI	Confidence interval
C_{max}	Maximum concentration
CS	Coated sugar beads
CSD	Cambridge Structual Database
CYP	Cytochrome P450
DC	Degree of crystallinity
D_o	Dose number
DoE	Design of Experiment
DSC	Differential scanning calorimetry
DVS	Dynamic vapour sorption
EMA	European Medicines Agency
f_2	Similarity factor
FDA	Food and Drug Administration
HME	Hot melt extrusion
HPC	Hydroxypropyl cellulose
HPLC	High performance liquid chromatography
HPMC	Hydroxypropyl methylcellulose
HSP	Hansen Solubility Parameter
HTS	High throughput screening
IBU	Ibuprofen
IDR	Intrinsic dissolution rate
INA	Isonicotinamide
IR	Infrared
J/g	Joules per gram
LCST	Lower critical solution temperature
LE	Loading efficiency

MCC	Microcrystalline cellulose
mm	millimetres
$MPa^{0.5}$	Unit of Hansen Solubility Parameter
MTDSC	Modulated temperature differential scanning calorimetry
mW	Milliwatts
NF	National Formulary
NSAID	Non-steroidal anti-inflammatory drug
P/P_o	Partial pressure
PSA	Particle size analysis
PSD	Particle size distribution
PTFE	Polytetrafluoroethylene
PVA	Polyvinyl alcohol
PVP	Polyvinyl pyrrolidone
PXRD	Powder X-ray diffraction
QbD	Quality by Design
R^2	Coefficient of determination
RH	Relative humidity
rpm	Rotations per minute
RSD	Relative standard deviation
SCXRD	Single crystal X-ray diffraction
SD	Spray dried
SDM	Sulfadimidine
SE	Specific energy
SEM	Scanning electron microscopy
SGLT2	Soldium-glucose co-transporter 2
SI	Stability index
SLS	Soldium laurly sulfate
StD	Standard deviation
TFA	Trifluoroacetic acid
T_g	Glass transition temperature
TGA	Thermogravimetric analysis
T_m	Melting temperature (onset)
T_{max}	Time at which Cmax is obtained
TS	Tensile strength
UATR	Universal attenuated total reflectance
US	Uncoated sugar beads
USP	United States Pharmacopoeia
UV	Ultraviolet
VTXRD	Variable temperature X-ray diffraction
W/g	Watts per gram
ZnSe	Zinc selenide
ΔHSP	Difference in Hansen Solubility Parameter
δt	Total solubility parameter

Origin and scope

In recent years, several active pharmaceutical ingredients (APIs) have been formulated as cocrystals and marketed as such. Cocrystals of an API can serve to increase the dissolution rate and solubility, enhance stability and improve downstream processing without chemical modification of the API. Cocrystallisation of an API is an attractive method to alter the solid state characteristics of a non-ionisable API, which is not amenable to modification by salt formation. However, research in this area focuses mainly on cocrystal formation, screening, structure determination and methods to produce cocrystals of an API and a coformer, with little emphasis on the preparation of a final formulated product.

This thesis focuses on the production of cocrystal-in-excipient systems by a variety of advanced pharmaceutical methods, such as spray drying, hot melt extrusion and spray coating. The production of cocrystal-in-excipient systems by a one step process can serve to reduce the number of unit operations required to produce a final pharmaceutical product, as a separate blending step of the cocrystal with excipients may be omitted. This concept, referred to as *process intensification*, can serve to increase the economic and ecological efficiency of industrial production routes (Becht et al., 2009). The production of cocrystal-in-excipient systems by a one step process could result in a powder which may be suitable for direct compression to tablets, or cocrystal coated beads which could be filled into capsules.

Processes such as spray drying and hot melt extrusion have previously been employed as methods for producing cocrystals (Alhalaweh and Velaga, 2010, Dhumal et al., 2010). However, the impact of adding an excipient on cocrystal formation has not been investigated. While both methods have previously been compared in the production of amorphous solid dispersions (Tian et al., 2014) and fixed dose combinations (Kelleher et al., 2018), comparison of both methods with respect to the production of cocrystal-in-excipient systems has not previously been made.

Spray coating has not previously been investigated as a method to prepare cocrystals. This method has previously been utilized to produce drug loaded beads, such as Sporanox™, in which an amorphous dispersion of itraconazole and hypromellose is coated onto sugar spheres. Spray coating is also employed in the production of Efexor™,

in which a solution of ethyl cellulose and hypromellose is used to coat spheronised drug pellets, resulting in an extended release formulation. However, studies in this thesis will extend the application of spray coating, and investigate this approach as a method to coat sugar beads with a thin layer of cocrystal, which could then be filled into capsules.

The overall objective of this thesis was to investigate if an excipient could be incorporated into a one step process with an API and coformer, while still retaining the cocrystal structure.

The following research interests were investigated and are presented in this thesis:

1. For the sulfadimidine:4-aminosalicylic acid cocrystal, investigate cocrystal formation in the presence of a range of excipients by spray drying. Also investigate the possibility of using differences in Hansen Solubility Parameter between the cocrystal and excipient to predict the success or otherwise of cocrystal formation in the presence of excipient, at different weight ratios.
2. Co-spray dry the same API and coformer in the presence of two excipients, and investigate the flow and tabletting properties of the co-spray dried powders.
3. Compare spray drying with hot melt extrusion as a method to produce cocrystal-in-excipient systems using a model cocrystal of ibuprofen:isonicotinamide.
4. Investigate the feasibility of spray coating as a method to produce a layer of cocrystals on the surface of sugar beads.
5. Propose a mechanism by which cocrystallisation can occur in the presence of excipient.

CHAPTER 1

Introduction

1.1 Pharmaceutical solids

Most Active Pharmaceutical Ingredients (APIs) are formulated as oral solid dosage forms, such as capsules and tablets. Tablets and capsules offer a number of advantages as a formulation strategy, due to their suitability for large scale production, chemical and microbiological stability and low cost of production compared to other dosage forms. They are also favoured by patients, as they are easy to administer and non-invasive.

However, oral solid dosage forms are also associated with a number of disadvantages, such as difficulty of swallowing in the case of children, elderly patients and unconscious patients, as well as difficulties with powder processing prior to tabletting or capsule filling.

There are a number of important issues to consider during the development stage of an API that is to be formulated as a solid oral dosage form, such as the solid form of the API, physical and chemical stability, hygroscopicity, dissolution rate and solubility (Figure 1.1). In the case of crystalline materials, the polymorphic form is also of importance. These factors can ultimately affect the bioavailability of an API.

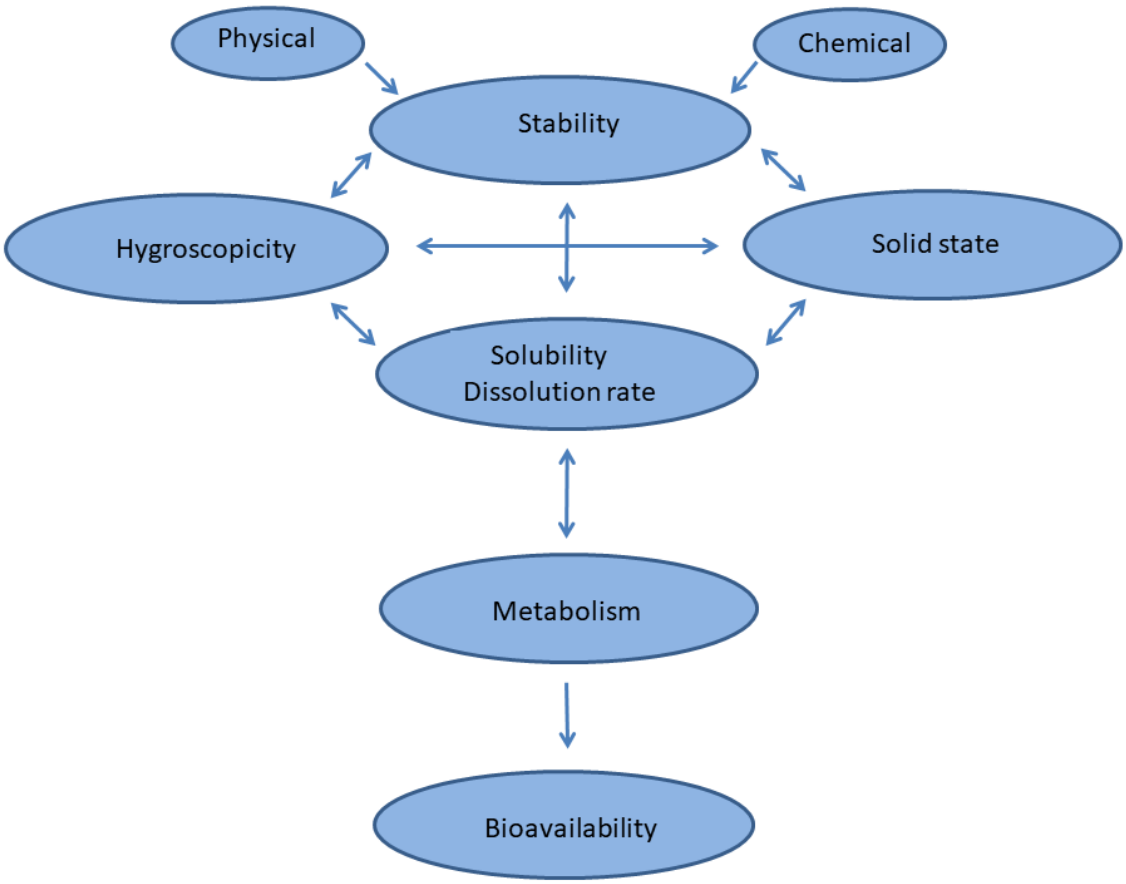

Figure 1.1. Factors that can influence the bioavailability of an API.

1.2 The solid state – crystalline and amorphous forms

The solid state of an API is of critical importance when developing oral dosage forms, as this will have a large impact on the physical stability of the API. The solid state can also impact on the dissolution rate of the API. Solids can be categorised into three groups based on their degree of long range order: crystalline, liquid crystalline and amorphous solids (Zhang and Zhou, 2017), depicted in Figure 1.2. Crystalline solids exhibit a three dimensional long range order in which the structural units, termed unit cells, are repeated regularly and indefinitely in three dimensions in space. Each crystal can be classified as a member of one of seven possible crystal systems that are defined by the relationships between the dimensions of the unit cells and between the individual angles of the unit cell (Brittain et al., 1999, Byrn et al., 1999). Different crystalline forms can exist, such as solvates and polymorphs. Solvates, which can also be referred to as pseudopolymorphs, are crystalline solids containing solvent molecules incorporated into the crystal structure, either in stoichiometric or nonstoichiometric amounts (Vippagunta et al., 2001). If the solvent molecule incorporated into the crystal structure is water, it is termed a hydrate.

There are several well-known pharmaceutical products in which the API exists as a hydrate include alendronate sodium trihydrate, amoxicillin trihydrate, atorvastatin calcium trihydrate and pantoprazole sodium sesquihydrate (Lee et al., 2011). Solvates generally crystallise more easily than single API molecules, as the solvent can potentially form hydrogen bonds with the API molecules in the crystal lattice, or can contribute to adduct-induced conformational changes (Morris, 1999). Solvates can exhibit differences in dissolution rate and solubility when compared to the non-solvated form of a drug. Several solvated forms of niclosamide, for example, demonstrated a lower solubility and intrinsic dissolution rate in aqueous media when compared to the anhydrous form (Van Tonder et al., 2004). This can be explained by the conversion of the solvate into the least soluble hydrate in solution. In most cases, the dissolution rate of an anhydrous API is higher than the hydrated form. However, in some cases, the dissolution rate of the hydrate can be faster. An example of this is the antibiotic erythromycin, in which the dihydrate form demonstrated a faster dissolution rate than the anhydrate and monohydrate forms of the API (Savjani et al., 2012). The pentanol and toluene solvates of glibenclamide have a higher solubility and dissolution rate when compared to two non-solvated polymorphs of the drug (Suleiman and Najib, 1989). However, solvent levels in solvated crystals can often be at concentrations that are not acceptable to regulatory authorities, as they may have toxicological consequences. Anhydrous crystalline solids are often preferable, as solvates can often be unstable, leading to desolvation during storage resulting in the formation of potentially less soluble forms, as solvent loss can lead to an amorphous phase, which can then crystallise into less soluble forms (Blagden et al., 2007). Desolvation of a solvate generally results in either a disordered noncrystalline state or a different crystalline form (Griesser, 2006).

As well as solvates, crystalline APIs can exist as a number of different polymorphs. Polymorphism is the ability of a compound to exist as more than one distinct crystal form. Crystal polymorphs have the same chemical composition but have different internal packing structures. Molecules can adopt more than one packing arrangement and/or conformation in the crystal lattice, resulting in polymorphism (Bernstein, 2002). Polymorphism can be divided into four categories: conformational polymorphism, packing polymorphism, synthon polymorphism and tautomeric polymorphism. Conformational polymorphs involve flexible molecules which can adopt more than one conformation in the solid state. Conformational polymorphism can be defined as

molecular moieties with varied rotational degrees of freedom which can result in different conformations in the unit cell (Dubey and Desiraju, 2015). Examples of conformational polymorphs include olanzapine and venlafaxine hydrochloride (Roy et al., 2005, Llinàs and Goodman, 2008, Di Maria et al., 2014). Packing polymorphism involves different packing arrangements of conformationally rigid molecules (Lee et al., 2011). In this structure, identical moieties pack into different periodic crystal structures (Li et al., 2014b). Aprepitant, an anti-emetic used to prevent nausea and vomiting caused by chemotherapy, displays packing polymorphism (Toziopoulou et al., 2017). Synthon polymorphism occurs when the primary synthons in the forms are different (Li et al., 2014b). These polymorphs can differ in their primary hydrogen-bond motifs. Interactions between molecules can occur via supramolecular synthons which can be assembled by known intermolecular interactions (Healy et al., 2017). Molecules which have multiple hydrogen bonding sites are more inclined to form synthon polymorphs. APIs displaying synthon polymorphism include cocrystals of 5-fluorouracil and 4-hydroxybenzoic acid (Li et al., 2014b) and furosemide (Babu et al., 2010). Tautomeric polymorphism exists when different tautomers of an API crystallise and co-exist in equilibrium in multiple crystal forms (Childs and Hardcastle, 2007). Tautomers that interconvert in solution rapidly between isomers are considered to be the same compound, and therefore can be classed as polymorph. However, tautomers that interconvert slowly are classed as different compounds (Bhatt and Desiraju, 2007). This can, however, be subjective, as interconversion can be temperature dependent. A cocrystal of piroxicam and 4-hydroxybenzoic acid displays tautomeric polymorphism. One polymorph of the cocrystal contains the API as the unionised form, while another polymorph contains the zwitterionic form of piroxicam (Childs and Hardcastle, 2007).

The lowest energy polymorph is generally chosen as the polymorph for development, as it is the most stable solid state form of the API, although this is commonly the polymorph with the lowest dissolution rate and solubility. As well as this, different polymorphs can exhibit differences in hardness, tabletability, density, refractive index and melting point (Vippagunta et al., 2001). It is imperative that appropriate screening for polymorphic forms of an API is carried out prior to development. During the development of ritonavir, only one crystal form was identified. This crystal form was formulated in a semi-solid gel as a hydroalcoholic solution. However, in 1998, several lots of ritonavir drug product failed the dissolution specification. The cause of this was found to be due to conversion

to a previously undiscovered polymorph which had a significantly lower solubility and dissolution rate. It was hypothesised that a degradation product of ritonavir promoted heterogeneous nucleation of the less soluble polymorph of the API. Ritonavir was found to exhibit conformational polymorphism (Bauer et al., 2001). As a result, ritonavir, marketed as Norvir, was withdrawn from the market, leaving tens of thousands of patients without medication (Bučar et al., 2015). The product was subsequently reformulated in an oily vehicle (Censi and Di Martino, 2015).

In the amorphous state, the three dimensional long range order that is seen in crystalline materials does not exist. The individual molecules are randomly oriented relative to each other and can exist in a number of conformational states (Hancock, 2002). Unlike crystalline solids which have a melting temperature, amorphous materials display a glass transition temperature. Below this temperature, the material behaves like a brittle solid, without the crystalline structure and displaying only short range order (Baghel et al., 2016). The amorphous state of an API has a higher heat capacity, entropy, enthalpy and free energy, and as a result can have significantly different properties when compared to the crystalline API (Zhang and Zhou, 2017).

The amorphous state of an API has a number of advantages relative to the crystalline solid. As the amorphous form of an API is more energetic, amorphous materials tend to have a higher solubility and dissolution rate than their crystalline counterparts (Hancock and Parks, 2000). In certain cases the amorphous state can confer other advantages, such as better compression characteristics, relative to the crystalline form (Yu, 2001). However, the amorphous form can be physically unstable, resulting in crystallisation during storage or during *in vitro* or *in vivo* dissolution (Van den Mooter et al., 2001, Newman et al., 2012). As well as physical instability, amorphous materials can exhibit greater chemical instability relative to the crystalline form, likely due to the greater molecular mobility of the amorphous form and the hygroscopic nature of the amorphous form (Yoshioka and Aso, 2007).

Liquid crystals can possess properties of a liquid, such as fluidity and an inability to support shear, as well as crystalline properties, such as a periodic arrangement of molecules in one or more spatial arrangements (Andrienko, 2018). Liquid crystals are related to liquids, but maintain a small degree of orientational order (Stevenson et al., 2005). Depending on the arrangement of the molecules, liquid crystals can further be split

into nematic and smectic phases. Nematic mesophases possess a long range order with molecular axes aligned along a preferred direction. Smectic mesophases can be distinguished from the nematic phase by its stratification. The molecules are arranged in layers, which can freely slide over one another. Smectic mesophases can be further split into smectic A, B and C. Smectic A mesophases have molecules aligned perpendicular to the layers. In smectic B, there is a hexagonal crystalline order between the layers, while smectic C have a biaxial symmetry. Examples of liquid crystals include itraconazole (Mugheirbi et al., 2016) and cyclosporin (Lechuga-Ballesteros et al., 2003).

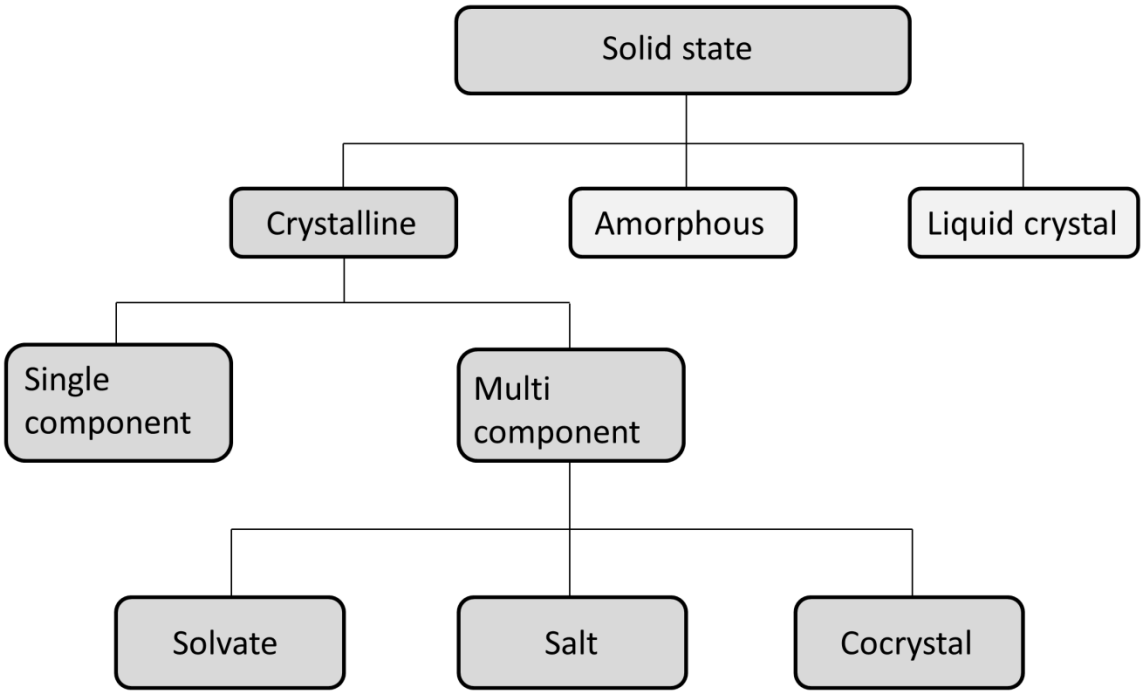

Figure 1.2. The solid state. Solids can be categorised into three groups based on their degree of long range order: crystalline, liquid crystalline and amorphous solids.

1.3 Solubility and dissolution

The solubility of a drug is defined as the maximum amount of solute that will dissolve in a given amount of solvent at a constant temperature and pressure under equilibrium conditions (Murdande et al., 2011). Solubility reflects the equilibrium competition of solute molecules between themselves (crystal energy) and the solvent (solvation energy) (Tasknen, 2007). Drugs must display acceptable aqueous solubility to be administered by the oral route. However, due to processes such as combinatorial chemistry and high-throughput screening (HTS), the number of APIs in the pipeline with poor aqueous

solubility is increasing. Almost 70 % of compounds in the early development pipeline exhibit aqueous solubility below 100 μg/ml (Ku and Dulin, 2012). Approximately 40 % of marketed immediate release oral drugs are defined as practically insoluble (< 100 μg/ml) (Kalepu and Nekkanti, 2015).

With low aqueous solubility APIs, it is important to take into account that the doses of different APIs may vary drastically. Dose number (D_o) has been defined the ratio of drug concentration in the administered volume (250 ml) to the saturation solubility in water at 37 ºC (Dahan et al., 2009). The highest dose of an API is used when calculating the D_o. The volume of 250 ml is chosen as this is considered to be the volume of a glass of water taken with an oral dosage form. The D_o therefore may be viewed as the number of glasses of water required to dissolve the drug dose. A D_o equal or lower than 1 indicates a high solubility compound.

$$Do = (Mo/Vo)/Cs$$ (Takagi et al., 2006)

Where M_o is the highest dose strength, V_o is 250 ml and C_s is the equilibrium solubility.

Drug dissolution refers to the rate at which the API solute enters into a solution. Noyes and Whitney determined that the rate at which a solid in its own solution will dissolve is proportional to the concentration difference between the concentration of the solution and the concentration of the saturated solution (Noyes and Whitney, 1897).

$$\frac{dc}{dt} = K\,(Cs - Ct)$$ (Noyes and Whitney, 1897)

Where dc/dt is the dissolution rate, K is a constant, Cs is the solubility of the substance, and Ct is the concentration of the substance in solution at time t. Modification of the Noyes-Whitney equation allows the important factors for drug dissolution to be identified. Nernst and Brunner conducted further studies based on the work of Noyes and Whitney, focusing on the meaning of the constant K in the Noyes-Whitney equation.

$$\frac{dm}{dt} = \frac{DA(Cs-Ct)}{h}$$ (Nernst, 1904, Brunner, 1904)

Where dm/dt is the rate of mass transfer per unit time, D is the diffusion coefficient, A is the surface area of the substance dissolving, C_s is the equilibrium solubility of the compound in the dissolution medium, C is the concentration of the substance at time t in the dissolution medium, and h is the thickness of the diffusion boundary through which

the dissolved solid diffuses. From the above equation, the difference between the equilibrium solubility and the concentration of dissolved drug in the gastric fluid is the driving force behind the rate at which dissolution occurs. In cases where the drug passes through the intestinal membrane at a faster rate than the rate at which the drug goes in to solution, the concentration of the drug in the dissolution medium is negligible, resulting in the equilibrium solubility of the drug being the main factor driving dissolution.

1.4 Methods to increase dissolution rate and solubility

Common methods to increase the dissolution rate and/or solubility of an API include the formation of amorphous solid dispersions, salt formation, cocrystallisation, prodrug formation and particle size reduction.

Amorphous APIs can have advantages over their crystalline counterparts, such as enhanced solubility and dissolution rate, often leading to a higher oral bioavailability (Hancock and Zografi, 1997). However, due to stability issues, pure amorphous drugs are rarely used in formulations. Instead, solid amorphous dispersions are formulated, containing an amorphous API and an amorphous carrier. Amorphous solid dispersions can be formulated as either a glass solution or a glass suspension. A glass solution is a one phase system exhibiting one glass transition in which the API molecules are mixed with the polymer, which is favourable in respect of dissolution properties (Van den Mooter, 2012). A glass suspension can be formulated when there is limited miscibility between the API and carrier. A glass suspension will typically contain at least two glass transitions, one attributable to a drug rich phase and one attributable to a polymer rich phase. In these systems, there is a higher likelihood for the API to crystallise from the amorphous form due to phase separation (Laitinen et al., 2014). The aim in formulating amorphous solid dispersions is to inhibit crystallisation and maintain a level of supersaturation in solution to allow dissolution and absorption of the API (Newman et al., 2012). ASDs can generate a highly supersaturated solution in which the API concentration is significantly greater than the equilibrium solubility of the crystalline API in solution. However, this state can be unstable in solution and revert back to the stable, crystalline form (Sun and Lee, 2013). The dissolution profile of an API from an amorphous solid dispersion typically exhibits the “spring and parachute” effect (Babu and Nangia, 2011). The “spring” refers to the initial dissolution of the API from the dosage form, while the “parachute” refers to the prolonged supersaturation of the API in

solution as the polymer prevents crystallisation of the API (Liu et al., 2016). Amorphous solid dispersions are commonly produced by spray drying or hot melt extrusion (Baird and Taylor, 2012).

Salt formation is commonly used to increase the solubility and dissolution rate of ionisable drugs (Kawabata et al., 2011). Salt formation involves an acid/base reaction, where an API forms an ionic interaction with an oppositely charged counter ion via a proton transfer or neutralisation reaction (Kumar et al., 2007) (Berge et al., 1977). A stable ionic bond can be formed when the difference in pK_a between the acid and base is greater than 3 (Childs et al., 2007). The counter ion can change the local pH at the dissolving surface in the diffusion layer, resulting in a higher dissolution rate and solubility of the salt compared to the unionised API (Serajuddin, 2007). As per the Henderson-Hasselbalch equation, the change in pH will alter the solubility of an ionisable API (Völgyi et al., 2010). pH dependent solubility can be calculated using the Henderson-Hasselbalch equation, and depends on the pH of the solution and the pK_a of the API. The below equation can be used to predict the pH-solubility for monoprotic acids:

$$pK\mathrm{a} = pH - \log[(S_{tot}\text{-}S_o)/S_o\} \qquad \text{(Tasknen, 2007)}$$

Where S_{tot} is the effective solubility (the sum of the concentrations of all the compound species dissolved in the aqueous medium at a particular pH (Takagi et al., 2006) and S_o is the intrinsic solubility (solubility of the uncharged species).

Salt formation can be favourable compared to the amorphous solid dispersion approach, as an enhanced dissolution rate and solubility can be achieved without compromising stability. However, only acidic and basic APIs are amenable to salt formation.

Prodrugs are derivatives of drug molecules that can undergo an enzymatic and/or chemical transformation *in vivo* to the active drug, which can then exert a pharmacological effect (Rautio et al., 2008). The prodrug itself should not be pharmacologically active, and any biological activity should come from the drug molecule. Prodrugs can be used to enhance the solubility and dissolution rate of an API (Chin Chung et al., 2011), improve the biopharmaceutical profile (Stella, 2010), reduce side effects (Chin Chung et al., 2011) or for targeted delivery to the site of action (Dhaneshwar and Vadnerkar, 2011). Sulindac sulfoxide, a prodrug of the Non-Steroidal Anti-Inflammatory Drug (NSAID) sulindac, is approximately 100 times more water

soluble than the pharmacologically active form (Duggan et al., 1977, Shen and Winter, 1977). The prodrug is more polar in this case, resulting in greater aqueous solubility. The use of a prodrug approach can also identify more efficacious drug candidates. The anti-helminthic API albendazole was found to be less active than the prodrug albendazole sulfoxide. The prodrug also displayed an improved dissolution rate and solubility profile (Domínguez et al., 1995). However, in practice, the prodrug approach is rarely used to improve the dissolution rate and solubility of poorly soluble drugs. Instead, this approach is mainly used to overcome permeability barriers (Stella and Nti-Addae, 2007).

Reduction of particle size can also be used to enhance the saturation solubility and dissolution rate of poorly soluble drugs (Chen et al., 2011, Kipp, 2004). The saturation solubility of an API can increase for particles with a mean particle size below 1 μm (Shahrin, 2013, Keck and Müller, 2006). Reduction in particle size below 1 μm can result in extreme curvature of the particles, which can increase the solvation pressure, resulting in an increase in solubility (Khadka et al., 2014, Muller and Keck, 2004). The increase in saturation solubility with respect to reduction of particle size can be explained by the Ostwald-Freundlich equation:

$$\frac{RT}{Vm}.Ln\frac{S}{So}=\frac{2\gamma}{r}$$ (Ostwald, 1900, Freundlich, 1909)

where R is the universal gas constant, T is the temperature, V_m is the molar volume, S is the solubility of small particles of radius r, S_0 is the solubility of drug in solution under equilibrium conditions, γ is the interfacial tension between the solid and liquid, and r is the radius of the particles. However, any small particle dispersed in a medium is thermodynamically unstable due to its large interfacial area. Particle growth can decrease this area, lowering the interfacial energy. Small particles have a higher saturation solubility than larger particles, creating a concentration gradient between small and large particles. The smaller particles diffuse through the concentration gradient, resulting in a supersaturated solution around the large particles, which then deposit onto the large particles (Wu et al., 2011, Voorhees, 1985). This phenomenon is referred to as Ostwald ripening and is responsible for changes in particle size and particle size distribution (Wu et al., 2011). As a result, it can be necessary to include stabilisers to inhibit Ostwald ripening (Verma et al., 2011). Small particles can also exhibit greater cohesion and adhesion than larger particles, resulting in downstream processing problems such as poor flowability (Han et al., 2011).

Reduction of the particle size will increase the surface area of the API exposed. As per the Nernst-Brunner equation, increasing the surface area will increase the dissolution rate. Dissolution enhancement can be seen with reduction to both micron-sized drug particles (Rasenack and Müller, 2004) and nano-sized drug particles (Kumar et al., 2015, Müller and Peters, 1998). The production of a nanocrystal suspension of cilostazol increased its bioavailability. As well as this, no significant food effect was seen for this system compared to other formulations of this API, reducing both intra- and inter-patient variability (Jinno et al., 2006). However, particle size reduction is normally produced by mechanical methods, such as crushing, grinding and milling (Rasenack and Müller, 2004). Mechanical activation of the crystalline API can occur, resulting in amorphous regions and/or the formation of metastable polymorphs (Boldyrev, 2004).

1.5 Bioavailability

The bioavailability of an API is the fraction of the dose that reaches the system circulation in its unchanged form, as well as the rate at which the API enters the systemic circulation. For orally administered drugs, the bioavailability is affected by the amount of drug that is absorbed across the intestinal epithelium as well as first pass metabolism, as the drug crosses the intestine and liver on its way to the systemic circulation. The bioavailability of an API can depend on factors such as the physicochemical properties of the API, API-excipient interactions, efflux transporters, and the fasted or fed state of the patient.

1.6 Biopharmaceutics Classification System (BCS)

The BCS is used to classify drugs based on their aqueous solubility and gastrointestinal permeability. It is based on the idea that the two most significant factors influencing oral drug administration are solubility and permeability, and divides drugs into four groups based on these parameters (Amidon et al., 1995), as shown in Figure 1.3. Drugs are considered to be highly soluble when the highest dose strength of an immediate release oral formulation is soluble at 37 ^{o}C in 250 ml or less of aqueous media over a pH range of 1–6.8, as defined by the Food and Drug Administration (FDA), or over a pH range of 1.2-6.8, as defined by the European Medicines Agency (EMA). The concept of BCS solubility is similar to that of the dose number of an API. Unlike the dose number, the BCS will assess solubility across a pH range. The dose number will, however, generate a dimensionless value based on the maximum dosage and aqueous solubility of an API.

D_o values below or equal to 1 indicate a high solubility API. D_o can be regarded as the number of glasses of water required to dissolve the maximum dose of an API.

Both the EMA and FDA state that in order for a drug to be considered highly permeable, the extent of absorption must be ≥ 85 % of the administered dose based on the absolute bioavailability or mass balance studies. The BCS can be used to allow waiver of *in vivo* bioavailability and bioequivalence testing of immediate release solid oral dosage forms for Class I drugs when the drug also exhibits rapid dissolution.

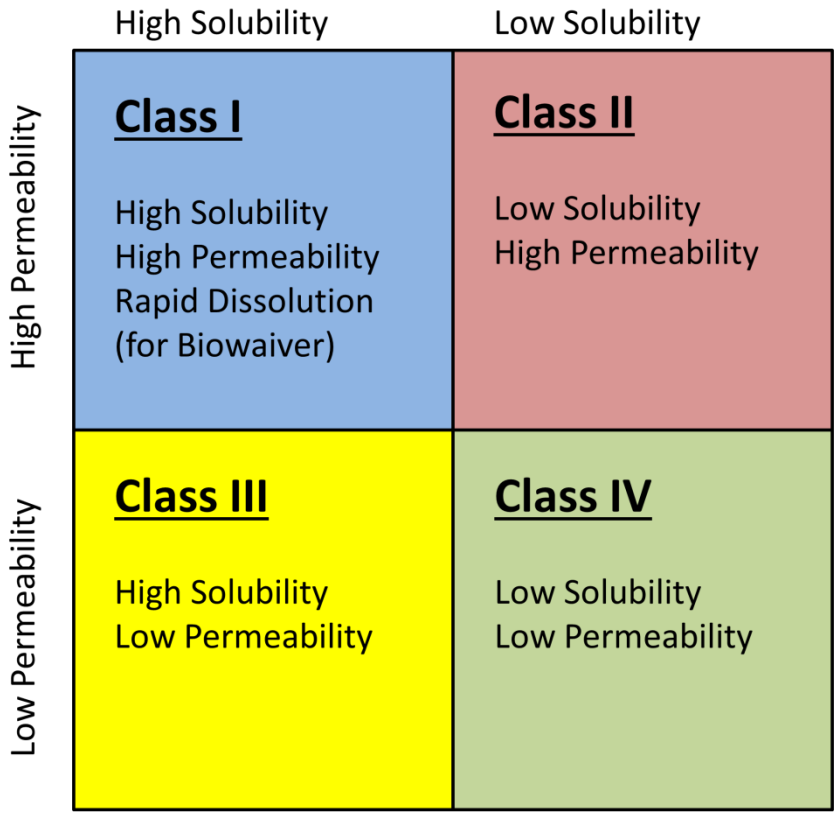

Figure 1.3. The Biopharmaceutics Classification System.

Class I drugs exhibit high solubility and high permeability. Examples of BCS Class I drugs include propranolol, metoprolol and diltiazem (Sachan et al., 2009). Gastric emptying is often the rate limiting step for absorption due to the fast rate of dissolution of Class I drugs. BCS Class II drugs, such as ibuprofen, sulfadimidine and carbamazepine, display low solubility and high permeability. For these drugs, the rate limiting step to absorption is dissolution of the API in the alimentary tract. Due to drug discovery strategies such as high throughput screening (HTS), lead molecules are

identified with greater efficacy and specificity for a particular target, but with poor physicochemical properties such as low aqueous solubility and dissolution rate (Lipinski et al., 2012). Approximately 40 % of marketed drugs and up to 75 % of drugs under development have poor solubility or are practically insoluble (Williams et al., 2013, Kalepu and Nekkanti, 2015). BCS Class III drugs exhibit high aqueous solubility and poor intestinal permeability. Permeation through the intestinal membrane is the rate limiting step for BCS Class III drugs, with drug dissolution being of negligible importance. However, some compounds may be eligible for biowaiver when they meet the criterion for very fast dissolution, defined as greater than 85 % within 15 minutes at pH 1.2-6.8 (EMA, 2010). Examples of BCS Class III drugs include atenolol, cefazolin and valsartan (Wu and Benet, 2005). BCS Class IV drugs exhibit both low solubility and low permeability. The bioavailability of BCS Class IV drugs can be significantly influenced by food, and such compounds can be substrates for the efflux transporter, P-glycoprotein, and for CYP 3A4, leading to extensive first pass metabolism. There can also be inter and intra subject variability associated with BCS Class IV drugs (Ghadi and Dand, 2017). As a result, the amount of BCS Class IV compounds absorbed into the systemic circulation can be erratic and unpredictable. BCS Class IV drugs include amphotericin B, mebendazole and chlorothiazide (Wu and Benet, 2005).

1.7 Pharmaceutical cocrystals

Pharmaceutical cocrystals offer an alternative method to alter the dissolution rate and solubility of BCS Class II drugs. Cocrystals consist of an API and a generally regarded as safe (GRAS) molecule, with specific stoichiometric compositions (Figure 1.4). However, there is no single definition as to what a pharmaceutical cocrystal is. Multiple definitions appear in the literature, but a common definition is “a stoichiometric multi-component system connected by non-covalent interactions where all the components present are solid under ambient conditions” (Jones et al., 2006, Bhogala and Nangia, 2008, Aakeröy and Salmon, 2005). As both the API and coformer in a cocrystal must be solid on their own under ambient conditions, solvates and hydrates are not classed as cocrystals. However, other restrictive definitions define a cocrystal as “a crystalline complex of two or more neutral molecular constituents bound together in the crystal lattice through non-covalent interactions, often including hydrogen bonding” (Jones et al., 2006). This definition specifies that the API and coformer must be in the neutral form. However, there are many reports of “ionic cocrystals” in the literature, where the

molecules in the crystal lattice interact via ionic bonds as well as hydrogen bonding (Yao et al., 2014, Braga et al., 2010, Duggirala et al., 2014). An article authored by 46 researchers in the area of cocrystals have proposed an inclusive definition of cocrystals, defining cocrystals as "solids that are crystalline single phase materials composed of two or more different molecular and/or ionic compounds generally in a stoichiometric ratio which are neither solvates nor simple salts" (Aitipamula et al., 2012).

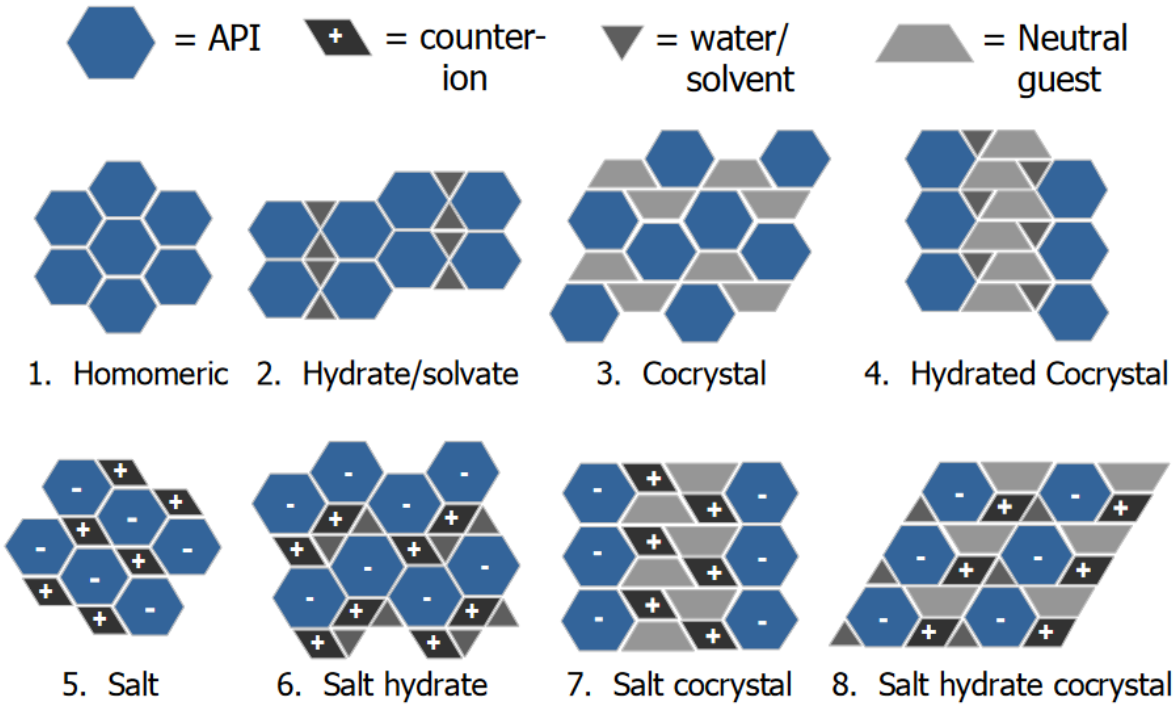

Figure 1.4. Multi-component crystals (Childs, 2009).

1.8 Cocrystal design

Crystal engineering can be used to design cocrystals with the aim of improving the solid state properties of an API without modification of the intrinsic structure of the API (Qiao et al., 2011). Cocrystals between the API and coformer molecules can form via non-covalent interactions such as hydrogen bonding, π-π stacking, van der Waals forces, halogen bonding and electrostatic interactions (Aakeröy et al., 2007, Cinčić et al., 2008, Miroshnyk et al., 2009, Saha et al., 2005). Based on the definition by Aitipamula et al. (2012), ionic interactions between the API and coformer can also exist within the cocrystal structure.

The selection of an appropriate coformer to form a cocrystal is often based on the concept of "supramolecular synthons" (Desiraju, 1995). These are functional groups within molecules that can interact with another molecule through non-covalent interaction, resulting in cocrystal formation. Examples of functional groups involved in cocrystallisation include carboxylic acids, amides, alcohols and pyridines (Qiao et al., 2011, Shan and Zaworotko, 2008). Supramolecular heterosynthons, where the two complementary, interacting functional groups are different, are favoured to supramolecular homosynthons. Examples of supramolecular heterosynthons commonly seen in cocrystals include carboxylic acid-aromatic nitrogen, carboxylic acid-amide and alcohol-pyridine interactions (Shan and Zaworotko, 2008). Interactions between supramolecular homosynthons can also occur, such as the carboxylic acid-carboxylic acid and amide-amide homosynthons, although these are less common (Groom et al., 2016). Appropriate coformers can be screened using Cambridge Structural Database (CSD) surveys, which can identify coformers containing functional groups which can potentially cocrystallise with the API. The CSD is a comprehensive repository of crystal structures, with over 900,000 entries. However, this approach does not take into account the ability of the coformer to pack into an ordered crystalline structure, as steric hindrance can prevent the interaction of complementary functional groups between the API and coformer. Furthermore, this approach does not consider competition between different functional groups present in the API and coformer (Thakuria et al., 2013).

Other approaches to coformer selection include the use of pK_a differences between the API and coformer and also the use of the difference in Hansen Solubility Parameter (HSP) between the two components. It has previously been reported that salt formation is likely to occur when the difference in pK_a between the acid and base is greater than two or three units (Cruz-Cabeza, 2012, Variankaval et al., 2006). The difference in pK_a can result in complete proton transfer from acid to base, resulting in salt formation. Cocrystal formation between an acid and a base can occur when the difference in pK_a is minimal, i.e., less than one (Bhogala et al., 2005, Childs et al., 2007). However, when the difference in pK_a is between 0 and 2, it can be difficult to predict the species which may form. It should also be noted that many exceptions to this rule exist; for example, neutral carboxylic acid-pyridine interactions have occurred when the pK_a difference is approximately 3.75 (Johnson and Rumon, 1965). Furthermore, pK_a measurements are

applicable to acidic and basic molecules in solution, and so this approach may not be successful in predicting cocrystals produced by solvent-free techniques.

Another approach to predict cocrystal formation involves the use of the difference in HSP between the API and potential coformers (Mohammad et al., 2011). This approach is based on the hypothesis that in order for an API and coformer to interact, they must be miscible on a molecular level. A small difference in HSP can indicate miscibility, and therefore cocrystallisation can occur. It has been reported that systems with a difference in solubility parameter of less than 7 $MPa^{0.5}$ are miscible, while systems with a difference greater than 7 $MPa^{0.5}$ are immiscible (Greenhalgh et al., 1999). It should, however, be noted that the studies of Greenhalgh et al. are based on Hildebrand Solubility Parameter. All cocrystals formed in the previously reported study by Mohammad et al. (2011) had a difference in HSP values between the coformer and model API, indomethacin, of less than 7 $MPa^{0.5}$. However, not all miscible coformers, defined as having a HSP difference of less than 7 $MPa^{0.5}$ between the API and coformer, resulted in cocrystal formation.

The concept of a solubility parameter was first introduced by Hildebrand and Scott. They suggested that compounds with a similar solubility parameter value would be miscible. The behaviour of specific solvents was given a numerical value, which was the square root of the cohesive energy density of the solvent. This quantity was referred to as the Hildebrand Solubility Parameter (Hildebrand, 1936). However, a limitation of the Hildebrand Solubility Parameter is that it does not take into account association between molecules, such as polar and hydrogen bonding interactions (Hansen, 2002). The use of multicomponent parameters such as the Hansen Solubility Parameter (HSP) can overcome these issues to a large extent. The basis of HSP is that the total cohesive bonding that holds a solvent together is broken when the solvent evaporates. The total energy of vaporisation of a solvent consists of several individual parts, which can be attributed to dispersion forces, hydrogen bonding forces and dipole-dipole forces (Hansen, 2004). This led to the three component HSP, which can be split in to disperse forces, dipolar forces and hydrogen bonding forces. These three component values are then combined to give the overall solubility parameter value. The use of HSP to predict miscibility has been widely used in the paint and ink industries (Hansen, 1969, Machui et al., 2012).

1.9 Advantages of cocrystals

Cocrystals can offer a number of advantages compared to other formulation strategies. Cocrystals can enhance the dissolution rate and solubility of an API without chemical modification of the API. The solubility of the API in a cocrystal is enhanced by two mechanisms: lowering the crystal lattice energy and increasing solvation. Both methods can enhance API solubility to different extents. Lowering of the crystal lattice energy is generally a more important mechanism to enhance cocrystal solubility in non-polar solvents. The crystal lattice energy is influenced mainly by hydrogen bonding, van der Waals forces and electrostatic forces (Perlovich et al., 2004). The lattice energy between the coformer and API is generally lower than the energy between the API molecules in a single component crystal structure. As a result, it may be reasonably expected that cocrystal solubility, and hence dissolution rate, may be correlated with the cocrystal melting temperature. However, this is not always the case, particularly in water, where the solvent-solvate barrier dominates over lattice energy (Good and Rodríguez-Hornedo, 2009). The second method by which cocrystals can exhibit enhanced solubility is by solvation of the API in the cocrystal structure. This is the main method by which solubility enhancement occurs in water, as hydrophobic BCS Class II drugs are often solubility-limited by reduced solvent-solute interactions. The introduction of a polar, water soluble molecule into the crystal structure can serve to more readily solvate the hydrophobic API. Cocrystal solubility can be correlated with coformer solubility. This is due to enhanced solvation with a higher solubility coformer (Good and Rodríguez-Hornedo, 2009, Childs et al., 2008).

Cocrystallisation can also serve to improve the stability profile of an API. Crystalline forms can show both a greater chemical and physical stability compared to amorphous forms. Further to this, cocrystallisation of an API can prevent the formation of hydrates during processing and storage. Crystalline theophylline has been shown to interconvert between the anhydrous and monohydrated form as a function of relative humidity. This can then present challenges during manufacturing (Khankari and Grant, 1995). It was demonstrated that cocrystals of theophylline are much less likely to form hydrates at high relative humidity. A cocrystal of theophylline and oxalic acid did not form a hydrate at high relative humidity, and also did not dissociate under these conditions, indicating that this cocrystal is more stable and can be less unpredictable during processing and storage (Trask et al., 2006).

The compaction properties of an API can also be improved by cocrystallisation. Paracetamol displays poor compression properties due to its low plasticity. Wet granulation with excipients is normally required to improve the tabletability of paracetamol. However, cocrystallisation of paracetamol with caffeine improved compaction and increased plastic deformation (Latif et al., 2018). Due to the relatively large dosage of paracetamol (500 mg), the addition of large amounts of excipients to improve production performance is not favoured, as this would lead to in an increase in tablet size. This may then be an issue for patients with swallowing difficulty. Another study compared the compaction properties of paracetamol with that of the paracetamol:5-nitroisophthalic acid cocrystal. The coformer in this case has a higher degree of interparticulate bonding, resulting in greater plasticity for the cocrystal. The improved tabletability and increase in tensile strength in this case may also be due to the presence of slip planes in the cocrystal structure, which can result in greater plasticity (Hiendrawan et al., 2016). It is important to note that coformer selection is an important aspect to consider when aiming to improve the tabletability of an API. Theophylline was found to demonstrate better tabletability than the theophylline:methyl gallate cocrystal (Chattoraj et al., 2010). The coformer in this case, methyl gallate, was found to be poorly tabletable. In order to improve the compression properties of an API, it is important to choose a coformer with desirable tabletting properties. Cocrystallisation of an API can improve downstream processing. Ertugliflozin, marketed as Steglatro, existed as a hygroscopic, amorphous form with a low glass transition temperature which is unsuitable for processing (Bowles et al., 2014). Cocrystallisation of this API resulted in a crystalline solid form which is suitable for processing.

Cocrystals can also impact the pharmacokinetic profile of an API. This can be attributed, but not limited to, the solubility advantage of the cocrystal compared to the API (Shan et al., 2014). Cocrystals of AMG-517, a poorly soluble small molecule, were compared to the free base. A 30 mg/kg dose in rat of the API in the cocrystal form demonstrated a comparable maximum plasma concentration (C_{max}) to a 500 mg/kg dose of the API in the free base form. Both the cocrystal and API were delivered as suspensions. This indicates improved oral absorption of the API by cocrystallisation (Bak et al., 2008). Another study compared the area under the curve (AUC) of meloxicam and 12 meloxicam cocrystals in rats dosed with the equivalent of 10 mg/kg of meloxicam. While most AUC values for the cocrystals were higher than for free meloxicam, some cocrystals demonstrated a

reduced AUC value relative to meloxicam, demonstrating that coformer selection is an important consideration when selecting a drug for cocrystallisation (Weyna et al., 2012).

One of the main advantages of cocrystallisation is cocrystal diversity. Cocrystals offer the ability to fine tune an API by rational coformer selection. Coformers can be selected to increase and decrease the dissolution rate and solubility of an API (Chow et al., 2012, Grossjohann et al., 2012, Levinthal, 1978), improve stability (Trask et al., 2006) and improve production performance of an API (Hiendrawan et al., 2016, Latif et al., 2018). Further to this unlike in salt formation, as APIs do not require an ionisable group to form cocrystals, cocrystallisation is a viable method to tailor the physicochemical properties of a large number of APIs. A study by Stahly found that 60 % of all APIs screened could form cocrystals (Stahly, 2007).

Formulating marketed drugs as cocrystals can also provide the opportunity to grant new intellectual property on an API, and therefore extend their patent life cycle (Newman and Wenslow, 2016). This is especially relevant due to the impact of the 'patent cliff' in the pharmaceutical industry on the Irish economy (Enright and Dalton, 2013). Cocrystals can also offer some disadvantages. Cocrystallisation of an API will increase the mass of drug substance to be incorporated into the formulation, which can be a disadvantage for high dose APIs. Also, in the case of drug-drug cocrystals, the ratio of one API to the other must be stoichiometric. Therefore, for these types of cocrystals, the loading of one API cannot increase without the other API.

1.10 Methods to produce cocrystals

Many methods currently exist to produce cocrystals. These methods can be split into solution based methods and solvent free methods. Solution based methods include solvent evaporation, cooling crystallisation, reaction crystallisation, spray drying, freeze drying and supercritical fluid technology. Solvent evaporation has previously been shown to produce pure cocrystals (Weyna et al., 2009, Bag et al., 2011). The API and coformer are dissolved in solvent, which is then allowed to evaporate. However, the downside of this method is the potential formation of single component crystals. When the API and coformer are incongruently saturating in solution, the less soluble component can crystallise, resulting in a mixture of cocrystal and crystalline API and coformer. Therefore, reactant solubilities are important to consider. Further to this, both components must be soluble in the solvent prior to evaporation.

Reaction crystallisation is a solution based method that has been successful in preventing the formation of single component crystals (Childs et al., 2008). Reaction crystallisation to produce cocrystals is performed by producing a saturated solution of reactant A (API or coformer), then adding reactant B to the saturated solution. The solution becomes supersaturated with respect to the cocrystal, resulting in cocrystal formation (Qiao et al., 2011).

Cooling crystallisation is another solution based method used in the production of cocrystals. Cocrystal formation by this method is more likely to occur when the API and coformer have similar solubilities in the solvent (Chiarella et al., 2007). However, this can limit the number of potential coformers. This method is the current method of choice in the pharmaceutical industry for crystallisation of APIs (Wittering et al., 2015). While this method is well understood and ubiquitous, control of the crystallisation process is significantly more complex with the addition of a second (coformer) molecule, especially when both components display differences in solubility in a particular solvent (Aakeröy et al., 2009). As a result, non-stoichiometric ratios of API: coformer are often required, with a higher proportion of the more soluble component. The API and coformer are dissolved in boiling solvent, generating a supersaturated solution. The solution is then cooled, reducing the solubilities of the API and coformer, resulting in nucleation and crystal growth of the cocrystal. Cocrystal phase diagrams are commonly used to predict cocrystal formation from solution. Phase diagrams are used to visualise solution and solid phase compositions based on thermodynamic considerations (Wouters and Quéré, 2011). However, the downside of this approach is the construction of a phase diagram can be quite time consuming, and is unique to each solvent. This can be a disadvantage during screening studies. Difficulty can also be encountered with scale up by this method (Ainouz et al., 2009).

Spray drying is a solution based method to produce pure cocrystals from congruently and incongruently saturating solutions (Alhalaweh and Velaga, 2010). Congruently saturating solutions are solutions in which the API and coformer have the same solubility in a given solvent, whereas solutions in which the API and coformer have different solubilities are termed incongruently saturating solutions. Spray drying is a method of generating dry powders from solution or suspension by rapidly evaporating the solvent with a hot air stream (Broadhead et al., 1992, Patel et al., 2009). Spray drying consists of three stages: atomisation of the liquid feed, drying of the fine droplets by a heated gas stream, and

separation of the fine powder from the drying gas (Cal and Sollohub, 2009). While spray drying is commonly used to produce amorphous dispersions (Caron et al., 2011, Paudel et al., 2013, Ambike et al., 2005), this method can also be used to generate crystalline forms (Chiou and Langrish, 2008, Vehring, 2008, Chiou et al., 2008). The production of crystalline forms by spray drying is likely due to the rapid supersaturation during the drying phase and due to the difference in inlet and outlet temperatures (Matsuda et al., 1984). It is thought that the production of cocrystals by spray drying is kinetically controlled by the amorphous state, where the liquid droplets are first converted to an amorphous state, and then converted from the amorphous to the crystalline state (Alhalaweh and Velaga, 2010). Spray drying parameters can also be altered to tailor the properties of the spray dried product. Spray drying can therefore be seen as a viable and scalable method to produce cocrystals.

Freeze drying has also been explored as method to produce cocrystals from solution. Freeze drying is a technique where a solution of API and cocrystal is prepared, frozen rapidly, and then held under vacuum, causing the solvent to sublime (Eddleston et al., 2013). Like spray drying, freeze drying is a technique primarily associated with generating amorphous powders (Yu, 2001). However, crystallisation from the amorphous form can occur if the glass transition temperature of the amorphous material is low (Craig et al., 1999). It is thought that, like spray drying, cocrystallisation by freeze drying proceeds via the amorphous state (Eddleston et al., 2013). As a result, freeze drying is less likely to produce single component crystals than solution based methods such as solvent evaporation or cooling crystallisation. This technique is also widely used to produce dry powders in the pharmaceutical industry, and is amenable to scale up.

Supercritical fluid technology has been explored as a method to produce cocrystals (Padrela et al., 2009, Padrela et al., 2010). A supercritical fluid is any substance at a temperature and pressure above its critical point, where distinct liquid and gas phases do not exist. Above its critical point, a substance has density and solvating power approaching that of a liquid, and can effuse through solids like a gas. Depending on the technique used, supercritical carbon dioxide can be employed as a solvent, anti-solvent or as an atomising fluid. This process can be used to control the morphology and size of the cocrystals produced (Padrela et al., 2009).

Solvent free methods to produce cocrystals include hot melt extrusion and grinding techniques. The production of cocrystals by hot melt extrusion has previously been demonstrated (Dhumal et al., 2010, Moradiya et al., 2014). This process involves premixing the API and coformer and pumping them with a rotating screw under elevated temperature through a die to produce a product of uniform shape (Crowley et al., 2007). The extrudate can then be milled to produce a pharmaceutically acceptable powder. Like spray drying and freeze drying, hot melt extrusion is normally associated with the production of solid amorphous dispersions (Lenz et al., 2017, Sarode et al., 2013, Sathigari et al., 2012). Hot melt extrusion can offer a number of advantages over other formulation methods, as it is a continuous, one step method to produce dry powders (Maniruzzaman et al., 2012). As hot melt extrusion is a solvent free method, the resulting powders will have negligible quantities of oxygen and water, which can be an advantage for APIs susceptible to oxidation and hydrolysis (Breitenbach, 2002). However, this process may not be suitable for certain APIs and excipients, as heat stress and shear forces can result in chemical degradation (Crowley et al., 2007). A study by *Dhumal et al.* investigated the impact of processing temperature, screw configuration and screw speed on the formation of the ibuprofen: nicotinamide 1:1 cocrystal by this method. Optimal conditions to produce cocrystals by hot melt extrusion were low screw speed, high mixing intensity and processing above the eutectic temperature of the API and coformer (Dhumal et al., 2010). A eutectic mixture comprises two compounds that display limited miscibility in the solid state, but are fully miscible in the molten state. The two components can crystallise simultaneously when cooled from the molten state (Laitinen et al., 2014).

Mechanochemistry is a popular method to produce cocrystals. Mechanochemical synthesis of cocrystals occurs due to mechanical energy, and therefore requires limited or no solvent (Fernández-Bertran, 1999, James et al., 2012). This process can be split in to dry (neat) grinding and liquid assisted grinding. Dry grinding involves mixing the API and coformer together and grinding them using a pestle and mortar, or by using a ball mill (Qiao et al., 2011). This can be an effective method to produce cocrystals, especially when the processing temperature is above the eutectic temperature of the API and coformer. Further to this, the closer the eutectic temperature to the cocrystal melt temperature, the longer it will take to complete the cocrystallisation process by dry grinding (Chadwick et al., 2007). The mechanism of cocrystallisation by neat grinding

has not been fully elucidated, and it is thought that several mechanisms are involved, such as molecular diffusion, eutectic formation and cocrystallisation mediated by the amorphous phase (Friščić and Jones, 2009). However, when the eutectic temperature is above the processing temperature, dry grinding can result in a poor yield of cocrystal (Chadwick et al., 2007, Shan et al., 2002). A number of drops of solvent can be added to improve the kinetics of cocrystal formation. This process is referred to as liquid assisted grinding, or wet grinding. In order to accelerate the process, at least one of the components must be at least partly soluble in the solvent (Shan et al., 2002). It is thought that small amounts of solvent can confer greater molecular freedom and additional degrees of orientational freedom, resulting in an increased opportunity for molecular collisions. Further to this, cocrystal seeds may form in the solvent during liquid assisted grinding which can promote the cocrystallisation process (Shan et al., 2002, Trask et al., 2004). However, this process may result in the formation of cocrystal solvates, or a powder with residual solvent. It should be noted that, as the mechanism of cocrystal formation differs between solution based methods and solid state methods, applying an API and coformer in a defined stoichiometric ratio to different processes can result in different cocrystal polymorphs. The SDM:4ASA cocrystal, for example, has been shown to have at least two polymorphs. Form I can be generated through liquid assisted grinding with ethanol, while form II can be generated through solution based methods such as solvent evaporation and spray drying (Grossjohann et al., 2015). However, it has been shown that polymorphic control of the cocrystal can be achieved during liquid assisted grinding by selection of an appropriate solvent. In one study, polymorphic control of the caffeine:glutaric acid 1:1 cocrystal could be achieved by adding four drops of either a polar or non-polar solvent (Trask et al., 2004). However, cocrystals produced by dry or liquid assisted grinding may not be amenable to scale up. Advantages and disadvantages of cocrystal production methods are presented in Table 1.1.

Technique	Synthesis	Advantages	Disadvantages	Examples		
				API	Coformer	Reference
Solution based methods	Solvent Evaporation	Highly crystalline product is formed; can select from a large number of solvents can to tailor final product	Formation of single component crystals from incongruently saturating solutions; both components must be soluble in solvent	Indomethacin Carbamazepine	Saccharin Nicotinamide	(Basavoju et al., 2008) (Weyna et al., 200
	Cooling Crystallisation	Suitable for scale up; cocrystal formation can be predicted by phase diagrams	Scale up can be complicated for multicomponent systems; phase diagrams can be time intensive to generate	Carbamazepine Theophylline	Nicotinamide Oxalic acid	(Gagnière et al., 2009) (Zhang and Rasmuson, 2012)
	Reaction Crystallisation	Less likely to form single component crystals; cocrystal formation can be predicted by phase diagrams	Large volumes of solvent required; phase diagrams can be time intensive to generate	Carbamazepine	Succinic acid Maleic acid	(Childs et al., 200
	Spray Drying	Can generate pure cocrystals from incongruently saturating solutions; suitable for scale up	Spray dried powders tend to have small particle size, poor flowability	Sulfadimidine Urea	4-aminosalicylic acid Succinic acid	(Grossjohann et al 2015) (Alhalaweh and Velaga, 2010)
	Freeze Drying	Can generate pure cocrystals from incongruently saturating solutions; suitable for scale up	Batch process, increased handling and processing times	Theophylline	Caffeine	(Eddleston et al., 2013)

Solid state methods	Hot Melt Extrusion	Final product will have negligible quantities of oxygen and water, suitable for scale up	Not suitable for APIs which are subject to thermal degradation; further processing (eg. milling) of extrudate is required	Ibuprofen	Nicotinamide	(Dhumal et al., 2010)
	Dry Grinding	Environmentally friendly, useful aid to screen for cocrystals not formed by solution methods	Poor kinetics of cocrystal formation if eutectic temperature is above processing temperature; not suitable for scale up	Benzophenone	Diphenylamine	(Chadwick et al., 2007)
	Liquid Assisted Grinding	Control of cocrystal polymorph is possible by rational solvent selection	Not suitable for scale up	Caffeine Sulfadimidine	Glutaric acid 4-aminosalicylic acid	(Trask et al., 2004 (Grossjohann et al 2015)

Table 1.1. Advantages and disadvantages of methods to produce cocrystals

1.11 Regulatory considerations

Both the European Medicines Agency (EMA) and the Food and Drug Administration (FDA) have published guidance relating to the classification of cocrystals in recent years. In both cases, a cocrystal of an existing API is classed as a polymorph of the API as opposed to a new chemical entity. Cocrystals of an existing API can be approved by the FDA through the 505(b)(2) New Drug Application pathway (Kalepu and Nekkanti, 2015). This pathway allows some of the safety and efficacy data to come from studies not conducted by the applicant. Existing drugs with new indications, changes in dosage form, formulation or strength and new combination products may be approved through this pathway. While the FDA had previously defined cocrystals as a drug product intermediate that must dissociate before reaching the site of action (FDA, 2016), new guidance published in February 2018 considers a cocrystal to have a similar regulatory classification to that of a polymorph of the API (FDA, 2018). As a result of this reclassification, cocrystals are now seen as an attractive formulation approach once again, as they are viewed as drug substances. If classified as a drug product intermediate, additional current good manufacturing practice (cGMP) requirements would apply to cocrystals. The EMA will not designate an existing API as a new active substance unless the cocrystal form shows differences with respect to efficacy and/or safety. However, for certain routes of administration, such as inhalation or topical formulations, the status of the cocrystal is dependent on what the therapeutic moiety is at the site of action. In these cases, dissociation of the API from the cocrystal may not have occurred when the cocrystal reaches the site of pharmacological action (EMA, 2015). In these cases, the cocrystal may be the active moiety at the site of action as opposed to the previously authorised API, which can have implications on efficacy and/or safety. An active substance which is a new therapeutic moiety will be treated as a new active substance regardless of whether the API is presented as a salt, cocrystal, solvate or anhydrous molecule (EMA, 2015). Cocrystals of an existing API can be considered for generic applications.

A number of medicines have been formulated as cocrystals and marketed in the last number of years. Entresto, a drug-drug cocrystal of sacubitril and valsartan, was approved for use by the EMA in 2015 and is licenced for the treatment of symptomatic chronic

heart failure with reduced ejection fraction. Entresto is a cocrystal salt hydrate, with each unit cell consisting of 6 sacubitril anions, 6 valsartan anions, 18 sodium cations and 15 water molecules (Feng et al., 2012). The cocrystal contains both a new active substance, sacubitril, a prodrug converted *in vivo* to sacubitrilat, and valsartan, which has previously been licenced for conditions such as hypertension and heart failure. Valsartan in this formulation is more bioavailable than valsartan in other marketed formulations. Doses of 26 mg, 51 mg, and 103 mg of valsartan as a cocrystal are equivalent to 40 mg, 80 mg, and 160 mg of valsartan in marketed formulations respectively, as measured by the maximum concentration in plasma (C_{max}) and total exposure (area under the curve (AUC)). Peak plasma concentrations of valsartan as a cocrystal formulation were achieved at approximately two hours, while the peak plasma concentration of valsartan in the marketed formulation was achieved at approximately four hours. No differences in the terminal half-life were observed (Gu et al., 2010).

Steglatro is an anti-hyperglycaemic drug which was approved for use by the EMA in March 2018. The active drug in Steglatro is ertugliflozin, a competitive inhibitor of the sodium-glucose co-transporter 2 (SGLT2), which inhibits reabsorption of glucose in the kidneys, therefore lowering blood glucose (Miao et al., 2013). After synthesis of the API, attempts to crystallise ertugliflozin proved unsuccessful. Instead, ertugliflozin existed as a hygroscopic, amorphous form with a low glass transition temperature which is unsuitable for processing (Bowles et al., 2014). However, cocrystallisation of the API with L-pyroglutamic acid resulted in an acceptable, anhydrous crystalline form which was suitable for pharmaceutical processing (Bernhardson et al., 2014). Ertugliflozin is a BCS Class I drug, displaying high solubility across the physiological pH range and high permeability (EMA, 2018). Cocrystallisation in this case was employed to improve the processability as opposed to improving the solubility and dissolution profile of the API. Steglujan, a fixed dose combination of ertugliflozin: L-pyroglutamic acid and sitagliptin, has also been approved for use by the EMA, as well as Segluromet, a fixed dose combination of ertugliflozin: L-pyroglutamic acid and metformin.

Suglat is a sodium-glucose co-transporter-2 (SGLT2) inhibitor marketed in Japan, which was approved for use in January 2014. This product was also in trials both in the US and Europe, and had completed three phase II trials. However, the development of Suglat in these markets was discontinued due to competition and prioritisation of other products in the pipeline (Poole and Dungo, 2014). The API in Suglat is ipragliflozin, which is

formulated as a cocrystal with L-proline in a 1:1 molar ratio. The cocrystal in this case is more stable and less hygroscopic than the free compound, resulting in less challenges during production (Aguillon et al., 2018).

Escitalopram oxalate, which is marketed as Lexapro as well as other generic versions, has been considered to be a salt of escitalopram and oxalic acid. However, each unit cell contains two escitalopram cations, one oxalate dianion and one neutral oxalic acid molecule (Harrison et al., 2007). In this structure, both ionic bonding and hydrogen bonding forces are present, and therefore this complex may be classified as a cocrystal salt. Another cocrystal-salt hybrid which exists and is marketed in the EU and US is Depakote, which contains valproic acid and sodium valproate (Brittain, 2013). Valproic acid is a clear, colourless liquid at room temperature, while sodium valproate is hygroscopic at ambient temperatures (Petruševski et al., 2008). It can be argued that the valproic acid:sodium valproate complex is not a cocrystal, as many definitions argue that the two individual components should exist in the solid state under ambient conditions (Jones et al., 2006, Bhogala and Nangia, 2008, Aakeröy and Salmon, 2005), therefore distinguishing cocrystals from solvates. However, the EMA and FDA argue that cocrystals should be seen as an extension of solvates, as opposed to a separate entity. The valproic acid:sodium valproate compound is more processable, and has shown superior anticonvulsant properties relative to the sodium valproate salt (Henry, 2003).

A drug-drug cocrystal of tramadol hydrochloride and celecoxib is currently under development by Esteve. Celecoxib is a BCS Class II API, exhibiting high permeability and low solubility, while tramadol is a BCS Class I API, exhibiting high permeability and solubility. Cocrystallisation results in a greater release of celecoxib, while the release of tramadol is slower compared to the pure component. This can be advantageous, as prolonged release of tramadol may result in less pronounced peaks and troughs. High peaks of tramadol are often associated with adverse effects. This approach can also provide a synergistic approach to pain management. Celecoxib is an NSAID and a preferential inhibitor of cyclo-oxygenase-2, while tramadol is an opioid receptor agonist as well as a reuptake inhibitor of both serotonin and noradrenaline, therefore providing pain relief by a number different mechanisms (Almansa et al., 2017). Pharmacokinetic parameters of both celecoxib and tramadol were found to be altered for the cocrystal when compared to marketed formulations of the individual APIs. Tramadol from the cocrystal showed a similar AUC to tramadol monotherapy, but showed a lower C_{max},

likely due to its slower dissolution rate. Lower peaks of tramadol can translate to fewer side effects. Celecoxib from the cocrystal formulation showed a reduction in AUC and C_{max}, as well as a faster T_{max}, when compared to celecoxib monotherapy. This can be attributed to a faster dissolution from the cocrystal (Videla et al., 2017).

TAK-020 is an investigational drug that is currently in clinical trials. TAK-020 is a Bruton's tyrosine kinase inhibitor developed for the treatment of rheumatoid arthritis (Chavan et al., 2018). TAK-020 is formulated as a cocrystal with gentisic acid and has recently completed phase I trials. Examples of marketed cocrystal formulations and cocrystals in clinical trials are presented in Table 1.2.

API	Coformer/API	Comments	Status
Sacubitril	Valsartan	Greater bioavailability of valsartan as a cocrystal compared to monotherapy.	Licenced for the treatment of symptomatic chronic heart failure with reduced ejection fraction
Ertugliflozin	L-pyroglutamic acid	Ertugliflozin could not be crystallised individually, and existed as a hygroscopic amorphous material which is unsuitable for processing.	Licenced for the treatment of type 2 diabetes mellitus in adults aged 18 or older.
Ipragliflozin	L-proline	The cocrystal is more stable and less hygroscopic than the free compound.	Licenced for the treatment of type 2 diabetes in Japan, South Korea and Thailand.
Escitalopram	Oxalic acid	Salt cocrystal hybrid with each unit cell containing two escitalopram cations, one oxalate dianion and one neutral oxalic acid molecule.	Licenced for the treatment of major depressive episodes, panic disorder, social anxiety disorder, generalised anxiety disorder and obsessive-compulsive disorder.
Sodium valproate	Valproic acid	The cocrystal is more processable, and has shown superior anticonvulsant properties relative to the sodium valproate salt.	Licenced for treatment of generalised, partial or other epilepsy, and for the treatment of manic episode in bipolar disorder when lithium is contraindicated or not tolerated.
Tramadol hydrochloride	Celecoxib	Lower peaks of tramadol due to slower dissolution from cocrystal, translating to fewer side effects. Faster dissolution of BCS Class II API celecoxib.	Currently in Phase II clinical trials.
TAK-020	Gentisic acid	Cocrystal developed for the potential treatment of rheumatoid arthritis.	Recently completed Phase I clinical trials.

Table 1.2. Examples of marketed cocrystals and cocrystals in clinical trials.

1.12 Formulation in the presence of excipients

Pharmaceutical dosage forms are formulated with a number of excipients as well as the API. Excipients can be used to enhance flow properties, disintegration properties and compression properties of oral dosage forms. For inhalation products, excipients are commonly added to prevent agglomeration, therefore increasing the respirable fraction

of the API (Bosquillon et al., 2001). For injectable formulations, excipients are commonly added to enhance the stability, as well as increasing the solubility of the API (Strickley, 2004). Other excipients can be used to increase the bioavailability of the API by mechanisms such as inhibition of efflux transporter P-glycoprotein (Hugger et al., 2002). While most excipients are pharmacologically inert, they can have an important impact on the chemical and physical stability of the API (Bharate et al., 2016). For example, non-hygroscopic excipients should be chosen when formulating an API which is susceptible to hydrolysis. For BCS Class I drugs, often the rate limiting step of absorption is disintegration of the tablet or capsule. In these cases, the time taken for the API to reach therapeutic levels in the body is often dependant on the excipients. However, the API is normally manufactured separately as a drug substance, and then blended with excipients to form the drug product.

Co-processing an excipient with an API can often provide a formulation advantage, as well as potentially reducing production costs by formulating an API with an excipient in a one-step process. Antisolvent precipitation of an API and excipient has been used to tailor the physicochemical properties of the poorly soluble API, siramesine hydrochloride. Adsorption of excipients such as sodium lauryl sulfate (SLS), hydroxypropyl methyl cellulose (HPMC) and hydroxypropyl cellulose (HPC) onto the surface of drug particles altered the size and morphology of the co-processed systems. The resulting systems showed increased wettability, resulting in an increase in the dissolution rate of the API (Zimmermann et al., 2009). Drying of peptides by processes such as freeze drying or spray drying from the liquid state to the solid state is commonly performed to increase the stability of the peptide (Millqvist-Fureby et al., 1999). However, these processes can remove water from the protein which can be responsible for protein activity. Replacing the water with excipients can compensate for the water loss and reduce the impact of dehydration induced inactivation (Carpenter and Crowe, 1989).

However, there is currently very little investigation into the impact of adding an excipient during the cocrystallisation manufacturing process. A number of studies have investigated the impact of an excipient on the phase behaviour and dissolution properties of the cocrystal (Remenar et al., 2007, Ullah et al., 2015, Li et al., 2014a), but studies incorporating an excipient during a one-step cocrystallisation process are limited.

CHAPTER 2

Materials and Methods

2.1 Materials

Material	Supplier
Sulfadimidine (SDM)	Sigma Aldrich (Ireland)
4-Aminosalicylic acid (4ASA)	Sigma Aldrich (Ireland)
Racemic ibuprofen (IBU)	Kemprotec (UK)
Isonicotinamide (INA)	Sigma Aldrich (Ireland)
Mannitol	Sigma Aldrich (Ireland)
Chitosan (avg. molecular weight 50,000 – 190,000)	Sigma Aldrich (Ireland)
Glycine	Sigma Aldrich (Ireland)
Polyvinyl Alcohol (PVA) (avg. molecular weight 70,000 – 100,000)	Sigma Aldrich (Ireland)
Polyvinylpyrrolidone K15 (PVP K15) (avg. molecular weight 10,000)	Sigma Aldrich (Ireland)
Dextran (avg. molecular weight 68,800)	Sigma Aldrich (Ireland)
Hydroxypropyl methylcellulose (HPMC) (4,000 cP)	Sigma Aldrich (Ireland)
Microcrystalline cellulose (MCC) Avicel CL-611	FMC Biopolymer (Belgium)
Inulin (avg. degree of polymerisation = 11)	Sensus (Netherlands)
Soluplus	BASF (Germany)
Xylitol	Lancaster (UK)
Non-pareil sugar beads 250, 500 and 1000 µm)	JRS Pharma (Germany)
Polyvinylpyrrolidone K90 (PVP K90) (avg. molecular weight 1,000,000 – 1,500,000)	BASF (Germany)
Sodium bromide	Fluorochem (UK)
Water (HPLC grade)	Elix 3 connected to Synergy UV system, Millipore (UK)
Water (deionised for DVS)	Sigma Aldrich (Ireland)

Ethanol (96 %)	Corcoran Chemicals (Ireland)
Ethanol (> 99.9 %) (for DVS)	Merck (Germany)
Methanol	Sigma Aldrich (Ireland)
Methanol (HPLC grade)	Fischer Scientific (Ireland)
Isopropanol	Corcoran Chemicals (Ireland)
Acetone	Corcoran Chemicals (Ireland)
Phosphoric acid	Merck (Germany)
Dipotassium phosphate	Sigma Aldrich (Ireland)
Trifluoroacetic acid (TFA)	Sigma Aldrich (Ireland)
Liquid nitrogen	BOC (Ireland)

2.2 Unit operations

2.2.1 Spray drying

Preparation of the SDM:4ASA cocrystal and cocrystal-in-excipient systems

A 1 % w/v solution of SDM and 4-ASA was prepared using ethanol as solvent. The solution was sonicated to dissolve the cocrystal components completely. An equal volume of 1 % w/v excipient aqueous solution (inulin, mannitol, glycine, PVA (heated to 60 ^{o}C), HPMC, PVP K15 and Soluplus) or suspension (MCC, chitosan and dextran) was added to the 1 % w/v solution of SDM and 4-ASA. The solution with the cocrystal components was mixed with the excipient solution/suspension prior to spray drying. For the excipients which were in suspension, the suspensions were stirred constantly during the spray drying process. The resultant solutions/suspensions were spray dried using a Büchi B-290 Mini Spray Dryer operating in the open mode. The solutions/suspensions were delivered to a 2-fluid atomisation nozzle using a peristaltic pump at a pump speed of 30 % (9-10 ml/min) and the aspirator was operated at 100 %, equivalent to 35 m^3/hr. The flowmeter for the standard 2-fluid nozzle was set at 4 cm, which is equivalent to 667 normlitres per hour (Nl/h) of gas flow at standard temperature and pressure conditions (p=1013.25 mbar and T=273.15 K) (Büchi Labortechnik, 93001). The inlet temperature was set at 105 °C (outlet temperature between 68 – 72 °C) for the systems which contained excipient in deionised water and 78 °C (outlet temperature between 50 – 57 °C) for the spray drying of cocrystal in ethanol alone. Based on whether cocrystal formation occurred at this ratio of cocrystal component to excipient (i.e. 1:1 % w/w), the ratio of cocrystal components to excipient was altered to assess the maximum ratio of excipient:cocrystal components which would allow cocrystal formation.

Preparation of the SDM:4ASA cocrystal-in-excipient systems with two excipients

As per the Design of Experiment formulation parameters detailed in chapter 4, the total excipient concentration and ratio of inulin: MCC varied according to each run. Inulin was added to water and stirred using magnetic stirrer until completely dissolved. MCC was added and suspended in the water. This suspension of MCC and inulin was then added to the solution containing the cocrystal components (a 1:1 molar ratio of SDM and 4-ASA was prepared in a mixture of 150 ml ethanol and 50 ml deionised water). The final concentration of solids in solution/suspension was 1 %w/v. The resultant suspensions

were spray dried using a Büchi B-290 Mini Spray Dryer operating in the open mode. The suspensions were delivered to a 2-fluid atomisation nozzle using a peristaltic pump at a pump speed of 30 % (9-10 ml/min) and the aspirator was operated at 100 %, equivalent to 35 m^3/hr. The inlet temperature was set at 105 °C (outlet temperature between 68 – 72 °C) for the systems which contained excipient.

Preparation of the IBU:INA cocrystal and cocrystal-in-excipient systems

For the cocrystal alone, a 1% w/v solution of IBU:INA (1:1 molar ratio) was prepared in ethanol or isopropanol (300 ml) and sonicated until completely dissolved. For the systems containing the cocrystal components and an excipient, a 1:1 molar ratio of IBU:INA was dissolved in a mixture of ethanol and water at a 90:10 v/v ratio. When the two cocrystal components were fully dissolved, the carrier excipient was then added and fully dissolved. For the system containing 50 % w/w of excipient, the ratio of ethanol to water was altered to 80:20 v/v to ensure complete dissolution of the excipient. The batch size for all spray drying experiments was 3 grams (300 ml of a 1 % w/v solution). Solutions were spray dried using a Büchi B-290 Mini Spray Dryer operating in the open mode (inlet temperature 90 ^oC, pump speed 30 % (equivalent to 9-10 ml/min), aspirator 100 % (equivalent to 35 m^3/hr), nitrogen flow rate 667 Normlitres/h). The spray dried cocrystal refers to the cocrystal spray dried from ethanol, unless indicated otherwise.

A solution of INA and Soluplus 50:50 weight ratio was dissolved in a mixture of 90:10 v/v of ethanol and water and spray dried under the same spray drying conditions. This was performed to assess the polymorphic form of INA after spray drying with Soluplus

For comparison purposes, a 1 %w/v solution of IBU was spray dried using ethanol as solvent. The inlet temperature was set at 65 ^oC due to the low melt temperature of IBU. All other processing conditions were kept the same, as above.

Investigation of cocrystallisation of API/coformer with excipient – Spray drying

IBU or INA was spray dried with mannitol to investigate the possible formation of a cocrystal between the API or coformer with the crystalline excipient. IBU was spray dried with mannitol at a weight ratio of 0.566: 0.1, which is the same ratio of IBU:mannitol used in the formulation comprising 90:10 (w/w) cocrystal components to excipient. INA was spray dried with mannitol at a weight ratio of 0.334:0.1. All process parameters were

unchanged relative to those used to spray drying the IBU:INA cocrystal. The solvent used was a mixture of 90:10 v/v ethanol and water.

2.2.2 Solvent evaporation

Preparation of the SDM:4ASA cocrystal by solvent evaporation

SDM (2.78 g) and 4ASA (1.53 g) were dissolved in 60 ml of acetone to give a 0.01 M solution and stirred until complete dissolution was achieved. The resulting solution was placed in a fumehood and allowed to evaporate for 72 hours (Serrano et al., 2015).

Preparation of the IBU:INA cocrystal by solvent evaporation

IBU (2.06 g) and INA (1.22 g) were added to a beaker containing 50 ml of isopropanol as solvent. Sonication was performed to ensure complete dissolution of the API and coformer. The beaker was covered with pierced parafilm to slow the evaporation of the solvent, which allowed larger crystals to form which could be used for single crystal X-ray diffraction studies, detailed in section 2.3.2. The beaker was placed in a fumehood and the solvent left to evaporate.

2.2.3 Physical mixture preparation

Physical mixtures of cocrystal and excipient, or API and coformer, were prepared by gentle mixing in an agate mortar and pestle.

2.2.4 Compaction

Tensile strength and ejection force of the co-spray dried systems and physical mixtures of cocrystal with excipient(s) were investigated. Flat tablets (n=6, 100 mg) were compressed using a Natoli NP-RD10 (Saint Charles, MO, USA) laboratory-scale single punch tablet press supplied with an Enerpac (Menomonee Falls, WI, USA) P-392 manual pump with a RC-104 hydraulic cylinder working in the range from 0 to 10 tonnes and standard 8-mm diameter punch and die tooling (I Holland Limited, UK). Compaction properties were quantified in terms of hardness achieved at the applied compaction pressure of 6 kN (0.612 tonnes). The pressure was released immediately after the desired compression pressure was reached. Tablets were pushed out of the die using the bottom punch and ejection force was recorded. A set of 6 tablets was subjected to radial hardness testing using a Dr Schleuniger, Pharmatron model 6D tablet tester (Thun, Switzerland) (Serrano et al., 2015). Tensile strength was calculated as indicated in Equation 2.1:

$$\sigma = \frac{2*F}{\pi*D*H} \quad \text{(Eq. 2.1)}$$

where σ is the tensile strength, *F* is the radial hardness, *D* is the tablet diameter, and *H* is the tablet thickness. After compaction, it was monitored whether or not the tablet capped under the applied pressure and if the breakage of the tablet occurred in a consistent manner. PXRD studies, detailed in section 2.3.1, of the formulation before and after compaction were compared.

2.2.5 Hot melt extrusion

Preparation of the IBU: INA cocrystal-in-excipient systems

A 1:1 molar ratio of IBU and INA was premixed with either xylitol, Soluplus or PVP K15 using a mortar and pestle for 5 minutes. The ratio of cocrystal components to excipient was 90:10 (w/w). HME was performed using a co-rotating, fully intermeshing twin-screw extruder (Microlab, Rondol Technology Ltd, France). The extruder die (Rondol Technology Ltd, France) was 2 mm in diameter, and was connected via screws to the end of the barrel. Only conveying elements were assembled on the screw shafts. The extruder contained five heating zones, which were set at 70, 80, 90, 90 and 80 ^{o}C from the feeding zone to the exit die. The batch size used was 10 grams for all extrusion studies. The cylindrical extrudate was air cooled and subsequently cryomilled, which is detailed in section 2.2.6.

Investigation of cocrystallisation of API/coformer with excipient – Hot melt extrusion
IBU or INA was extruded with xylitol to investigate the possible formation of a cocrystal between the API or coformer with the crystalline excipient. IBU was extruded with xylitol at a weight ratio of 0.566:0.1, which is the same ratio of IBU:xylitol used in the formulation comprising 90:10 (% w/w) cocrystal components to excipient. INA was hot melt extruded with xylitol at a weight ratio of 0.334:0.1. All process parameters were unchanged relative to the extrusion studies performed in section 2.2.5.

2.2.6 Cryomilling

HME samples were pulverised using a high-energy cryogenic ball mill (Retsch Cryomill, Haan, Germany) with circulating liquid nitrogen for 3 cycles consisting of 5 minutes of grinding followed by a 2-minute break before physicochemical analysis.

2.2.7 Spray coating

Spray coating studies of the cocrystal on to non-pareil beads were performed. A total of eight formulations were prepared. Non-pareil sugar starter cores (either 500 or 1000 µm) were coated with an ethanolic solution containing a binder (inulin or PVP K90) and SDM and 4ASA in a 1:1 molar ratio. The cocrystal components were initially dissolved in ethanol at a concentration of 1 % and then the corresponding binder was added to the mixture at a concentration of either 1 % or 5 %. The ethanolic solution was sprayed using a fluidised bed coater equipped with a Wurster insert (Mini-Glatt, Glatt®, Binzen, Germany). The process parameters were as follow: 60℃ inlet temperature, 0.5 mm nozzle diameter, 1.6 or 2.5 g/min spray rate, 25 or 35 m^3/h nitrogen flow rate and 0.7 or 1 bar atomisation pressure. Once the ethanolic solution was sprayed, the coated beads were dried inside the fluidised bed until the product temperature reached 40℃.

A seven-factor eight-run Taguchi design (L2^7) was employed for factor screening studies in order to identify the formulation and process variables that critically influence the product quality. Seven factors and two levels of each factor affecting the cocrystal-coating process were selected. Seven factors were numerical (i - vi) and one categorical (vii):

i) Spray rate of feed solution: 0.4 (1.6 g/min) or 0.6 (2.5 g/min);
ii) Nitrogen flow rate: 25 or 35 m^3/h;
iii) Atomisation pressure: 0.7 or 1 bar;
iv) Non-pareil sugar bead size: 500 or 1000 µm;
v) Amount of sprayed mass onto the beads: 30 or 50%;
vi) Amount of binder: 1 or 5%
vii) Type of binder: inulin or PVP K90.

Based on the preliminary studies (factor screening studies), the critical material attributes that affected the spray coating process were identified. A Box-Behnken design was then employed for systematic optimisation using Design Expert® software. The central point (0, 0, 0) was studied in quintuplicate. Three factors and three levels of each factor affecting the cocrystal coating process were selected: atomisation pressure (0.6, 0.8 and 1 bar), the amount of mass sprayed onto the beads (15, 30 and 45%) and the amount of binder (5, 12.5 and 20%). The remainder of the process and formulation parameters were

kept constant: 500 µm sugar bead size, 25 m^3/h nitrogen flow rate, 60 ℃ inlet temperature, PVP K90 as a binder, 0.5 mm nozzle diameter and 2.5 g/min spray rate.

2.3 Solid state characterisation

2.3.1 Powder X-ray diffraction (PXRD)

Powder X-ray analysis was performed using a Miniflex II Rigaku diffractometer with Ni-filtered Cu Kα radiation (1.54 Å). The tube voltage and tube current used were 30 kV and 15 mA, respectively. The PXRD patterns were recorded (n=3) for 2 theta ranging from 5° to 40° at a step scan rate of 0.05° per second. Rigaku Peak Integral software was used to determine peak intensity for each sample using the Sonneveld-Visser background edit procedure.

The programme Mercury (version 3.9, Cambridge Crystallographic Data Centre, Cambridge, UK) was used for calculation of X-ray powder patterns on the basis of the single crystal structure obtained from the Cambridge Crystallographic Data Centre.

2.3.2 Single crystal X-ray diffraction

This analysis was performed by Brendan Twamley (School of Chemistry, Trinity College Dublin, Ireland). X-ray structural analysis for crystals of IBU:INA ($C_{19}H_{24}N_2O_3$), prepared by solvent evaporation from isopropanol, was performed on a Bruker APEX Duo CCD at 100 K with an Oxford Cobra cryostat, with the sample mounted on a MiTeGen microloop using Cu Kα radiation (λ = 1.54178 Å). Bruker APEX (Bruker, 2014) software was used to collect and reduce data and determine the space group. Absorption corrections were applied using SADABS (Bruker, 2014/5). Structures were solved with the XT structure solution program (Sheldrick, 2015), using Intrinsic Phasing and refined with the XL refinement package (Sheldrick, 2008) using Least Squares minimisation. All non-hydrogen atoms were refined anisotropically. Hydrogen atoms were assigned to calculated positions using a riding model with appropriately fixed isotropic thermal parameters, except for amide hydrogens (N1, N25) which were located on the difference map and refined as semi-free. The sample was weakly diffracting leading to a high wR_2 and poor high angle data. Apart from the acid moiety, each ibuprofen group is fully disordered and is modelled in two positions with O10/O12 64:36% and O34/O36 53:47% occupancy, and restraints were used for convergence of the least squares refinements (DFIX, SADI, SIMU).

2.3.3 Differential scanning calorimetry (DSC)

DSC was performed using a Mettler Toledo DSC 821e instrument under nitrogen purge. Powder samples (4-6 mg) were placed in aluminium pans (40 μl), sealed, pierced to provide three vent holes and heated at a rate of 10 °C/min in the temperature range of 25 to 250 °C for the SDM:4ASA cocrystal, associated cocrystal-in-excipient systems and all raw materials in chapters 3 and 4. Quantification of crystallinity for the spray coated systems in chapter 6, described in section 2.2.2.7, was also performed using this DSC method. The heating rate for the IBU:INA cocrystal, associated cocrystal-in-excipient systems and raw materials in chapter 5 was 10 °C/min in the temperature range of 25 to 200 °C. Temperature and enthalpy were calibrated using indium as standard. The DSC was controlled by Mettler Toledo STARe software (version 6.10) working on a Windows NT operating system. All reported temperatures refer to onset of melting. All DSC analyses were performed in triplicate.

2.3.4 Modulated temperature differential scanning calorimetry (MTDSC)

MTDSC scans for the SDM:4ASA coated beads in chapter 6 were performed using a DSC Q200 (TA instruments, Elstree, United Kingdom) calorimeter using nitrogen as the purge gas. Intact beads were weighed (4-6 mg) and sealed in closed aluminium pans with one pin-hole. A scanning rate of 5 °C/min, amplitude of modulation of 0.796 °C and modulation rate of 60 seconds was employed. The temperature range was from 25 °C to 210 °C. The instrument was calibrated for temperature and cell constant using indium as standard. MTDSC data was analysed using TA Universal Analysis software (TA Instruments, Leatherhead, UK) version 4.5 A. Temperatures of melting events (n = 3) refer to onset temperatures.

MTDSC scans for the IBU:INA cocrystal systems in chapter 5 were performed using a DSC Q200 (TA Instruments, Elstree, United Kingdom) calorimeter using nitrogen as the purge gas. Samples were loaded into sealed standard aluminium pans, held at 105 °C for 10 minutes to remove any residual moisture and scanned over a temperature range of -70-180 °C with a modulation rate of 0.53 °C every 40 seconds, with a scanning rate of 5 °C/min. The instrument was calibrated for temperature and cell constant using indium as standard. MTDSC data was analysed using TA Universal Analysis software (TA Instruments, Leatherhead, UK) version 4.5 A. Temperatures of melting events (n = 3) refer to onset temperatures.

2.3.5 Attenuated total reflectance Fourier Transform infrared spectroscopy (ATR-FTIR)

Infrared spectra were recorded on a PerkinElmer Spectrum 1 FT-IR Spectrometer equipped with a UATR and a ZnSe crystal accessory. Each spectrum was scanned in the range of 650-4000 cm^{-1} with a resolution of 4 cm^{-1}. Data were evaluated using Spectrum v 5.0.1. software. Four scans of each sample were taken.

2.3.6 Physical stability studies

Spray dried samples (100 mg) were placed in glass vials and stored in conditions of 25 ^{o}C and 60% relative humidity, with the required humidity provided by using a saturated solution of sodium bromide. After seven days, samples were removed and analysed by PXRD.

2.3.7 Particle size analysis (PSA)

The geometric particle size distributions (PSD) were determined by laser diffraction using a Malvern Mastersizer 2000 (Malvern Instruments Ltd., Worcestershire, UK). Particles were dispersed using a Scirocco dry feeder instrument with 3 bar pressure. An obscuration of 0.5-3% was obtained under a vibration feed rate of 75%. Values reported are D_{50} (median particle size) results. Mastersizer 2000 software (Version 5.61) was used for the analysis of the particle size. Results reported are the average of three analyses for each sample.

2.3.8 Solubility of cocrystal in excipient

Physical mixtures of cocrystal and excipient were prepared by mixing in a pestle and mortar at different weight ratios. The melting enthalpy of the crystalline phase was determined by DSC, as described in section 2.3.3, and plotted as a function of excipient weight fraction. The solubility of the cocrystal in excipient was determined by extrapolating the linear plot of the mass fraction against melting enthalpy to zero melting enthalpy, as previously described (Amharar et al., 2014). Annealing was not performed due to the thermal instability of 4ASA.

2.3.9 Scanning electron microscopy (SEM)

The surface images of the samples were captured at various magnifications by SEM using a Zeiss Supra Variable Pressure Field Emission Scanning Electron Microscope (Germany) equipped with a secondary electron detector at 5 kV. Samples were glued on to carbon tabs, mounted onto aluminium pin stubs and sputter-coated with gold/palladium under vacuum prior to analysis.

2.3.10 High performance liquid chromatography (HPLC)

The concentration of SDM and 4ASA in solution were determined as previously described (Grossjohann et al., 2015) using an Alliance HPLC with a Waters 2695 Separations module system and Waters 2996 photodiode array detector. The mobile phase consisted of methanol and phosphate buffer pH 6.5 in 40:60 (v/v) ratio. The buffer was prepared from a 50 mM dipotassium phosphate solution adjusted to pH 6.5 with phosphoric acid. The mobile phase was vacuum filtered through a 0.45 µm membrane filter (Pall Supor® 0.45 µm, 47 mm) and bath sonicated for 5 min. Separation was performed on a Phenomenex Inertsil ODS (3) C18 column (150 mm length, diameter 4.6 mm, particle size 5 µm) at a UV detection wavelength of 265 nm. An injection volume of 20 µL was used. The elution was carried out isocratically at ambient temperature with a flow rate of 1 mL/min. Elution times for 4ASA and SDM were 1.9 min and 4.0 min respectively. Empower software was used for peak evaluation. HPLC analysis was performed for assay in chapter 3, dissolution studies in chapters 3 and 6, and to determine cocrystal loading efficiency and degree of crystallinity in chapter 6. The loading efficiency was measured by weighing out an exact mass of beads after coating and adding to mobile phase. Sonication was performed to ensure complete dissolution of the cocrystal. The resultant solution was filtered prior to HPLC analysis. The concentration range for the calibration curves of SDM and 4ASA was 0.1 – 100 µg/ml. The ratio of signal to noise at 0.1 µg/ml was > 10 for both SDM and 4ASA. This was considered to be the limit of quantification, with a limit of detection of 0.033 µg/ml.

In chapter 5, the concentration of IBU in solution was determined using an Alliance HPLC with a Waters 2695 Separations module system and Waters 2996 photodiode array detector. The mobile phase consisted of 85% HPLC grade methanol and 15% HPLC grade water containing 0.2% trifluroracetic acid (Li et al., 2016). The mobile phase was degassed by sonicating for 10 minutes. Separation was performed on a Waters XBridge

C18 column with a length of 150 mm, an internal diameter of 3 mm and a particle size of 3.5 µm. Samples were analysed at a UV detection wavelength of 220 nm. An injection volume of 20 µL was used. The elution was carried out isocratically with a flow rate of 0.5 mL/min. The temperature of the column chamber was maintained at 40 ^{o}C for the entire analytical process. Elution times for IBU and INA were 2.2 and 1.5 minutes respectively. With the systems containing Soluplus, the ratio of aqueous to organic phase was altered to 70:30 v/v due to peak interference. The elution time for IBU was 5.7 minutes. Empower software was used for peak evaluation. The concentration range for the calibration curve for IBU was 0.14 – 115 µg/ml. The signal to noise ratio at 0.14 µg/ml was > 10. This was considered to be the limit of quantification, with a limit of detection of 0.046 µg/ml.

2.3.11 Density measurement

A 1-cm^3 syringe was used in the bulk volume determination of samples in chapter 4, as previously described (Ógáin et al., 2011). The syringe was filled by allowing the powder to flow into the syringe until 1 ml was reached. The tap volume was determined similarly to the bulk volume, but the volume taken for calculations was that after 100 strokes. Each average result is calculated based on two measurements. Carr's compressibility index was calculated using the bulk and tapped values according equation 2.2.

$$Carr's\ Index = \frac{bulk\ volume - tapped\ volume}{bulk\ volume} * 100 \qquad \text{(Eq. 2.2)}$$

2.3.12 Quantification of crystallinity for co-spray dried systems

The relative crystallinity for the co-spray dried systems compared to the physical mixtures of cocrystal and excipients in chapter 4 was calculated according to equation 2.3. All runs were performed as described in section 2.3.3, in the temperature range of 25-250 ^{o}C. Physical mixtures were prepared by mixing in an agate mortar and pestle.

$$\%\ Crystallinity = \frac{Average\ enthalpy\ of\ cospray\ dried\ cocrystal}{Average\ enthalpy\ of\ physical\ mix\ of\ cocrystal}\ x100 \qquad \text{(Eq. 2.3)}$$

2.3.13 Quantification of crystallinity for spray coated systems

The degree of crystallinity (DC) was calculated taking into consideration the actual percentage of cocrystal that was coated on the beads (loading efficiency), measured by HPLC, described in section 2.3.10, and the melting enthalpy (J/g) corresponding to the melting of the cocrystal. The melting enthalpy of the cocrystal coated beads was compared with the melting enthalpy of the cocrystal prepared by solvent evaporation (SE) described in section 2.2.2 (Eq. 2.4). The DSC method used to calculate the melting enthalpy is the method for the SDM:4ASA system described in section 2.3.4.

$$DC\ (\%) = \frac{\Delta Hf\ cocrystal\ coated\ on\ beads}{(LE(\%) * \Delta Hf\ cocyrstal\ SE)/100} * 100 \qquad \text{(Eq. 2.4)}$$

2.3.14 Thermogravimetric analysis (TGA)

TGA was performed using a Mettler TG50 measuring module coupled to a Mettler Toledo MT5 balance (Schwerzenbach, Switzerland). Approximately 8−10 mg samples were analysed in open aluminium pans, using nitrogen as the purge gas. Samples were heated from 25 to 300 °C at a rate of 10 °C/min. All TGA studies were performed in triplicate.

2.3.15 Dynamic vapour sorption (DVS)

Vapour sorption experiments on the IBU:INA cocrystal and associated cocrystal-in-excipient systems in chapter 5 were obtained using a DVS Advantage-1 automated gravimetric sorption analyser (Surface Measurement Systems, Alperton, UK) at 25.0 ± 0.1 ºC. Ethanol was used as the probe vapour. A mass of 15-20 mg of powder was loaded on to the sample basket. Samples were dried for 1 hour at 0 % partial pressure (P/P_o) and then subjected to step changes of 10 % P/P_o up to 90 % P/P_o, and the reverse for desorption. The sample mass was allowed to reach equilibrium, defined as $dm/dt \leq 0.002$ mg/min over 10 min, before the P/P_o was changed (Grossjohann et al., 2015). Two cycles of sorption and desorption were performed for each sample. Samples were recovered and analysed by PXRD and DSC. All studies were performed in duplicate.

Vapour sorption experiments on the SDM:4ASA coated beads in chapter 6 were obtained using a DVS Advantage-1 automated gravimetric sorption analyser (Surface Measurement Systems, Alperton, UK) at 25.0 ± 0.1°C. Water was used as the probe vapour. A mass of 15-20 mg of powder was loaded on to the sample basket. Samples

were dried at 0 % RH for 1 h and then subjected to step changes of 10 % RH up to 90 % RH, and the reverse for desorption. The sample mass was allowed to reach equilibrium, defined as dm/dt ≤ 0.002 mg/min over 10 min, before the RH was changed (Grossjohann et al., 2015). One cycle of sorption and desorption was performed. All studies were performed in duplicate.

2.3.16 Surface area measurements

To determine the specific surface area by the Brunauer, Emmett, Teller (BET) isotherm method, a Micromeritics Gemini VI (Micromeritics, Norcross, GA, USA) surface area analyser was used. The specific surface area of the samples was determined by the N_2 adsorption BET multipoint method, with 6 points in the relative pressure range of 0.05-0.3, using a Micromeritics Gemini 2385c (Micromeritics, Norcross, USA). Each average result was calculated on the basis of three measurements. Samples were prepared by purging under N_2 overnight at 25 °C using a SmartPrep degassing unit (Micromeritics, Norcross, GA, USA).

2.3.17 Flow measurements

The basic flow energy (BFE), specific energy (SE) and stability index (SI) of both the uncoated 250, 500 and 1000 µm beads, and the coated 250, 500 and 1000 µm beads were measured using a FT4 Powder Rheometer (Freeman Technology Ltd., Gloucestershire, UK) in chapter 6. All tests were performed in 25 ml batch samples in a 25 mm diameter cylinder with a fitted blade. The material was subject to a standard conditioning cycle, to ensure that the state of each sample was reproducible before every test. The BFE and SE were measured by rotating a precision blade anti-clockwise downward and clockwise upward, respectively, in a helical path through a fixed volume of conditioned material. During the downward traverse, the torque and axial force acting on the blade were measured, and the resistance to flow was calculated and expressed as energy (Narang et al., 2016, Chaudhari and Dave, 2015). The SI, defined in equation 2.5, is the ratio of energy in test 1 to energy in test 7. Stable powders will have an SI value of approximately 1 (Davis et al., 2018, Freeman, 2007).

$$Stability\ Index\ (SI) = \frac{Energy\ test\ 7}{Energy\ test\ 1} \qquad \text{(Eq. 2.5)}$$

2.3.18 Attrition

Attrition measurements of the beads after spray coating was performed by attempting to pass the uncoated and coated beads through a sieve. Initially, sieving was performed to ensure that none of the uncoated beads could pass through the sieve. After spray coating, the beads were again subject to the same process. 425 µm and 850 µm sieves were used to perform studies on the 500 µm and 1000 µm beads respectively. The attrition value (calculated as % broken beads) was calculated from equation 2.6.

$$\%\ Broken\ beads = \frac{Mass\ of\ beads\ passed\ through\ sieve}{Total\ mass\ of\ beads\ tested} * 100 \qquad \text{(Eq. 2.6)}$$

2.4 Dissolution studies

2.4.1 Intrinsic/constant surface area dissolution studies

Dissolution studies of solid materials were performed using a Wood's intrinsic dissolution apparatus (Elementec, Ireland). This allowed the dissolution to be measured from constant surface area discs. Discs were prepared by compressing the powder (200 mg) into compacts using a Perkin Elmer hydraulic press with an 8 mm (diameter) punch and die set at a pressure of 3 tonnes for a 1 min dwell time. The dissolution studies for the SDM:4ASA cocrystal systems in chapter 3 were carried out in deionised water (volume: 900 mL, temperature: 37 ^{o}C) at a rotation speed of 100 rpm. All dissolution studies were performed under sink conditions. Aliquots (5 ml) were withdrawn with volume replacement at appropriate time intervals. Samples were taken at 2, 4, 6, 8, 10, 15, 20, 25, 30, 40, 50 and 60 minutes. Samples were filtered through 0.45 µm filters and analysed for SDM and 4ASA content by HPLC. The study was performed in triplicate. The intrinsic dissolution rate (IDR) was determined from the slope of the dissolution time profiles over the first 10 minutes. All dissolution studies were carried out for samples with a 50 % (w/w) ratio of excipient and cocrystal. At the end of the experiments, the discs were recovered, dried at ambient temperature and analysed by PXRD for process induced phase transformation.

With regard to the studies for the IBU:INA cocrystal systems, dissolution studies were performed in phosphate buffer (pH: 7.2, volume: 900 mL, temperature: 37 ^{o}C) at a rotation speed of 100 rpm as indicated in the USP Pharmacopeia 38/NF 33. All dissolution studies were performed under sink conditions. Aliquots (5 ml) were withdrawn with volume replacement at appropriate time intervals. Samples were filtered through 0.45 µm PTFE filters and analysed for IBU content by HPLC. The study was performed in triplicate. Samples were taken at 2, 4, 6, 8, 10, 15, 20, 25, 30, 40, 50 and 60 minutes. The dissolution rate was determined from the slope of the dissolution time profiles over the first 10 minutes. At the end of the experiments, the discs were recovered, dried at ambient temperature and analysed by PXRD for process induced phase transformation.

For some samples in chapter 5, additional intrinsic dissolution studies were carriedut at 20 ^{o}C, with all other conditions being kept the same. This was performed to investigate the impact of Soluplus on the release of the cocrystal from constant surface area disks.

Statistical analysis of dissolution profiles was performed using DDSolver (Zhang et al., 2010). Univariate ANOVA analysis was performed to compare drug dissolution profiles considering a p-value < 0.05 as significant (Yuksel et al., 2000). An f_2 value between 50-100 indicates that dissolution profiles are similar.

2.4.2 Dissolution from capsules

Cocrystal coated beads were weighed (200 mg) and filled into HPMC capsules size 1 (Vcaps®). Dissolution studies in chapter 6 were performed according to USP Method I (basket method) utilising a Sotax dissolution apparatus with a rotation speed of 100 rpm. The dissolution medium was 900 ml of simulated intestinal fluid without enzymes adjusted to pH 6.8 at 37°C (Serrano et al., 2015). Samples (5 ml) without replacement were obtained at: 5, 10, 15, 20, 30, 40, 50 and 60 min. For comparison purposes, dissolution studies were also performed on non-pareil sugar beads coated with SDM. SDM was dissolved in ethanol at 1% concentration and sprayed onto non–pareil sugar beads using the same process parameters as for the optimised cocrystal formulation.

2.5 Hansen solubility parameter

2.5.1 Hansen solubility parameter calculation

Hansen solubility parameters were calculated from the chemical structures using the Van Krevelen method (Van Krevelen and Te Nijenhuis, 2009). The weight average molecular weights were used to determine the solubility parameters for polymeric excipients (Scott, 1992). The total HSP contribution was divided into three partial solubility parameters: dispersion (δ_d), polar (δ_p) and hydrogen bonding (δ_h). The total solubility parameter was calculated as indicated in Equations 2.6 – 2.9:

$$\delta_t = (\delta_d^2 + \delta_p^2 + \delta_h^2)^{0.5} \quad \text{(Eq. 2.6)}$$

$$\delta_d = \frac{\sum_{i=1}^{n} F_{di}}{\sum_{i=1}^{n} v_i} \quad \text{(Eq. 2.7)}$$

$$\delta_p = \frac{\left(\sum_{i=1}^{n} F_{pi}^2\right)^{0.5}}{\sum_{i=1}^{n} v_i} \quad \text{(Eq. 2.8)}$$

$$\delta_h = \left(\frac{\sum_{i=1}^{n} F_{hi}}{\sum_{i=1}^{n} v_i}\right)^{0.5} \quad \text{(Eq. 2.9)}$$

where i is the structural group within the molecule, F_{di} is the group contribution of the dispersion forces, F_{pi} is the group contribution of the polar forces, F_{hi} is the group contribution of the hydrogen bonding forces, and V_i is the group contribution of the molar volume (Mohammad et al., 2011).

2.6 Statistical analysis

Statistical analysis for both Box-Behnken and Taguchi Design of Experiments was performed using Design Expert software (version 10.0) Optimisation of the process and formulation factors was also performed using this software.

CHAPTER 3

Co-spray drying an excipient in the presence of an API and coformer to produce cocrystal-in-excipient systems

3.1 Introduction

This chapter investigates the introduction of an excipient, in the presence of an API and coformer, in to a one-step spray drying process. Such processes could result in a cheaper and more efficient process to produce a final product, which in turn could make medicines more accessible to patients. A cocrystal of SDM and 4ASA was chosen as a model cocrystal. This cocrystal is well characterised, and has previously been studied extensively by this research group.

It has been shown that the reason less than 1% of drug candidates make it to market is not only due to a lack of efficacy, safety or an unfavourable side effect profile, but also due to poor biopharmaceutical properties (Cook et al., 2014, Aakeröy et al., 2009). It has been suggested that drug discovery strategies, such as high throughput screening, are increasingly leading to lead candidates which have unfavourable physicochemical properties (Lipinski et al., 2012). Many of these compounds have poor aqueous solubility, which can lead to a low dissolution rate (Hörter and Dressman, 2001). Over half of marketed drug products are formulated as salts to modify the physical properties of the active pharmaceutical ingredient (API). However, a major limitation of this approach is the requirement of the API to possess a basic or acidic ionisable group. Pharmaceutical cocrystals offer an alternative to salt forms as a means of improving the solubility, dissolution and bioavailability of poorly water soluble drugs. Cocrystals of an API and coformer are formed by noncovalent, freely reversible interactions, and so the presence of an ionisable group is not a necessity. The solubility and dissolution rate of an API in a cocrystal are improved by lowering the lattice energy and/or increasing the solvent affinity (Thakuria et al., 2013). Cocrystallisation of an API can confer a number of advantages over other formulation strategies such as amorphisation. One of the major limitations of amorphous forms is the fact that they are thermodynamically unstable, making them prone to conversion to the lower energy crystalline forms (Hancock et al., 1995).

Various methods exist to produce cocrystals. Common approaches include grinding and solution methods. However, a disadvantage of solution methods to produce cocrystals can be the formation of single component crystals when crystallised from an incongruently saturating solution (Qiao et al., 2011). Spray drying is commonly used to produce amorphous solid dispersions (Zhao et al., 2012, Van den Mooter et al., 2001) but

also, in some instances, results in the formation of crystalline materials (Kumar et al., 2015). This technique has been shown to be a viable and scalable method to produce pure cocrystals from both congruent and incongruently saturating solutions. Carbamazepine-glutaric acid, theophylline-nicotinamide, urea-succinic acid and caffeine-glutaric acid all formed pure cocrystals when spray dried from incongruently saturating solutions. Further to this, the urea-succinic acid 1:1 cocrystal was discovered and consistently generated in pure form by spray drying. Cocrystallisation of this system was unsuccessful by slurry or reaction crystallisation methods (Alhalaweh and Velaga, 2010).

The approach of using Hansen Solubility Parameters calculated using the group contribution method has enabled the prediction of solid-solid solubility of pharmaceutical materials (Hancock et al., 1997). For drug-excipient combinations, a $\Delta\delta t$ (i.e. difference in HSP) of less than 7.0 $MPa^{1/2}$ is considered to be indicative of significant miscibility, while a $\Delta\delta t$ of greater than 10.0 $MPa^{1/2}$ denotes a lack of miscibility and limited ability to form glass solutions (Greenhalgh et al., 1999, Forster et al., 2001). However, it is important to note that the studies conducted by Greenhalgh et al. utilised Hildebrand Solubility Parameters as opposed to Hansen Solubility Parameters.

Calculation of the HSP of drug and coformer and the difference in HSP values for the two components can be used as a tool to predict the success of cocrystal formation on spray drying. It has been shown that, in order for an API to form a cocrystal with a coformer, the two molecules must be miscible at a molecular level, with the difference in HSP being less than 7 $MPa^{0.5}$ (Mohammad et al., 2011). However, to the best of our knowledge, the effect on cocrystal formation of introducing a third (excipient) component into the feed solution during the spray drying process has never been investigated, nor has the relative differences in HSP between excipient and cocrystal components been probed in relation to success or otherwise of cocrystal formation on spray drying.

The hypothesis underlying this work is that a larger difference in HSP between the cocrystal components and the excipient will promote cocrystal formation during spray drying in the presence of a carrier excipient, as the cocrystal components will not be miscible with the excipient, and so will remain phase separated from the excipient but still interact with one another. In contrast, excipients which have a similar HSP to the cocrystal components may be miscible and may not allow for cocrystal formation to

occur, rather there may be a high probability that an amorphous dispersion of individual coformer molecules, rather than a cocrystal suspension would form within the carrier.

The aim of this work was to investigate the impact of including a carrier excipient on cocrystal formation during the spray drying process. A range of pharmaceutical excipients was selected and co-spray dried with the cocrystal components. Solid state characterisation was performed as well as solubility studies of the cocrystal in the excipient using a thermal analysis approach. Dissolution studies were performed from constant surface area disks.

The feasibility of co-spray drying cocrystals and a third carrier excipient component in order to reduce the number of unit processes to produce a final pharmaceutical product was investigated by means of compaction studies.

3.2 Results

3.2.1 Effect of the type and composition of excipient on cocrystal formation by spray drying

SDM:4-ASA cocrystal:excipient 50:50 (% w/w)

The form II polymorph of the SDM:4ASA cocrystal, the crystal structure of which has previously been determined by single crystal XRD (Grossjohann et al., 2015), was generated by spray drying. The X-ray diffraction pattern of SDM:4ASA cocrystal and individual components are depicted in Figure 3.1, as well as the cocrystal prepared by slow solvent evaporation from acetone. DSC analysis of the cocrystals produced by solvent evaporation and spray drying showed a single endothermic peak, characteristic of cocrystal melting. The cocrystal produced by solvent evaporation had a higher melting point (175.84 ± 0.85 ^{o}C) and melting enthalpy (239.15 ± 6.84 J/g) compared to that produced by spray drying, which had a melting point of 170.08 ± 0.23 ^{o}C and a melting enthalpy of 216.52 ± 3.69 J/g. This is in agreement with previously reported data (Grossjohann et al., 2015). This finding can be explained by the fact that rapid drying processes, such as spray drying, are likely to induce crystal lattice imperfections such as point defects, line defects and plane defects, which can affect the thermal properties of the spray dried product (Corrigan, 1995).

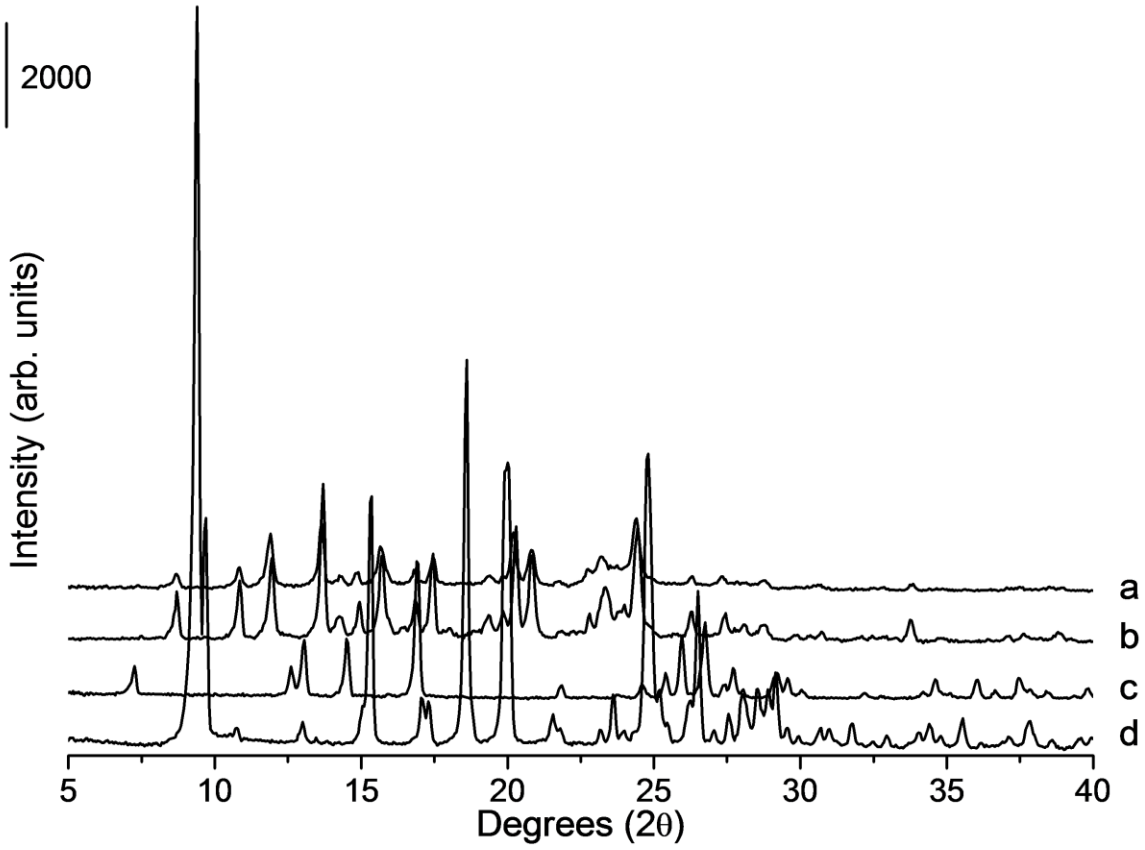

Figure 3.1. PXRD patterns a) Cocrystal produced by spray drying, b) Cocrystal produced by slow solvent evaporation from acetone, c) Unprocessed 4ASA, d) Unprocessed SDM.

PXRD demonstrated cocrystal formation was preserved when cocrystal components were spray dried in the presence of inulin, MCC, dextran and mannitol at a 50 % (w/w) ratio of cocrystal components to 50 % (w/w) of excipient (Figure 3.2). PXRD analyses showed that the same diffraction peaks were present when compared to the spray dried cocrystal. Characteristic diffractions peaks of the cocrystal are observed at 11.9^o, 13.65^o, 20.25^o and 24.4^o 2θ (Serrano et al., 2015). It would be expected that cocrystal formation would occur in the presence of a suspended excipient (which was the case for MCC, chitosan and dextran), as the cocrystal components in solution would be phase separated from the excipient in suspension. Extra diffraction peaks were present for the cocrystal in mannitol system which were attributed to mannitol (both alpha and delta polymorphs). Characteristic peaks of delta mannitol are present at 9.75^o and 25.2^o 2θ, while characteristic alpha mannitol peaks are observed at 17.3^o and 33.2^o 2θ. Spray drying of mannitol and lysosome has previously been shown to produce a system containing a mixture of mannitol polymorphs, and both beta and delta polymorphs of mannitol were

observed (Hulse et al., 2009). However, the intensity of the diffraction peaks was decreased for the co-spray dried cocrystal-in-excipient system when compared to a physical mixture of the spray dried cocrystal and excipient, probably due to the interaction between the cocrystal components and the excipient, and partial amorphisation of cocrystal within the excipient matrix. Reduction in peak intensity may also be attributed to crystal imperfections and/or the preferred orientation effect (Grant and York, 1986). The observed decrease in intensity varied for each excipient used. PXRD analyses of physical mixtures of cocrystal and excipient are shown in Figure A.1.1, Appendix 1.

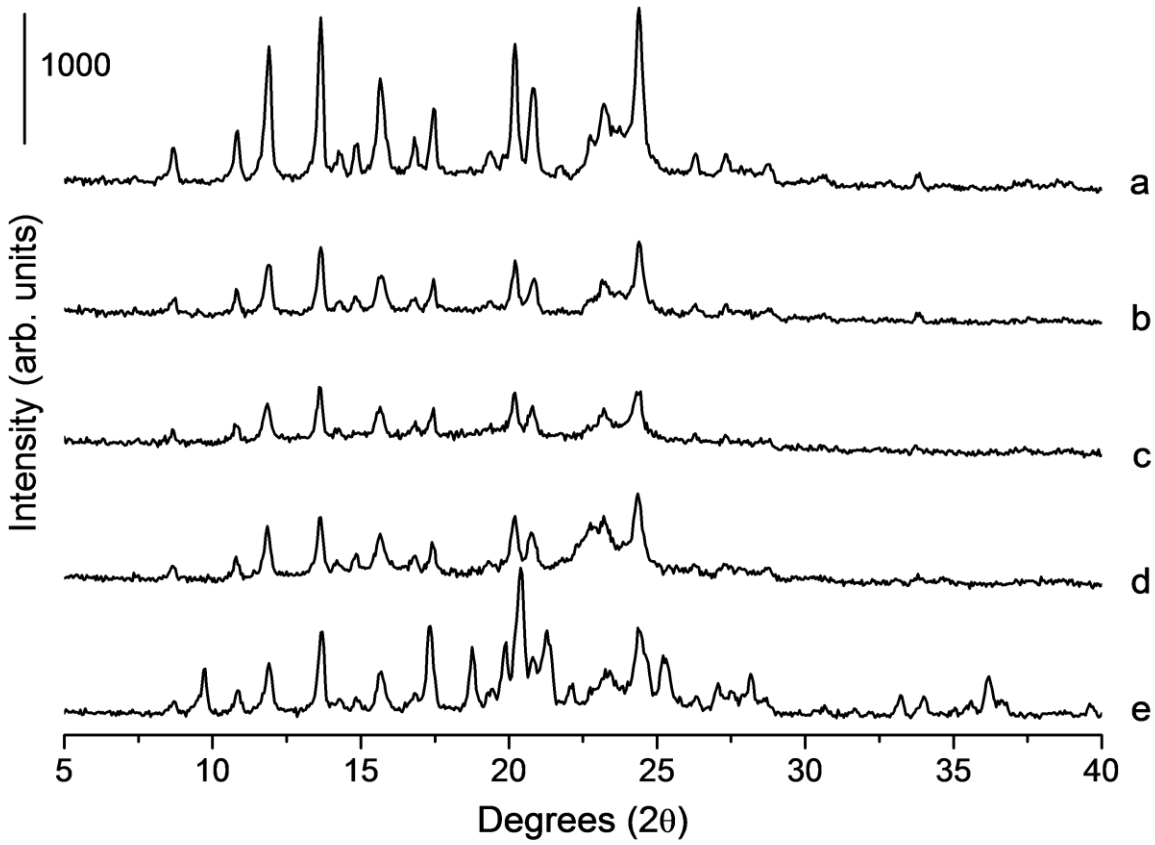

Figure 3.2. PXRD pattern of co-spray dried systems with excipient at 50% w/w ratio. a) Cocrystal produced by spray drying, b) Cocrystal components co-spray dried with dextran, c) Cocrystal components co-spray dried with inulin, d) Cocrystal components co-spray dried with MCC, e) Cocrystal components co-spray dried with mannitol.

The melting enthalpy associated with the co-spray dried cocrystal in inulin system was 91.81 ± 2.62 J/g, compared with a value of 98.7 ± 5.45 J/g for a physical mixture of the

spray dried cocrystal and inulin. The co-spray dried dextran in cocrystal system showed an enthalpy of 99.11 ± 5.4 J/g, compared to a value of 103.21 ± 9.13 J/g for the physical mixture of dextran and spray dried cocrystal. The excipient which showed the largest difference in enthalpy between the co-spray dried system and the physical mixture was MCC, with values of 83.52 ± 4.23 J/g and 101.02 ± 9.59 J/g respectively. In all cases, the only endothermic event was attributed to the melting of the cocrystal, and no exothermic events were observed (Figure 3.3). It was not possible to accurately measure the enthalpy of melting for the cocrystal when mannitol was used as an excipient. Mannitol melted at 165.46 ± 0.47 ^{o}C, which overlapped with the melting of the cocrystal. Based on the DSC analyses, the relative crystallinities of the co-spray dried systems compared to the physical mixtures were 93.02 %, 96.03 % and 82.68 % for the systems containing inulin, dextran and MCC respectively. The co-spray dried systems had a similar melting temperature as the physical mixture of cocrystal and excipient for all systems, with the exception of MCC, where a significant melting point depression was seen for the co-spray dried formulation when compared to the physical mixture. DSC analyses of the physical mixtures are shown in Figure A.1.2, Appendix 1.

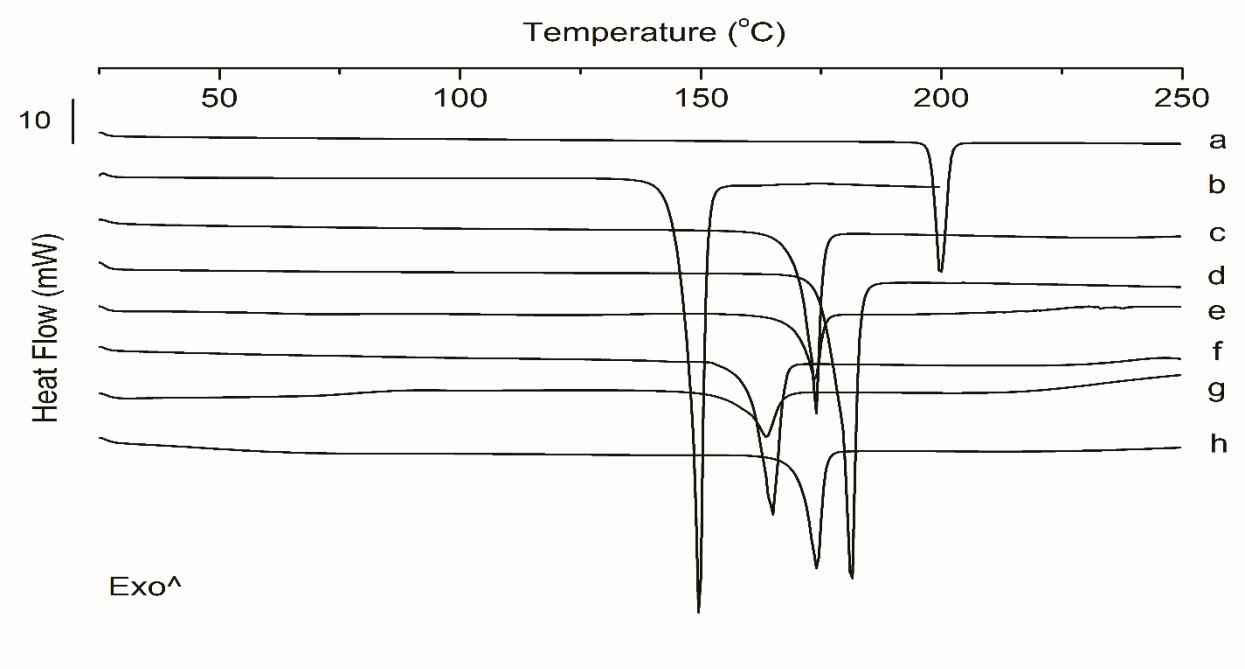

Figure 3.3. DSC thermograms. a) Unprocessed SDM, b) Unprocessed 4ASA, c) Cocrystal produced by spray drying, d) Cocrystal produced by solvent evaporation, e) Cocrystal components co-spray dried with inulin, f) Cocrystal components co-spray dried with mannitol, g) Cocrystal components co-spray dried with MCC, h) Cocrystal components co-spray dried with dextran.

Bragg diffraction peaks attributable to the cocrystal, as well as the individual components (API and coformer), were observed when cocrystal components were spray dried in the presence of PVA, glycine and chitosan at a 50:50 % w/w ratio. Characteristic diffraction peaks of glycine were also present in that particular system (Figure 3.4). An amorphous solid dispersion was produced when cocrystal components were spray dried in the presence of Soluplus, HPMC and PVP K15 at the 50:50 % w/w ratio (Figure 3.5).

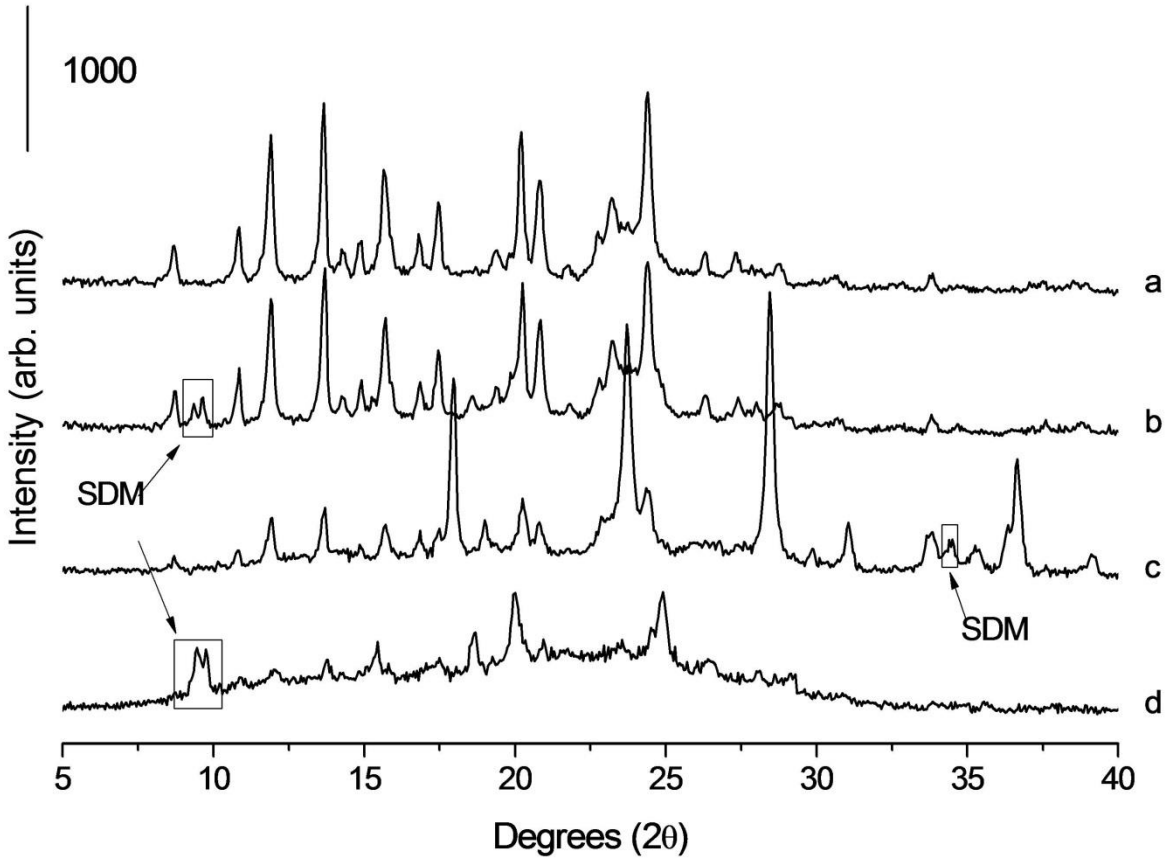

Figure 3.4. PXRD analyses of co-spray dried systems with excipient at 50:50%w/w ratio. a) Cocrystal produced by spray drying, b) Cocrystal components co-spray dried with PVA, c) Cocrystal components co-spray dried with glycine, d) Cocrystal components co-spray dried with chitosan. Extra diffraction peaks attributable to crystalline glycine can be seen in c).

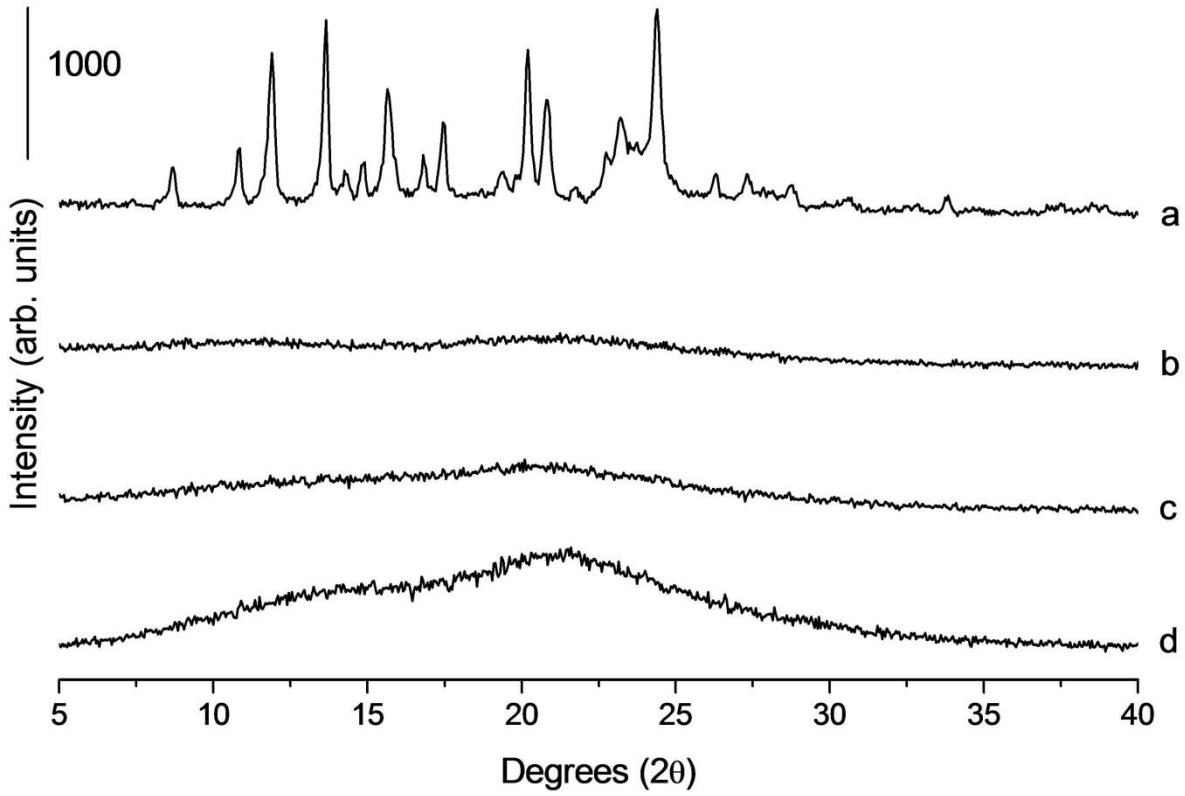

Figure 3.5. PXRD analyses of co-spray dried systems with excipient at 50:50%w/w ratio. a) Cocrystal produced by spray drying, b) Cocrystal components co-spray dried with HPMC, c) Cocrystal components co-spray dried with Soluplus, d) Cocrystal components co-spray dried with PVP K15.

Based on the calculated HSP, inulin, MCC, mannitol, chitosan and dextran are immiscible with the cocrystal components with a difference in HSP between the excipient and cocrystal ranging from 9.6 $MPa^{0.5}$ – 18.6 $MPa^{0.5}$ (Table 3.1). All of these spray dried systems, with the exception of chitosan, resulted in the formation of a cocrystal and there was no evidence of other (individual API or coformer) components present by PXRD. Characteristic diffraction peaks of the cocrystal and SDM were observed for the spray dried system containing chitosan. As chitosan is a basic polymer, there may be an interaction with the acidic coformer, resulting in the presence of Bragg peaks attributed to "free" SDM.

The differences in HSP between PVA and glycine and the cocrystal are 4.9 $MPa^{0.5}$ and 6.6 $MPa^{0.5}$, respectively which can explain the presence of diffraction peaks of both the

cocrystal and the individual components, due to the partial miscibility of the cocrystal components within these excipients. It may be hypothesised that the interaction of the excipient with the cocrystal components can result in the formation of an amorphous dispersion. The diffraction peaks observed may be as a result of the rapid crystallisation of a binary, ternary or single component amorphous domains. The crystallisation of materials by spray drying is thought to be a two stage process, with material transforming from the liquid to an amorphous phase first, and then from the amorphous phase to a crystalline phase (Chiou and Langrish, 2008) The differences in HSP between PVP K15, Soluplus and HPMC and the cocrystal were even lower (4.4 $MPa^{0.5}$, 3.9 $MPa^{0.5}$ and 1.9 $MPa^{0.5}$ respectively). Spray drying led to the formation of an amorphous solid dispersion instead of a cocrystal (Figure 3.5) probably due to the higher miscibility of the cocrystal components in these excipients.

Table 3.1. Cocrystal formation in excipient matrix when spray dried at a ratio of 50:50 (% w/w) cocrystal components: excipient. The calculated HSP of SDM:4ASA cocrystal was 26.8 $MPa^{0.5}$. Key, CC, cocrystal. HSP values of excipient which are not referenced were calculated.

Excipient	**Excipient in solution or suspension**	**Crystalline or amorphous nature of the excipient**	**δ_t ($MPa^{0.5}$) of excipient (Reference)**	**$\Delta\delta_t$ ($MPa^{0.5}$) between excipient and Cocrystal**	**PXRD of co-spray dried systems**
Cocrystal	N/A	-	26.8	-	-
Inulin	Solution	Amorphous	45.4	18.6	CC
MCC	Suspension	Semi-crystalline	39.3 (Rowe, 1988)	12.5	CC
Mannitol	Solution	Crystalline	39.1 (Forster et al., 2001)	12.3	CC
Chitosan	Suspension	Amorphous	38 (Ravindra et al., 1998)	11.2	CC+API+coformer
Dextran	Suspension	Amorphous	36.4 (Antoniou et al., 2010)	9.6	CC
Glycine	Solution	Crystalline	33.4	6.6	CC+API+coformer
PVA	Solution	Amorphous	31.7 (Forster et al., 2001)	4.9	CC+API+coformer
PVP K15	Solution	Amorphous	22.4 (Forster et al., 2001)	4.4	Amorphous
Soluplus	Solution	Amorphous	22.9	3.9	Amorphous
HPMC	Solution	Amorphous	28.7	1.9	Amorphous

3.2.2 Effect of different ratios of excipient on cocrystal formation during spray drying

PVP K15, Soluplus and HPMC

The ratio of cocrystal components to excipient was altered to assess whether the HSP difference reflected the ratio at which a cocrystal would form when co-spray dried with an excipient. PVP K15, Soluplus and HPMC were chosen and different cocrystal:excipient weight ratios (75:25, 80:20, 90:10 % w/w) investigated.

At the lowest ratio of excipient (10 % w/w), the cocrystal was formed when PVP K15 and Soluplus were the excipients used. However, an amorphous dispersion was formed in the case of HPMC (Figure A.1.3, Appendix 1). It has previously been determined that viscous polymers can inhibit the crystallisation process. The fast evaporation of solvent which occurs during the drying process can lead to a rapid viscosity increase and permit kinetic trapping of the cocrystal components in the excipient matrix as an amorphous form or disordered system (Paudel et al., 2013). As the HPMC solution has a higher viscosity than the PVP K15 and Soluplus solutions, both the higher viscosity and the lower difference in HSP between the cocrystal components and HPMC may contribute to the formation of an amorphous dispersion.

For PVP K15 and Soluplus, cocrystal formation was observed when excipients were co-spray dried at a ratio of 80:20 (% w/w) cocrystal components to excipient (Figures 3.6i and 3.7i respectively). When the ratio was altered to 75:25 (% w/w) cocrystal components to excipient, an amorphous dispersion was formed in the case of both excipients. The three co-spray dried PVP K15 and Soluplus systems at different ratios were then stressed under conditions of 25 ^{o}C and 60 % relative humidity (RH) for one week. An increased intensity of the Bragg peaks was observed in those co-spray dried systems containing 80% and 90% cocrystal. Co-spray dried cocrystal components and PVP K15 at a 75 (% w/w) cocrystal components to 25 (% w/w) ratio crystallised from an amorphous dispersion to the metastable polymorph II cocrystal (Grossjohann et al., 2015) under these conditions. Peaks attributable to individual components or to the form I cocrystal were not observed. In contrast, when the 75:25 (% w/w) cocrystal components: Soluplus system was stressed, diffraction peaks attributable to both the form II and more stable form I cocrystal were present (Figures 3.6ii and 3.7ii respectively). When the spray dried cocrystal alone (which presents as form II) was stressed under the same conditions, a polymorphic transition to the form I cocrystal was not observed, suggesting that stressing

co-spray dried cocrystal: Soluplus (75:25 % w/w) from the amorphous state results in a metastable form II.

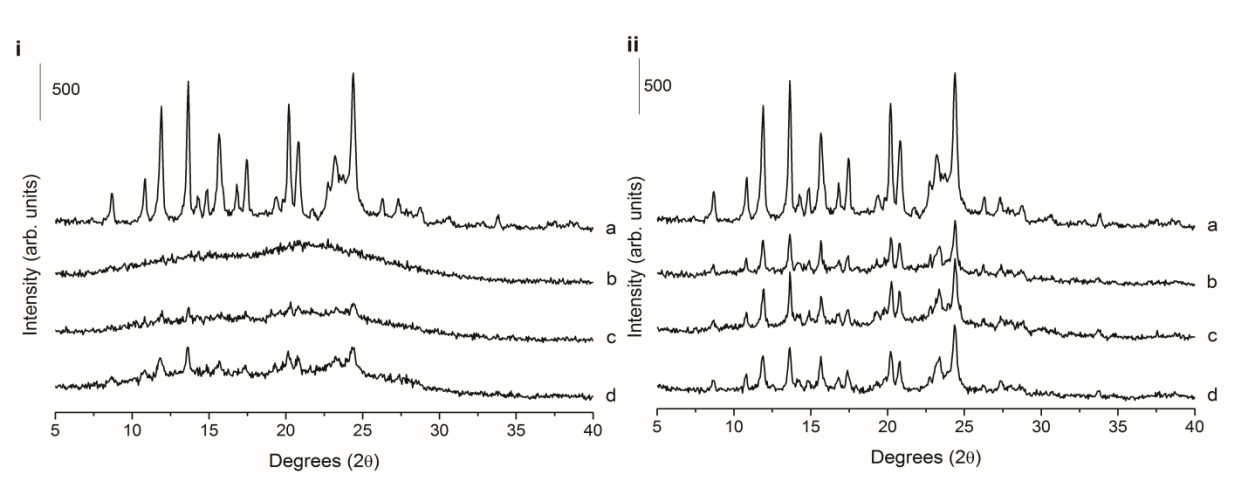

Figure 3.6. PXRD patterns of co-spray dried systems with PVP K15. i) Co-spray dried with PVP K15 and ii) Co-spray dried with PVP K15 after stressing at 25 ^{o}C and 60 % RH for seven days, a) Spray dried cocrystal, b) Cocrystal:PVP K15 (75:25 % w/w), c) Cocrystal:PVP K15 (80:20 % w/w), d) Cocrystal:PVP K15 (90:10 % w/w).

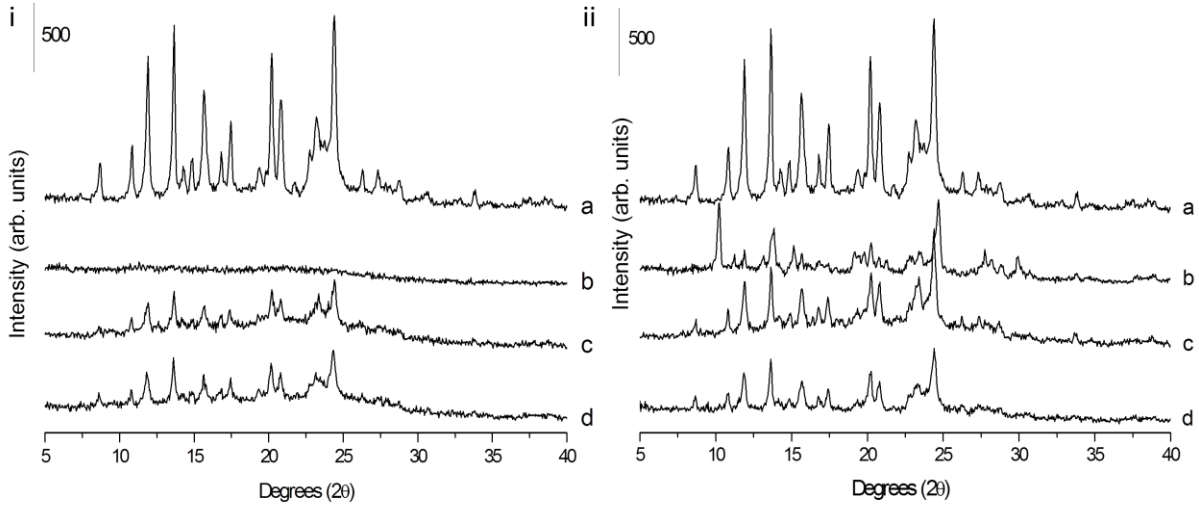

Figure 3.7. PXRD patterns of co-spray dried systems with Soluplus. i) Co-spray dried with Soluplus and ii) Co-spray dried with Soluplus after stressing at 25 ^{o}C and 60 % RH for seven days. a) Spray dried cocrystal, b) Cocrystal:Soluplus (75:25 % w/w), c) Cocrystal:Soluplus (80:20 % w/w), d) Cocrystal:Soluplus (90:10 % w/w).

Chitosan

Diffraction peaks attributable to both the cocrystal and individual components were seen when chitosan was co-spray dried with cocrystal components (50 % w/w). This ratio was altered to determine the maximum ratio at which cocrystal formation will occur without the presence of individual components. Cocrystal formation occurred when 10, 20 and 25 (% w/w) chitosan was co-spray dried with the cocrystal components. When 30 % of chitosan was used, cocrystal as well as the peaks of individual components were observed, probably due to the interaction between the chitosan and the 4ASA, as previously commented (Figure 3.8). DSC thermograms showed that the melting temperature of the co-spray dried system with chitosan varied between 164 to 167 ^{o}C (Figure 3.9) .

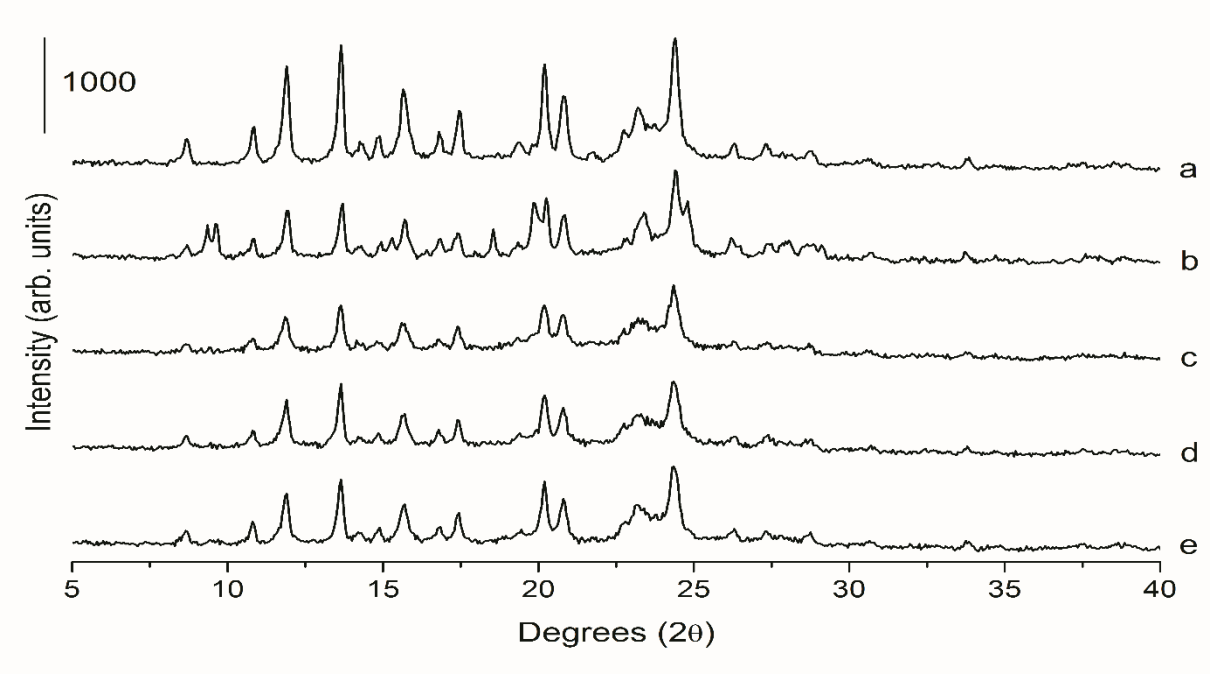

Figure 3.8. PXRD pattern of a) Spray dried cocrystal, b) Cocrystal:chitosan (70:30 % w/w), c) Cocrystal:chitosan (75:25 % w/w), d) Cocrystal:chitosan (80:20 % w/w), e) Cocrystal:chitosan (90:10 % w/w).

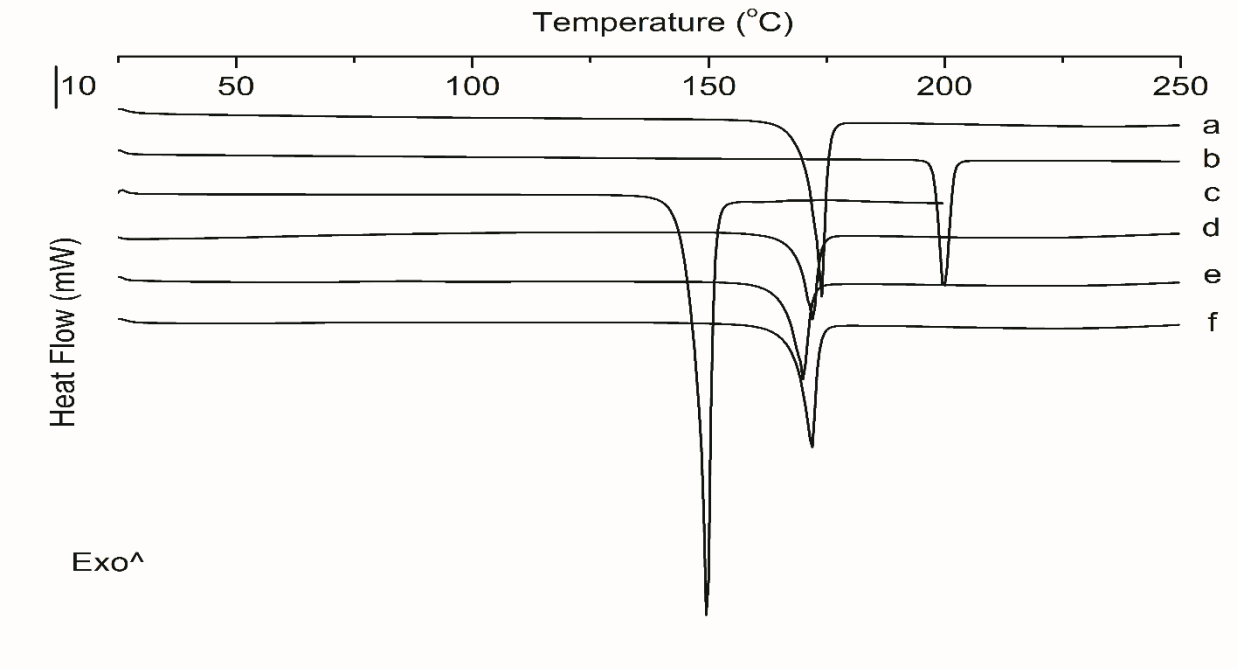

Figure 3.9. DSC thermograms of a) Spray dried cocrystal, b) Unprocessed SDM, c) Unprocessed 4ASA, d) Cocrystal:chitosan (75:25 % w/w), e) Cocrystal:chitosan (80:20 % w/w), f) Cocrystal:chitosan (90:10 % w/w).

MCC

A cocrystal was formed in the presence of MCC when the cocrystal components were co-spray dried with MCC (50 % w/w). As a cocrystal formed at this ratio, the amount of MCC relative to cocrystal components was increased to assess the maximum ratio at which cocrystal formation would occur. Cocrystal formation was observed up to a 30:70 % w/w, cocrystal:MCC weight ratio. A reduction in intensity of Bragg peaks attributable to the cocrystal was seen when the ratio of MCC to cocrystal components was increased (Figure 3.10i). The diffraction pattern was devoid of characteristic Bragg peaks of the individual cocrystal components. The melting point depression of the cocrystal with increasing MCC composition suggests the formation of a more imperfect crystalline form of the cocrystal when higher ratios of MCC are used. A broader melting peak can be attributed to imperfect crystalline form (Figure 3.11). After stressing at 25 ^{o}C and 60 % RH for seven days, characteristic Bragg peaks of the cocrystal were observed even at the lowest ratio (cocrystal: MCC, 20:80 % w/w) (Figure 10ii).

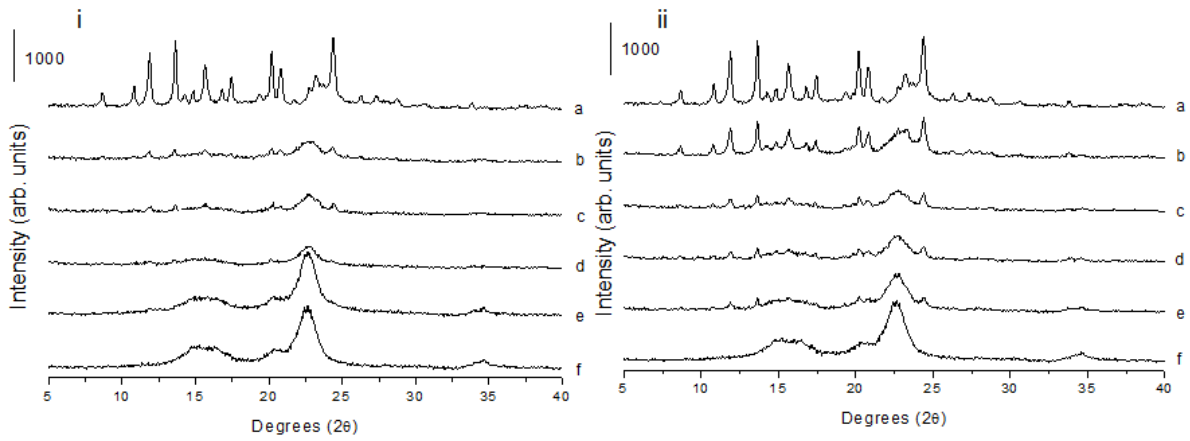

Figure 3.10. PXRD patterns of co-spray dried systems with MCC before (i) and after stressing (ii) at 25 ^{o}C and 60 % RH for seven days. Key: a) Spray dried cocrystal, b) Cocrystal:MCC (50:50 % w/w), c) Cocrystal:MCC (40:60 % w/w), d) Cocrystal:MCC (30:70 % w/w), e) Cocrystal:MCC (20:80 % w/w), f) Unprocessed MCC.

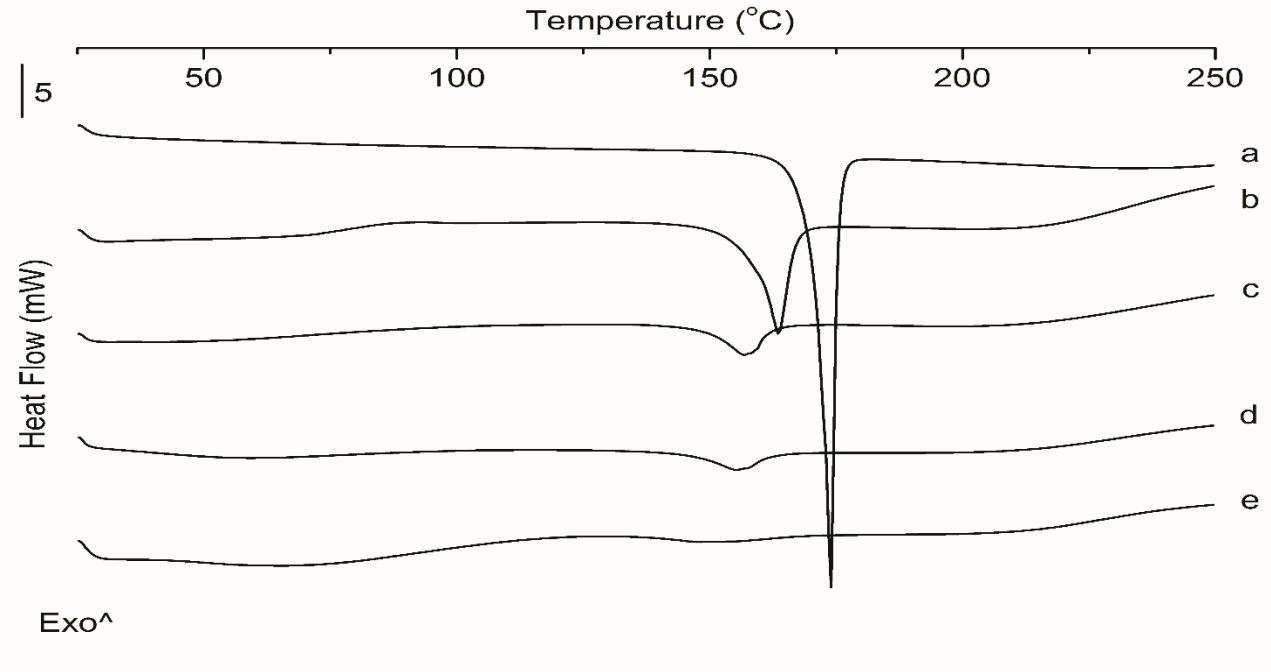

Figure 3.11. DSC thermograms of co-spray dried systems with MCC. Key: a) Spray dried cocrystal, b) Cocrystal:MCC (50:50 % w/w), c) Cocrystal:MCC (40:60 % w/w), d) Cocrystal:MCC (30:70 % w/w), e) Cocrystal:MCC (20:80 % w/w).

3.2.3 Morphology

Spray drying resulted in cocrystal microspheres between 1 and 10 µm (Figure 3.12). Microparticle surface and morphology was dependent on the excipient used, but also on the excipient-cocrystal ratio. In those systems where the cocrystal was formed, microspheres exhibited rough surfaces with embedded crystals at the surface (Figure 3.12a-d) whereas, in those systems where an amorphous solid dispersion was formed, microspheres exhibited smooth surfaces (for example with PVP K15 at 50 %). When the ratio of PVP K15 was reduced to 10 %, cocrystal formation occurred and microspheres with rough surfaces were observed (Figure 3.12f).

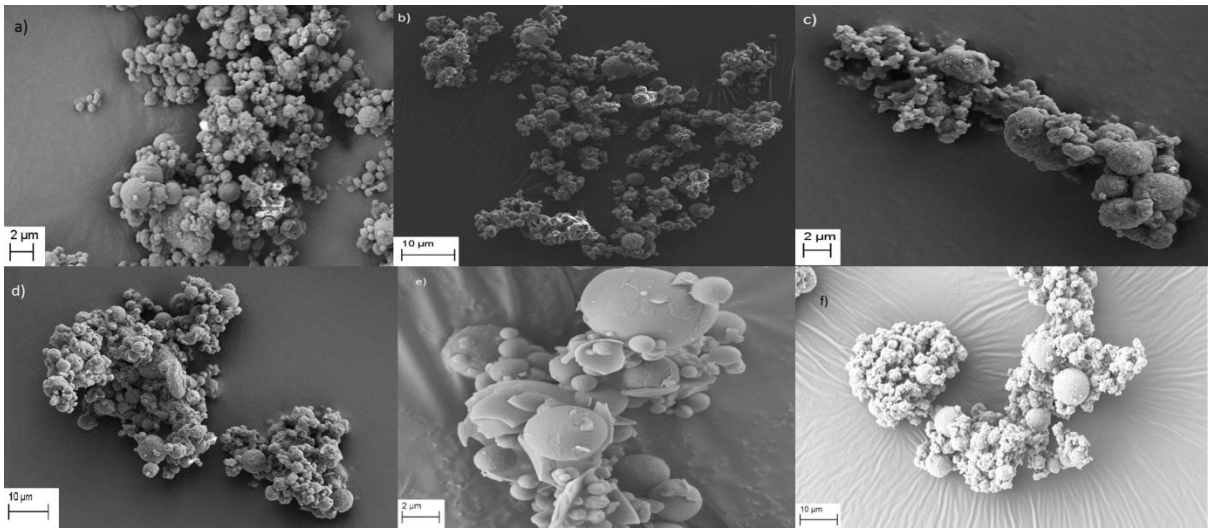

Figure 3.12. SEM micrographs. Key: a) Spray dried cocrystal, b) Co-spray dried cocrystal with inulin (50:50 % w/w), c) Co-spray dried cocrystal with mannitol (50:50 % w/w), d) Co-spray dried cocrystal with MCC (50:50 % w/w), e) Co-spray dried cocrystal with PVP K15 (50:50 % w/w), f) Co-spray dried cocrystal with PVP K15 (90:10 % w/w).

3.2.4 ATR-FTIR

The H-bonding interaction between the cocrystal in the presence of excipients was analysed by ATR-FTIR. The co-spray dried system with inulin is displayed in Figure 3.13. Distinctive bands in the higher frequency range were observed for the single components. Asymmetric and symmetric stretching bands of -NH_2 of 4ASA were observed at 3493 cm^{-1} and 3386 cm^{-1}. SDM displays asymmetric and symmetric stretching bands of the NH_2 group at 3441cm^{-1} and 3339 cm^{-1} respectively. The

sulphonamide NH group shows a stretching band at 3235 cm^{-1}. The molecular interaction through hydrogen bond formation between SDM and 4ASA spray dried cocrystal was characterised by: i) two broad bands, one at 3482 cm^{-1} and one at 3372 cm^{-1} with a shoulder attributable to the N-H stretching of the NH_2 amine group of 4ASA which were shifted towards lower wavenumbers from 3493 cm^{-1} and 3386 cm^{-1} and ii) sulfone ($-SO_2$) stretching in SDM and -OH deformation in 4ASA at 1315 cm^{-1} and 1275 cm^{-1}, respectively (Grossjohann et al., 2015). The same bands were seen for both the spray dried cocrystal alone and the co-spray dried systems (containing inulin, mannitol, MCC and dextran), indicating no interaction between the cocrystal and the excipient on spray drying. Hydrogen bonding attributable to cocrystal formation is not seen when PVP and Soluplus were co-spray dried with the cocrystal components at the 50:50 % w/w ratio. In Figure 3.13, the co-spray dried system with inulin is illustrated. Co-spray dried systems with dextran, MCC, mannitol, PVP K15 and Soluplus at the 50 (% w/w) ratio are presented in Figures A.1.4-A.1.8, Appendix 1).

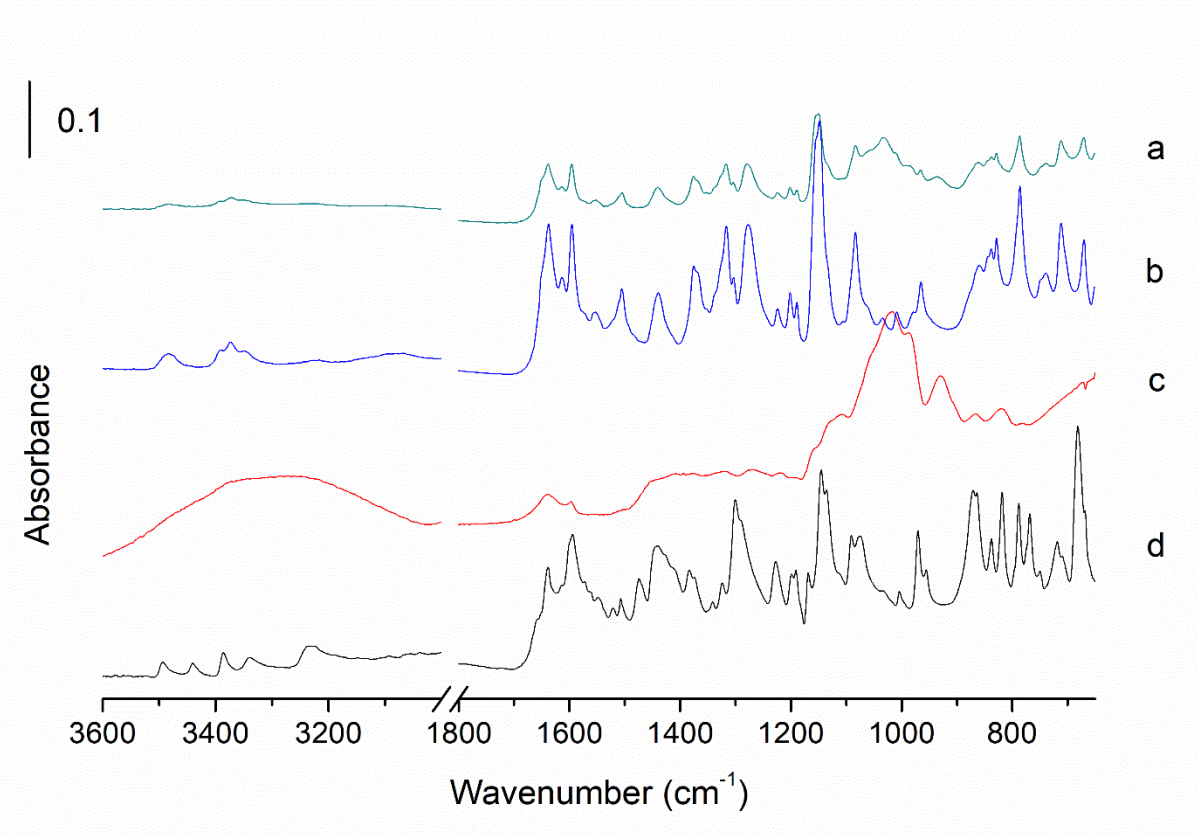

Figure 3.13. FTIR analyses of a) Co-spray dried cocrystal in inulin (50:50 % w/w), b) Spray dried cocrystal, c) inulin, d) a physical mixture of SDM and 4ASA (1:1 molar ratio).

3.2.5 Solubility of cocrystal in excipient

It was hypothesised that cocrystal formation occurs in the presence of an excipient when the single components are not miscible with the excipient, as determined by the difference in HSP between the components and excipient. In order to correlate the difference in HSP with the miscibility of the cocrystal with the excipient matrix, the solubility of the spray dried cocrystal and the individual cocrystal components in the amorphous excipients (inulin, MCC, dextran, chitosan, PVA, PVP K15, Soluplus and HPMC) was determined by the zero enthalpy extrapolation method (Amharar et al., 2014). The solubility of the cocrystal in inulin, MCC and dextran was 3.69 % w/w, 3.85 % w/w and 3.83 % w/w, respectively, which was relatively low (Figure 3.14). Based on these low solubilities, it is not surprising to see that the cocrystal is immiscible with these excipients based on

HSP differences, with values of 18.6 $MPa^{0.5}$, 12.5 $MPa^{0.5}$ and 9.6 $MPa^{0.5}$ respectively, indicating that the formation of the cocrystal at higher excipient ratios is likely to happen. The solubility of cocrystal in chitosan was determined to be 3.23 %. This value is in agreement with the calculated HSP difference of 11.2 $MPa^{0.5}$ between the cocrystal and chitosan. However, a cocrystal only formed at low ratios of chitosan, possibly due to the interaction between basic chitosan and acidic 4ASA.

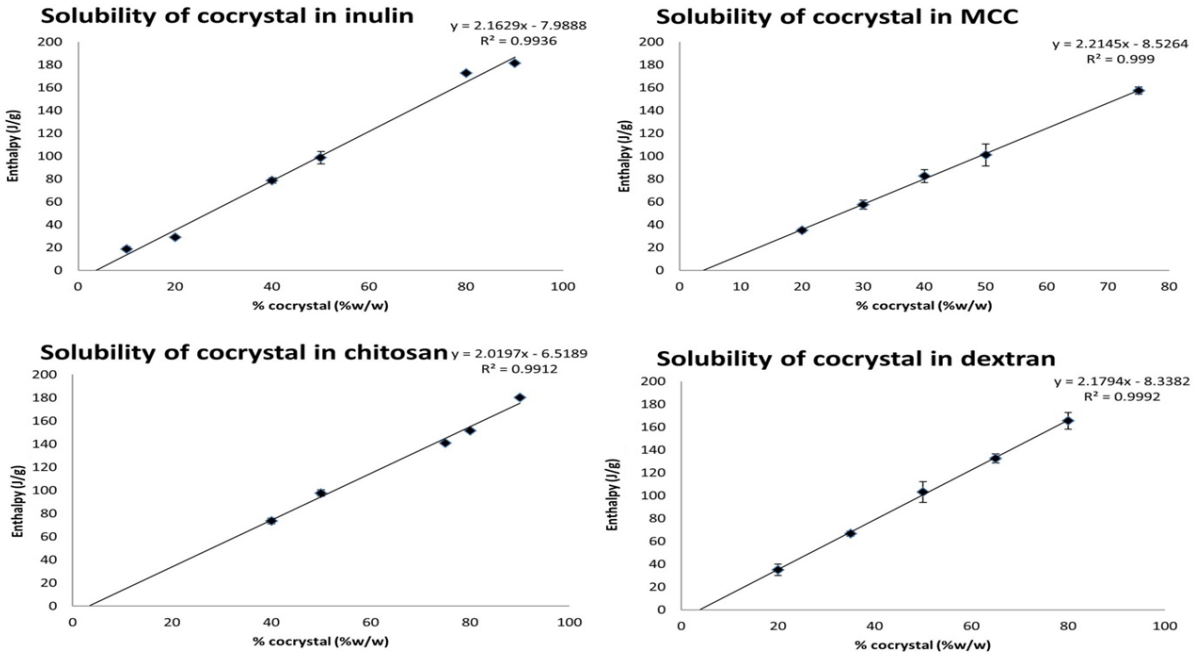

Figure 3.14. The solubility of the cocrystal in inulin (i), MCC (ii), chitosan (iii) and dextran (iv).

The solubility of the cocrystal in PVA was 13.74 % w/w and the difference in HSP between the cocrystal and PVA was 4.9 $MPa^{0.5}$. Cocrystal solubility in PVP K15, Soluplus and HPMC was much higher, 24.43 % w/w, 25.21 % w/w and 18.77 % w/w respectively (Figure 3.15). These solubility values are higher than for the immiscible excipients. Also, the difference in HSP between these excipients and the cocrystal indicate miscibility, as $\Delta HSP < 7$ $MPa^{0.5}$ in all cases, justifying why cocrystal formation only occurred when a low ratio of excipient was used. Similar solubility values between the single components and the excipients were observed as the solubility values between the cocrystal and respective excipients (values in Table 3.2) (Figure A.1.9 – A.1.11, Appendix 1).

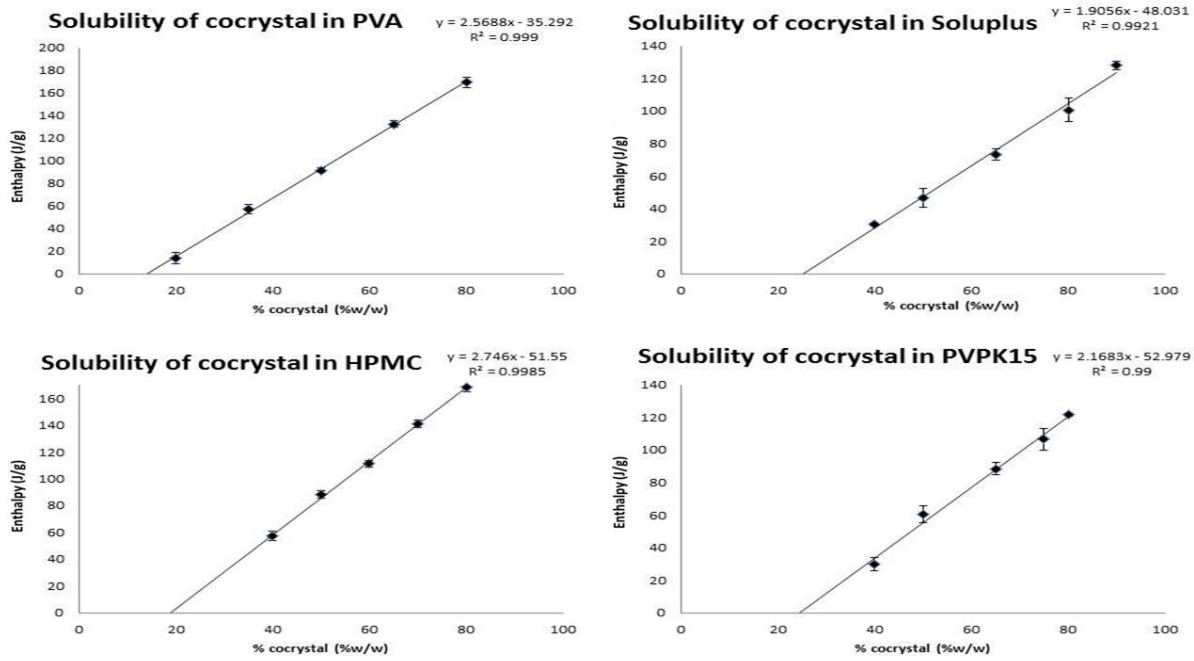

Figure 3.15. The solubility of the cocrystal in PVA (i), Soluplus (ii), HPMC (iii) and PVP K15 (iv).

Table 3.2. Solubility values of cocrystal and individual components in excipients and the associated difference in HSP.

System	**Solubility (% w/w)**	**Difference in HSP ($MPa^{0.5}$)**
Cocrystal in Inulin	3.69	18.6
Cocrystal in MCC	3.85	12.5
Cocrystal in Chitosan	3.23	11.2
Cocrystal in Dextran	3.83	9.6
Cocrystal in PVA	13.74	4.9
Cocrystal in PVP K15	24.43	4.4
Cocrystal in Soluplus	25.21	3.9
Cocrystal in HPMC	18.77	1.9
SDM in Inulin	2.85	19.2
4ASA in Inulin	4.14	16.8
SDM in MCC	1.76	13.1
4ASA in MCC	1.77	10.7
SDM in Chitosan	2.50	11.8
4ASA in Chitosan	9.41	9.4
SDM in Dextran	5.68	10.2
4ASA in Dextran	5.10	7.8
SDM in PVA	13.88	5.5
4ASA in PVA	11.77	3.1
SDM in Soluplus	15.93	3.3
4ASA in PVP K15	27.52	6.2

3.2.6 Dissolution studies

Dissolution of SDM and 4-ASA from the cocrystal started incongruently over the first 10 min and became congruent subsequently (Figure 3.16). During spray drying, 4ASA can partially sublime, resulting in a mass loss of 4ASA, as previously reported (Grossjohann et al., 2015). HPLC analysis of the spray dried cocrystal showed 3.5 % less molar amount of 4ASA relative to SDM. It is surmised that this resulted in an excess of SDM in the spray dried product which can transform to the amorphous state upon spray drying (Caron

et al., 2011). Once the excess amorphous SDM crystallised, dissolution became congruent.

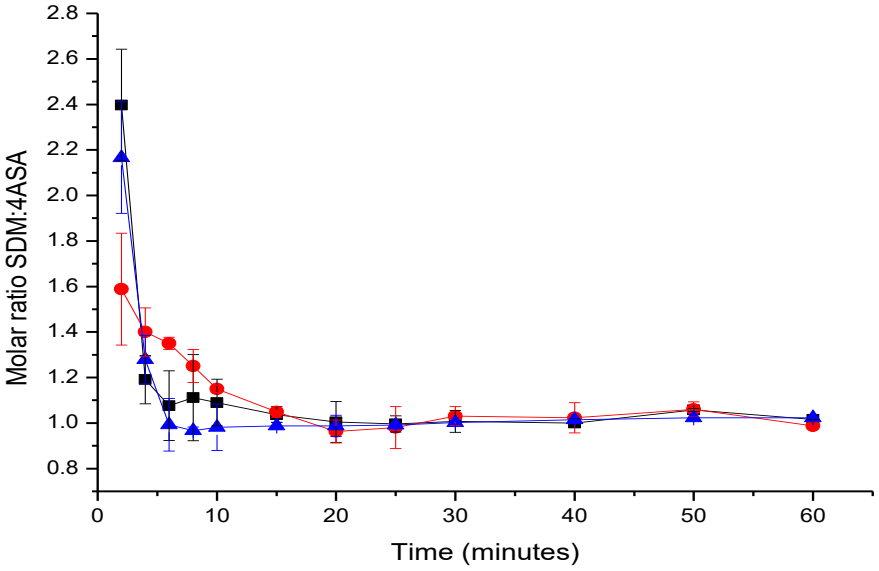

Figure 3.16. Stoichiometry (SDM:4ASA) of the systems co-spray dried with inulin (black ■), mannitol (red ●) and dextran (blue ▲) during dissolution, as measured by HPLC.

No statistically significant differences in the f_2 value were found among the dissolution profiles of the co-spray dried systems (50:50 % w/w ratio) with inulin, mannitol or dextran (Figure 3.17). Dissolution from a constant surface area could not be tested when MCC was used as an excipient since, due to the disintegrant properties of MCC, the disk quickly disintegrated. No differences were found between the constant surface area dissolution rates of the three co-spray dried systems (Table 3.3). Therefore, it was concluded that the excipient used had no impact on the dissolution of the cocrystal from the co-spray dried system.

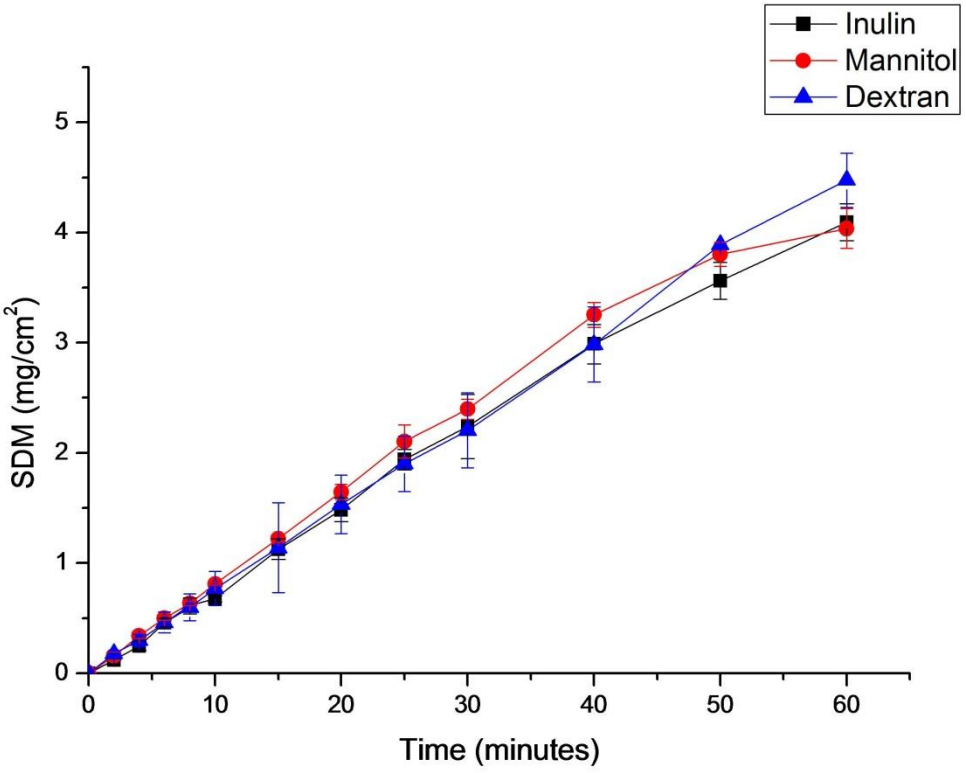

Figure 3.17. The release of SDM for the systems co-spray dried with inulin (black ■), mannitol (red ●) and dextran (blue ▲) with a 50:50% w/w ratio of excipient and cocrystal.

Table 3.3. Constant surface area dissolution rates of SDM calculated over the first 10 min.

System, 50:50 % w/w ratio	**Initial Dissolution Rate (mg/cm^2/min)**
Cocrystal in inulin system	0.0712 ± 0.0027
Cocrystal in mannitol system	0.0812 ± 0.0013
Cocrystal in dextran system	0.0764 ± 0.0150

After dissolution, the compacts were dried and analysed by PXRD for surface changes. A polymorphic transformation from the form II to form I was observed for the co-spray dried system with mannitol. In contrast, no polymorphic transformation was seen when dissolution studies were performed with inulin and dextran (Figures A.1.12 – A.1.14, Appendix 1). The compacts were smooth and homogenous in texture before dissolution.

After dissolution, the surface was observed to be pitted due to the different dissolution rates of the excipient and cocrystal.

3.2.7 Compactability of spray dried cocrystal:excipient systems

As a proof of concept, the feasibility of co-spray dried systems to reduce the number of unit processes to produce a final pharmaceutical product was investigated by means of compaction studies. As MCC is commonly used as a tablet filler due to its excellent compression properties (David and Augsburger, 1977), the compactability of the co-spray dried system with MCC (50 % w/w) and its corresponding physical mixture were assessed. Including more than one excipient in the feed solution/suspension may allow for a blending step to be omitted, going directly from a spray drying process to a direct compression. For this reason, the compaction properties of a co-spray dried system containing 60 % w/w cocrystal, 20 % w/w inulin and 20 % w/w MCC was also assessed, along with a physical mixture with identical composition. It has previously been reported that the SDM:4ASA cocrystal produced by spray drying is less prone to capping than the cocrystal produced by solvent evaporation (Serrano et al., 2015). For the MCC systems, both the co-spray dried system and physical mixture produced tablets with similar tensile strengths. A significant difference in ejection force was observed however, with the co-spray dried system requiring a 5-fold lower force to eject the tablets (Figure 3.18). No capped tablets were observed for both the co-spray dried system and the physical mixture. PXRD analyses were performed to assess possible alteration of the crystal structure during the tabletting process. While an increase in Bragg peak intensity was observed for the co-spray dried system after compaction, no deformation induced phase transformation changes were observed (Figure A.1.15, Appendix 1). For the system containing both MCC and inulin, the co-spray dried system showed no tendency to capping during compaction. Two capped tablets were observed for the physical mixture. These two tablets were not tested further. Two extra tablets were made and tested. No differences were observed in tensile strength between the co-spray dried system and the physical mixtures. However, a significantly lower ejection force (19-fold) was observed for the co-spray dried system (Figure 3.18), suggesting that the compaction properties of the co-spray dried system were notably improved, due to less sticking characteristics. Possible alteration of the cocrystal structure was evaluated by PXRD analysis before and after the compaction. No deformation induced phase transformation changes were observed (Figure A.1.16, Appendix 1).

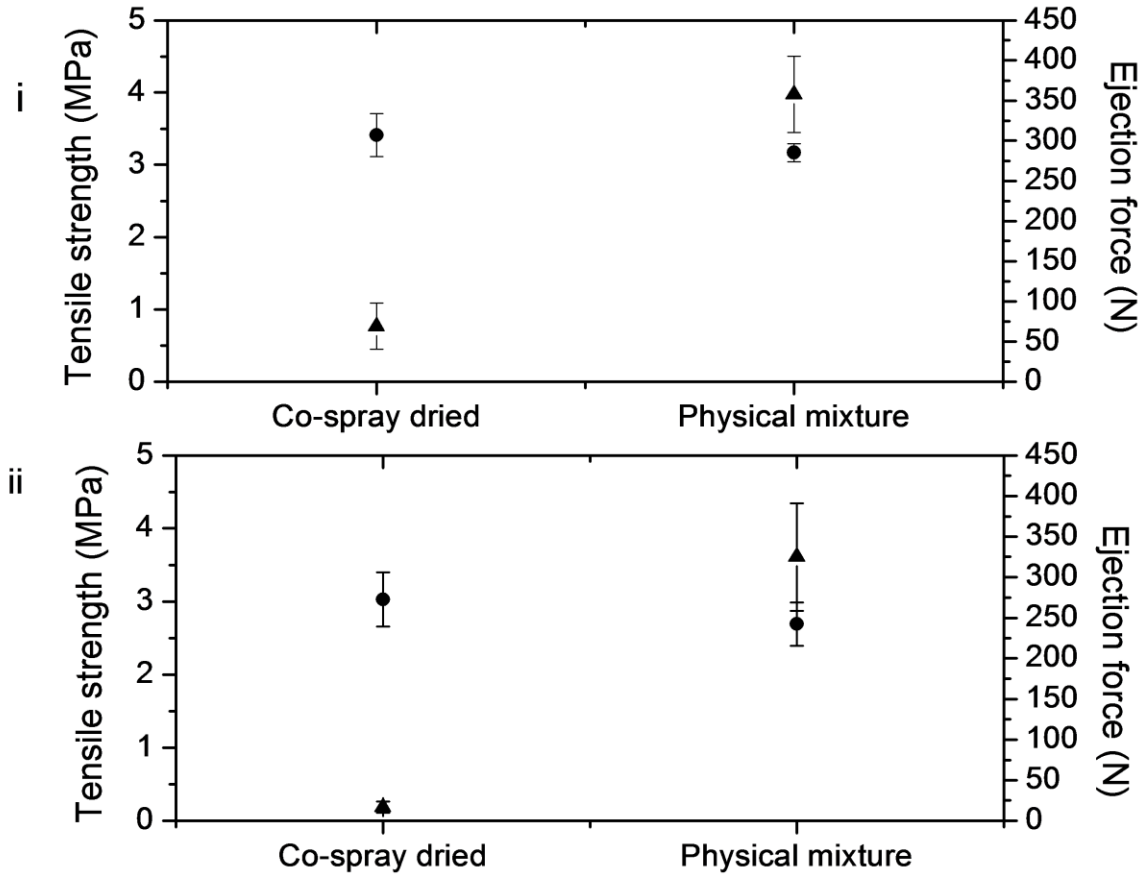

Figure 3.18. Tensile strength (circles) and ejection force (triangles) of i) co-spray dried system and physical mixtures of cocrystal 50 %, MCC 50 %, and ii) co-spray dried system and physical mixtures of cocrystal 60 %, inulin 20 % and MCC 20 %, compacted at 6 kN.

3.3 Conclusions

This work demonstrates that the introduction of a third component into the feed solution/suspension prior to spray drying can result in a cocrystal embedded in excipient matrix. Cocrystal formation can also occur when more than one excipient is added to the spray drying feed solution/suspension. The difference in HSP between the cocrystal components and the excipient can be used as a general parameter to predict if cocrystal formation will occur. However, as was seen when the cocrystal components were co-spray dried with chitosan, other factors such as the acidic/basic nature of the excipient can influence whether cocrystal formation can occur. The difference in HSP can also be used to predict the ratio at which a cocrystal can form when co-spray dried with an

excipient. Co-spray drying an excipient with the cocrystal components can result in cocrystal formation, regardless of the crystalline or amorphous nature of the excipient. As spray drying is a scalable unit operation used in the pharmaceutical industry, co-spray drying with an excipient can reduce the number of unit operations required to produce a final pharmaceutical product, as a separate blending step of the cocrystal and excipient could be avoided.

CHAPTER 4

Using a design of experiment approach to optimise the incorporation of cocrystals into an excipient matrix by spray drying

4.1 Introduction

Tablets are the preferred drug delivery system, due to ease of patient administration and the relative ease of manufacturing large amounts of tablets (Sinka et al., 2009). Cocrystallisation of an API has previously been performed to enhance its tabletability. Cocrystals of caffeine and methyl gallate exhibited an improved compaction behaviour compared to that of the API alone, by the formation of flat slip planes in the cocrystal structure (Chattoraj et al., 2010). Cocrystallisation of SDM with 4ASA can result in a solid which is less prone to capping, when compared to a physical mixture of the two components (Serrano et al., 2015). In chapter 3, it was shown that cocrystals of SDM and 4ASA can form in the presence of an excipient by a one-step spray drying process. Research in chapter 3 also demonstrated that cocrystal formation can occur in the presence of two immiscible excipients, as defined by differences in HSP. The aim of this work is to form tablets from a cocrystal containing powder produced from a one-step spray drying process. The concept of reducing the number of steps required to make a final product can result in more efficient technologies (Buchholz, 2010).

Statistical design of experiment (DoE) is a powerful approach used to optimize pharmaceutical and other processes. DoE has become increasingly prevalent in formulation design, as it allows the identification of critical formulation and process parameters (Wang et al., 2018). In order to carry out a DoE, a problem is defined and the variables are chosen. A design space, or region of interest, is also identified. This involves setting a range of variability for each variable (Cavazzuti, 2013).

The DoE chosen in this case was the Box-Behnken design. This is an incomplete three level factorial design. This design was introduced to limit the sample size as the numbers of parameters grow. The sample size is kept to a value that is sufficient for the estimation of the coefficients in a second degree least squares approximating polynomial. In a Box-Behnken design, the block of samples corresponding to a three-level factorial design is repeated over a number of different sets of parameters. The parameters that are not included in the factorial design remain at their mean level throughout the block. The type (full or fractional), the size of the factorial, and the number of blocks which are evaluated, depend on the number of parameters and it is chosen so that the design meets, either exactly or approximately, the criterion of rotatability. A design is rotatable if the variance of the predicted response at any point depends only on the distance of the design point

from the centre point. Rotatability in statistical design of experiments is a desirable property. This design requires fewer design points than a full factorial design, and avoids extreme conditions. Extreme conditions are represented by the corners of the cube in the graphical example of the Box-Behnken design in Figure 4.1, which are avoided in this type of DoE approach. In this project, a Box-Behnken design with three factors, three levels and five centre points was used. Graphically, the samples are at the midpoints of the edges of the design space. The Box-Behnken design used in this project has three input factors: excipient percentage, excipient ratio (i.e ratio of inulin:MCC), and spray dryer airflow, and three responses: % crystallinity, Carr's index and tensile strength.

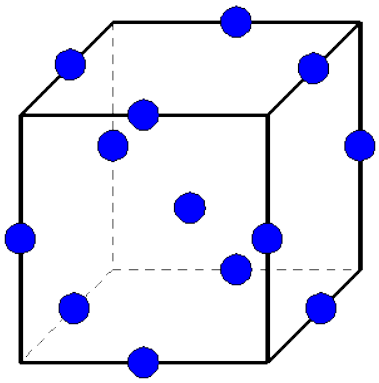

Figure 4.1. Graphic example of Box-Behnken design.

Excipient percentage and excipient ratio were chosen as input factors as it was previously observed in chapter 3 that different excipients can have an impact on the crystallinity of the cocrystal. High excipient loadings of MCC were observed to negatively impact the crystallinity of the cocrystal, while high excipient loadings of inulin had less of an impact on cocrystal crystallinity, as was seen in chapter 3. It was also hypothesised that a faster drying of the atomised feed may result in a greater number of crystal imperfections, which could be reflected in the thermal properties of the spray dried product (Corrigan, 1995), and could have further processing implications. Carr's index is a straight forward, commonly used method to measure the flowability of a powder. Carr's index is a useful quantitative parameter for indicating the cohesiveness of a powder. Carr's index considers bulk density which is the mass of powder that can be packed into a specific volume and tapped bulk density which is obtained by tapping the syringe holding the aerated sample (Abdullah and Geldart, 1999). In general, the structure of a cohesive powder will collapse significantly on tapping while a free-flowing material has low tendency for further consolidation. A low Carr's index therefore indicates that the powder

is not cohesive (Leturia et al., 2014). Carr's index can be calculated from the following equation (Eq. 2.2):

$$Carr's\ Index = \frac{bulk\ volume - tapped\ volume}{bulk\ volume} * 100 \qquad \text{(Eq. 2.2)}$$

The third response assessed was the tensile strength of the tablets prepared. Tabletability is defined as the ability of a powdered material to be transformed into a tablet of specified strength under the effect of compaction pressure (Thoorens et al., 2015). An ideal target for a cocrystal is one that is suitable for direct compression with only a low amount of excipient, has good flowability and can form a stable compact at low punch forces (Serrano et al., 2015). Changing the crystal structure by means of cocrystallisation of an API can affect the compression and tableting behaviour. Regarding tableting behaviour, a free-flowing powder can be filled homogenously into the die. The contact area between the particles can vary depending on the alignment of the crystals in the die. Therefore, an exclusive variation only of the external crystal structure, as can be seen when an API is cocrystallised, can optimize substance properties (Rasenack and Müller, 2002). The addition of different excipients and excipient ratios may also impact on the ability of the powder to form a tablet, especially if the cocrystal itself has poor compression properties.

One of the aims of this chapter was to investigate the processability of the 1:1 SDM:4ASA cocrystal in an excipient matrix when three inputs (excipient percentage, excipient ratio and airflow) were varied. Serrano et. al. have demonstrated that when the cocrystal alone was prepared in numerous ways (liquid assisted milling, solvent evaporation, spray drying), the flowability of the powder was poor in all cases, with Carr's index values above 25 (Serrano et al., 2015). It has also been reported that when the SDM:4ASA cocrystal is produced by spray drying it is less prone to capping in comparison to the cocrystal produced by solvent evaporation (Serrano et al., 2015). The effect of adding inulin and MCC as excipients at different ratios and varying the airflow during the spray drying process has on compactibility and flowability is unknown, and was investigated in this study.

4.2 Results

The three factors and three responses assessed in the Box-Behnken DoE are presented in Table 4.1. The airflow values expressed throughout this chapter refer to the rotameter setting on the spray dryer, in which 40, 50 and 60 mm are equivalent to 667, 1052 and 1744 Normlitres/hour respectively.

Run	**Factor 1**	**Factor 2**	**Factor 3**	**Response 1**	**Response 2**	**Response 3**
	A: Excipient %	B: Excipient ratio (inulin: MCC)	C: Airflow	Crystallinity	Tensile Strength	Carr's Index
			mm	%	MPa	%
1	35	50:50	50	94.19	2.37	47.5
2	35	75:25	40	94.25	2.50	45
3	35	25:75	60	94.63	2.63	50
4	20	50:50	60	97.01	2.24	42.5
5	50	50:50	60	95.77	2.51	47.5
6	35	75:25	60	95.78	2.55	35
7	35	50:50	50	92.33	2.44	37.5
8	50	25:75	50	97.95	2.68	42.5
9	20	50:50	40	96.98	2.42	47.5
10	50	75:25	50	94.73	2.44	32.5
11	35	50:50	50	93.69	2.31	40
12	35	50:50	50	93.98	2.43	35
13	20	25:75	50	99.69	2.30	42.5
14	35	25:75	40	97.32	2.40	40
15	20	75:25	50	103.64	2.24	42.5
16	35	50:50	50	97.73	2.49	37.5
17	50	50:50	40	99.61	2.71	40

Table 4.1. Box-Behnken design used in this study. The airflow values refer to the rotameter setting on the spray dryer. 40, 50 and 60 mm are equivalent to 667, 1052 and 1744 Normlitres/hour.

The PXRD and DSC patterns of the starting materials are presented in Figures 4.2 and 4.3. Both 4ASA and SDM are crystalline, with 4ASA displaying a melting endotherm at 145.76 ± 0.64 ºC (348.29 ± 2.71 J/g), while SDM displays a melt endotherm at 197.25 ± 0.12 ºC (127.40 ± 0.70 J/g). Inulin is an amorphous material, while MCC is semi-crystalline. Characterisation of the cocrystal produced by spray drying and solvent evaporation has previously been discussed in chapter 3.

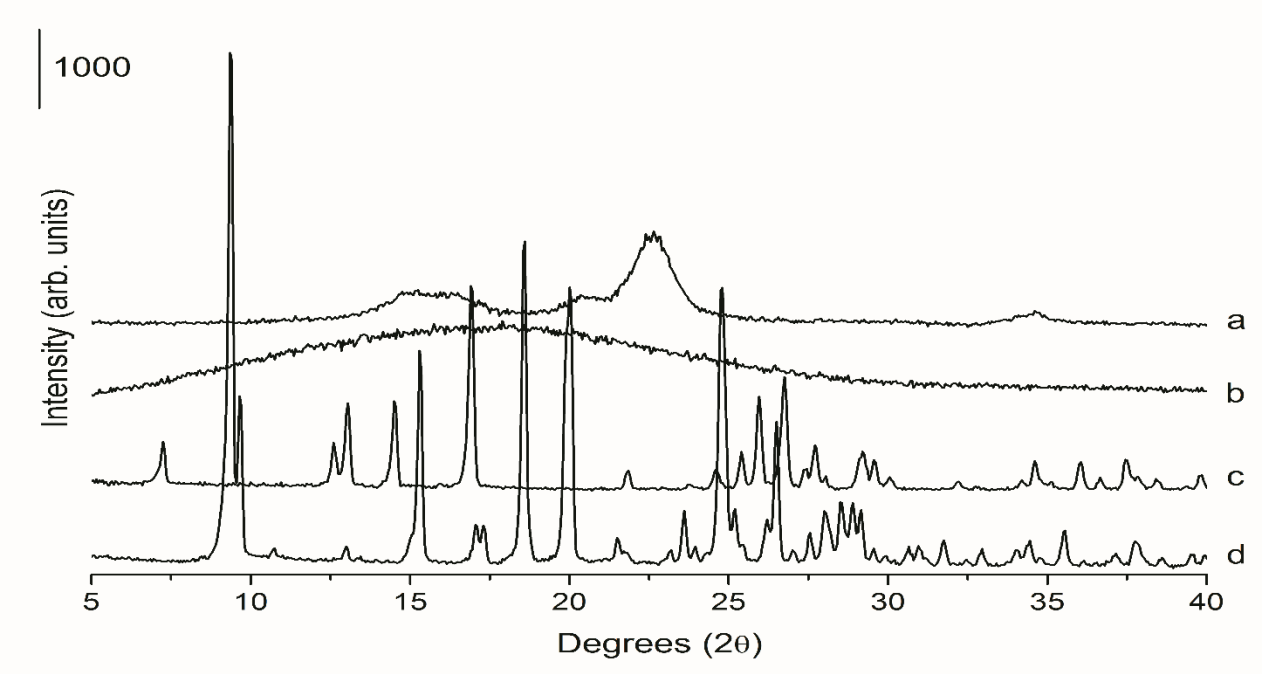

Figure 4.2. PXRD patterns of raw materials. a) MCC, b) inulin, c) 4ASA, d) SDM.

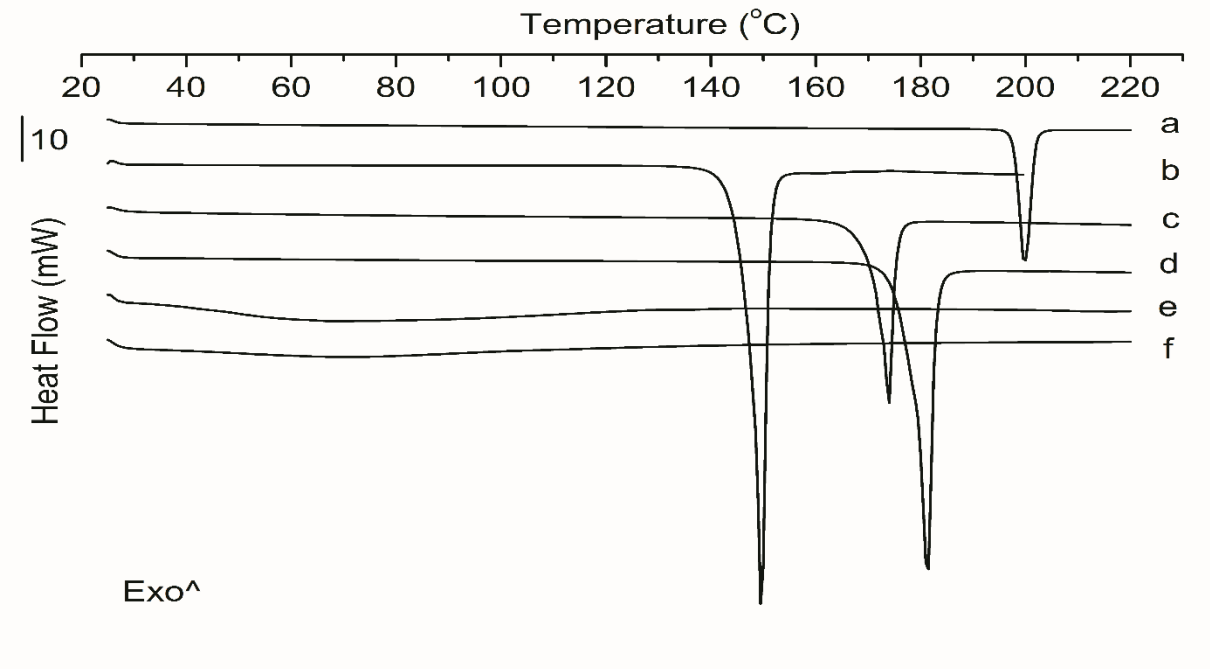

Figure 4.3. DSC curves of a) SDM, b) 4ASA, c) Cocrystal produced by spray drying, d) Cocrystal produced by solvent evaporation from acetone, e) Inulin and f) MCC.

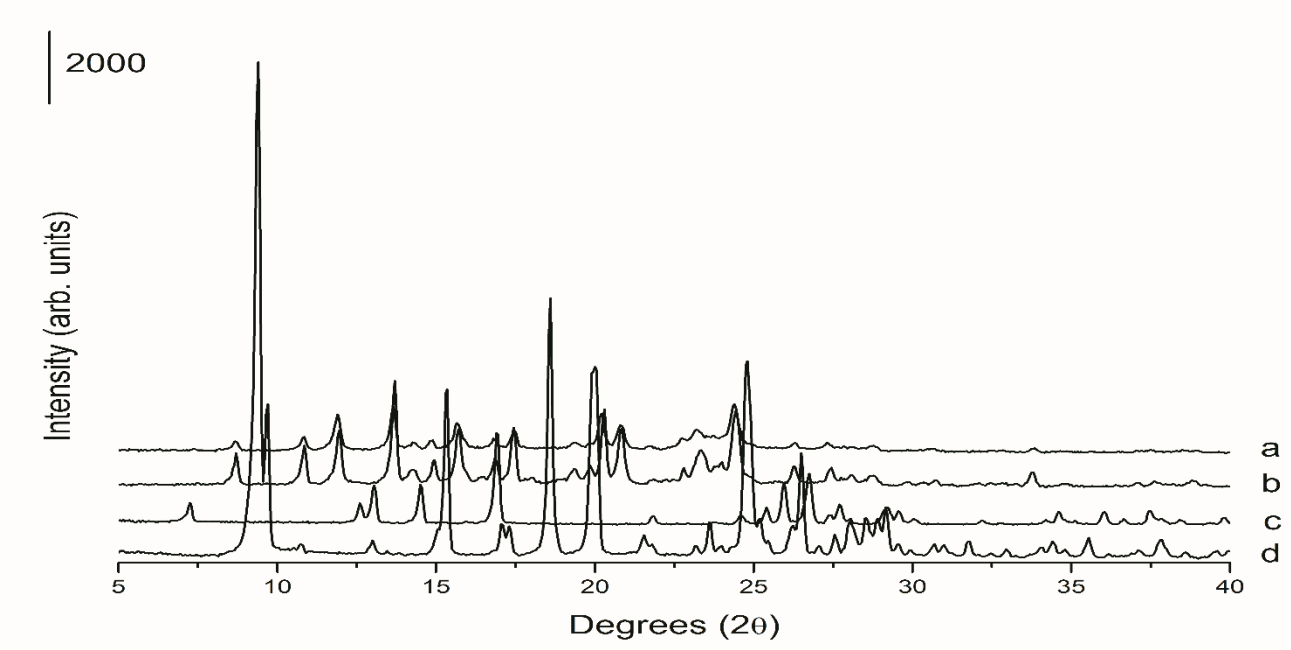

Figure 4.4. PXRD patterns of a) Cocrystal produced by spray drying, b) Cocrystal produced by solvent evaporation from acetone, c) 4ASA, d) SDM.

4.2.1 PXRD analysis

The PXRD analyses in Figures 4.5 – 4.7 show that all the diffraction peaks of the samples with varying excipient: cocrystal ratios and excipient percentages can be superimposed

with the diffraction peaks of the cocrystal itself and that the peaks are in the same position regardless of the ratio used. Therefore, cocrystal formation is retained for all cocrystal:excipient ratios and for all ratios of inulin:MCC. PXRD and DSC analysis showed no evidence of the presence of single components.

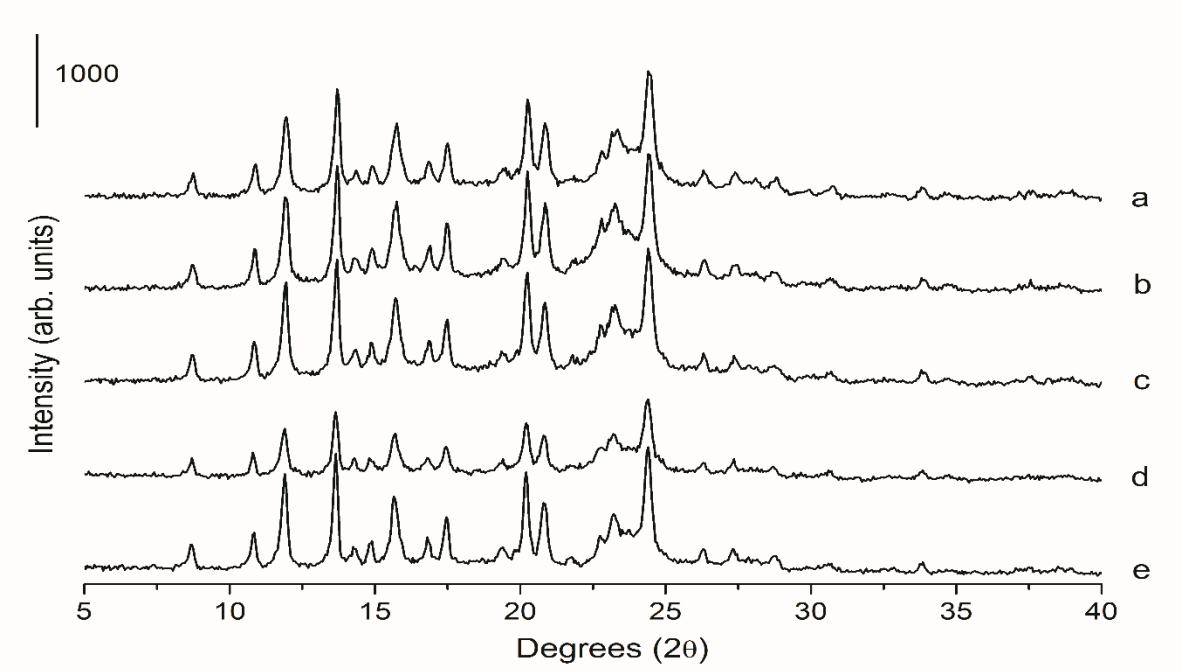

Figure 4.5. DoE runs containing 20 % total excipient fraction. a) Run 15, b) Run 13, c) Run 9, d) Run 4, e) Cocrystal produced by spray drying.

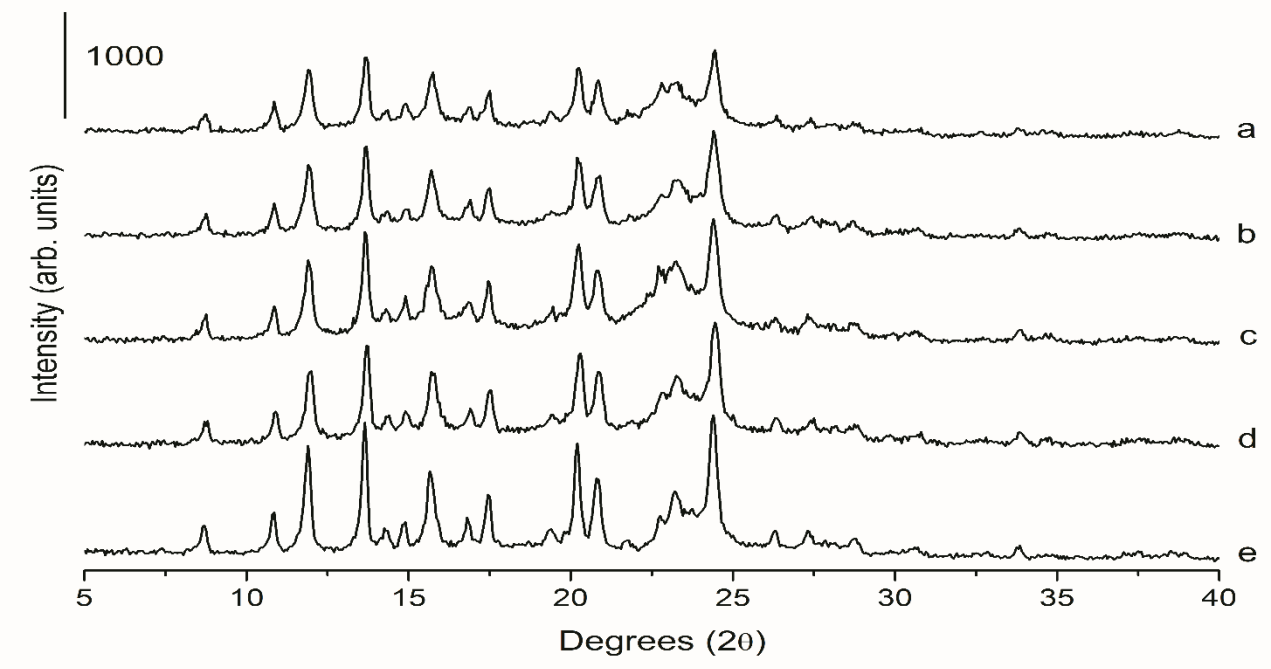

Figure 4.6. DoE runs containing 35 % total excipient fraction. a) Run 14, b) Run 6, c) Run 3, d) Run 2, e) Cocrystal produced by spray drying.

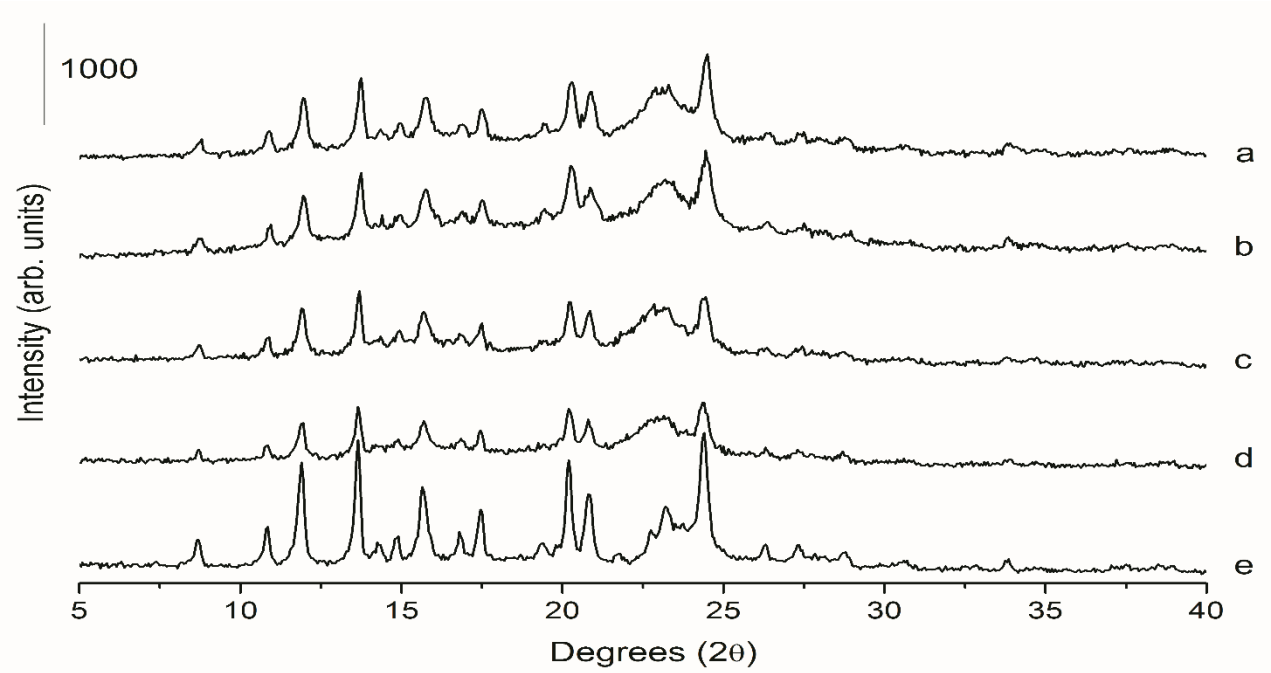

Figure 4.7. PXRD patterns of DoE runs containing 50 % total excipient fraction. a) Run 17, b) Run 10, c) Run 8, d) Run 5, e) Cocrystal produced by spray drying.

4.2.2 DSC analysis

The relative crystallinity of the co-spray dried systems was calculated by comparing each formulation to an equivalent physical mixture of cocrystal (produced by spray drying), inulin and MCC. The physical mixtures of cocrystal and excipients generally have higher enthalpies than the co-spray dried systems, possibly due to partial amorphisation of the cocrystal components and due to more imperfect cocrystals being formed due to the presence of the excipients in the spray drying process. DSC curves of all co-spray dried formulations are presented in Figures 4.8 – 4.10.

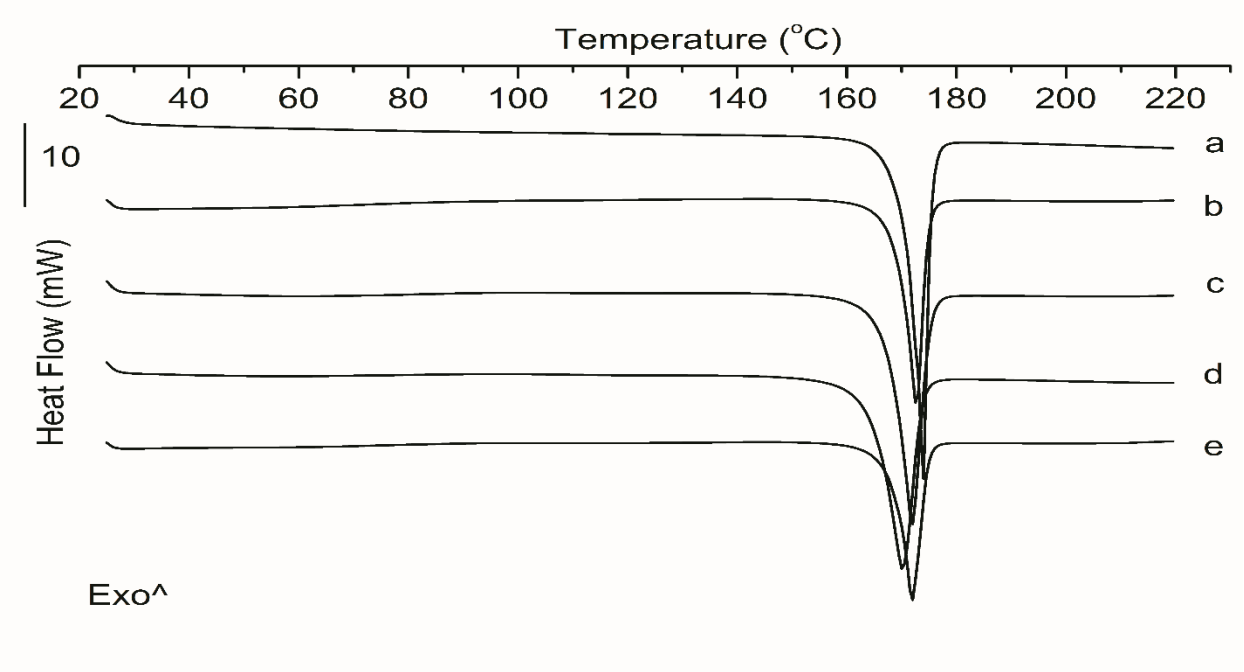

Figure 4.8. DSC curves of DoE runs containing 20% total excipient fraction. a) Cocrystal produced by spray drying, b) Run 4, c) Run 9, d) Run 13, Run 15.

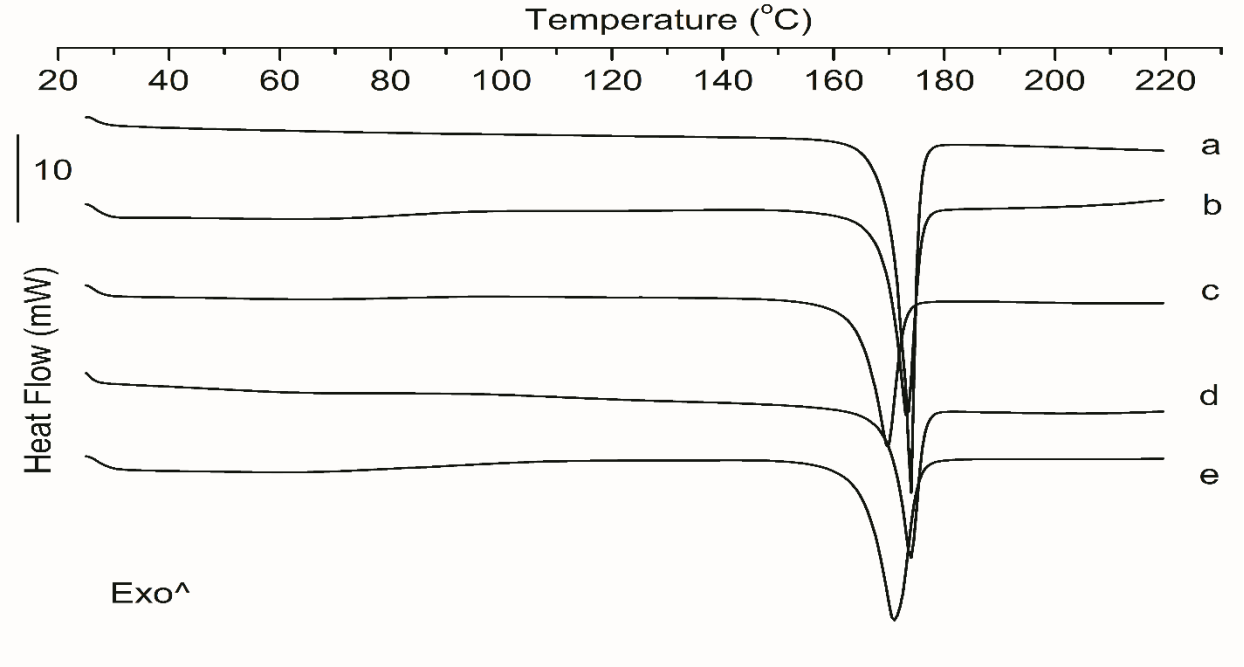

Figure 4.9. DSC curves of DoE runs containing 35% total excipient fraction. a) Cocrystal produced by spray drying, b) Run 2, c) Run 3, d) Run 6, Run 14.

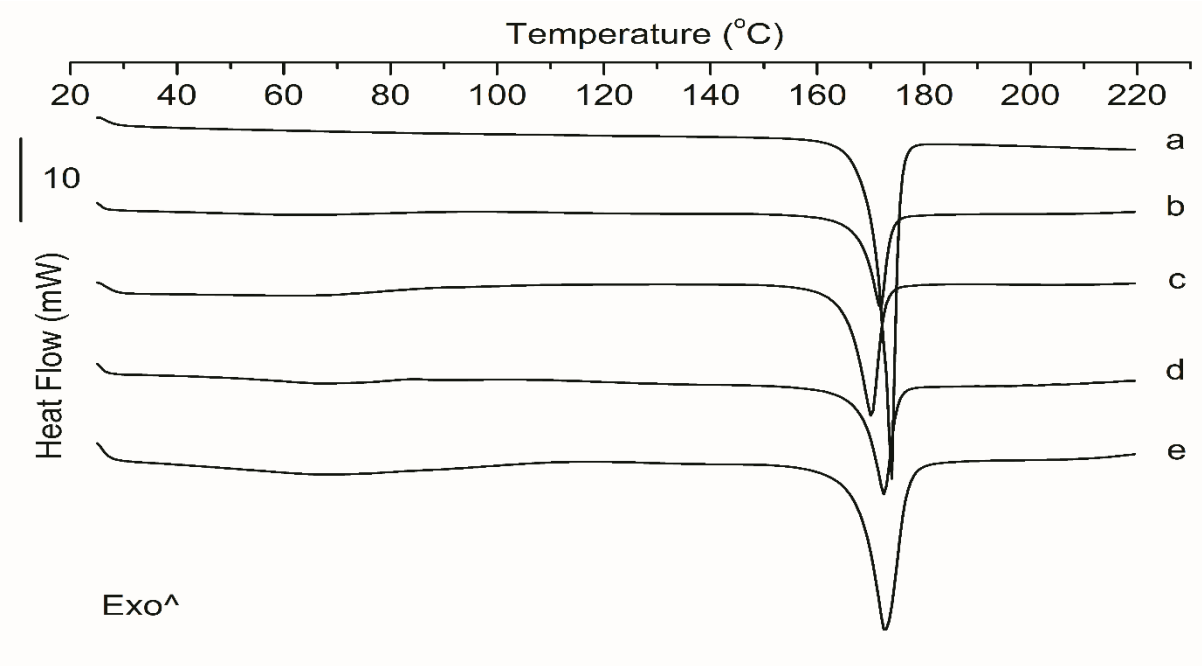

Figure 4.10. DSC curves of DoE runs containing 50% total excipient fraction. a) Cocrystal produced by spray drying, b) Run 5, c) Run 8, d) Run 10, Run 147.

4.2.3 Statistical analysis

Multilinear regression analysis was performed based on the results of the experiments. Linear models were found to be the best fit for the assessed parameters for all responses. For all three models generated, there were no statistically significant interactions between the factors, and so these interactions were excluded from the final models. The coefficients of the model generated for the tensile strength showed that the model was significant with a p-value of < 0.05. In all cases, the lack of fit was not significant. This is desirable, as a significant lack of fit can indicate that the model does not adequately describe the functional relationship between the experimental factors and response variables. The models generated for crystallinity and Carr's index were not statistically significant ($p > 0.05$).

The 2D contour plot and 3D surface plot depicted in Figures 4.11 and 4.12 revealed that the crystallinity was negatively influenced by all three input factors. However, none of these factors had a statistically significant impact on the relative crystallinity of the cocrystal. Also, the overall model was not statistically significant, with a p-value > 0.05.

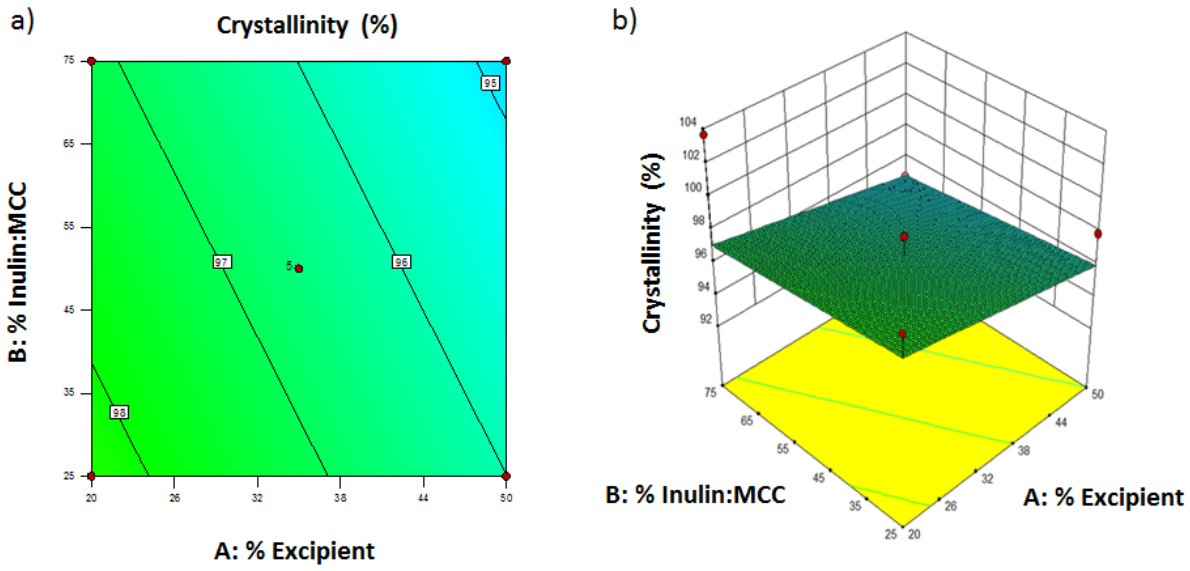

Figure 4.11. 2D contour plot (a) and 3D surface response (b) showing the influence of the total excipient percentage and the excipient ratio on the cocrystal crystallinity.

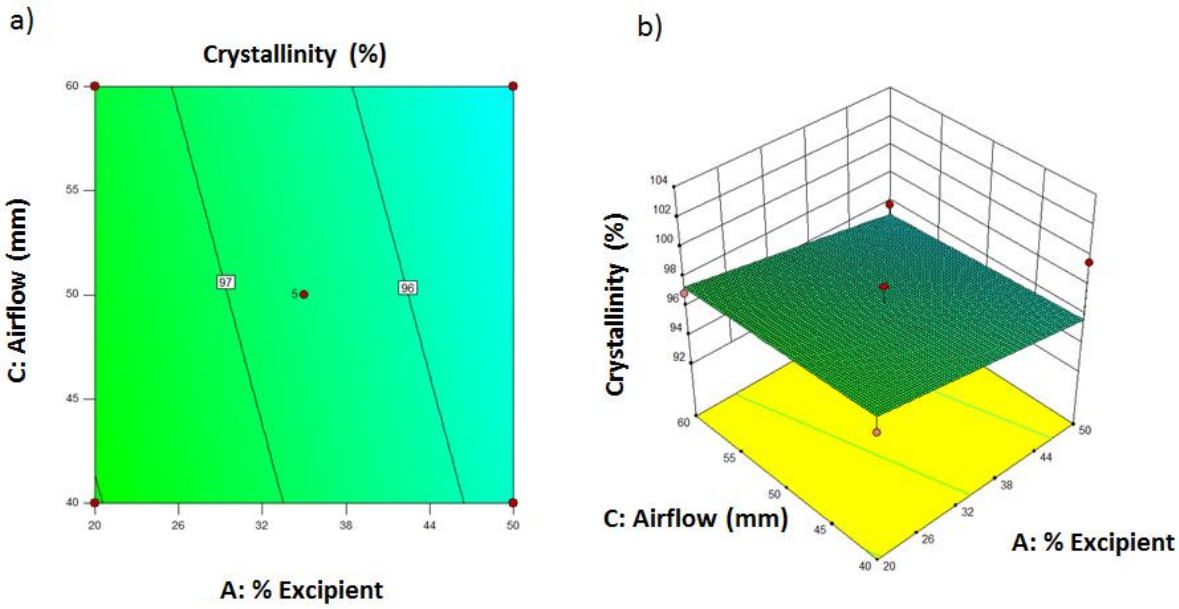

Figure 4.12. 2D contour plot (a) and 3D surface response (b) showing the influence of the total excipient percentage and the airflow on the cocrystal crystallinity.

With regard to the tensile strength of the tablets formed, a linear model was found to be the best fit for the data. The p-value for the model generated was 0.0126. Further to this, the total excipient fraction had a highly statistically significant impact on tensile strength, with a p-value of 0.0019 for this input factor. Both the excipient ratio and the airflow were not significant ($p > 0.05$). The excipient fraction positively affected the tensile strength of the tablets formed, while the excipient ratio negatively affected the tensile strength, suggesting that a higher amount of MCC in the tablets would positively affect the tensile strength. The airflow also had a negative effect on the tensile strength. 2D contour plots and 3D surface responses showing the effect of the input factors on tensile strength are presented in Figures 4.13 and 4.14.

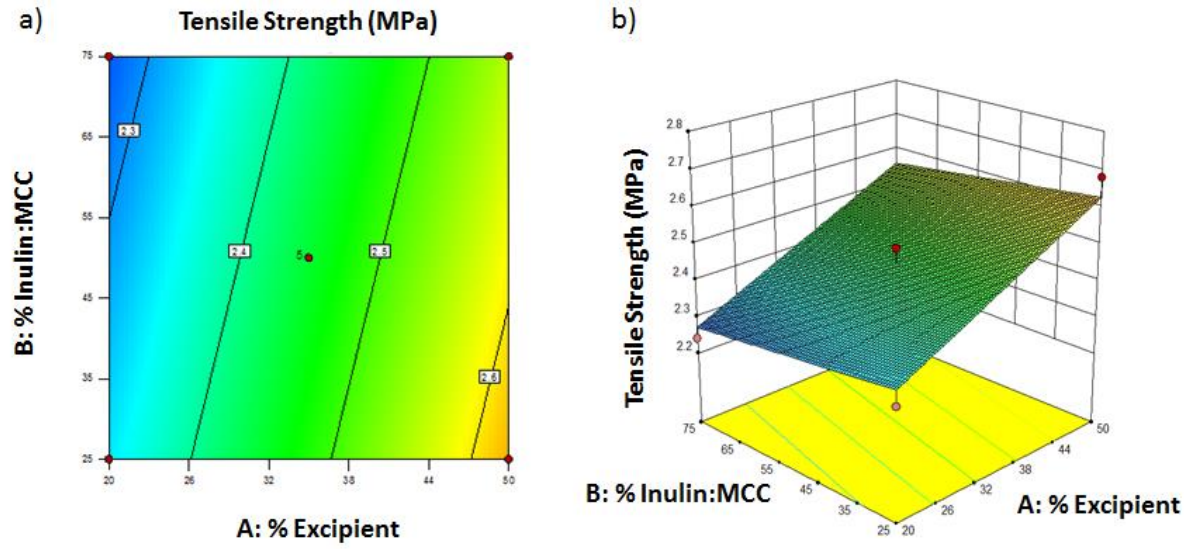

Figure 4.13. 2D contour plot (a) and 3D surface response (b) showing the influence of the total excipient percentage and the excipient ratio on the tensile strength of the tablets formed.

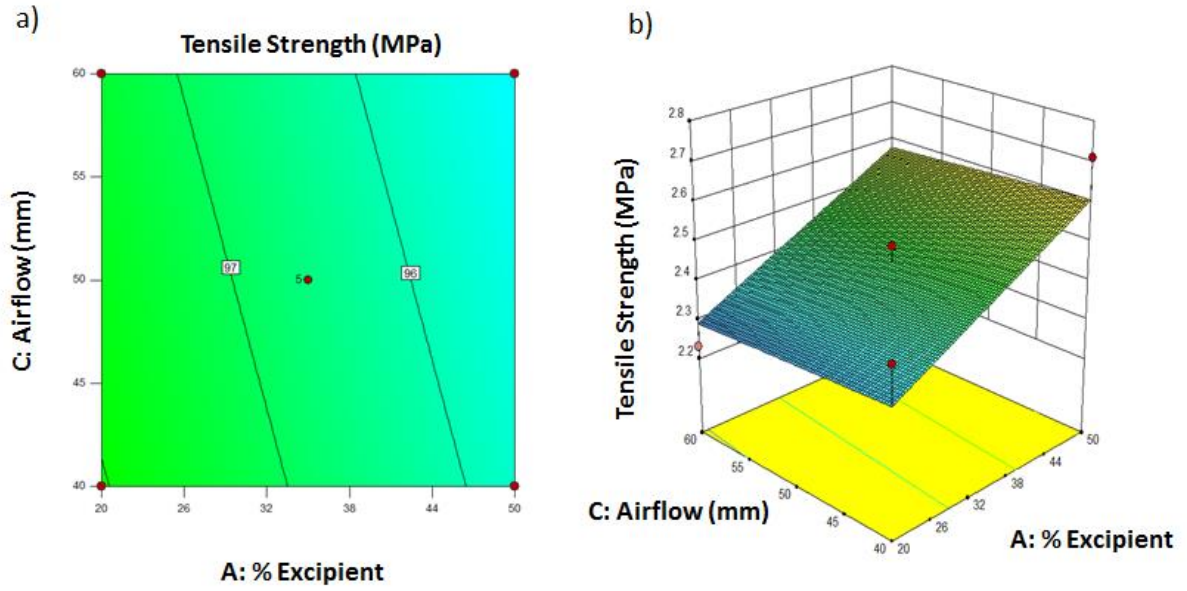

Figure 4.14. 2D contour plot (a) and 3D surface response (b) showing the influence of the total excipient percentage and the airflow on the tensile strength of the tablets formed.

Differences in Carr's index are shown in Table 4.1. Powders with a Carr's index > 25 are poorly flowable, cohesive powders (De Villiers, 2005). All samples in this study

demonstrated a value greater than 25. The poor flowability is likely due to the small particle size of the spray dried powders an unfavourable crystal habit. SEM analysis in Chapter 3 showed that the cocrystals produced by spray drying were in the shape of microspheres, which are likely to have better flow properties compared to crystal habits such as needles. However, particle size analysis performed in Chapter 3 also demonstrated that the cocrystal produced by spray drying had a D_{50} of 5.7 μm. As a result, there is a larger surface area for interaction between the particles, resulting in a cohesive powder. Spray dried particles can also be electrostatic in nature, which can promote cohesion between the particles and adhesion to surfaces. It had been anticipated that a lower airflow rate would improve the Carr's index, as it should result in a larger particle size due to less energy for fluid dispersion. The particle size of the co-spray dried powders was not measured in this study due to the small sample size. Other process factors that could increase particle size of spray dried powders, and therefore improve Carr's index, are increasing the feed rate, decrease the ratio of organic solvent: water, and increasing the concentration of the feed solution. It should also be noted that, due to the batch sizes of the runs performed, a 1 ml syringe was used to perform the bulk and tapped density measurements for Carr's index, as previously described (Ógáin et al., 2011). Due to the small syringe size, and considering that the syringe was graduated in 0.05 ml measurements, there may also be some error associated with the measurement process.

Statistical analysis of the Carr's index of the spray dried powders revealed that the model was not significant with a p-value > 0.05. The model chosen was a linear model, as there were no significant interactions. Further to this, there were no significant model terms. 2D contour plots and 3D surface responses showing the effect of the input factors on Carr's index are presented in Figures 4.15 and 4.16. The predicted equations for all three responses in terms of actual factors are presented in Table 4.2. As the models generated and the individual responses for crystallinity and Carr's index are not statistically significant, these models may not be valid, and may not be suitable to predict responses based on these input factors and parameters.

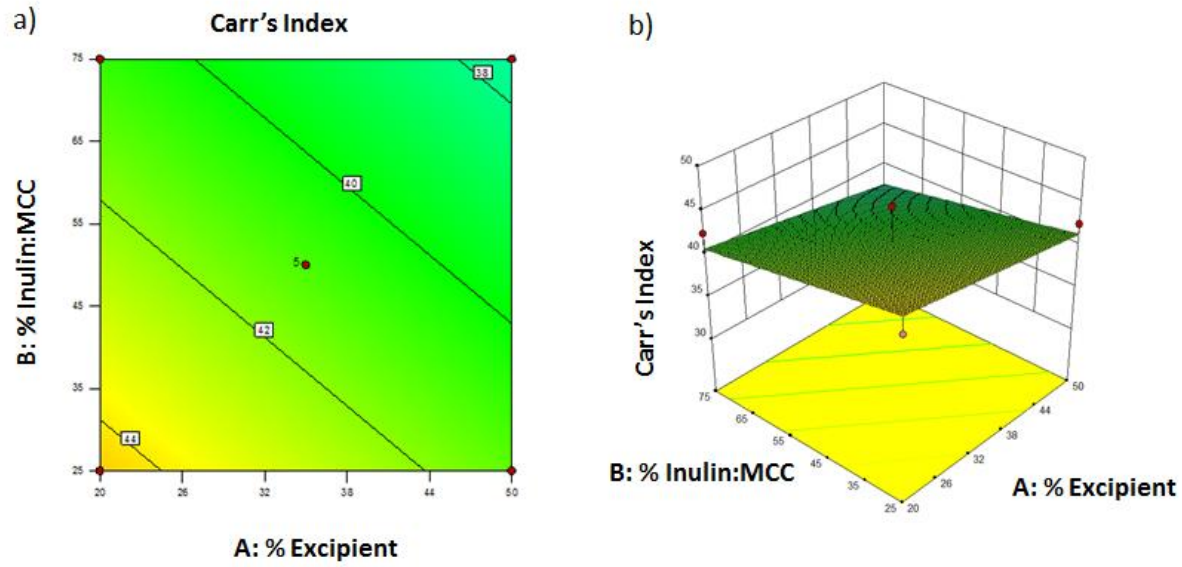

Figure 4.15. 2D contour plot (a) and 3D surface response (b) showing the influence of the total excipient percentage and the excipient ratio on Carr's index of the co-spray dried powders.

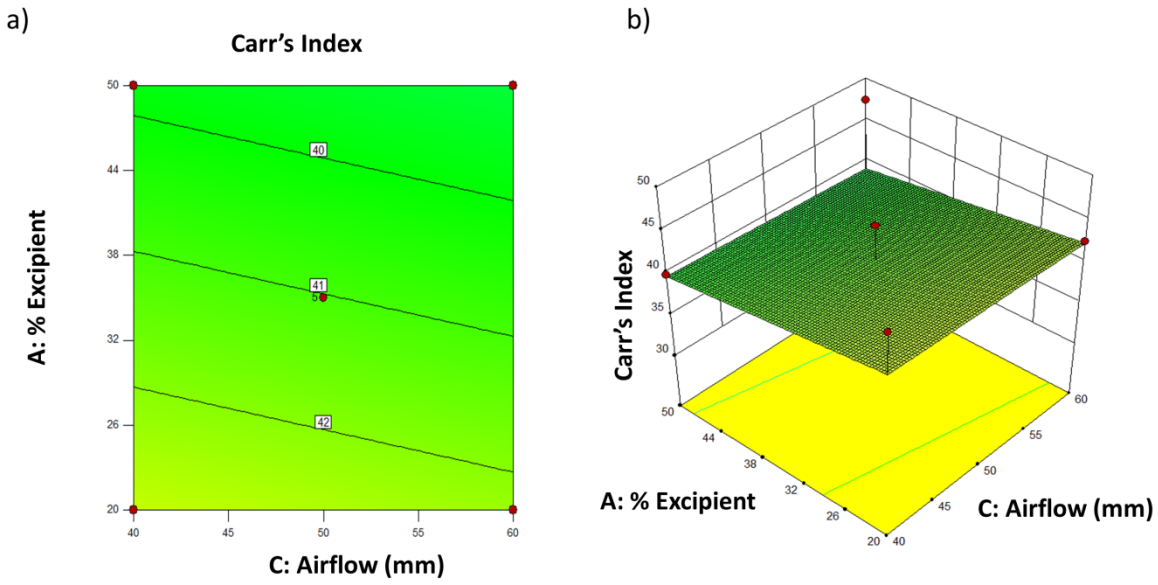

Figure 4.16. 2D contour plot (a) and 3D surface response (b) showing the influence of the total excipient percentage and the airflow on Carr's index of the co-spray dried powders.

Model (p-value)	**Predicted equation in terms of actual factors**
Linear (p>0.05)	**Crystallinity** = + 101.992 – 0.077*Excipient % - 0.023*Excipient ratio – 0.031*Airflow.
Linear (p<0.02)	**Tensile Strength** = + 2.262 + 0.010*Excipient % - 0.001*Excipient ratio – 0.002*Airflow.
Linear (p>0.05)	**Carr's Index** = + 49.988 – 0.104*Excipient % - 0.080*Excipient ratio – 0.031*Airflow.

Table 4.2. Model generation and predicted equations obtained from the Box-Behnken DoE.

4.2.4 Validation studies

The search for the optimum process and formulation parameters was carried out with the aim of maximising crystallinity and tensile strength, while minimising Carr's index. The optimum parameters were: 50 % excipient, 44.18 % inulin as excipient fraction, and an airflow setting of 40 mm, equivalent to 667 Nl/hour. These parameters were predicted to give a relative crystallinity of 95.86 %, a tensile strength of 2.61 MPa, and a Carr's index of 40.22. Validation of the QbD methodology revealed close proximity between the predicted value of the response with the observed response for tensile strength, presented in Table 4.3. The percent error between the experimental and predicted validation runs was 0.29 %, 1.53 % and 0.55 % for crystallinity, tensile strength and Carr's index respectively, demonstrating excellent goodness of fit. However, the small experimental error for the crystallinity and Carr's index may be due to chance, as these models were not statistically significant.

Response	Experimental results		Predicted results			
	Mean	**Standard deviation**	**Predicted response**	**Percent error**	**95 % CI Low**	**95 % CI High**
Crystallinity (%)	96.58	0.78	96.86	0.29 %	92.34	99.38
Tensile Strength (MPa)	2.57	0.23	2.61	1.53 %	2.49	2.74
Carr's Index	40	0	40.22	0.55%	34.73	45.68

Table 4.3. Comparison of experimental results with predicted responses. Key: CI, Confidence intervals.

4.3 Conclusions

Spray drying has been successfully been employed to produce a cocrystal-in-excipient matrix. Two excipients were incorporated into a one-step spray drying process to produce a cocrystal-in-excipient powder which could be directly compressed, eliminating the need for a separate blending step of cocrystal and excipients. A Box-Behnken DoE was performed to assess the impact of formulation and process parameters on the crystallinity of the cocrystal, tensile strength of the tablets formed and Carr's index of the co-spray dried powders. Linear models were chosen as the best fit in all cases. However, the only statistically significant model was the model generated for tensile strength, indicating that higher excipient to cocrystal fractions will result in tablets with a higher tensile strength. The ratio of inulin:MCC did not have a statistically significant effect on any of the three responses. The process parameter which was assessed, the airflow of the drying gas, did not have a significant impact on any response. This may be an indication that spray drying is a robust process in which to produce a cocrystal-in-excipient system.

CHAPTER 5

Comparing spray drying versus hot melt extrusion to prepare cocrystal-in-excipient systems

5.1 Introduction

Spray drying has previously been shown to be an effective method to produce cocrystals (Alhalaweh and Velaga, 2010). It can offer an advantage compared to other solution based methods such as cooling crystallisation, which can result in a mixture of phases (Fucke et al., 2012). Further to this, spray drying is favourable as it is a scalable, continuous one-step process often employed in the pharmaceutical industry (Broadhead et al., 1992, do Amaral et al., 2018). Spray drying parameters can also be altered to tailor the properties of particles produced by spray drying, such as particle size, shape and density (Vehring et al., 2007). However, disadvantages of spray drying include the requirement of large volumes of organic solvent (Ré, 2006), residual solvent of spray dried powders (Patel et al., 2009), the production of poorly flowable powders (Walton, 2000) and the expense of the equipment at large scale.

Hot melt extrusion (HME) has been explored as a method to produce cocrystals (Moradiya et al., 2014, Dhumal et al., 2010, Li et al., 2017). This process can offer a number of advantages as a formulation processing method, as it is a scalable and continuous process. Unlike spray drying, it is a solvent free method, and is therefore often regarded as a 'greener' method in comparison to spray drying, as large volumes of solvent are not required. As a result, the product obtained will have negligible amounts of oxygen and water, an advantage for pharmaceuticals which are susceptible to oxidation and hydrolysis (Breitenbach, 2002, Li et al., 2013). However, extrusion can also confer a number of disadvantages, as heat stress and shear force can cause chemical degradation of an active pharmaceutical ingredient (API) (Crowley et al., 2007). In the case of cocrystallisation (processing of drug and coformer) by extrusion, it has previously been demonstrated that cocrystallisation can occur when processed above the eutectic temperature (Dhumal et al., 2010).

Ibuprofen (IBU) is a Non-Steroidal Anti-Inflammatory Drug (NSAID) included in Class II of the Biopharmaceutics Classification System (BCS), demonstrating poor aqueous solubility and high permeability (Alvarez et al., 2011). Various attempts to increase the bioavailability of IBU, such as salt formation (Tung et al., 1991) and the formation of amorphous dispersions (Marsac et al., 2009, Shen et al., 2010), are abundant in the literature. Cocrystallisation of IBU can offer an alternative formulation approach to increase the bioavailability of the API without altering the chemical integrity, while

maintaining the physical stability of the API. Cocrystals of IBU with a number of different coformers have been generated by methods such as solvent evaporation (Chow et al., 2012), cooling crystallisation (Friščić and Jones, 2007), liquid assisted grinding (Friščić and Jones, 2007), dry grinding (Alshahateet, 2010, Alshahateet, 2011), HME (Kelly et al., 2012, Dhumal et al., 2010, Moradiya et al., 2014), and freeze drying (Eddleston et al., 2013). A review of the literature revealed no previous reports of an IBU cocrystal produced by spray drying. The IBU:INA cocrystal was chosen as a model cocrystal for this study as it was found that the SDM:4ASA cocrystal was not processable by HME, due to the thermal degradation of 4ASA. The IBU:INA cocrystal is amenable to both spray drying and HME.

Previous studies, presented in chapters 3 and 4, described the production of cocrystals of another BCS Class II drug, sulfadimidine, in the presence of a third component by a one-step spray drying process in order to reduce the number of unit operations which are required to produce a final pharmaceutical product. Cocrystal integrity was preserved when the cocrystal components were immiscible with the excipient, based on the difference in Hansen Solubility Parameter (HSP). However, our previous work did not consider the use of HME as an alternative continuous process to produce a cocrystal-in-excipient matrix system.

Attempts have previously been made to form the IBU:INA cocrystal by HME in the presence of xylitol, Soluplus and Eudragit EPO (Li et al., 2016). Cocrystal formation occurred only in the presence of xylitol (which has a melt temperature of 93.68 ^{o}C) at a 90:10 weight ratio of cocrystal components to xylitol, but not with Soluplus or Eudragit EPO, probably due to IBU amorphisation during the extrusion process (Li et al., 2016). Ratios of 70:30 and 50:50 (by weight) of cocrystal components to xylitol resulted in cocrystal formation, but individual crystalline IBU and INA were also detected in the extruded products. However, alteration of the processing temperature and screw configuration during extrusion led to cocrystal formation even with a higher xylitol load of 50 % by weight (Li et al., 2017).

The aim of this work was to fully investigate the impact of including a carrier excipient on cocrystal formation during spray drying and to compare it to HME. Spray drying and HME techniques have previously been compared in the context of the production of amorphous solid dispersions (Tian et al., 2014) and fixed dose combinations (Kelleher et

al., 2018), but the production of cocrystals in an excipient matrix by both methods has not been compared. The combination of IBU:INA was used as a model cocrystal. A range of pharmaceutical excipients was selected for processing. The ratio of cocrystal components to excipient was altered to assess the ratios at which cocrystal formation occurs. Due to the low melt temperature of xylitol and the low yield of xylitol on spray drying, mannitol (a six carbon polyol which is amenable to spray drying and has a similar HSP to xylitol, Table 5.2) was chosen as a model crystalline excipient for spray drying. Soluplus and PVP K15 were selected as amorphous excipients for comparison purposes. Solid state characterisation was performed as well as dissolution studies from constant surface area discs to compare the product characteristics of materials processed by the two different methods.

5.2 Results

5.2.1 Single crystal X-ray diffraction characterisation of solvent evaporated cocrystal

Using an equimolar ratio of IBU:INA, the solvent evaporation method produced a colourless crystalline sample of the cocrystal. A suitable crystal was analysed via single crystal X-ray diffraction yielding a formula of $C_{13}H_{18}O_2$:$C_6H_6N_2O$, a 1:1 cocrystal. The asymmetric unit consists of two independent IBU and two INA molecules, linked via hydrogen bonding, almost as predicted (Li et al., 2016). Each IBU is disordered over two positions and Figure 5.1 only shows the majority occupied moiety (see Figures A.3.1 and A.3.2, Appendix 3 for further figures). The hydrogen bonding between the INA moieties are formed via the amide NH and the opposite carbonyl group (N1…O27 = 2.963(4), N25…O3 = 2.926(4) Å). IBU also forms a hydrogen bond with the INA (O…N 2.575(4), 2.607(4) Å with angles > 157°) tying the four molecules into a linear array. One IBU is pointing up and the other pointing down. Each linear array is hydrogen bonded to a neighbouring array through the free INA amine NH to the IBU carbonyl (N1…O36^{ii}, 3.113(4) Å; symmetry transformations used to generate equivalent atoms: ii -x,-y+2,-z+1) forming a sheet (Figure 5.2). Each successive layer packs on the nearest layer by slotting the IBU between each other (Figure A.3.3, Appendix 3). There are several heterosynthon IBU cocrystals known in the literature (Walsh et al., 2003, Chen et al., 2010, Alshahateet, 2010, Berry et al., 2008, Alshahateet, 2011, Stone et al., 2009). Many are trimers e.g. IBU:X:IBU. Only a few display the same packing motif seen here where a tetramer is formed IBU:INA:INA:IBU (Berry et al., 2008, Alshahateet, 2011). Crystallographic data of the cocrystal are presented in Table 5.1. Crystallographic data, CCDC 1862812, can be obtained free of charge from the Cambridge Crystallographic Data Centre via www.ccdc.cam.ac.uk/ data_request/cif.

Table 5.1. Crystal data and structure refinement for IBU:INA cocrystal.

Empirical formula	$C_{19}H_{24}N_2O_3$
Formula weight	328.40
Temperature/K	100(2)
Crystal system	Triclinic
Space group	P-1
a/Å	5.7025(3)
b/Å	11.5514(6)
c/Å	27.6754(13)
α/°	95.551(3)
β/°	93.326(4)
γ/°	102.210(3)
Volume/Å^3	1767.65(16)
Z	4
ρ_{calc}g/cm^3	1.234
μ/mm^{-1}	0.675
F(000)	704.0
Crystal size/mm^3	0.27 × 0.17 × 0.16
Radiation	CuKα (λ = 1.54178)
2Θ range for data collection/°	3.218 to 138.392
Index ranges	$-6 \leq h \leq 6$, $-13 \leq k \leq 13$, $-33 \leq l \leq 33$
Reflections collected	24654
Independent reflections	6444 [R_{int} = 0.0600, R_{sigma} = 0.0759]
Data/restraints/parameters	6444/669/669
Goodness-of-fit on F^2	1.069
Final R indexes [I>=2σ (I)]	R_1 = 0.0985, wR_2 = 0.2875
Final R indexes [all data]	R_1 = 0.1223, wR_2 = 0.3155
Largest diff. peak/hole / e Å^{-3}	0.40/-0.41

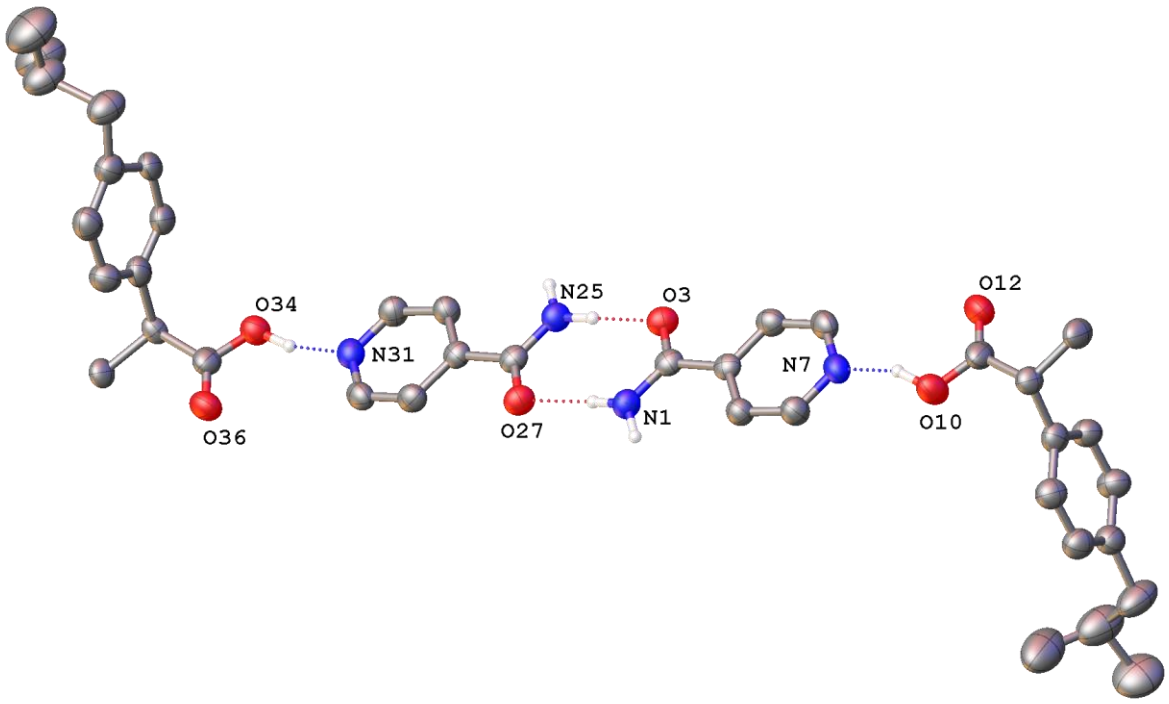

Figure 5.1. Cocrystal structure determined from SCXRD studies. Hydrogen bonded tetramer of the cocrystal $C_{13}H_{18}O_2$:$C_6H_6N_2O$, IBU:INA, with only the majority occupied disordered IBU moiety shown. Only heteroatoms labelled and only hydrogen atoms involved in hydrogen bonding are shown. Displacement parameters shown at 50 % probability.

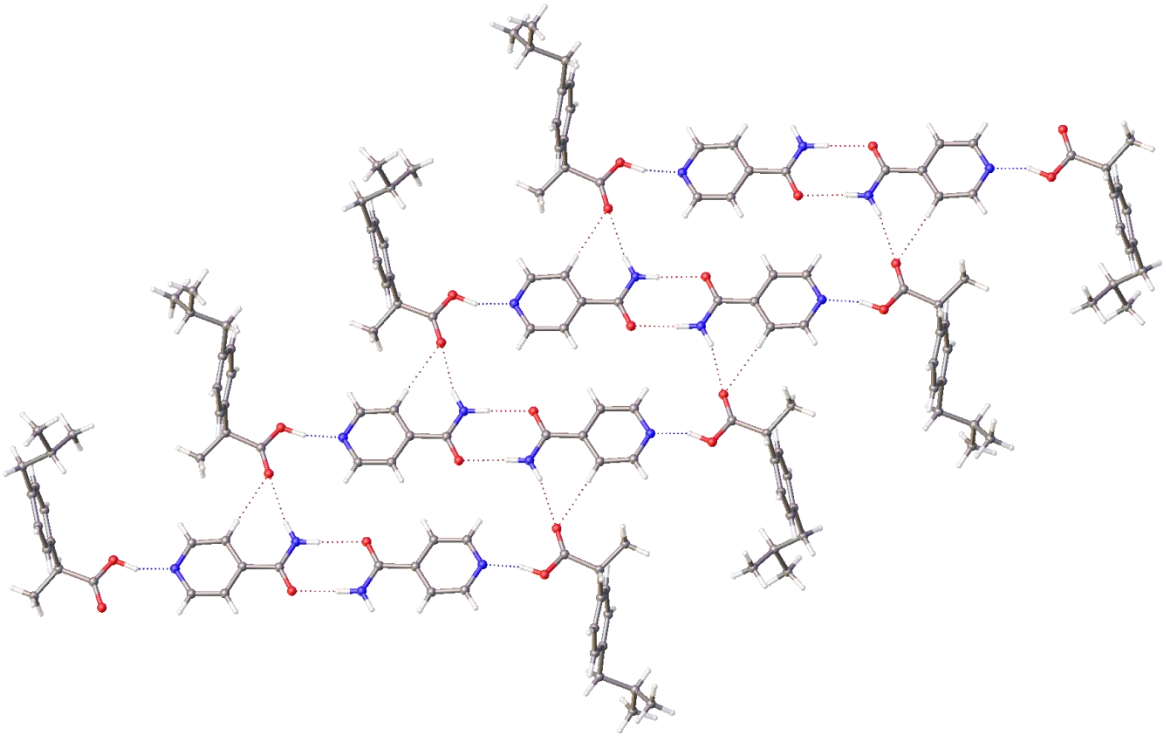

Figure 5.2. Cocrystal structure determined from SCXRD studies. Hydrogen bonded sheet structure of the IBU:INA cocrystal showing the amide-ketone and hydroxide-INA donor acceptors as dotted lines as well as weak CH…O interactions (C5…O36ii = 3.316(4) Å; ii = symmetry equivalent transformation, -x,-y+2,-z+1).

5.2.2 Powder X-ray diffraction

Spray drying

Spray drying the solution of IBU:INA at a 1:1 molar ratio resulted in cocrystal formation. Similar Bragg peak intensity was seen for the cocrystal produced by spray drying from ethanol and the cocrystal produced by spray drying from isopropanol. Bragg peaks attributable to IBU and INA were not present. Characteristic peaks of IBU raw material may be observed at 6.15°, 12.25°, 16.7° and 24.6° 2θ, and peaks of INA raw material at 17.85°, 18.9°, 20.85° and 23.5° 2θ (Figure 5.3). Similarly to Li et al. who prepared the cocrystal by coextrusion (Li et al., 2016), Bragg peaks attributed to the IBU:INA cocrystal were observed at 6.4°, 17.45°, 18.95° and 20.1° 2θ (Figure 5.3), indicating that the same form of the cocrystal was obtained by both hot melt extrusion and spray drying. Spray drying can produce a different polymorphic form of a cocrystal than other methods

of cocrystal formation, as previously seen with the SDM:4ASA cocrystal (Grossjohann et al., 2015). However, polymorphism of the IBU:INA cocrystal has not been reported to date. The cocrystal produced by solvent evaporation from isopropanol resulted in more intense Bragg peaks compared to the cocrystals produced by spray drying. Spray dried IBU resulted in crystalline IBU, with the same polymorph obtained as the raw material (Figure 5.3).

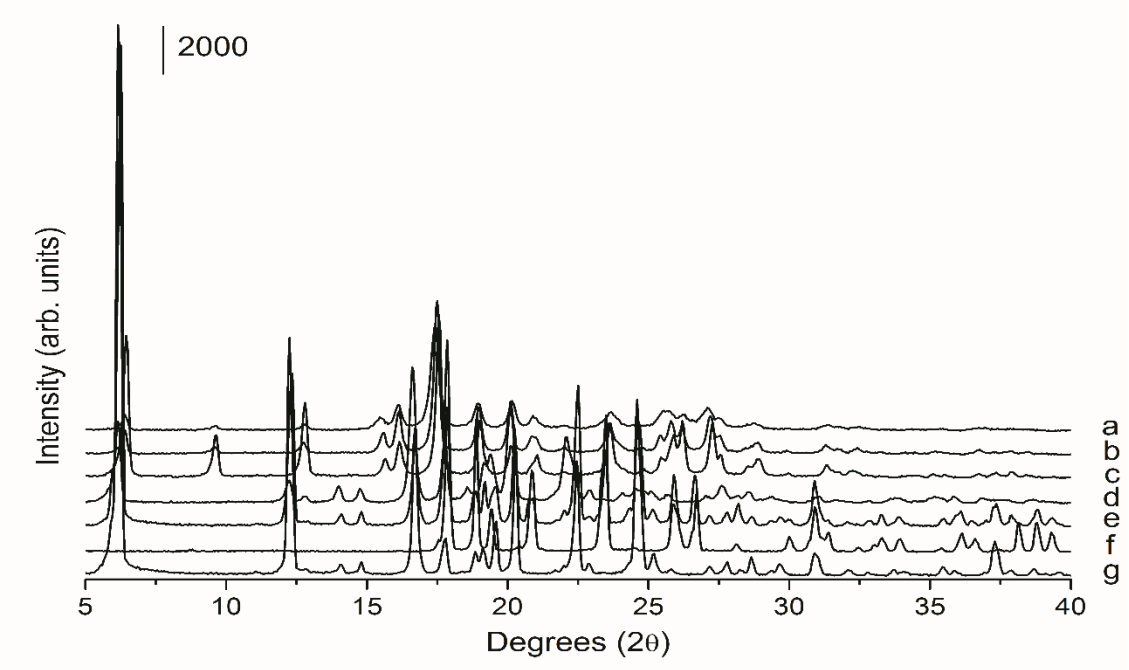

Figure 5.3. PXRD analyses of raw materials, cocrystals produced by spray drying and solvent evaporation. a) Cocrystal produced by spray drying from ethanol, b) Cocrystal produced by spray drying from isopropanol, c) Cocrystal produced by solvent evaporation from isopropanol, d) Spray dried IBU, e) Physical mixture of IBU and INA (1:1 molar ratio), f) INA, g) IBU.

Each formulation is named in this chapter with reference to the method of production (spray drying (SD) or hot melt extrusion (HME)), excipient used (M = mannitol, X = xylitol, P = PVP K15, S = Soluplus) and excipient weight fraction. For example, the co-spray dried system with 10 % mannitol is referred to as SD-M-10.

Cocrystal formation was observed for the spray dried formulations with mannitol, i.e. SD-M-10, SD-M-30 and SD-M-50 formulations (Figure 5.4). Bragg peaks attributable to the individual cocrystal components were not observed. However, Bragg peaks attributable to both the cocrystal and to different polymorphic forms of mannitol were

seen. Both beta and delta mannitol peaks were present in the PXRD diffractogram for all ratios of cocrystal components to excipient (Figure A.3.4, Appendix 3). Co-spray drying mannitol with lysozyme has previously been shown to produce a mix of mannitol polymorphs (Hulse et al., 2009). The API and coformer have similar HSP values, 19.4 $MPa^{0.5}$ and 24.4 $MPa^{0.5}$ respectively, whereas mannitol HSP is 39.1 $MPa^{0.5}$ (Table 5.2). It has previously been determined that cocrystallisation can occur when the difference in HSP between the API and coformer is less than 7 $MPa^{0.5}$ (Mohammad et al., 2011), while cocrystal formation in the presence of a third component occured when the difference in HSP between the cocrystal and excipient (i.e. third component) was above 9.6 $MPa^{0.5}$, as was observed in chapter 3.

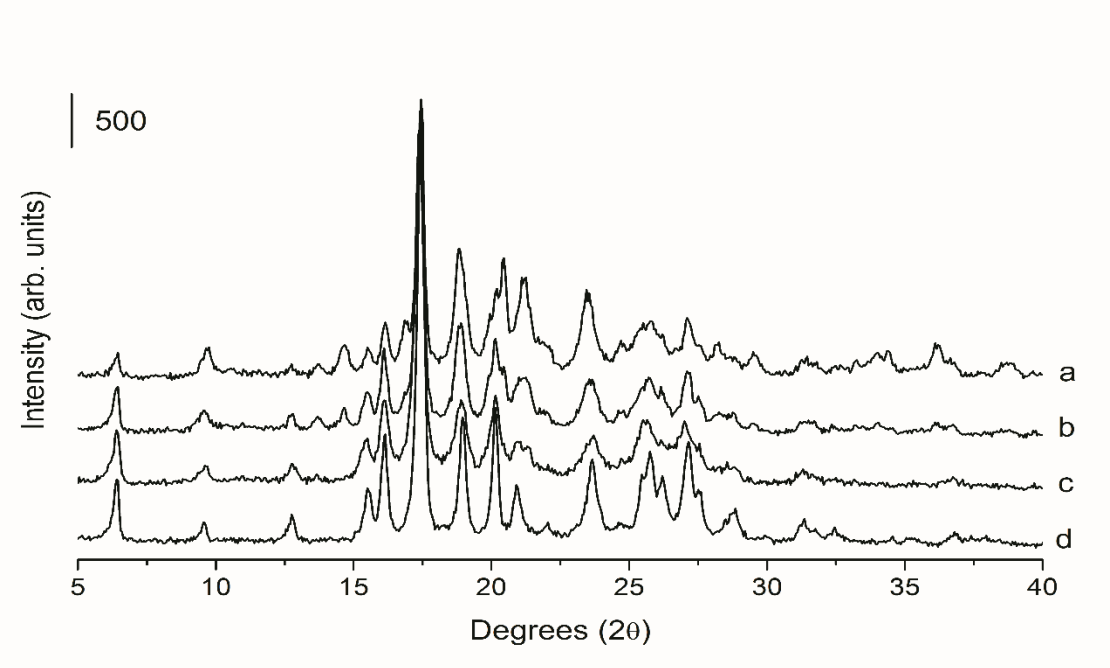

Figure 5.4. PXRD analyses of co-spray dried systems with mannitol; a) IBU:INA 50 %, mannitol 50 %, b) IBU:INA 70 %, mannitol 30 %, c) IBU:INA 90 %, mannitol 10 %, d) Spray dried cocrystal.

Cocrystal formation by spray drying with different ratios of cocrystal components to Soluplus was also assessed. The SD-S-10 formulation resulted in cocrystal formation (Figure 5.5). The ratio of Soluplus to cocrystal components was increased and cocrystal formation at these ratios was assessed. Bragg peaks attributable to the cocrystal were also observed for the SD-S-15, SD-S-20 and SD-S-30 formulations, as well as crystalline INA and what was taken to be an amorphous phase comprising IBU and Soluplus, given the

observed shift in the T_g of Soluplus when loads of ≥ 15 % Soluplus were incorporated into the feed solution. The PXRD patterns of the polymorphic forms of INA were obtained from single crystal data obtained from the Cambridge Crystal Database (Figure A.3.5, Appendix 3). Form I (CSD ref code: EHOWIH01) is the unprocessed raw material polymorph used in these experiments (Groom et al., 2016).

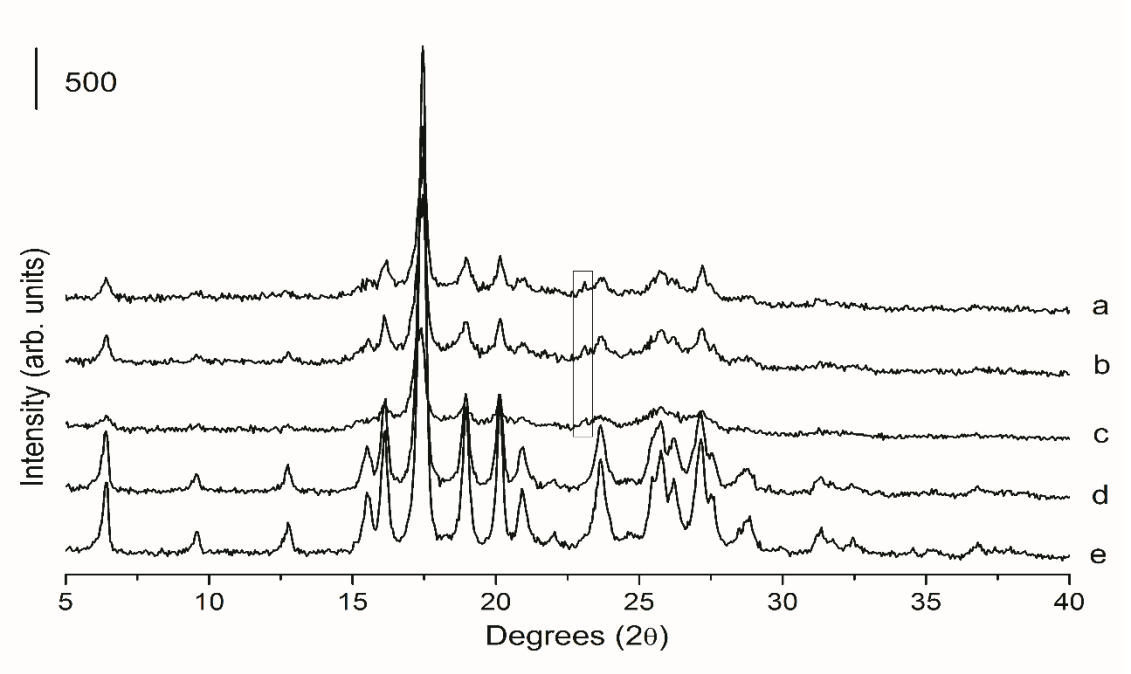

Figure 5.5. PXRD analyses of co-spray dried systems with Soluplus; a) IBU:INA 70 %, Solulpus 30 %, b) IBU:INA 80 %, Soluplus 20 %, c) IBU:INA 85 %, Soluplus 15 %, d) IBU:INA 90 %, Soluplus 10 %, e) Spray dried cocrystal. Bragg peaks attributable to INA can be observed at 23º 2θ when the Soluplus loading was ≥ 15 %.

A peak attributable to a polymorph of INA (form IV, CSD ref code: EHOWIH04) can be seen at 23º 2θ when Soluplus loads ≥ 15 % were incorporated into the process. Attempts were made to co-spray dry the cocrystal components with Soluplus at a ratio of 60:40 (% w/w). However, when this ratio was used, the yield was significantly affected, with negligible amounts of product reaching the collection vessel of the spray dryer. Cocrystal formation, without other separated coformer or API components, was only seen when 10 % Soluplus was used. Above this excipient loading, a mixture of cocrystal, a glass solution of IBU and Soluplus, and crystalline INA was formed, which can be explained by the fact that the difference in HSP between Soluplus and cocrystal is 2.1 $MPa^{0.5}$. It has previously been demonstrated in chapter 3 that when the HSP values of cocrystal and

excipient are very close, cocrystal formation only occurs when low excipient loads are used.

Cocrystal formation in the presence of PVP K15 by spray drying and HME was also assessed. PVP K15 was chosen as, unlike Soluplus, its glass transition temperature is above the extrusion processing temperature. It was hypothesised that this could prevent the formation of a glass solution being formed as a side reaction. A shorter chain PVP was chosen as higher chain length polymers can be more viscous in solution, which can result in kinetic trapping of the API/coformer during the fast solvent evaporation when spray drying, resulting in the formation of an amorphous dispersion (Paudel et al., 2013).

Cocrystal formation was assessed by spray drying in the presence of PVP K15 at a ratio of 90:10 (% w/w) cocrystal components to excipient. Bragg peaks attributable only to the cocrystal were seen for the SD-P-10 formulation (Figure 5.6). When the SD-P-20 formulation was processed, again peaks attributable only to the cocrystal were observed.

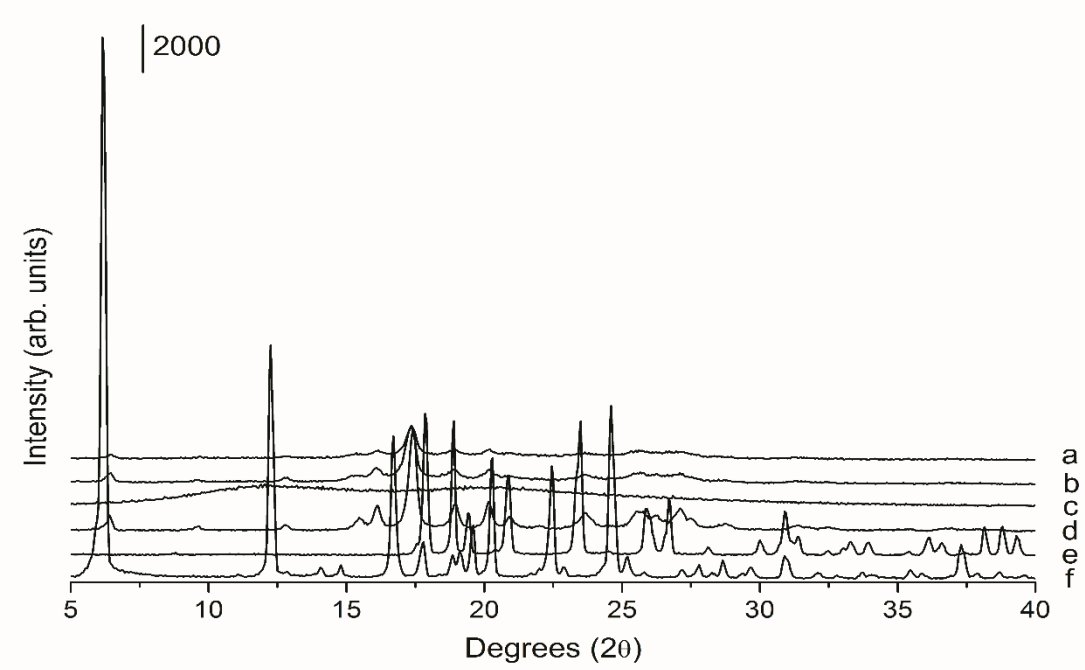

Figure 5.6. PXRD analyses of co-spray dried systems with PVP K15; a) IBU:INA 80 %, PVP K15 20 %, b) IBU:INA 90 %, PVP K15 10 %, c) PVP K15, d) Spray dried cocrystal, e) INA, f) IBU.

Due to the abundance of potential hydrogen bonding sites in mannitol, spray drying experiments were prepared to investigate the potential for cocrystal formation between the crystalline excipient (mannitol) and the API or the coformer. PXRD analyses of the

control powders showed no new peaks which could be attributed to a 'cocrystal cocktail'. Results of PXRD analyses are presented in Figures A.3.6-A.3.8, Appendix 3.

Table 5.2. Calculated HSP values of cocrystal components and carrier excipients.

Molecule	**HSP value ($MPa^{0.5}$)**	**ΔHSP ($MPa^{0.5}$)**
IBU	19.4	1.4
INA	24.4	3.6
Cocrystal 1:1 molar ratio	20.8	-
Mannitol	39.1	18.3
Xylitol	41.5	20.7
Soluplus	22.9	2.1
PVP K15	22.4	1.6

Hot Melt Extrusion

When the cocrystal components were processed with xylitol, HME-X-10, the hot melt extruded product showed characteristic diffraction peaks of the cocrystal, as well as peaks attributable to crystalline xylitol, which are indicated by arrows (Figure 5.7). Altering the extrusion temperature and screw configuration has been previously shown to result in cocrystal formation when higher xylitol loads are incorporated into the extrusion process (Li et al., 2017).

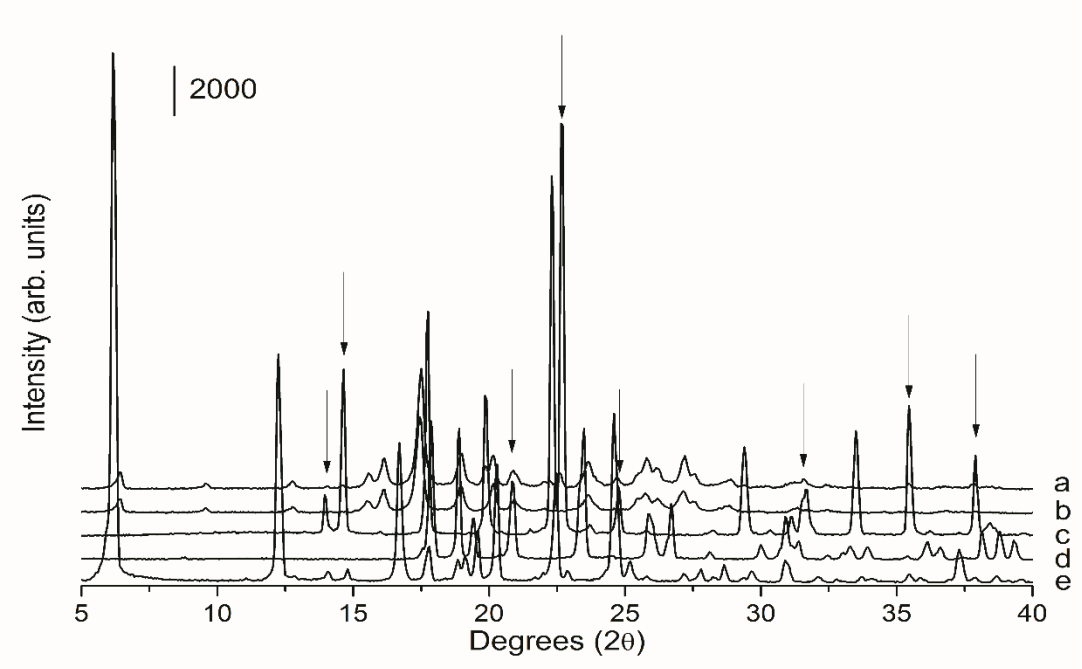

Figure 5.7. PXRD analyses of cocrystal produced by hot melt extrusion. A) Cocrystal in the presence of xylitol. a) Extruded IBU:INA 90 %, xylitol 10 %, b) Spray dried cocrystal, c) Xylitol, d) INA, e) IBU. Xylitol peaks are highlighted by arrows.

Hot melt extrusion was also performed using Soluplus and PVP K15, HME-S-10 and HME-P-10 respectively, as amorphous excipients. The processing temperature was above the T_g of Soluplus, and below the T_g of PVP K15. In both cases, the presence of cocrystal as well as amorphous and crystalline API/coformer was observed by PXRD (Figure 5.8). Peaks attributable to INA are highlighted by arrows. However, a cocrystal was obtained with both PVP K15 and Soluplus by spray drying at the same ratio, suggesting that spray drying may offer a processing advantage over hot melt extrusion.

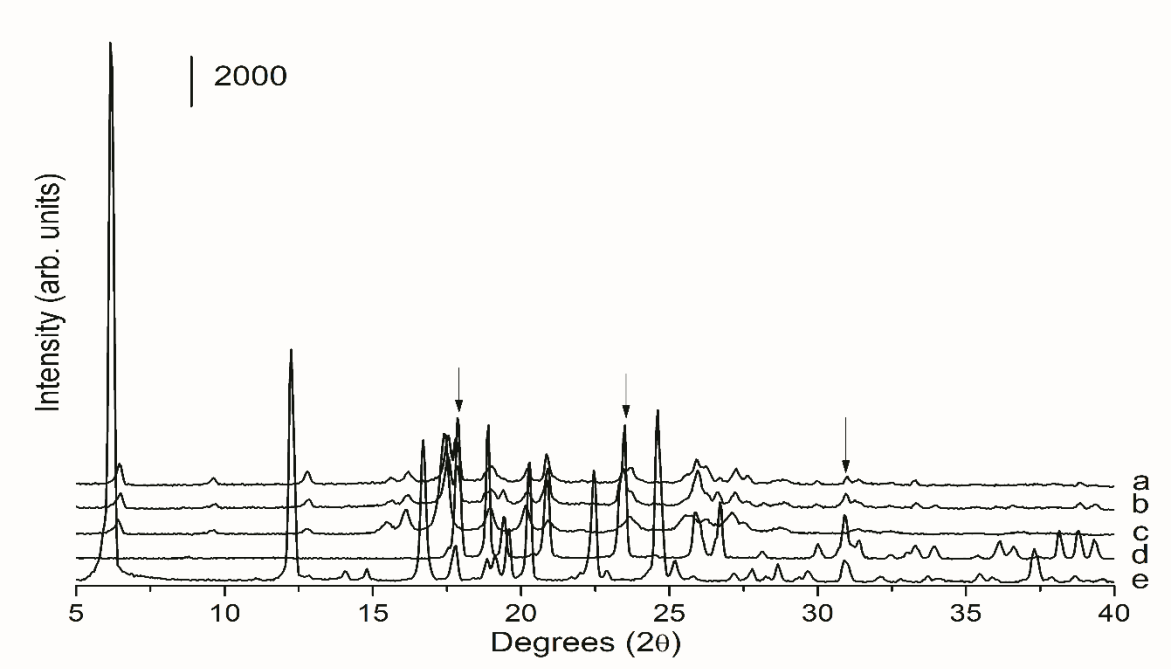

Figure 5.8. PXRD analyses of cocrystal produced by hot melt extrusion. A) Cocrystal in the presence of Soluplus and PVP K15; a) IBU:INA 90 %, PVP K15 10 %, b) IBU:INA 90 %, Soluplus 10 %, c) Spray dried cocrystal, d) INA, e) IBU. Peaks attributable to INA in the HME formulations are highlighted by arrows.

HME experiments were also performed with xylitol and the API or coformer to investigate the potential for cocrystal formation between the excipient and the API or coformer. No new peaks attributable to a cocrystal between the excipient and API/coformer were observed. Results of PXRD analyses are presented in Figure A.3.9-A.3.11, Appendix 3.

5.2.3 Differential scanning calorimetry

Spray drying

At a heating rate of 10 ^{o}C/min, IBU displayed a characteristic melting point at 75.26 ± 0.13 ^{o}C (130.96 ± 0.16 J/g), with INA displaying a polymorphic transformation at 120.08 ± 0.63 ^{o}C (13.34 ± 0.06 J/g) and a melting point at 156.40 ± 0.13 ^{o}C (196.14 ± 0.57 J/g) (Figure 5.9 and Table 5.3). For the physical mixture of IBU and INA, two endothermic events were present, one of which was below the IBU melt temperature, which may be attributed to a eutectic melt. In systems forming eutectics, cocrystal formation can occur by heating in the DSC past the eutectic temperature (Lu et al., 2008). The second

endotherm can be attributed to the cocrystal. No thermal event attributable to INA was observed.

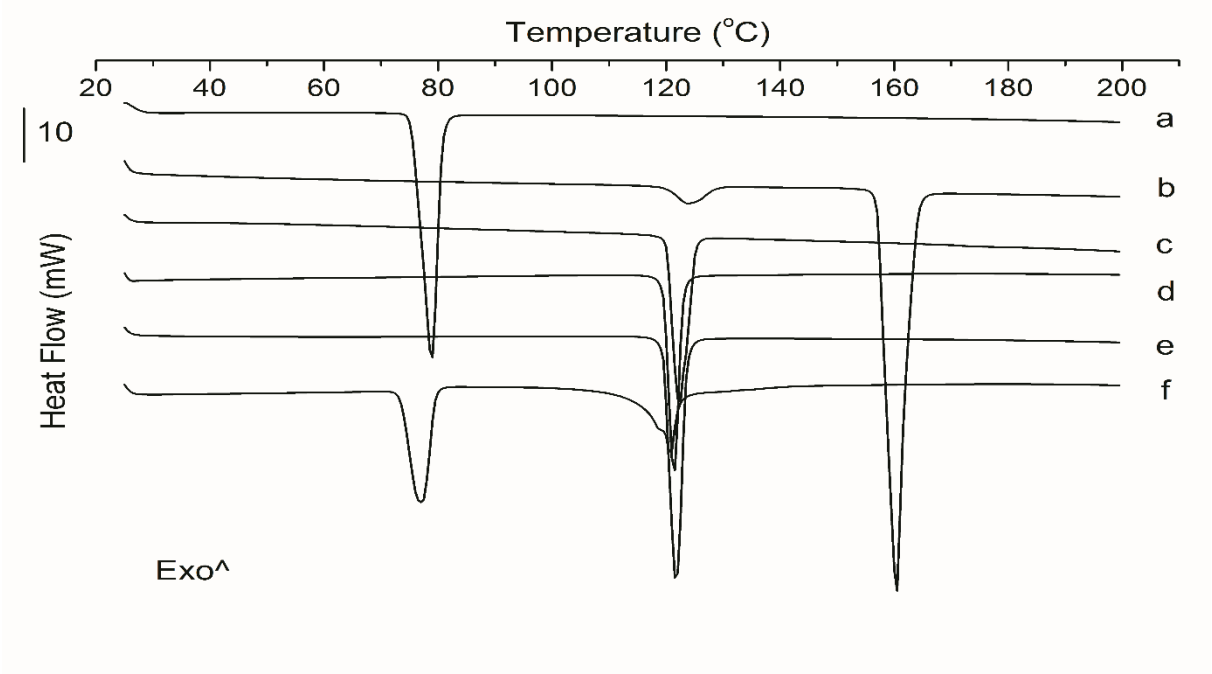

Figure 5.9. Cocrystal formation by spray drying and solvent evaporation; a) IBU, b) INA, c) Cocrystal produced by slow solvent evaporation from isopropanol, d) Cocrystal produced by spray drying from ethanol, e) Cocrystal produced by spray drying from isopropanol, f) Physical mixture of IBU and INA.

Xylitol displayed a characteristic melting point at 93.68 ± 0.16 ºC (249.56 ± 9.15 J/g) (Figure 5.13), while mannitol had one endothermic event characteristic of melting at 165.59 ± 0.21 ºC (307.14 ± 5.87 J/g) (Figure 5.10). The spray dried product of IBU and INA from ethanol at a 1:1 molar ratio displayed one endothermic peak at 119.33 ± 0.14ºC (139.10 ± 0.98 J/g) and no exothermic peaks, indicating that cocrystal formation had occurred. The spray dried cocrystal from isopropanol displayed an endothermic peak at 119.31 ± 0.16 ºC (138.64 ± 0.25 J/g), similar to that of the cocrystal produced by spray drying from ethanol with a slight reduction in the melt enthalpy. Solvent evaporation from isopropanol resulted in a material that displayed one single endothermic peak in the DSC at 119.72 ± 0.09ºC (139.43 ± 0.56 J/g) (Table 5.4).

Table 5.3. Melting temperatures and heat of fusion of raw materials and physical mixture of IBU and INA (1:1 molar ratio). *Denotes glass transition temperature. **Denotes polymorphic transformation. N/A, non-applicable.

System	T_{m1} or T_g (ºC)	ΔH_f (J/g)	T_{m2} (ºC)	ΔH_f (J/g)
IBU	75.26 ± 0.13	130.96 ± 0.16	N/A	N/A
INA	120.08 ± 0.64**	13.14 ± 0.06	156.40 ± 0.13	196.14 ±0.57
Physical mixture	73.67 ± 0.29	85.01 ± 1.82	117.72 ± 0.12	50.75 ± 4.84
Mannitol	165.59 ± 0.21	307.14 ± 5.87	N/A	N/A
Xylitol	93.68 ± 0.16	249.56 ± 9.15	N/A	N/A
Soluplus*	61.98 ± 0.22	N/A	N/A	N/A
PVP K15*	127.53 ± 0.23	N/A	N/A	N/A

Co-spray dried IBU:INA with mannitol at all three ratios, SD-M-10, SD-M-30 and SD-M-50, displayed two melting peaks, one attributable to the melting of the cocrystal and one attributable to the melting of crystalline mannitol (Figure 5.10). No melting peaks attributable to the individual cocrystal components were observed, even when high mannitol loads (50 % w/w) were incorporated into the feed solution prior to spray drying. Melting point depression of the cocrystal was observed with increasing mannitol loads, as well as broad melting peaks. This was observed for both the co-spray dried systems and the physical mixtures of cocrystal and mannitol. Melting point depression and broad melting peaks were also seen for mannitol. The melting enthalpy of the co-spray dried systems and the physical mixtures were compared, and the relative crystallinity of the co-spray dried systems compared to a physical mixture of cocrystal and excipient was calculated. A relative crystallinity of 98.36 %, 97.43 % and 91.79 % was calculated for the SD-M-10, SD-M-30 and SD-M-50 formulations respectively, showing a small loss in crystallinity for the co-spray dried formulations compared to the physical mixtures.

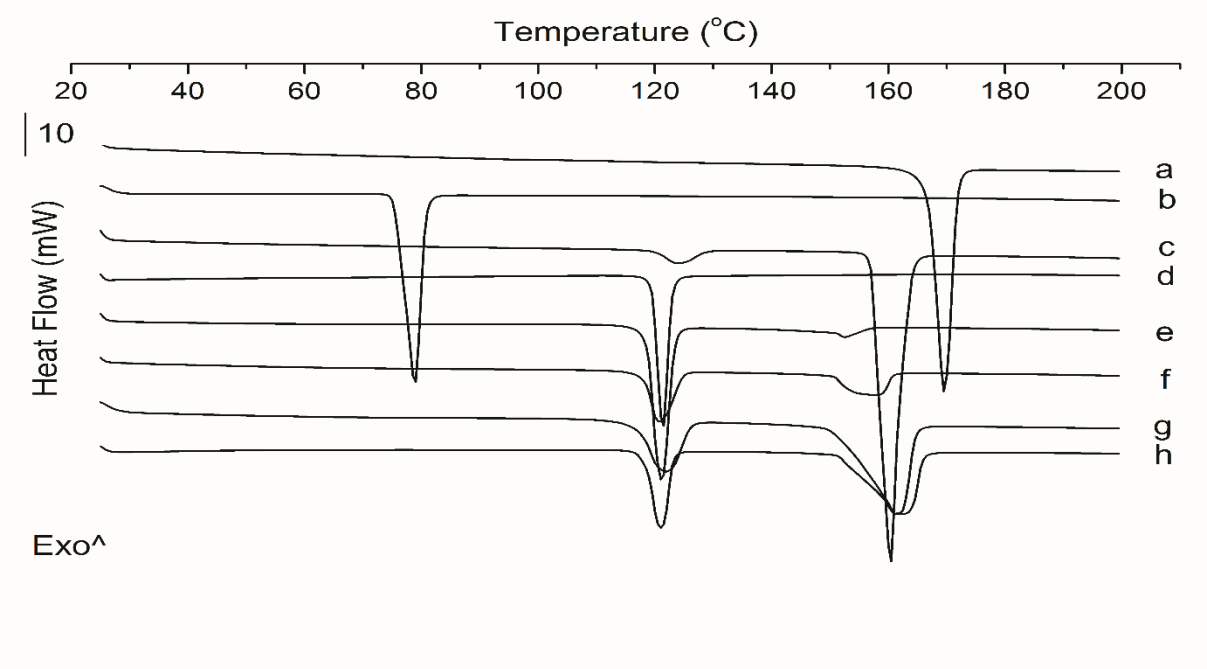

Figure 5.10. Cocrystal co-spray dried with mannitol; a) Mannitol, b) IBU, c) INA, d) Spray dried cocrystal, e) Spray dried IBU:INA 90 %, mannitol 10 %, f) Spray dried IBU:INA 70 %, mannitol 30 %, g) Spray dried IBU:INA 50 %, mannitol 50 %, h) Physical mixture of spray dried cocrystal 50 % and mannitol 50 %.

The SD-S-10 formulation resulted in cocrystal formation, with one endothermic peak present on the DSC curve, which can be attributed to cocrystal melting (Figure 5.11). When the ratio of Soluplus in the feed solution was increased, a second endothermic event was observed directly after cocrystal melting. However, this shoulder peak was not present in physical mixtures of spray dried cocrystal and Soluplus at the same ratios (Figure A.3.12, Appendix 3). This double melting peak could be attributed to two different crystal morphologies (Blundell, 1987). Nevertheless, as this peak occurred after cocrystal melting, it is unlikely to be morphology related. This peak can probably be attributed to a significantly depressed INA melting event which can be observed when 15 %, 20 % and 30 % Soluplus was incorporated into the feed solution prior to spray drying.

A polymorphic form of INA (form IV, CSD ref code: EHOWIH04) was generated, as well as the cocrystal, when Soluplus loads ≥ 15 % were used. This polymorph was also generated when INA was spray dried with Soluplus (50:50 % w/w), resulting in one endothermic event at 140 ^{o}C (Figure A.3.13, Appendix 3). This polymorph has been

shown to demonstrate one endothermic event on DSC analysis. No phase change is seen during DSC analysis, as only a melting event is observed (Eccles et al., 2011). At Soluplus loads ≥ 15 %, a mixture of an amorphous phase, cocrystal and crystalline INA can be observed. When ≥ 15 % Soluplus is incorporated into the feed solution, a shift in the T_g of Soluplus is seen, indicating a glass solution of polymer and IBU is formed, as well as crystalline INA. MTDSC results are presented in Figure A.3.14, Appendix 3, which shows the shift in glass transitions of the systems with ≥ 15 % Soluplus. The relative crystallinities of the co-spray dried samples were obtained by comparing the melt enthalpies to the relevant physical mixtures of cocrystal and Soluplus. A relative crystallinity of 94.11 %, 66.68 %, 56.58 % and 32.69 % was calculated for the systems containing 10 %, 15 %, 20 % and 30 % of Soluplus respectively, indicating a significant amount of amorphous IBU, present as a glass solution with Soluplus, and crystalline INA are present in the formulations containing ≥ 15 % Soluplus.

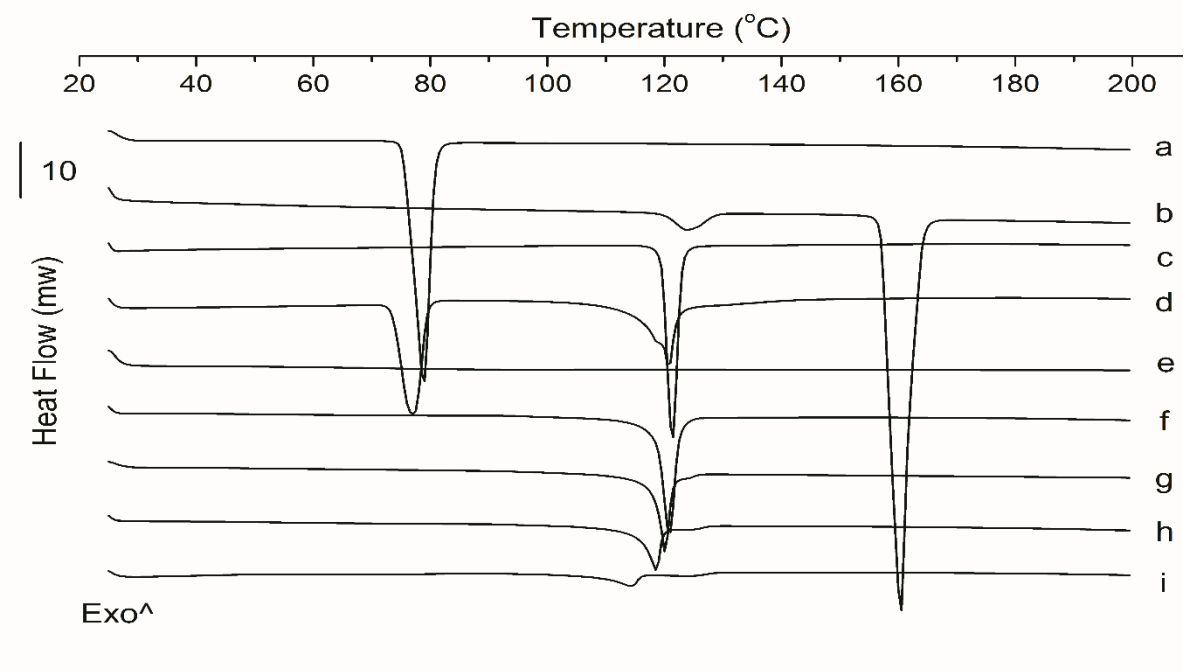

Figure 5.11. Cocrystal co-spray dried with Soluplus; a) IBU, b) INA, c) Spray dried cocrystal, d) Physical mixture of IBU and INA (1:1 molar ratio), e) Soluplus, f) Spray dried IBU:INA 90 %, Soluplus 10 %, g) Spray dried IBU:INA 85 %, Soluplus 15 %, h) Spray Dried IBU:INA 80 %, Soluplus 20 %, i) Spray dried IBU:INA 70 %, Soluplus 30 %.

The SD-P-10 formulation showed one endothermic peak at the cocrystal melting temperature (Figure 5.12). The relative crystallinity of the co-spray dried product compared to the physical mixture of cocrystal and PVP was 98.94 %. A T_g was observed at 10.66 ± 0.67 ºC, indicating the presence of a glass solution between the polymer, API and/or coformer. A melting event of the individual components was not observed. It was not possible to determine if a separate phase of polymer was present, as the T_g of this was obscured by the melting of the cocrystal. The SD-P-20 formulation showed two endothermic peaks, one attributable to the cocrystal and a second peak after the cocrystal temperature. Like the systems with ≥ 15 % Soluplus, this can be attributed to crystalline INA, although this was not detected by PXRD. A T_g was also observed at 3.65 ± 0.28 ºC, which is likely a glass solution of polymer, IBU and/or INA, Figure A.3.15, Appendix 3.

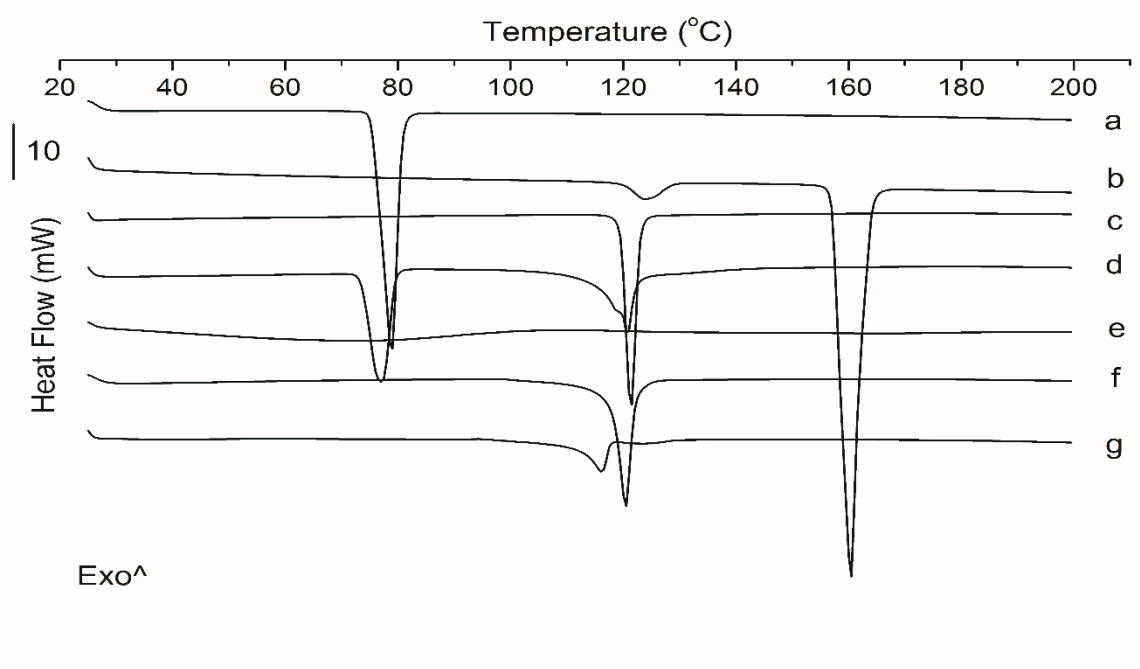

Figure 5.12. Cocrystal co-spray dried with PVP K15; a) IBU, b) INA, c) Cocrystal produced by spray drying, d) Physical mixture of IBU and INA, e) PVP K15, f) Co-spray dried IBU:INA 90 %, PVP K15 10 %, g) IBU:INA 80%, PVP K15 20 %.

Hot melt extrusion

The HME-X-10 formulation displayed two characteristic melting peaks, a depressed xylitol peak at 84.95 ± 0.16 ºC (21.98 ± 0.82 J/g) and a cocrystal melting peak at 115.28 ± 0.07 ºC (119.66 ± 2.27 J/g) (Figure 5.13). The melting enthalpy of the hot melt extruded cocrystal in xylitol was slightly lower than the spray dried cocrystal in mannitol. However, this may be attributed to the cocrystal melting into liquid xylitol in the case of

the hot melt extruded product, while the cocrystal melts in the presence of solid mannitol in the case of the spray dried product. A relative crystallinity of 97.99 % was measured for the hot melt extruded product compared to the physical mixture of cocrystal and xylitol.

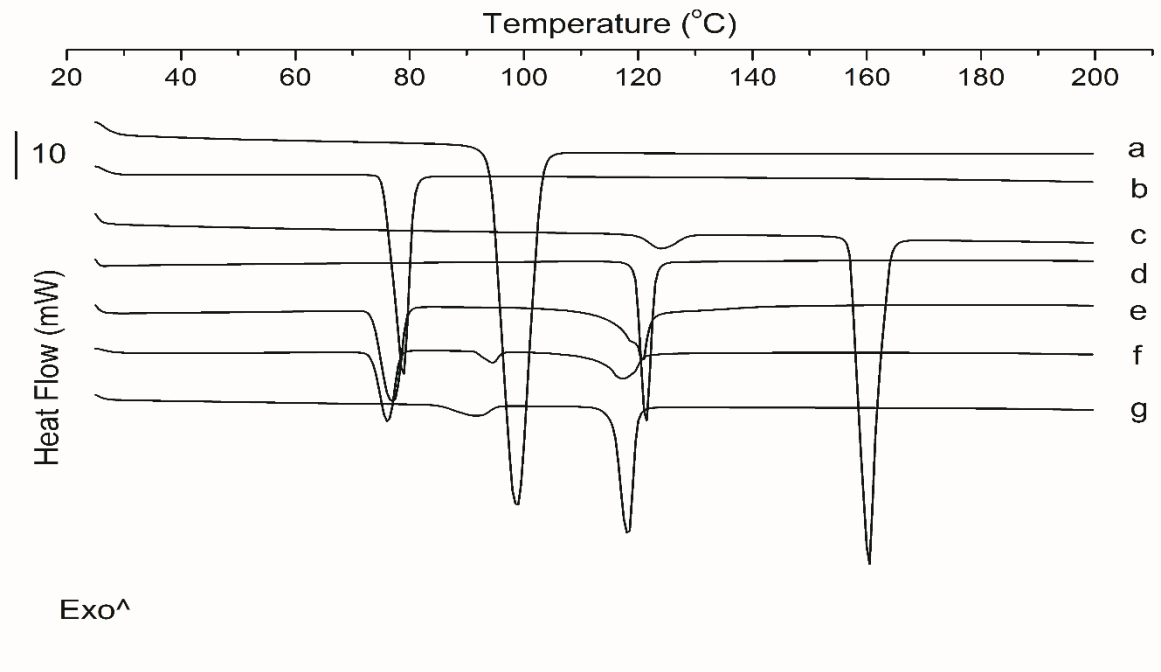

Figure 5.13. DSC analyses of cocrystal in the presence of xylitol; a) Xylitol, b) IBU, c) INA, d) Spray dried cocrystal, e) Physical mixture of IBU:INA 1:1 molar ratio, f) Physical mixture of IBU, INA 90 % and Xylitol 10 %, g) Hot melt extruded IBU:INA 90 %, Xylitol 10 %.

The hot melt extruded products with Soluplus and PVP K15 were also analysed (Figure 5.14). The HME-S-10 formulation showed an endothermic peak attributable to a eutectic melting, as well as a cocrystal melt. It is likely that the eutectic phase comprises IBU and INA, as Bragg peaks attributable to INA were observed in the PXRD diffractogram (Figure 5.8). The HME-P-10 formulation showed a melting event attributable to the cocrystal, as well as a depressed INA melt, indicating that only crystalline INA was observed by DSC, and any excess IBU was rendered amorphous.

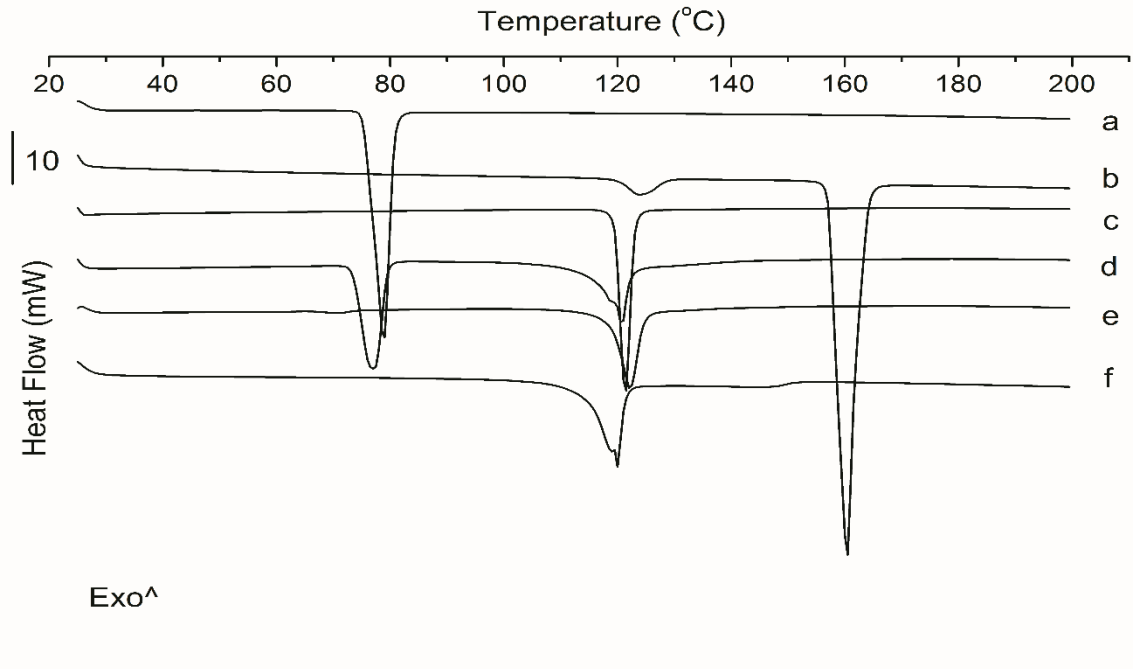

Figure 5.14. DSC analyses of Cocrystal in the presence of Soluplus and PVP K15; a) IBU, b) INA, c) Spray dried cocrystal, d) Physical mixture of IBU and INA at 1:1 molar ratio, e) Hot melt extruded IBU:INA 90 %, Soluplus 10 %, f) Hot melt extruded IBU:INA 90 %, PVP K15 10 %.

It should be noted that TGA experiments were performed on the raw materials prior to HME to demonstrate suitability of the processing temperatures used. All chemicals showed less than 5 % mass loss at the extrusion processing temperature, with the exception of PVP K15. However, the weight loss observed for PVP K15 can mainly be attributed to water loss. Results of TGA experiments can be seen in Figure A.3.16, Appendix 3.

Cocrystal: excipient (ratio, % w:w)	**Method of production**	**Result**	**Cocrystal melting temperature (ºC)**	**ΔH_f (J/g)**	**Excipient/ other melting temperature (ºC)**	**ΔH_f (J/g)**
IBU:INA	Spray drying (from ethanol)	Cocrystal	119.33 ± 0.14	139.10 ± 0.98	N/A	N/A
IBU:INA	Spray drying (from isopropanol)	Cocrystal	119.31 ± 0.16	138.64 ± 0.25	N/A	N/A
IBU:INA	Solvent evaporation from isopropanol	Cocrystal	119.72 ± 0.09	139.43 ± 0.56	N/A	N/A
IBU:INA, mannitol (90:10 % w/w) (SD-M-10)	Spray drying	Cocrystal	118.48 ± 0.16	123.45 ± 1.75	150.37 ± 0.21	4.04 ± 0.56
IBU:INA, mannitol (70:30 % w/w) (SD-M-30)	Spray drying	Cocrystal	117.90 ± 0.06	91.30 ± 2.16	150.07 ± 0.11	70.43 ± 2.74
IBU: INA, mannitol (50:50 % w/w) (SD-M-50)	Spray drying	Cocrystal	117.09 ± 0.18	59.55 ± 0.50	151.94 ± 0.54	135.12 ± 1.78
IBU:INA, xylitol (90:10 % w/w) (HME-X-10)	HME	Cocrystal	115.28 ±0.07	119.66 ± 2.27	84.95 ± 0.16	21.98 ± 0.82
IBU:INA, Soluplus (90:10 % w/w) (SD-S-10)	Spray drying	Cocrystal	118.35 ± 0.01	103.01 ± 1.48	N/A	N/A
IBU:INA, Soluplus (85:15 % w/w) (SD-S-15)	Spray drying	Cocrystal, amorphous API and crystalline coformer	117.78 ± 0.13	67.34 ± 1.04	123.17 ±0.47	0.15 ± 0.06
IBU:INA, Soluplus (80:20 % w/w) (SD-S-20)	Spray drying	Cocrystal, amorphous API and crystalline coformer	115.57 ± 0.53	48.69 ± 1.19	122.39 ± 0.57	1.03 ± 0.29
IBU:INA, Soluplus (70:30 % w/w) (SD-S-30)	Spray drying	Cocrystal, amorphous API and crystalline coformer	108.82 ± 0.42	26.98 ± 0.76	118.77 ± 0.34	4.29 ± 0.23
IBU:INA, Soluplus (90:10 % w/w) (HME-S-10)	HME	Cocrystal, crystalline coformer and crystalline and amorphous API	118.30 ± 0.40	77.06 ± 1.54	65.81 ± 1.03	2.35 ± 0.49
IBU:INA, PVP K15 (90:10 % w/w) (SD-P-10)	Spray drying	Cocrystal, amorphous API/coformer	117.58 ± 0.16	90.30 ± 1.24	N/A	N/A
IBU:INA, PVP K15 (80:20 % w/w) (SD-P-20)	Spray drying	Cocrystal, amorphous API and crystalline coformer	111.67 ± 0.30	43.49 ± 1.35	119.31 ± 0.48	4.73 ± 0.34
IBU:INA, PVP K15 (90:10 % w/w) (HME-P-10)	HME	Cocrystal, amorphous API and crystalline coformer	114.31 ± 0.11	61.11 ± 2.60	139.22 ± 0.46	3.98 ±0.77

Table 5.4. Summary table including thermal events of all spray dried and hot melt extruded systems. The ratio of IBU:INA cocrystal was 1:1 molar ratio for all systems.

5.2.4 Investigation of H-bonding interactions by Fourier Transform infrared spectroscopy

The FTIR spectra of IBU, INA, cocrystal, mannitol, xylitol, Soluplus, PVP K15, the hot melt extruded system with xylitol and the spray dried formulations with mannitol, Soluplus and PVP K15 are presented. The FTIR spectra of the co-spray dried systems with mannitol are presented in Figure 5.15, while the FTIR analyses of the co-spray dried systems with Soluplus and PVP K15, and the hot melt extruded formulation with xylitol are presented in Figures A.3.17-A.3.19, Appendix 3. Cocrystal formation between an API and coformer can form between supramolecular heterosynthons or homosynthons (Desiraju, 1995). The FTIR spectrum for IBU showed a broad vibrational band from 3400-2800 cm^{-1}, characteristic of O-H stretching of the carboxylic acid group. Medium intensity peaks are observed from 3100-2900 cm^{-1}, representing C-H stretching in the C-H, C-H_2 and C-H_3 groups of IBU and the C-H bonds in the aromatic ring (Vueba et al., 2008). A strong band was present at 1708 cm^{-1}, indicative of stretching of the C=O group of the carboxylic acid (Maheshwari et al., 2003). INA showed vibrational bands at 3361 cm^{-1} and 3178 cm^{-1}, representing asymmetric and symmetric stretching N-H respectively, for the H-bonded primary amide groups among closely packed INA molecules (Iogansen et al., 1977, Bakiler et al., 2007). Vibrational stretching at 1654 cm^{-1} represented the amide carbonyl group, while 1621 cm^{-1} represented bending of the N-H bond in the primary amide (Filho et al., 2006).

Some shifts in the IR peaks were observed for the cocrystal (prepared by spray drying) when compared to a physical mixture of IBU and INA, which can be attributed to H-bonding interactions between the two components. The IBU:INA cocrystal consists of two acid:amine interactions and an amide homodimer between the INA molecules. INA contains two competing H-bond acceptor sites, the pyridine N and the amide carbonyl. The nitrogen on the pyridine ring is considered a stronger H-bond acceptor than the amide carbonyl (Laurence and Berthelot, 2000). In crystalline INA, the pyridine N forms a hydrogen bond with the amide N-H. This bond is broken in the cocrystal, resulting in the formation of an N-H···O of the amide homodimer. The symmetric N-H stretching shifted from 3178 cm^{-1} to 3171 cm^{-1}, indicating the formation of the N-H···O bond in the amide

homodimer. The amide N-H asymmetric stretching shifted from 3361 cm^{-1} to 3431 cm^{-1}, representing formation of an N-H···O bond between the amide of INA and the IBU carboxylic acid carbonyl on the adjacent IBU molecule (Saha and Desiraju, 2018). NH_2 bending of INA shifted from 1621 cm^{-1} to 1630 cm^{-1}, resulting in the formation of the amide homodimer (Chow et al., 2012).

The broad peak attributable to O-H stretching in IBU is absent for the cocrystal, with the formation of a single peak at 3317 cm^{-1}, which can be attributed to H-bonding between the pyridine N and the O-H group of the carboxylic acid of IBU. The carboxylic acid carbonyl of IBU shifted from 1708 cm^{-1} to 1698 cm^{-1}, due to H-bond formation between the carbonyl and the pyridine hydrogen. The C-H bending of the pyridine ring also shifted from 794 cm^{-1} to 779 cm^{-1}. The same peaks were present when the API and coformer was co-spray dried with mannitol, xylitol, PVP K15 and Soluplus, and the hot melt extruded product with xylitol, as well as peaks attributable to the excipient, indicating that cocrystal formation occurred in the presence of the excipient.

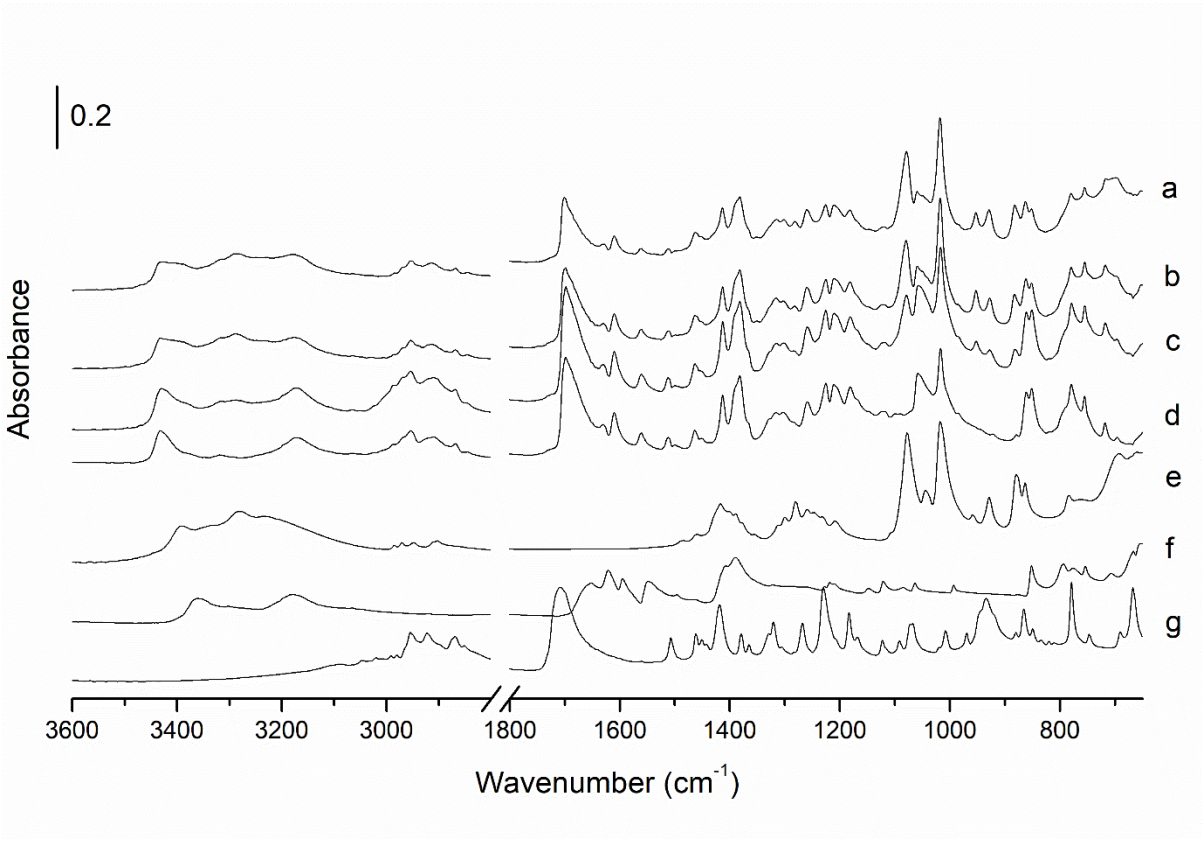

Figure 5.15. Investigation of H-bonding by FTIR. Cocrystal co-spray dried with mannitol; a) Co-spray dried IBU:INA 50 %, Mannitol 50 %, b) Co-spray dried IBU:INA 70 %, Mannitol 30 %, c) Co-spray dried IBU:INA 90 %, Mannitol 10 %, d) Cocrystal, e) Mannitol, f) INA, g) IBU.

5.2.5 Moisture uptake and sorption-desorption profile

DVS analysis of the spray dried cocrystal, the spray dried formulations with mannitol and Soluplus and the hot melt extruded cocrystal with xylitol was performed using ethanol as the probe vapour. Initial experiments were performed using water as the adsorbate. However, due to the hydrophobic nature of IBU, samples showed negligible water uptake (data not shown). It was hypothesised that any amorphous content in the samples would be crystallised when subject to moisture, which would then be detected by PXRD or DSC post analysis. The sorption and desorption isotherms of the formulations are illustrated in Figures 5.16, 5.17. The maximum ethanol sorption of the spray dried cocrystal was 0.54 % (Figures 5.16, 5.17), with most vapour uptake being between 50 % and 90 % P/P_o. The desorption profile showed a hysteresis effect from 90 % to 40 % P/P_o. No hysteresis effect was seen on the second cycle. The spray dried

formulations with mannitol showed a maximum ethanol sorption of 0.93 %, 1.63 % and 2.88 % for the SD-M-10, SD-M-30 and SD-M-50 formulations respectively. The increase in ethanol uptake with increasing mannitol loads may be due to the high surface area of the porous, spray dried mannitol particles (Littringer et al., 2011, Maa et al., 1997). The HME-X-10 formulation showed a maximum moisture uptake of 0.33 % at 90 % P/P_o, showing a hysteresis at all points from 90 % to 20 % P/P_o. A significant difference in moisture uptake between the first and second cycles was not seen for any system, indicating that the spray dried samples contained a negligible amorphous content prone to crystallisation. The samples were recovered and analysed by PXRD and DSC. No change in solid form was observed with any of the systems containing mannitol as carrier excipient post DVS analysis (Figure A.3.20, Appendix 3).

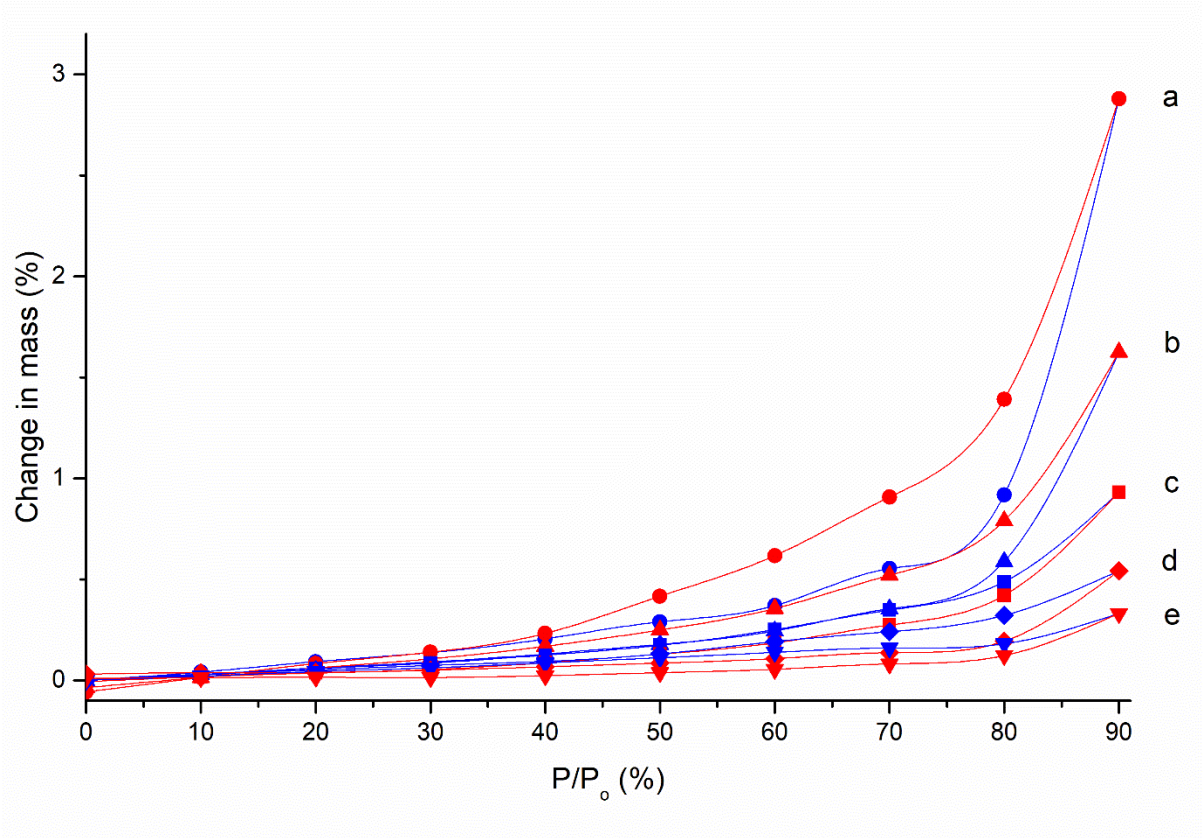

Figure 5.16. DVS sorption (blue) and desorption (red) isotherms of co-spray dried systems with mannitol and HME with xylitol using ethanol as the probe vapour; a) Co-spray dried IBU:INA 50 %, mannitol 50 %, b) Co-spray dried IBU:INA 70 %, mannitol 30 %, c) Co-spray dried IBU:INA 90 %, mannitol 10 %, d) Spray dried cocrystal, e) Hot melt extruded IBU:INA 90 %, xylitol 10 %.

The co-spray dried systems with Soluplus all showed a significantly higher moisture uptake than the co-spray dried systems with mannitol. This can be mainly attributed to the amorphous nature of Soluplus. However, no hysteresis effect was observed at any P/P_o step. The ethanol uptake at 90 % P/P_o was 8.29, 14.01, 18.65 and 28.64 (% w/w) for the SD-S-10, SD-S-15, SD-S-20 and SD-S-30 formulations respectively. PXRD analysis of these systems after DVS showed a Bragg peak attributable to INA at 23^o 2θ for systems containing ≥ 15 % Soluplus. This is not the case for the SD-S-10 formulation, as only peaks attributable to the cocrystal were present, suggesting that any amorphous content in this system crystallises to the cocrystal, or is stable as a glass solution at this ratio (Figure A.3.21, Appendix 3).

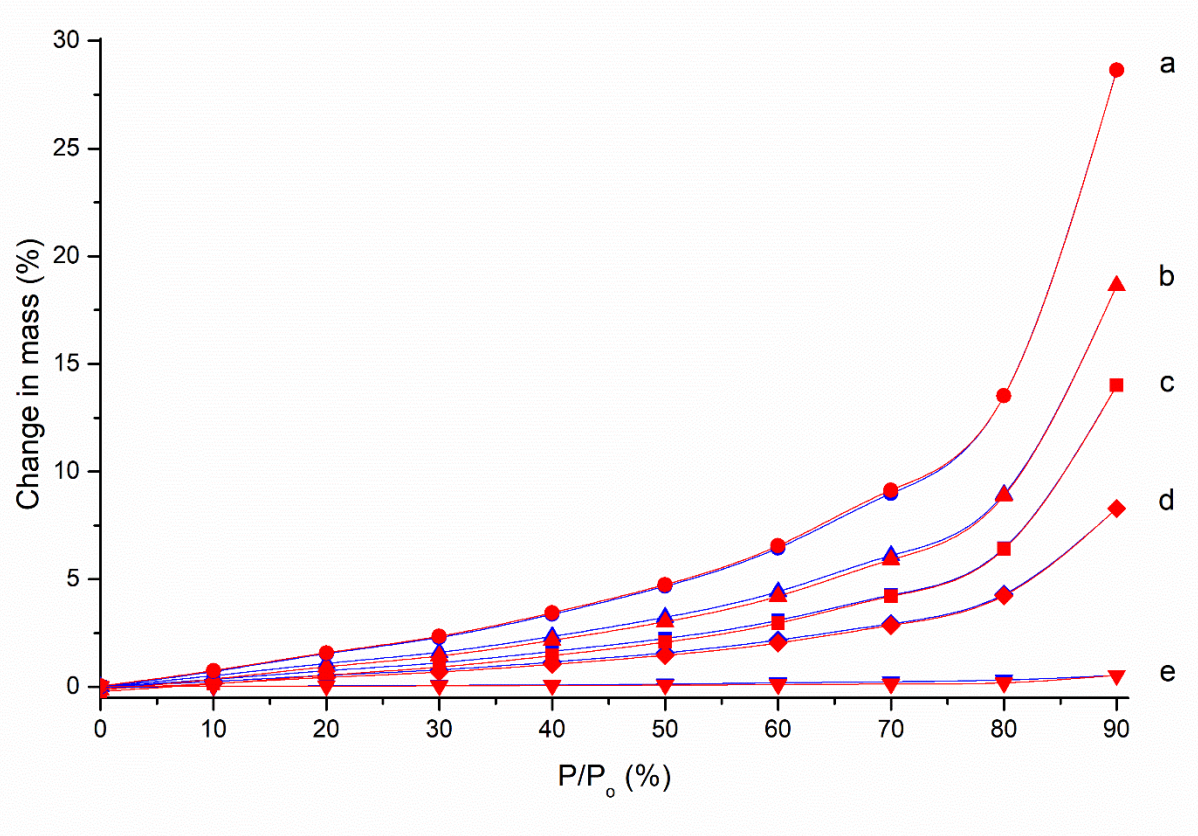

Figure 5.17. DVS sorption (blue) and desorption (red) isotherms of co-spray dried systems with Soluplus using ethanol as the probe vapour; a) Co-spray dried IBU:INA 70 %, Soluplus 30 %, b) Co-spray dried IBU:INA 80 %, Soluplus 20 %, c) Co-spray dried IBU:INA 85 %, Soluplus 15 %, d) Co-spray dried IBU:INA 90 %, Soluplus 10 %, e) Spray dried cocrystal.

5.2.6 Particle size distribution (PSD)

PSD analysis of the spray dried formulations and hot melt extruded formulation were evaluated (Table 5.5). Spray drying resulted in a particle size reduction when compared to the raw API and coformer materials. The spray dried cocrystal displayed a D_{50} of 6.92 ± 0.13 µm. A similar particle size was measured in the hot melt extruded product with xylitol after cryomilling (6.63 ± 0.36 µm). An increase in D_{50} was observed when mannitol was added compared to the cocrystal spray dried alone, with the largest particle size being the formulation containing 50 % mannitol. The samples which resulted in cocrystal formation with the amorphous excipients, Soluplus and PVP K15, displayed a 1.7 and 1.6-fold higher D_{50} value of 11.75 ± 0.27 µm and 10.95 ± 0.46 µm, respectively, compared to the spray dried cocrystal without excipients.

5.2.7 Morphology characterisation by SEM

The spray dried IBU:INA cocrystal presented as plate shaped particles, with a significantly smaller particle size than the raw materials (Figure 5.18). Co-spray drying of the cocrystal components with mannitol and Soluplus resulted in cocrystal plates, whereas more spherical particles were obtained when PVP K15 was used as the carrier excipient. The smaller particle size of the spray dried particles could result in poorly flowing and cohesive powder from a manufacturing point of view, but this could be negated by altering spray drying parameters, such as decreasing the airflow of the drying gas, and increasing the feed rate and concentration of the feed solution (Cal and Sollohub, 2009); however, this is not the main aim of this work and has not been further investigated.

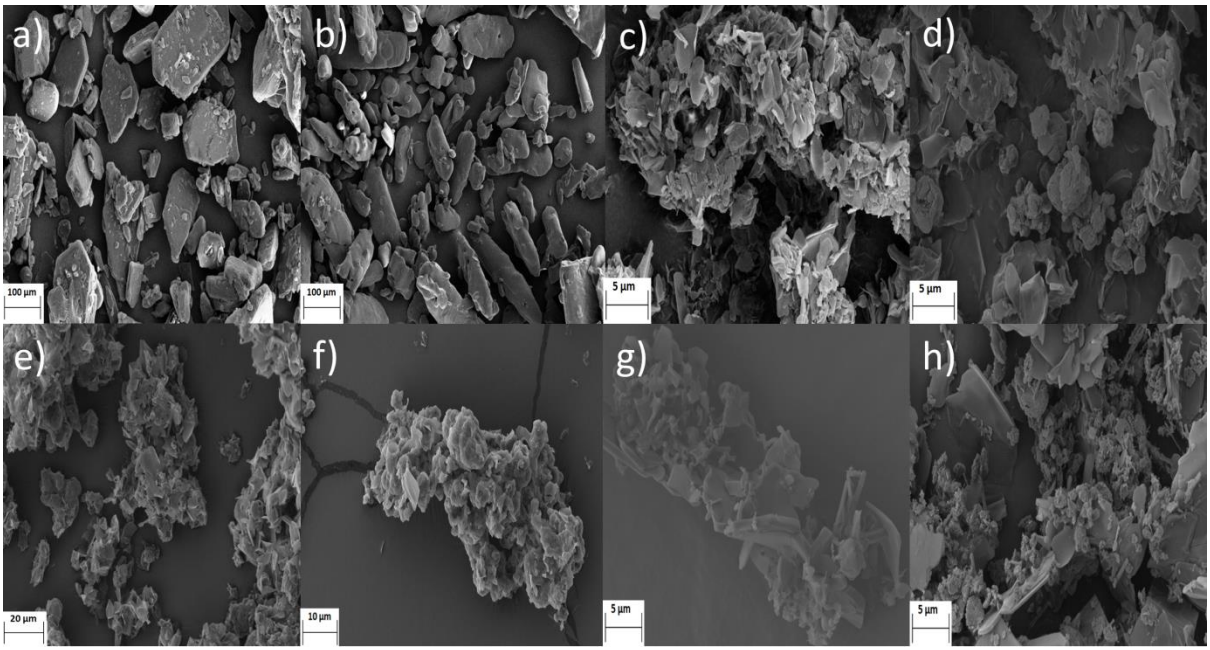

Figure 5.18. SEM images. Key: a) IBU, b) INA, c) Spray dried cocrystal, d) Spray dried IBU:INA 90 %, mannitol 10 %, e) Spray dried IBU:INA 90 %, Soluplus 10 %, f) Spray dried IBU:INA 90 %, PVP K15 10 %, g) Hot melt extruded IBU:INA 90 %, xylitol 10 %, h) Spray dried IBU:INA 50 %, mannitol 50 %.

5.2.8 Dissolution studies

Constant surface area dissolution studies of the spray dried cocrystal, HME-X-10, SD-M-10, SD-S-10 and SD-P-10 at 37 ^{o}C were performed (Figure 5.19). Intrinsic dissolution studies of unprocessed IBU were also performed (Figure A.3.22, Appendix 3).

Dissolution studies of the cocrystal, SD-M-10 and HME-X-10 all resulted in similar dissolution profiles. All three formulations showed a similar IDR and release after 60 minutes. The SD-S-10 formulation showed a lower release compared to the cocrystal, while the SD-P-10 formulation showed a higher release compared to the reference cocrystal. This formulation showed a 2.3-fold greater IDR for IBU compared to the spray dried cocrystal as well as the highest release of IBU after 60 minutes amongst all the tested formulations. The highest release was for the unprocessed raw material. However, it is important to note that the starting material is different for this system, as IBU is the starting material as opposed to the cocrystal. The dissolution studies were performed in pH 7.2 phosphate buffer, a medium in which IBU is very soluble (Dhingra et al., 2010). The pH-solubility curve for cocrystals can be significantly different to that of the API (Bethune et al., 2009), which can in turn impact dissolution of the API. Therefore, dissolution of the unprocessed API may not be directly comparable with dissolution from the cocrystal when pH-solubility studies of the cocrystal have not been performed. These experiments have not been performed as part of this study.

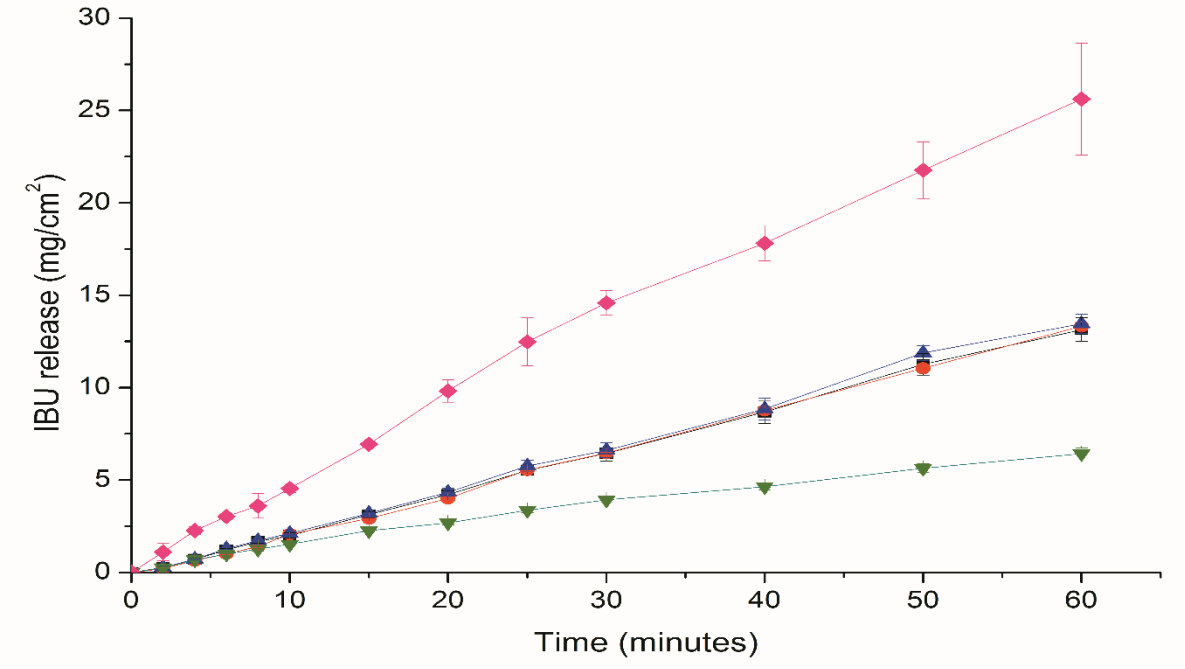

Figure 5.19. Dissolution profiles of spray dried and hot melted extruded formulations performed at 37 ºC. Key: co-spray dried IBU:INA 90 %, PVP K15 10 % (pink ◆), co-spray dried IBU:INA 90 %, mannitol 10 % (blue ▲), cocrystal produced by spray drying (black ■), hot melt extruded IBU:INA 90 %, xylitol 10 % (red ●) and co-spray dried IBU:INA 90 %, Soluplus 10 % (green ▼).

Univariate ANOVA analysis was also performed to compare the dissolution profile of the spray dried cocrystal to the dissolution profiles of the co-spray dried and hot melt extruded formulations. The co-spray dried system with PVP K15 was the only system which was statistically significantly different from the reference at each time point, indicating the IDR of this system was statistically higher than that of the cocrystal, as was the total release after 60 minutes.

Exposure of the cocrystal to the dissolution medium resulted in the transformation of the cocrystal to the individual components (Figure 5.20). PXRD analysis of the surface of the disk after dissolution revealed peaks attributable mainly to IBU. No INA peaks were observed, suggesting that the more soluble INA was in solution, leaving the less soluble IBU on the surface of the disk. A cocrystal peak was also present at 17.4 2θ. It has previously been reported that when a large difference in solubility exists between the API and the coformer, the cocrystal can be unstable in solution and recrystallisation to the individual components can occur. Recrystallisation to individual components is less

likely to occur when the solubilities of the API and coformer are similar (Schultheiss and Newman, 2009).

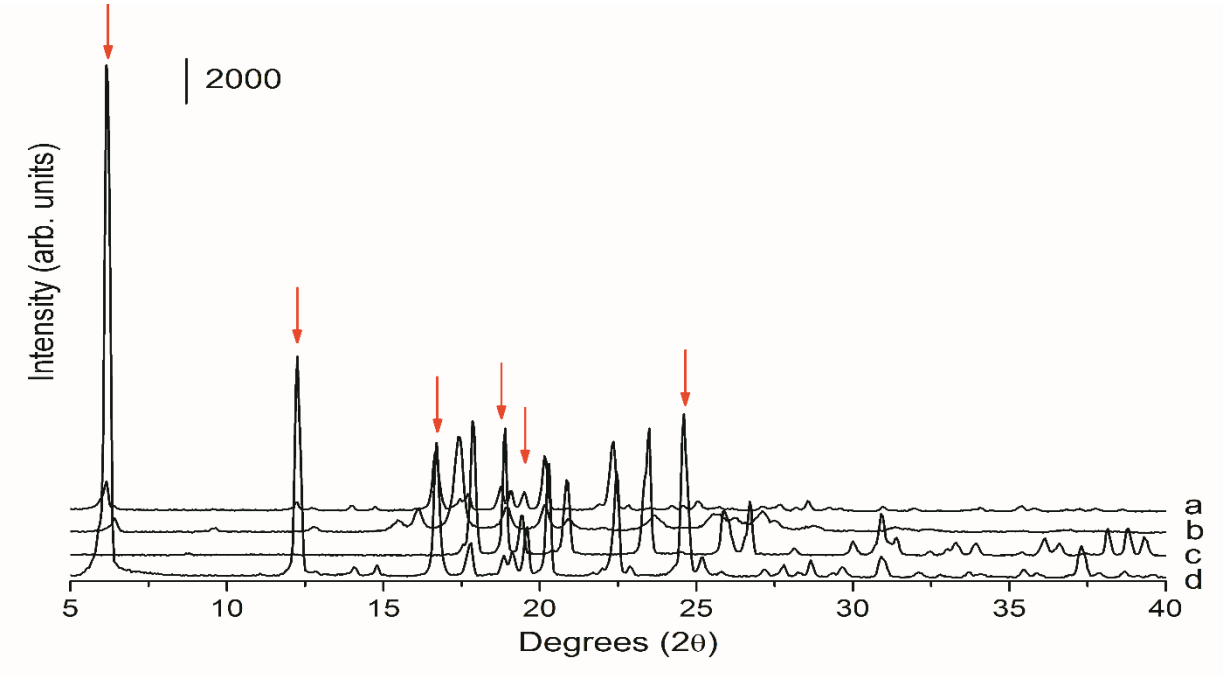

Figure 5.20. PXRD analyses after cocrystal dissolution; a) Cocrystal after dissolution, b) Cocrystal produced by spray drying, c) INA, d) IBU. Some peaks attributable to IBU are highlighted by arrows.

Transformation to the individual components was also observed when the hot melt extruded cocrystal with xylitol and the spray dried cocrystal with mannitol were analysed by PXRD after dissolution (Figure 5.21, 5.22). Bragg peaks attributable to IBU are indicated by arrows.

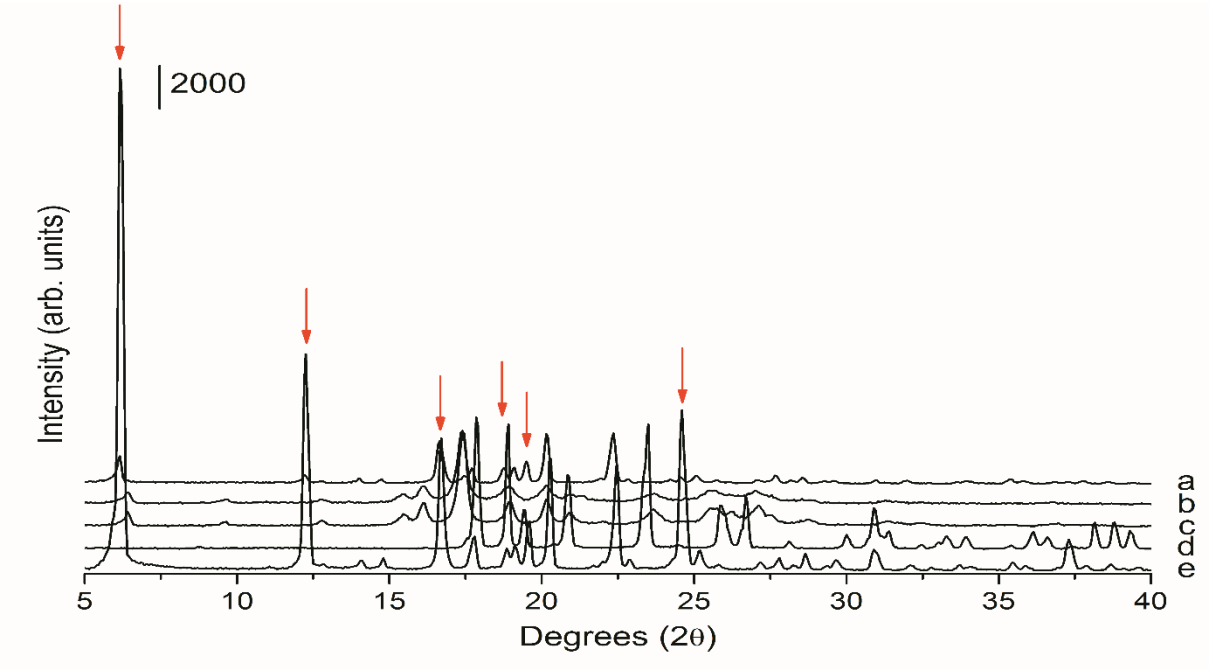

Figure 5.21. PXRD analyses after dissolution of the co-spray dried cocrystal with mannitol; a) Co-spray dried IBU:INA 90 %, mannitol 10 % after dissolution, b) Co-spray dried IBU:INA 90 %, mannitol 10 %, c) Cocrystal produced by spray drying, d) INA, e) IBU. Some peaks attributable to IBU are highlighted by arrows.

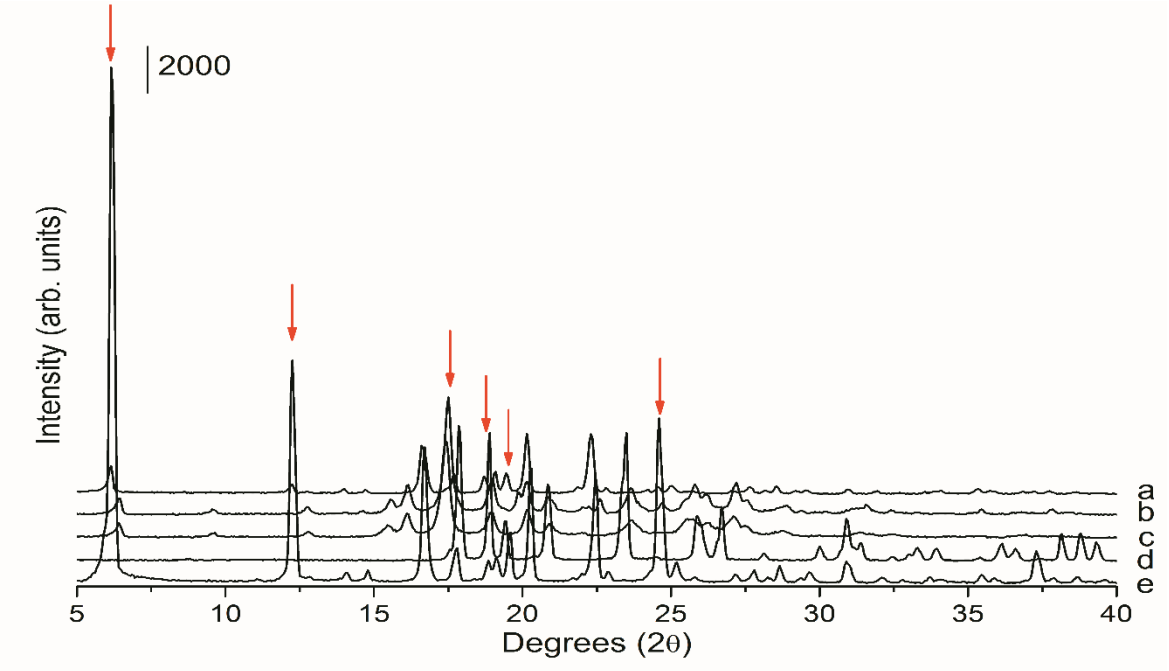

Figure 5.22. PXRD analyses after dissolution of hot melt extruded cocrystal with xylitol; a) Hot melt extruded IBU:INA 90 %, xylitol 10 % after dissolution, b) Hot melt extruded IBU:INA 90 %, xylitol 10 %, c) Cocrystal produced by spray drying, d) INA, e) IBU. Some peaks attributable to IBU are highlighted by arrows.

Analysis of the disk after dissolution of the SD-S-10 formulation showed the same diffraction peaks as the cocrystal, indicating that Soluplus polymers prevented the recrystallisation of the cocrystal to the individual components (Figure 5.23).

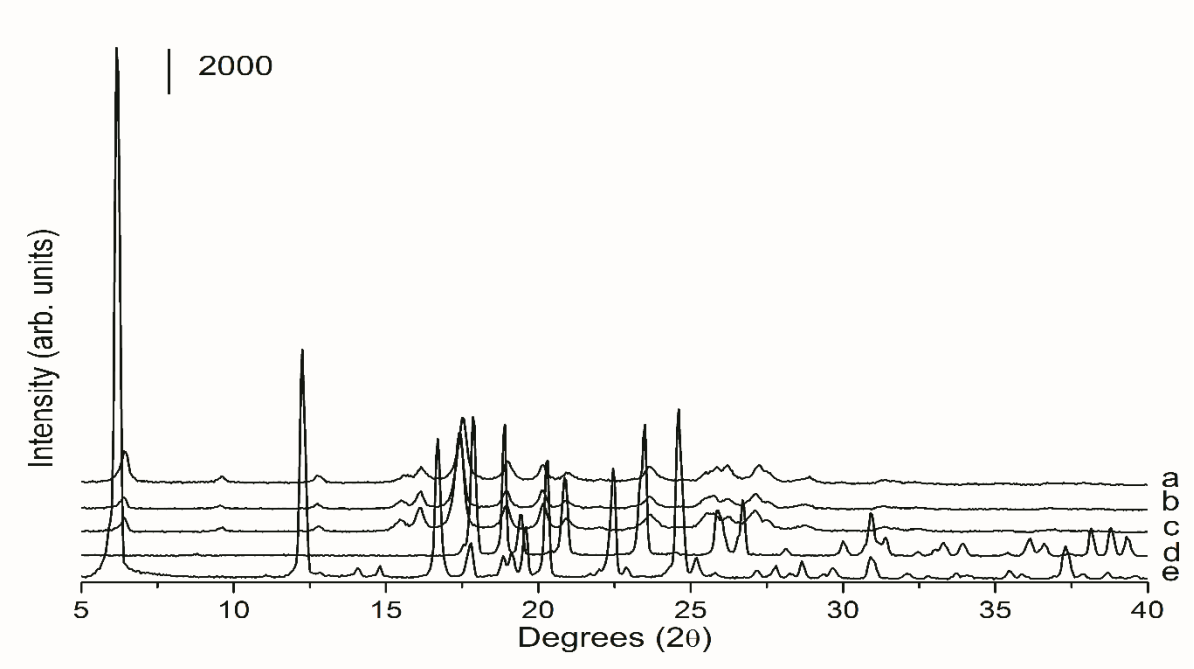

Figure 5.23. PXRD analyses of co-spray dried cocrystal with Soluplus at 37 ºC; a) Co-spray dried IBU:INA 90 %, Soluplus 10 % after dissolution, b) Co-spray dried IBU:INA 90 %, Soluplus 10 %, c) Cocrystal produced by spray drying, d) INA, e) IBU.

For the SD-P-10 formulation, PXRD analysis of the disk after dissolution showed mainly Bragg peaks attributable to the cocrystal. However, a characteristic peak of IBU at 6.15º can also be seen, suggesting some recrystallisation to the individual components, or crystallisation of trace amounts of amorphous IBU present in the system. (Figure 5.24).

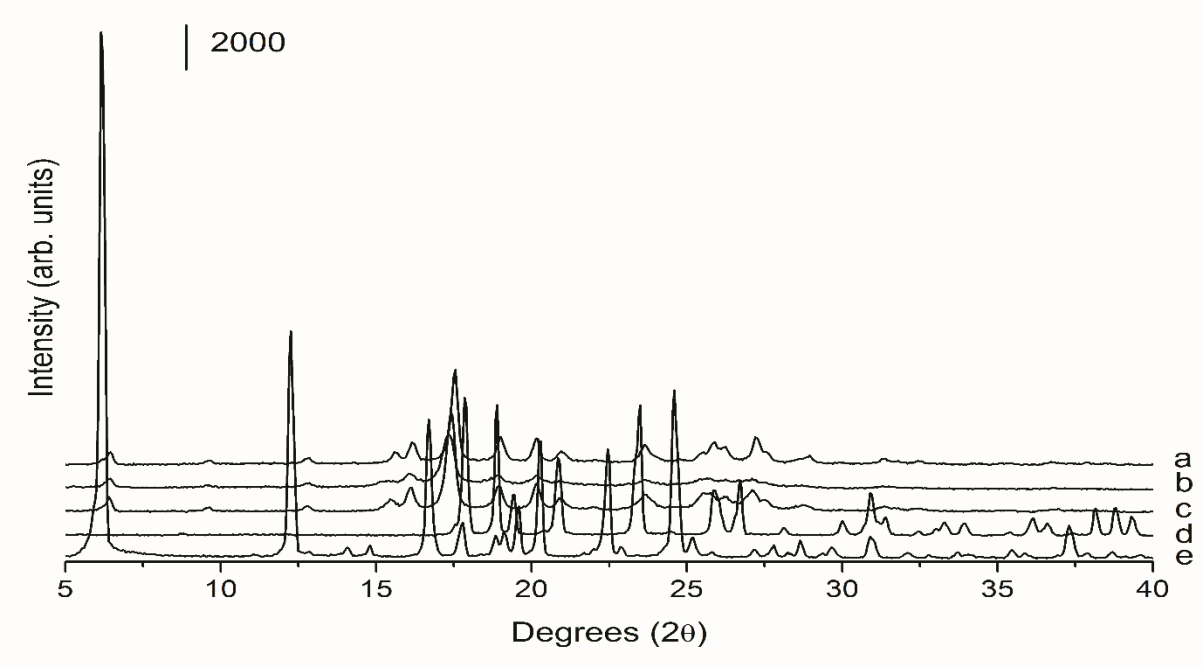

Figure 5.24. PXRD analyses of co-spray dried cocrystal with PVP K15; a) Co-spray dried IBU:INA 90 %, PVP K15 10 % after dissolution, b) Co-spray dried IBU:INA 90 %, PVP K15 10 %, c) Cocrystal produced by spray drying, d) INA, e) IBU.

The lowest IDR and release after 60 minutes of IBU was for the spray dried system with Soluplus (Table 5.5). However, the low IDR may be due to the presence of Soluplus as this excipient exhibits a lower critical solution temperature (LCST) in water near 40 ^{o}C (Hughey et al., 2013). Polymers can demonstrate good aqueous solubility at low temperature, but can demonstrate partial miscibility and separate from solution above the LCST (Feil et al., 1993). At the LCST, Soluplus chains lose hydration and progressively associate, decreasing their solubility and forming a cloudy suspension that can precipitate. This behaviour is responsible for the gel-forming property of Soluplus (Fini, 2016). Attempts to measure the IDR of IBU and carvedilol from solid dispersions containing Soluplus have resulted in lower values than expected, which has been attributed to the gelling properties of Soluplus (Genina et al., 2017).

To test our hypothesis that the lower release of IBU from the co-spray dried system with Soluplus was due to the LCST of Soluplus, dissolution studies of both this system and the spray dried cocrystal were performed at 20 ^{o}C (Figure 5.25). The dissolution rate of the cocrystal was significantly ($p<0.05$) lower than that of the co-spray dried system with Soluplus at 20 ^{o}C.

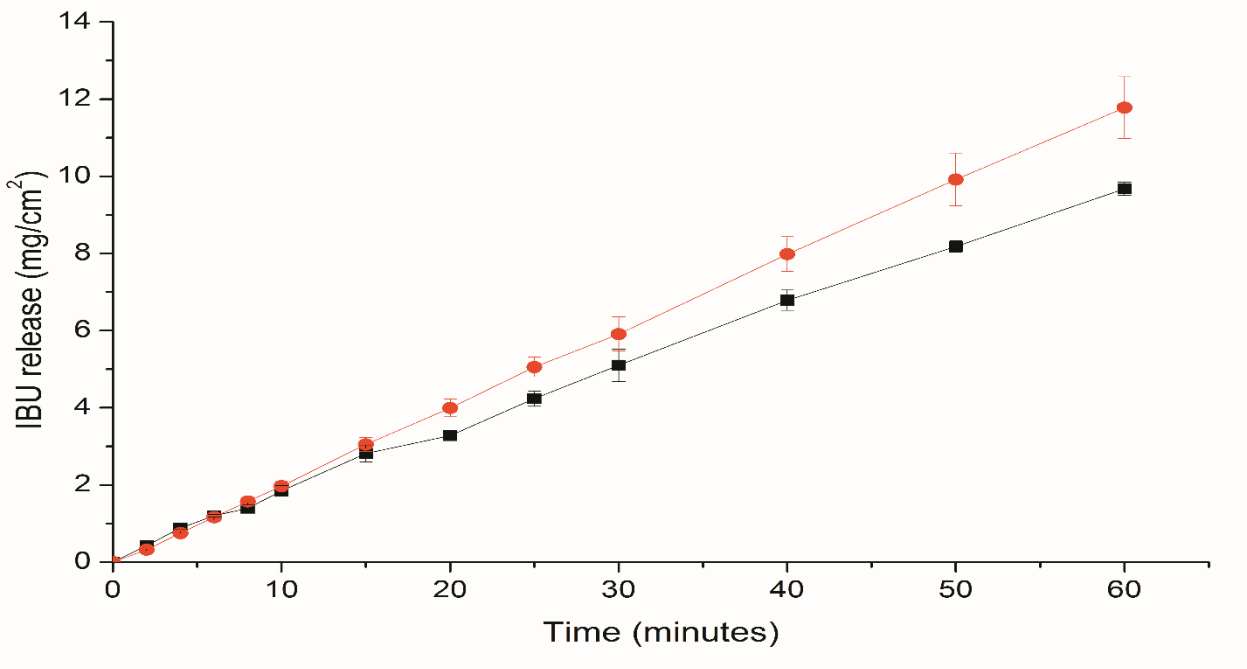

Figure 5.25. Dissolution profiles at 20 ºC of: the cocrystal produced by spray drying (black ■) and co-spray dried IBU:INA 90%, Soluplus 10% (red ●).

Disks were also analysed by PXRD after dissolution. Similar to the results obtained at 37 ºC, the diffractogram of the SD-S-10 formulation after dissolution showed the same Bragg peaks of the cocrystal after dissolution (Figure 5.26).

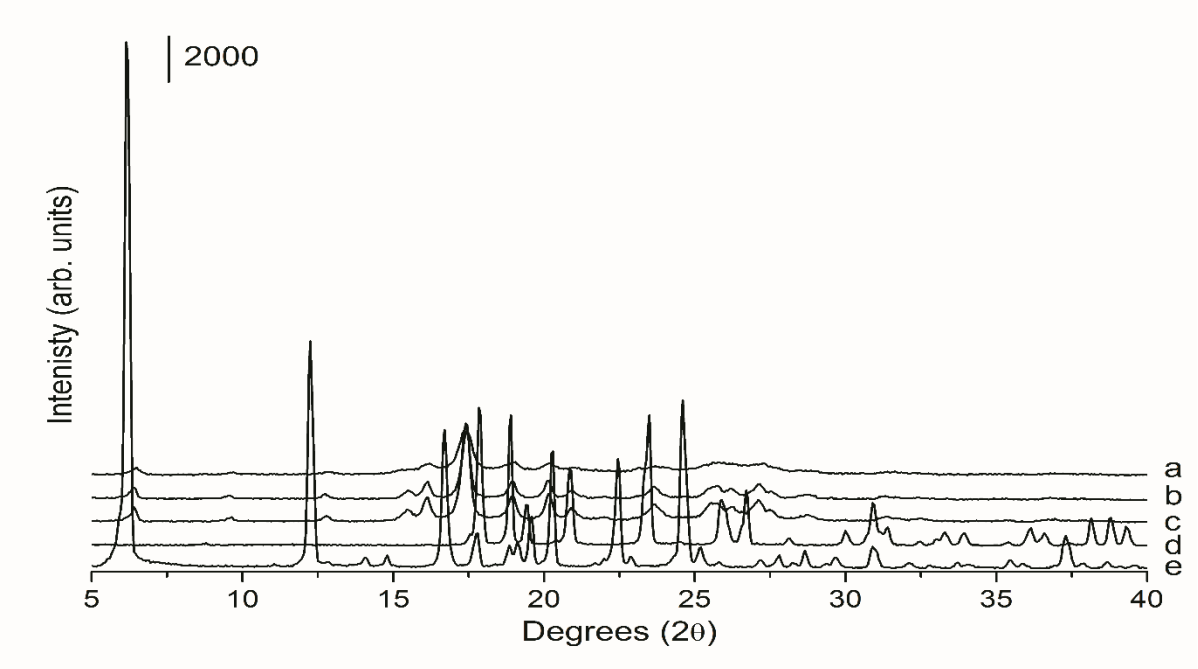

Figure 5.26. PXRD analyses of co-spray dried cocrystal with Soluplus post dissolution at 20 ºC; a) Co-spray dried IBU:INA 90 %, Soluplus 10 % after dissolution, b) Co-spray dried IBU:INA 90 %, Soluplus 10 %, c) Spray dried cocrystal, d) INA, e) IBU.

However, dissolution of the cocrystal without a carrier excipient at 20 ºC showed Bragg peaks attributable to IBU and also multiple cocrystal peaks (Figure 5.27), which differs from results at 37 ºC. This can be explained by the higher temperature, which may accelerate the dissociation of the cocrystal into its individual components.

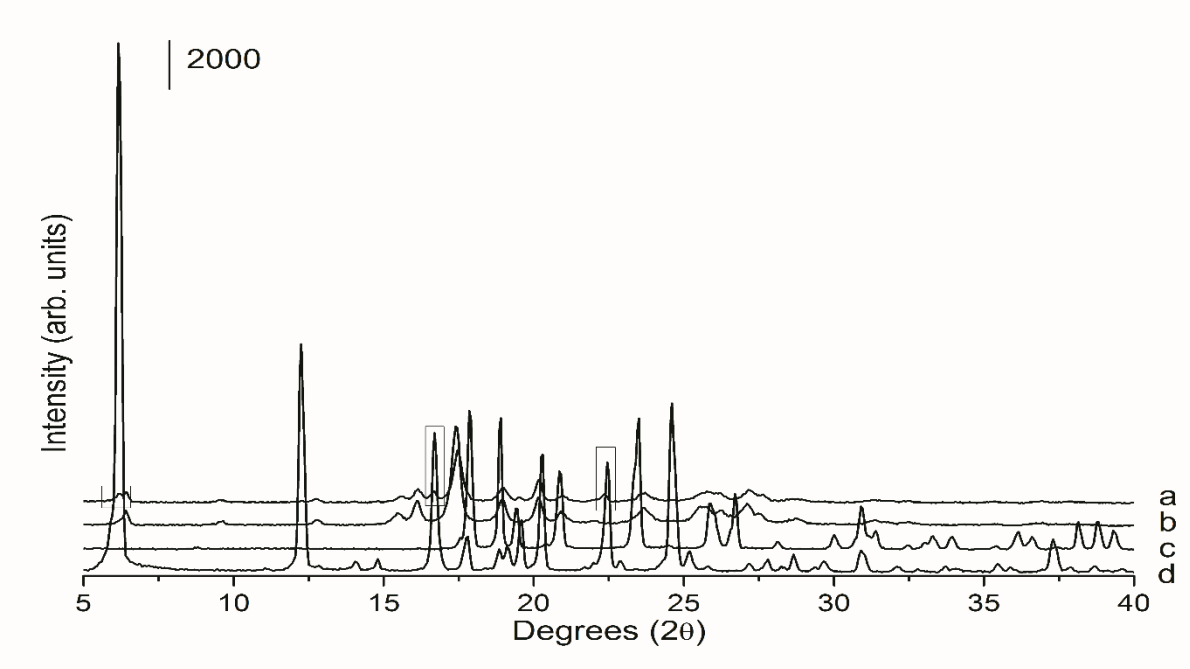

Figure 5.27. PXRD analyses cocrystal post dissolution at 20 ºC; a) Spray dried cocrystal after dissolution, b) Spray dried cocrystal, c) INA, d) IBU. Peaks of both the cocrystal and IBU can be seen after dissolution.

Table 5.5. Particle size distribution of raw materials and spray dried and hot melt extruded IBU and INA cocrystal (1:1 molar ratio). Intrinsic dissolution rates (of IBU) were calculated at 37°C for the spray dried cocrystal and those systems containing 90 % cocrystal: 10 % carrier excipient**.** Intrinsic dissolution rates were calculated over the first 10 minutes at 37 ºC.

System	**D_{50} (µm)**	**Intrinsic Dissolution Rate ($mg/cm^2/min$)**
IBU	23.69 ± 1.73	0.513 ± 0.003
INA	31.78 ± 1.74	-
Cocrystal	6.92 ± 0.13	0.199 ± 0.013
SD-M-10	9.47 ± 0.51	0.211 ± 0.006
SD-M-30	7.86 ± 0.12	-
SD-M-50	11.40 ± 0.57	-
SD-S-10	11.75 ± 0.27	0.152 ± 0.006
SD-P-10	10.95 ± 0.46	0.454 ± 0.022
HME-X-10	6.63 ± 0.36	0.207± 0.004

5.3 Conclusions

Cocrystallisation of an API and coformer in the presence of an excipient can be achieved through both spray drying and hot melt extrusion. However, the results obtained with the IBU:INA cocrystal suggest greater feasibility of spray drying over HME as a process for producing cocrystals within a carrier excipient, intended to reduce the number of unit operations required to produce a final pharmaceutical product. The use of HSP differences can be useful to predict cocrystal formation within a carrier excipient. However, ΔHSP values should not be used as the only indicator, as the manufacturing process, the ratio of carrier excipient:cocrystal and the overall miscibility among drug, coformer and carrier have also a major impact.

CHAPTER 6

Fluidised bed coating as a method to produce cocrystal coated beads

6.1 Introduction

Spray drying has previously been proven to be successful in producing pure cocrystals from solution (Alhalaweh and Velaga, 2010). Further to this, spray drying is a scalable method that is commonly used in the pharmaceutical industry. Cocrystals produced by spray drying are commonly spherical in nature (Serrano et al., 2015), which can result in advantageous flow properties compared to other cocrystal habits such as needles. However, due to the small particle size of spray dried powders, cocrystals produced by this method may have unfavourable flow properties. Cocrystals of SDM:4ASA produced by spray drying were more prone to aggregate in aqueous media compared to the cocrystal produced by solvent evaporation and milling methods. The cocrystal produced by spray drying had more hydrophobic surfaces exposed to the dissolution media, resulting in aggregation and subsequently a lower dissolution rate than cocrystals prepared by other methods (Serrano et al., 2015).

Fluidised bed spray coating has been successfully employed in the formation of drug-coated beads with enhanced dissolution properties and oral bioavailability (Kolašinac et al., 2013). One example is Sporanox^{TM}, which consists of an amorphous solid dispersion of itraconazole and hypromellose coated on sugar spheres (Namburi and Kerr, 2003). Spray coating is also employed to coat Efexor^{TM} pellets with ethyl cellulose to produce an extended release formulation. However, to the best of our knowledge, this technique has not been employed in the production of cocrystal coated beads. Research presented in the previous chapters in this thesis has determined that cocrystals can form in the presence of an excipient by spray drying and HME. The aim of this work was to assess if cocrystals can be formed by spray coating on to inert beads.

The hypothesis underpinning this work is that fluidised bed spray coating can be used to form *in situ* cocrystals deposited as a thin layer on different substrates, such as non-pareil sugar beads, resulting in particulates that are large enough to avoid aggregation in liquid medium, while improving dissolution and oral bioavailability. Quality by design (QbD) experiments (Taguchi and Box-Behnken) were performed to understand the effect of different process parameters, such as spray rate, air flow rate and nozzle air pressure, as well as formulation parameters such as size of the starter cores and the amount and type of binder excipient, on cocrystal formation during fluidized bed spray coating. The optimal parameters for loading efficiency, degree of crystallisation and yield were

identified. The cocrystal coated beads were evaluated and characterized. The SDM:4ASA cocrystal was used as the model cocrystal in this study. The spray coating process does not subject the API, coformer and excipients to high temperatures which may cause degradation, unlike the HME process. The aim of this study was to produce cocrystal loaded beads, which may then be suitable for capsule filling.

6.2 Results

6.2.1 Taguchi DoE

Seven process and formulation factors were identified, each at two levels. A Taguchi design was subsequently performed. Implementation of the design helped to identify the most important factors which would be subjected to further detailed investigation with minimal experimentation. The seven factors and three responses assessed in the Taguchi design are presented in Table 6.1. This design has the advantages of requiring minimal runs for a large number of independent variables. Screening works on the 'Pareto Principle', also known at the '80/20 rule' or the 'principle of factor sparsity', which states that roughly 80% of the effects come from 20% of the causes (Sanders, 1987).

	Factor							**Response**		
Run	**1**	**2**	**3**	**4**	**5**	**6**	**7**	**1**	**2**	**3**
1	2.5	25	1	1000	50	1	Inulin	80.87	6.18	87.68
2	1.6	35	0.7	1000	50	5	Inulin	83.58	6.96	80.24
3	1.6	25	0.7	500	30	1	Inulin	67.64	10.21	3.68
4	1.6	25	1	500	50	5	PVP K90	85.83	10.89	90.7
5	1.6	35	1	1000	30	1	PVP K90	28.51	1.18	92.8
6	2.5	35	0.7	500	50	1	PVP K90	91.70	19.32	2.77
7	2.5	25	0.7	1000	30	5	PVP K90	67.85	9.92	35.14
8	2.5	35	1	500	30	5	Inulin	81.75	2.60	71.66

Table 6.1. Taguchi design matrix for the cocrystal coated beads. Factor 1: spray rate (g/min), factor 2: airflow (m^3/hr), factor 3: atomisation pressure (bar), factor 4: bead size (μm), factor 5: amount of mass sprayed (as a percentage of total mass, which is the mass of the API, coformer and binder in solution as well as the mass of the beads), factor 6: amount of binder (%), factor 7: type of binder. Response 1: degree of crystallinity (%), response 2: loading efficiency (%), response 3: attrition (broken beads) (%).

In all cases, cocrystal formation was observed. PXRD analyses did not reveal any peaks attributable to the individual components or to the form I polymorph of the cocrystal. PXRD analyses of the experiments performed as part of the Taguchi DoE are presented in Figures 6.1, 6.2. Bragg peaks of both the crystalline beads and the cocrystal can be observed in the PXRD diffractogram. Bragg peaks attributable to the cocrystal are observed in the spray coated formulations at 11.9, 13.65 and 24.4 2θ. Bragg peaks attributable to the non-pareil beads are observed at 11.8, 19 and 22.15 2θ. No differences were seen in the PXRD diffractogram between beads of different sizes, as the beads were crushed before PXRD analysis.

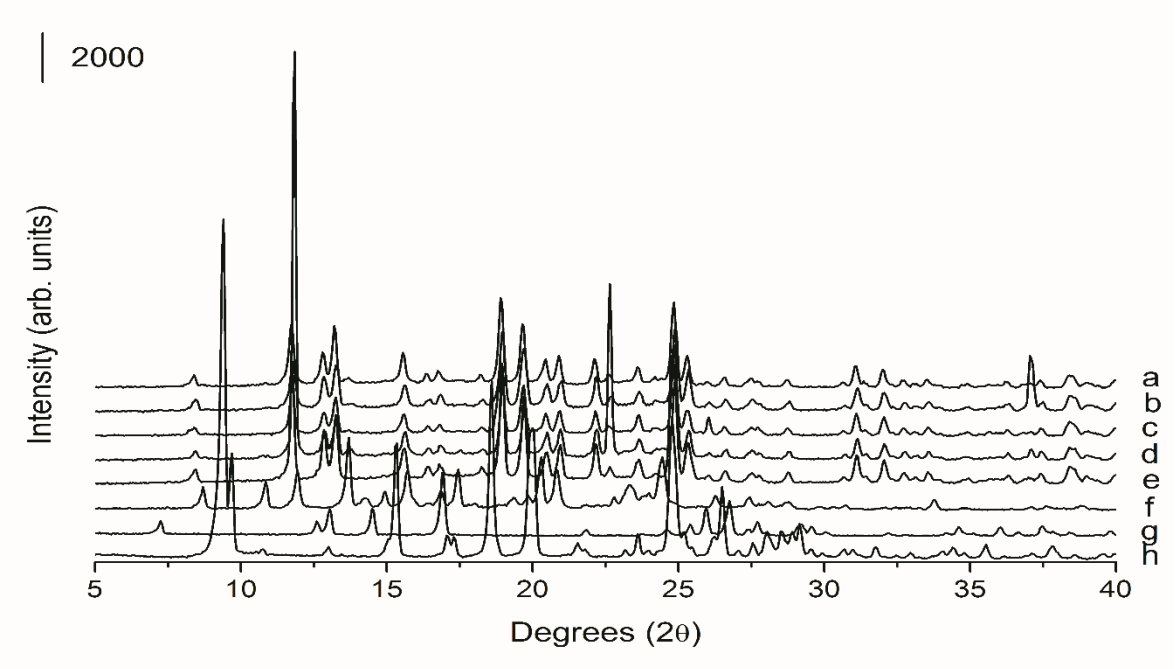

Figure 6.1. PXRD analyses of experiments performed as part of Taguchi DoE with 30 % spray dried mass. a) Run 8, b) Run 7, c) Run 5, d) Run 3, e) Blank beads, f) Cocrystal produced by solvent evaporation, g) 4ASA, h) SDM.

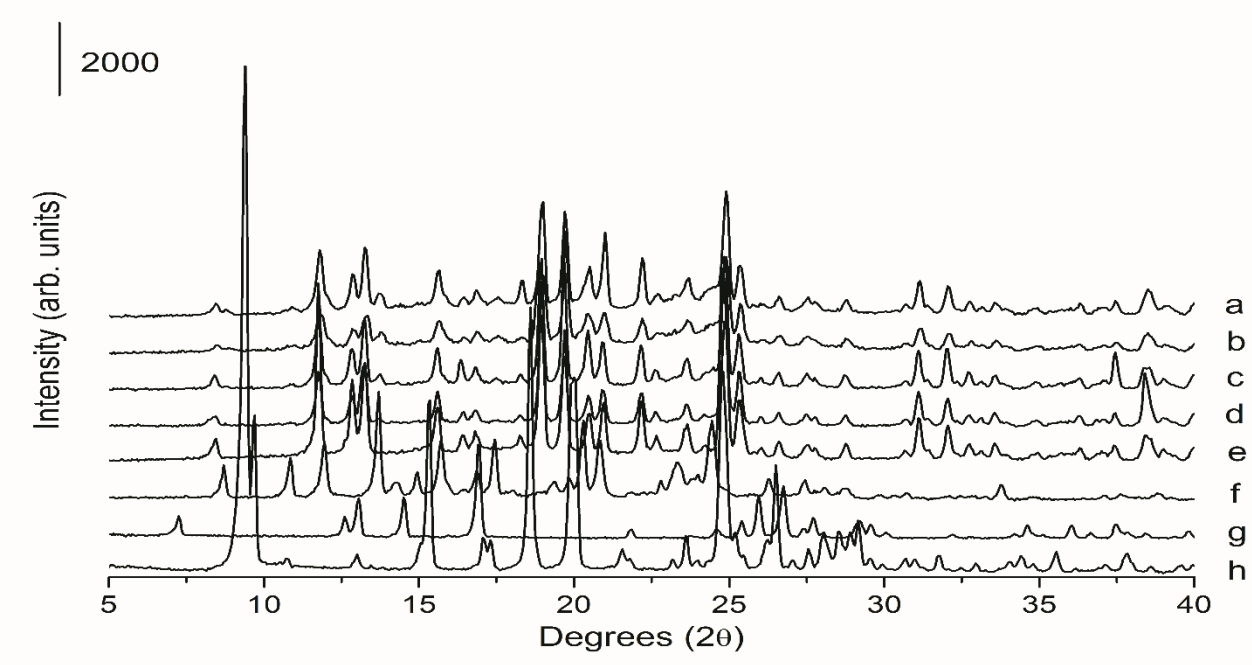

Figure 6.2. PXRD analyses of experiments performed as part of Taguchi DoE with 50 % spray dried mass. a) Run 6, b) Run 4, c) Run 2, d) Run 1, e) Blank beads, f) Cocrystal produced by solvent evaporation, g) 4ASA, h) SDM.

MTDSC analyses of all samples from experimental runs were also performed. SDM showed a melting onset at 193.94 ± 0.56 ^{o}C (125.76 ± 2.59 J/g). The melting temperature is slightly lower than previously reported (Grossjohann et al., 2015), however this can be attributed to the lower heating rate. DSC analysis of 4ASA at the lower heating rate of 5 ^{o}C/min resulted in thermal degradation of the coformer, due to decarboxylation of 4ASA to 3-aminophenol (Rotich et al., 2001). This was not previously observed at the heating rate of 10 ^{o}C/min (Grossjohann et al., 2015), which was also seen in chapters 3 and 4. Melting of the non-pareil beads occurred at 185.61 ± 0.82 ^{o}C. Melting of the cocrystal produced by spray drying occurred at 157.67 ± 0.26 ^{o}C. A melting peak attributable to SDM is also observed. This peak is only observed at the lower heating rate. In the majority of cases, melting of the cocrystal coated beads occurred at a higher temperature than the cocrystal produced by spray drying. This may be due to a greater number of crystal imperfections due to the spray drying process compared to spray coating. For the spray coated beads, two melt endotherms are present, one attributable to the cocrystal and another attributable to the beads. DSC analyses of all raw materials and experiments performed as part of the Taguchi DoE are presented in Figures 6.3, 6.4.

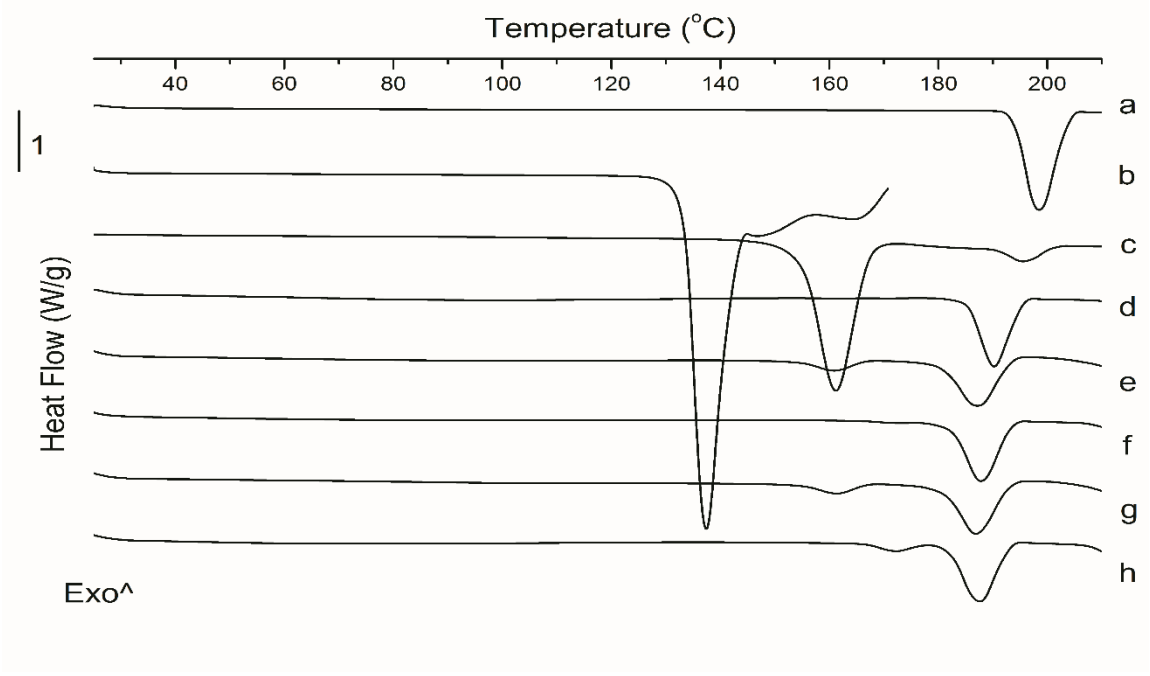

Fig 6.3. DSC curves of experiments performed as part of the Taguchi DoE with 30 % sprayed mass. a) SDM, b) 4ASA, c) Cocrystal produced by spray drying, d) Non-pareil beads, e) Run 3, f) Run 5, g) Run 7, h) Run 8.

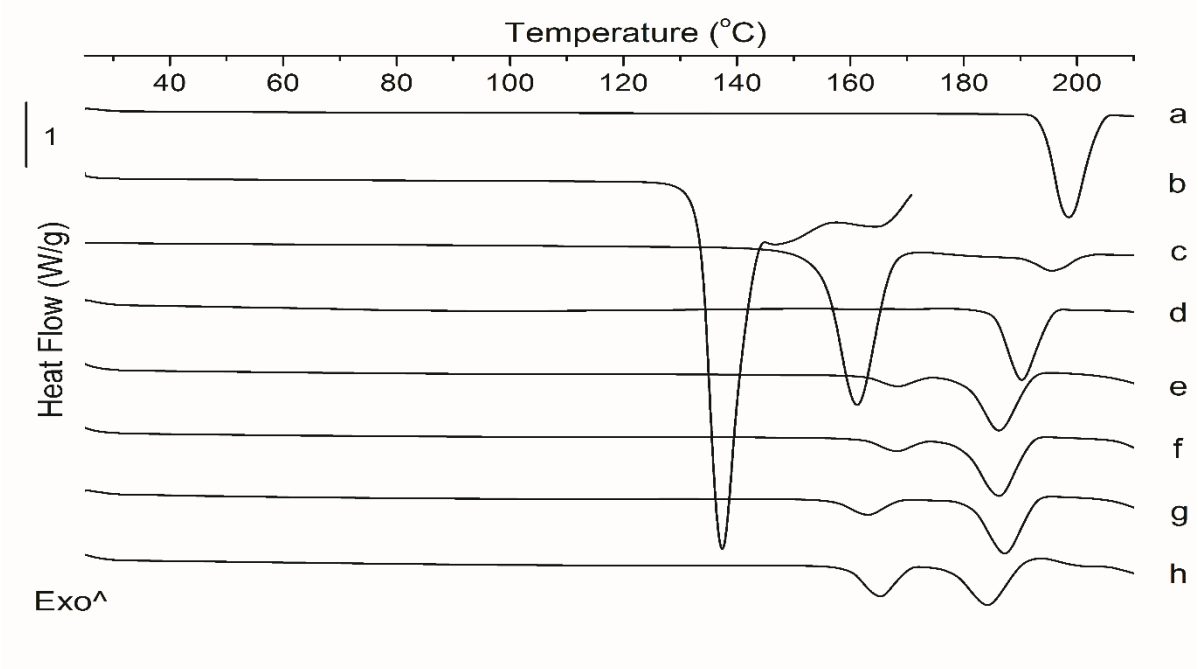

Fig 6.4. DSC curves of experiments performed as part of the Taguchi DoE with 50 % sprayed mass. a) SDM, b) 4ASA, c) Cocrystal produced by spray drying, d) Non-pareil beads, e) Run 1, f) Run 2, g) Run 4, h) Run 6.

In Figure 6.5, Pareto charts show the most influential variables during the spray coating process. The Bonferroni limit in this case is higher than the t-value, as the Bonferroni correction required that the individual significance level be divided by the number of effects. The atomisation pressure had a significant negative effect on the loading efficiency and promoted attrition, meaning that the higher the pressure, the lower the loading efficiency and the smaller the amount of intact beads at the end of the process. For this reason, this effect was studied in more depth in the second DoE (Box-Behnken), which included three levels. The amount of sprayed mass had an overall positive effect on the process, in particular, the higher the amount of sprayed mass, the higher the degree of crystallinity and the loading efficiency. As for the atomisation pressure, three levels of sprayed mass were established in the Box-Behnken design to explore in more detail. The nitrogen flow rate had a negative impact on the loading efficiency probably because, at higher rates, a greater percentage of sprayed solution was stuck onto the filters located at the top part of the fluidised bed coater. For this reason, the lower flow rate (25 m^3/h) was selected and kept constant in the second DoE. Lower flow rates were not tested as beads did not flow well when the flow rate was below 20 m^3/h.

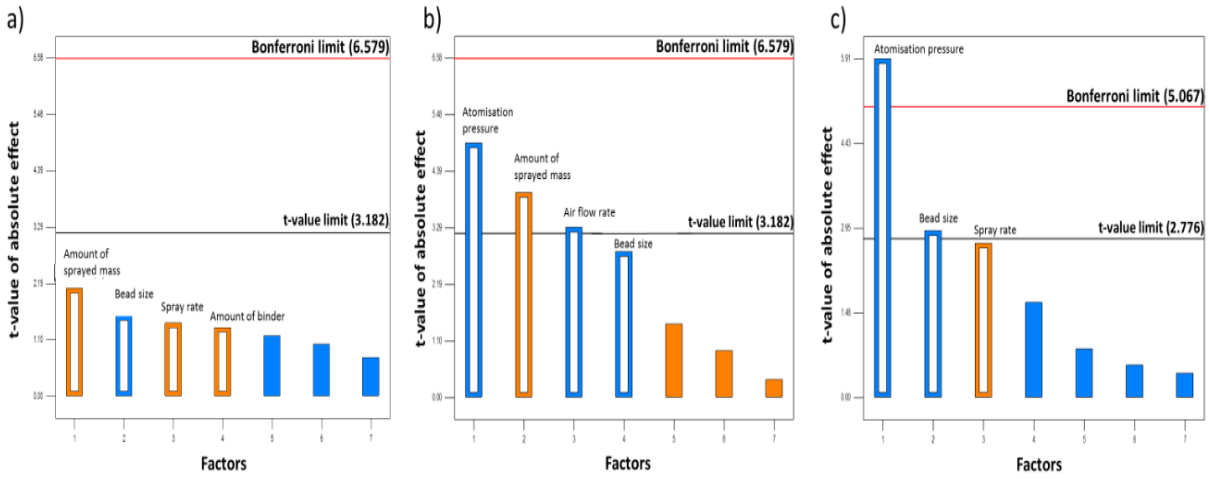

Figure 6.5. Pareto charts depicting the influence of the seven factors assessed in the Taguchi design. a) Degree of crystallinity, b) Loading efficiency, c) Attrition. Orange bars represent a positive effect, while blue bars reflect a negative effect.

Regarding the bead size, the larger size (1000 µm) resulted in a negative effect on the loading efficiency, degree of crystallinity and attrition. The reduced loading efficiency and crystallinity are a consequence of the smaller surface area available for coating compared to the 500 and 250 µm beads. Also, due to the larger size, the 1000 µm beads impact with more energy on the top of the filter, promoting attrition. For all these reasons, a 500 µm bead size was selected and kept constant in the second DoE. A smaller particle size was not included in the Box-Behnken design because, in preliminary assessments, it was observed that the electrostatic interactions of the particles were much higher when 250 µm beads were used, resulting in poor flow and sticking to the walls of the equipment and thus, high variability in the content uniformity.

The spray rate of the feed solution positively affected the degree of crystallinity and prevented attrition, so the higher spray rate (2.5 g/min) was kept constant in the next DoE. Higher spray rates were not selected because in preliminary studies it was observed that very fast rates (> 3 g/min) resulted in agglomeration of beads as the drying time was insufficient.

Regarding the amount and type of binder, no significant effect was observed, probably because the range selected was insufficient to observe differences in the responses. For this reason, the amount of binder included in the formulation was assessed in the second DoE at three different levels. Based on preliminary studies, PVP K90 was selected as the

binder, as inulin promoted higher attrition levels than PVP K90. PVP K90 was chosen over other grades of PVP, as this chain length typically results in high viscosity and better binding properties than lower chain PVP grades (Agnese et al., 2010).

While the experiments performed as part of the Taguchi DoE gave some information on the most important input factors, three levels and a wider range for each factor were analysed for the Box-Behnken DoE. This was done to ensure that the optimal parameters for each input factor were within the range of the DoE.

6.2.2 Box-Behnken DoE

Seventeen experimental runs were performed as part of the Box-Behnken DoE. Three factors were assessed, each at three levels, and five centre point experiments were performed. The factors, levels and responses are presented in Table 6.2.

	Factor			**Response**				
Run	**1**	**2**	**3**	**1**	**2**	**3**	**4**	**5**
1	0.6	45	12.5	24.27	81.58	0.01	76.00	0.09
2	1	30	20	14.72	65.95	1.89	83.84	0.50
3	0.8	45	20	21.84	70.87	2.32	70.56	0.32
4	1	30	5	12.4	88.29	2.27	76.84	1.47
5	0.8	30	12.5	13.84	82.27	4.57	75.66	0.71
6	0.6	30	5	11.68	88.73	0.50	79.20	0.87
7	0.6	30	20	14.27	78.66	0.28	83.94	20.8
8	0.8	30	12.5	15.34	84.50	0.56	83.65	1.28
9	0.6	15	12.5	7.27	77.94	0.63	91.90	20.8
10	0.8	15	5	6.53	81.89	1.23	90.01	1.84
11	0.8	45	5	22.43	93.60	0.34	90.64	0.15
12	1	15	12.5	4.93	76.29	19.41	76.60	2.83
13	0.8	30	12.5	16	83.39	0.49	85.00	0.24
14	1	45	12.5	20.84	96.21	0.13	75.71	0.33
15	0.8	15	20	6.89	84.25	1.79	90.38	0.74
16	0.8	30	12.5	15.84	79.75	0.62	84.08	0.03
17	0.8	30	12.5	13.32	86.17	5.35	75.64	5.09

Table 6.2. Box-Behnken design matrix for cocrystal coated beads. Factor 1: atomisation pressure (bar), factor 2: amount of sprayed mass (%), factor 3: amount of binder (%). Response 1: loading efficiency (%), degree of crystallinity (%), response 3: attrition (% broken beads), response 4: yield (%), response 5: Relative standard deviation of content uniformity (RSD) (%).

Cocrystal formation occurred in all cases, as confirmed by PXRD. Peaks attributable to the cocrystal are more prominent on the runs containing 45 % sprayed mass. This can be

attributed to sprayed mass having a positive effect on degree of crystallinity and loading efficiency of the cocrystal. In all cases, only Bragg peaks attributable to the beads and the form II polymorph of the cocrystal were observed. No peaks of SDM, 4ASA or the form I polymorph were observed in the PXRD diffractogram. PXRD analyses of experiments performed as part of the Box-Behnken DoE are presented in Figures 6.6 – 6.8. PXRD analyses of the centre points are presented in Figure A.4.1 (Appendix 4).

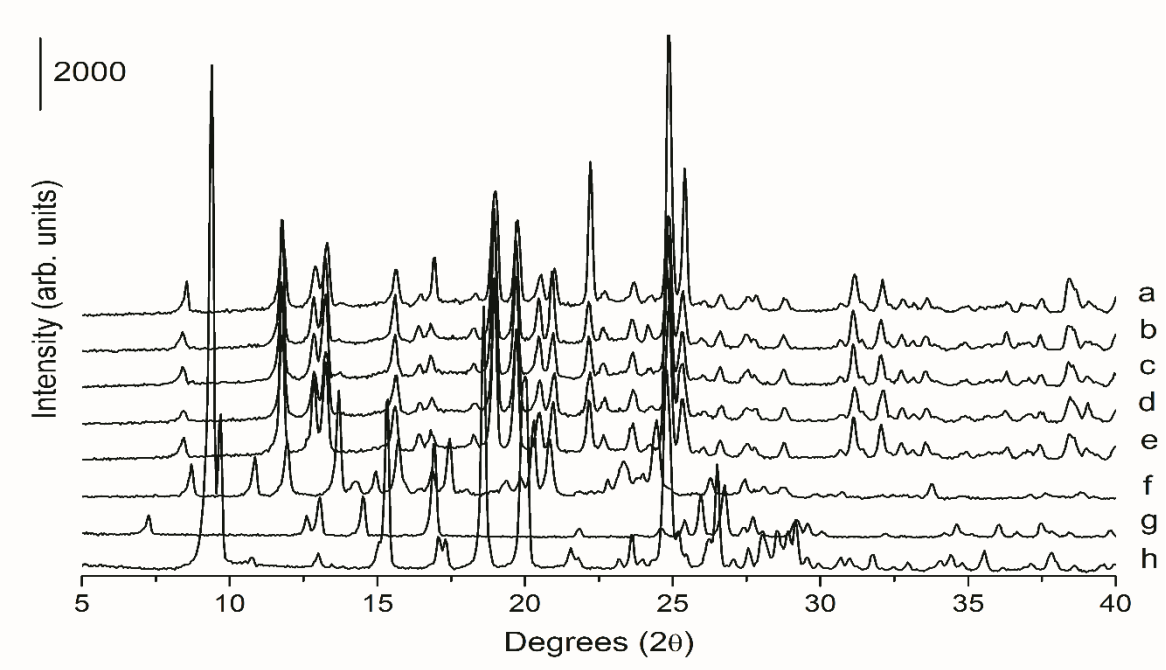

Figure 6.6. PXRD analyses of experiments performed as part of the Box-Behnken DoE with 15 % spray dried mass. a) Run 15, b) Run 12, c) Run 10, d) Run 9, e) Blank beads, f) Cocrystal produced by solvent evaporation, g) 4ASA, h) SDM.

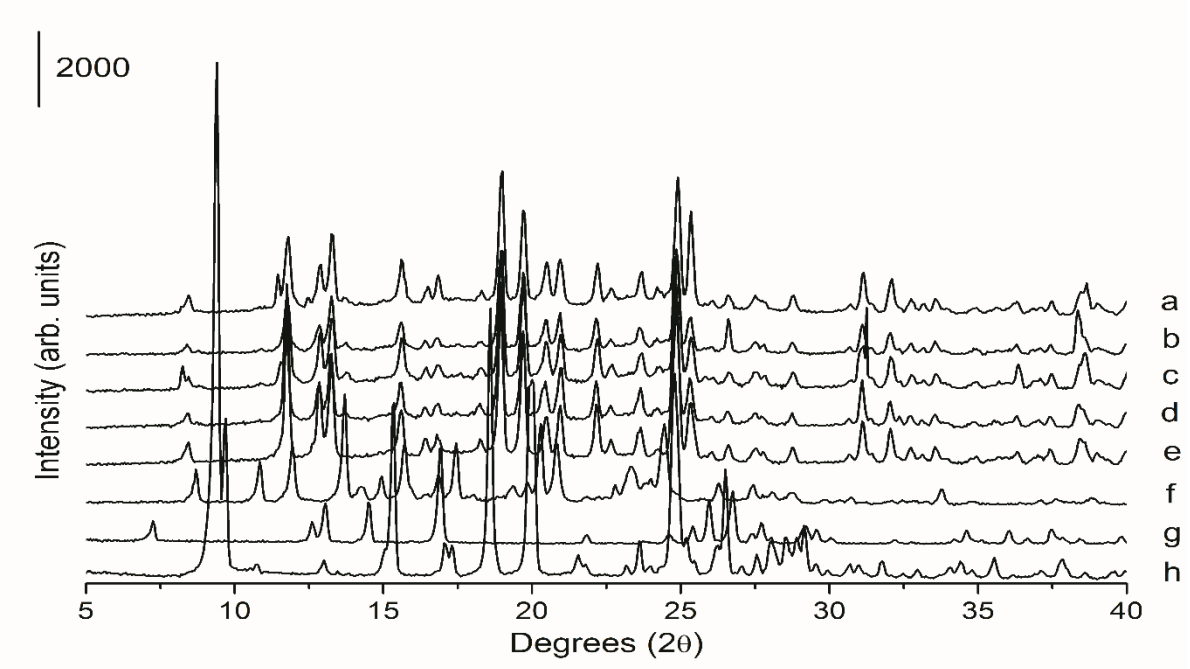

Figure 6.7. PXRD analyses of experiments performed as part of the Box-Behnken DoE with 30 % spray dried mass. a) Run 7, b) Run 6, c) Run 4, d) Run 2, e) Blank beads, f) Cocrystal produced by solvent evaporation, g) 4ASA, h) SDM.

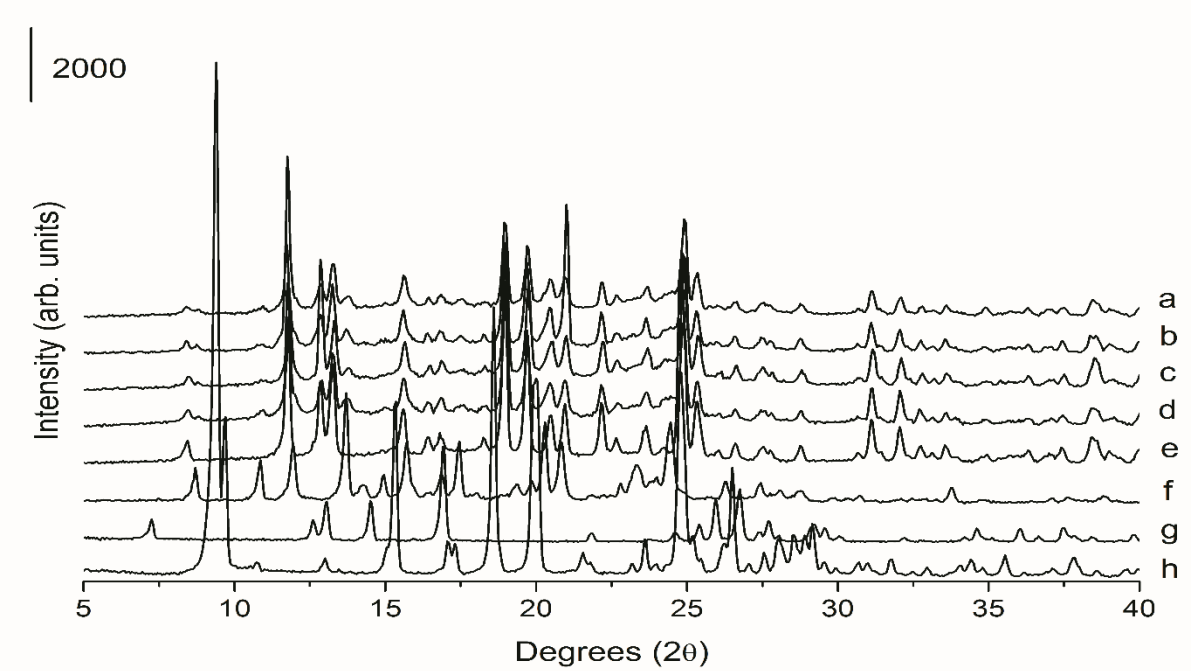

Figure 6.8. PXRD analyses of experiments performed as part of the Box-Behnken DoE with 45 % spray dried mass. a) Run 14, b) Run 11, c) Run 3, d) Run 1, e) Blank beads, f) Cocrystal produced by solvent evaporation, g) 4ASA, h) SDM.

DSC analyses of the experiments performed as part of the Box-Behnken DoE were also performed. In all cases, two melting endotherms were observed, one attributable to the cocrystal and one attributable to the beads. DSC analyses of all experiments performed as part of the Box-Behnken DoE are presented in Figures 6.9 – 6.11. DSC analyses of the centre points are presented in Figure A.4.2 (Appendix 4).

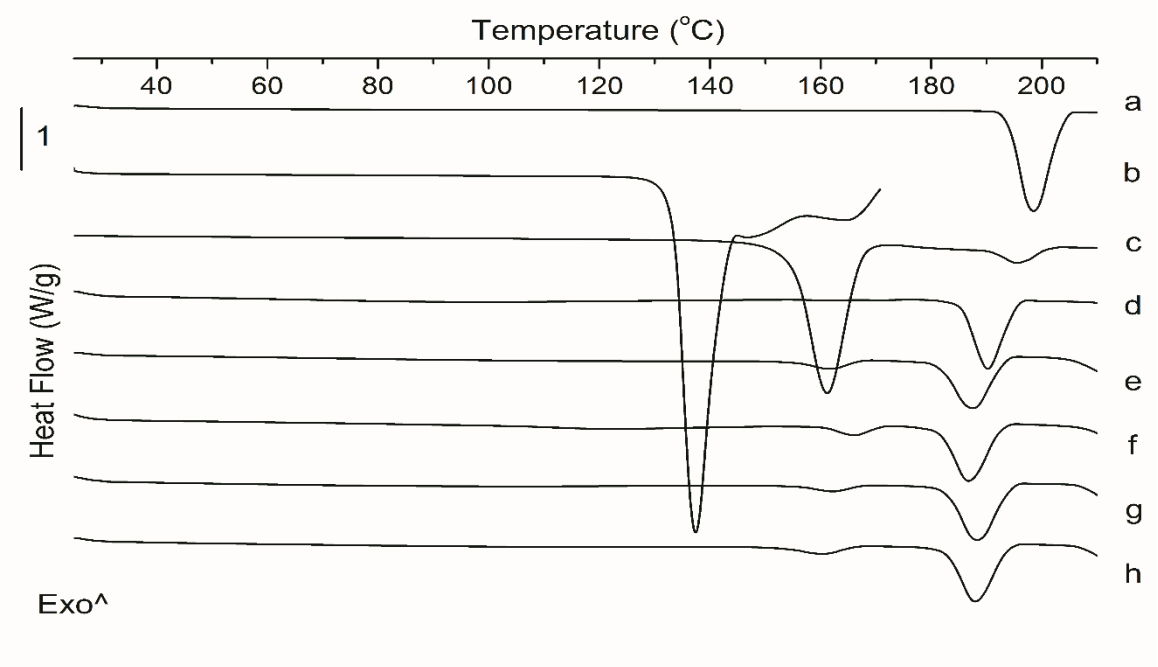

Fig 6.9. DSC curves of experiments performed as part of the Box-Behnken DoE with 15 % sprayed mass. a) SDM, b) 4ASA, c) Cocrystal produced by spray drying, d) Non-pareil beads, e) Run 9, f) Run 10, g) Run 12, h) Run 15.

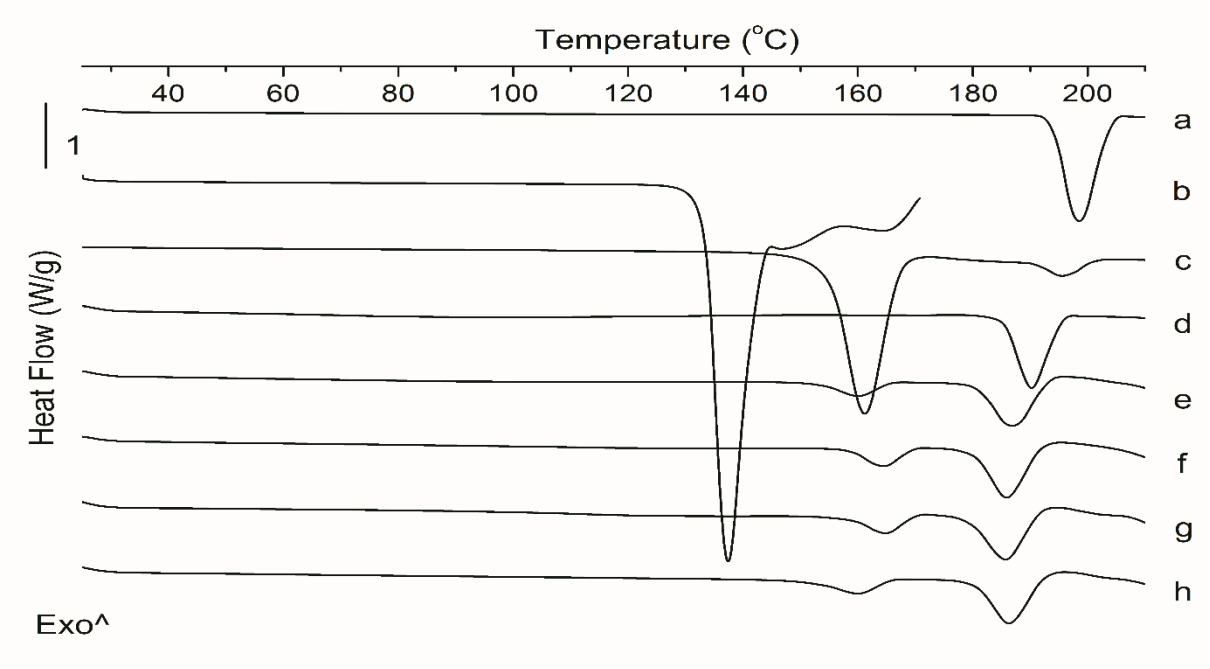

Fig 6.10. DSC curves of experiments performed as part of the Box-Behnken DoE with 30 % sprayed mass. a) SDM, b) 4ASA, c) Cocrystal produced by spray drying, d) Non-pareil beads, e) Run 2, f) Run 4, g) Run 6, h) Run 7.

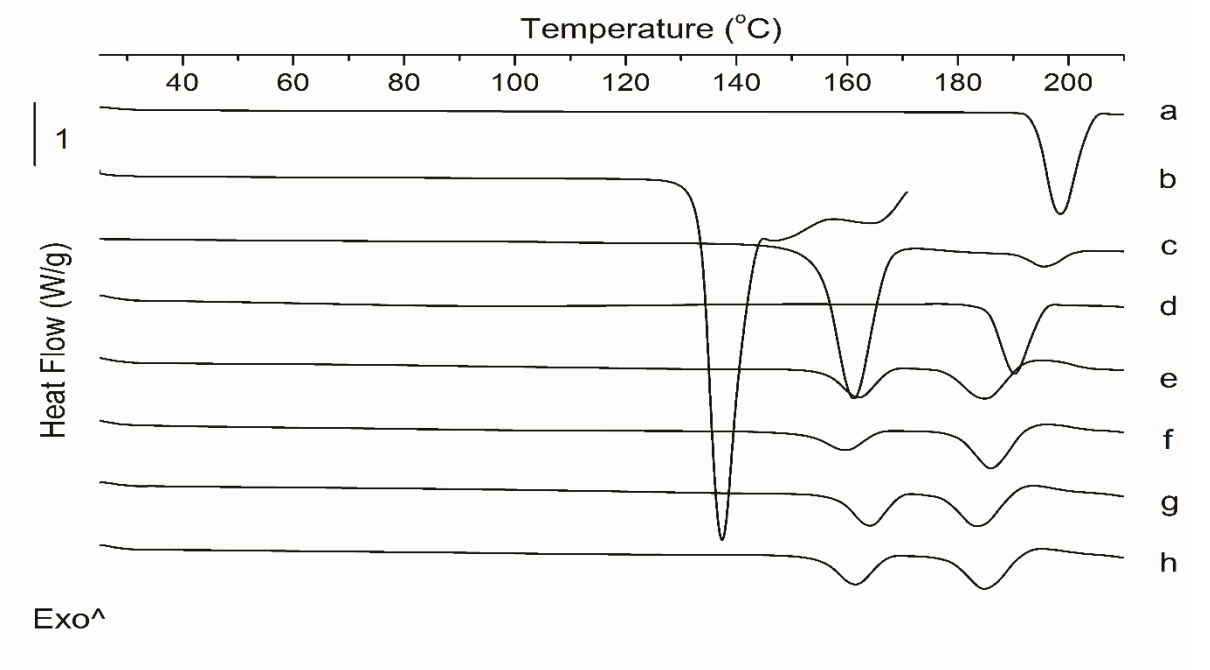

Fig 6.11. DSC curves of experiments performed as part of the Box-Behnken DoE with 45 % sprayed mass. a) SDM, b) 4ASA, c) Cocrystal produced by spray drying, d) Non-pareil beads, e) Run 1, f) Run 3, g) Run 11, h) Run 14.

6.2.3 Statistical analysis

Polynomial analysis was carried out by a multilinear regression analysis method suggesting that the linear and two factor interaction models were the best fit for the parameters assessed. The coefficients of the model equations generated for each critical quality attribute, presented in Table 6.3, revealed goodness of fit of the experimental data to the selected model with high values of R^2 and low p-values < 0.05 for three of the responses: loading efficiency, the degree of crystallinity and yield. No significant differences were observed in the percentage of attrition and content uniformity ($p > 0.05$).

The 2D-contour plot and 3D-response surface plot depicted in Figure 6.12 revealed a higher influence of the amount of mass sprayed on the loading efficiency, whereas the influence of the amount of binder was found to be negligible. Higher loading efficiency was obtained when greater amounts of mass were sprayed onto the beads and also at lower atomisation pressures.

Regarding the degree of crystallisation, the most influential variables were the amount of binder and sprayed mass (Figure 6.13). Higher values of crystallinity were achieved when low amounts of binder and high amounts of mass was sprayed. When the amount of binder was too high, the degree of crystallinity decreased significantly due to the generation of an amorphous system. The effect of the atomisation pressure was found to be negligible.

In contrast, opposite effects were observed for the yield (Figure 6.14). Yield increased significantly when higher amounts of binder were used, as it ensured the sprayed mass had a better adhesion to the beads. The atomisation pressure also played a key role in affecting yield, which was reduced when higher atomisation pressures were used due to the limited contact time of the sprayed mass with the flowing beads.

Most of the factors exhibited a negligible effect on the attrition and content uniformity ($p > 0.05$). However, it is noteworthy that high atomisation pressure promoted high attrition rates (Figure 6.15) and low amounts of mass sprayed led to poor content uniformity (RSD > 3 %) (Figure 6.16).

As previously discussed in chapter 4, models which are not statistically significant may not be accurate to predict the response. Therefore, the models generated for attrition and content uniformity may not be suitable to predict a response based on the input variables.

Model (p-value)	**Predicted equation in terms of actual factors**
Two factor interaction ($p < 0.01$)	**Crystallinity**= + 79.17 -15.24*Atomisation pressure - 0.21*Amount of mass sprayed + 2.43*Amount of binder + 1.36*Atomisation pressure*Amount of mass sprayed - 2.04*Atomisation pressure*Amount of binder - 0.06*Amount of mass sprayed*Amount of binder
Linear (< 0.0001)	**Loading efficiency**= - 0.36 - 2.87*Atomisation pressure + 0.53*Amount of mass sprayed + 0.08*Amount of binder
Two factor interaction ($p < 0.12$)	**Attrition**= - 39.17 + 59.16*Atomisation pressure + 0.98*Amount of mass sprayed - 0.04*Amount of binder - 1.47*Atomisation pressure*Amount of mass sprayed - 0.03*Atomisation pressure*Amount of binder + 0.003*Amount of mass sprayed*Amount of binder
Linear ($p<0.03$)	**Yield**= + 101.08 - 11.28*Atomisation pressure - 0.47*Amount of mass sprayed + 0.21*Amount of binder
Linear ($p<0.09$)	**Log10(RSD of content uniformity)** = + 0.63 + 0.17*Atomisation pressure - 0.03*Amount of mass sprayed - 0.002*Amount of binder

Table 6.3. Model generation and predicted equations obtained from the Box-Behnken DoE.

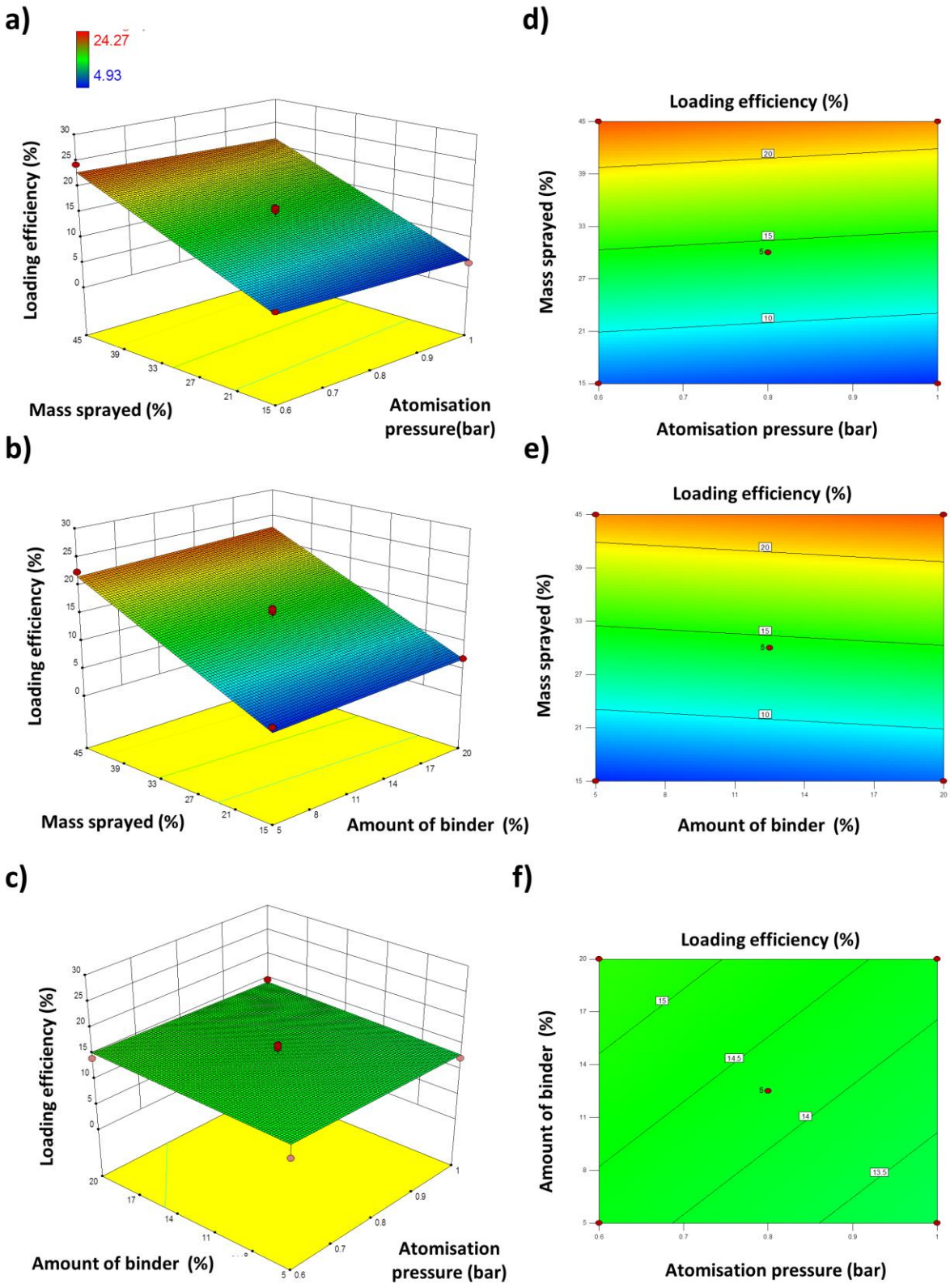

Figure 6.12. 3D response surface (a, b, c) and 2D contour plots (d, e, f) showing the influence of the atomisation pressure, the amount of sprayed mass and the amount of binder on the loading efficiency.

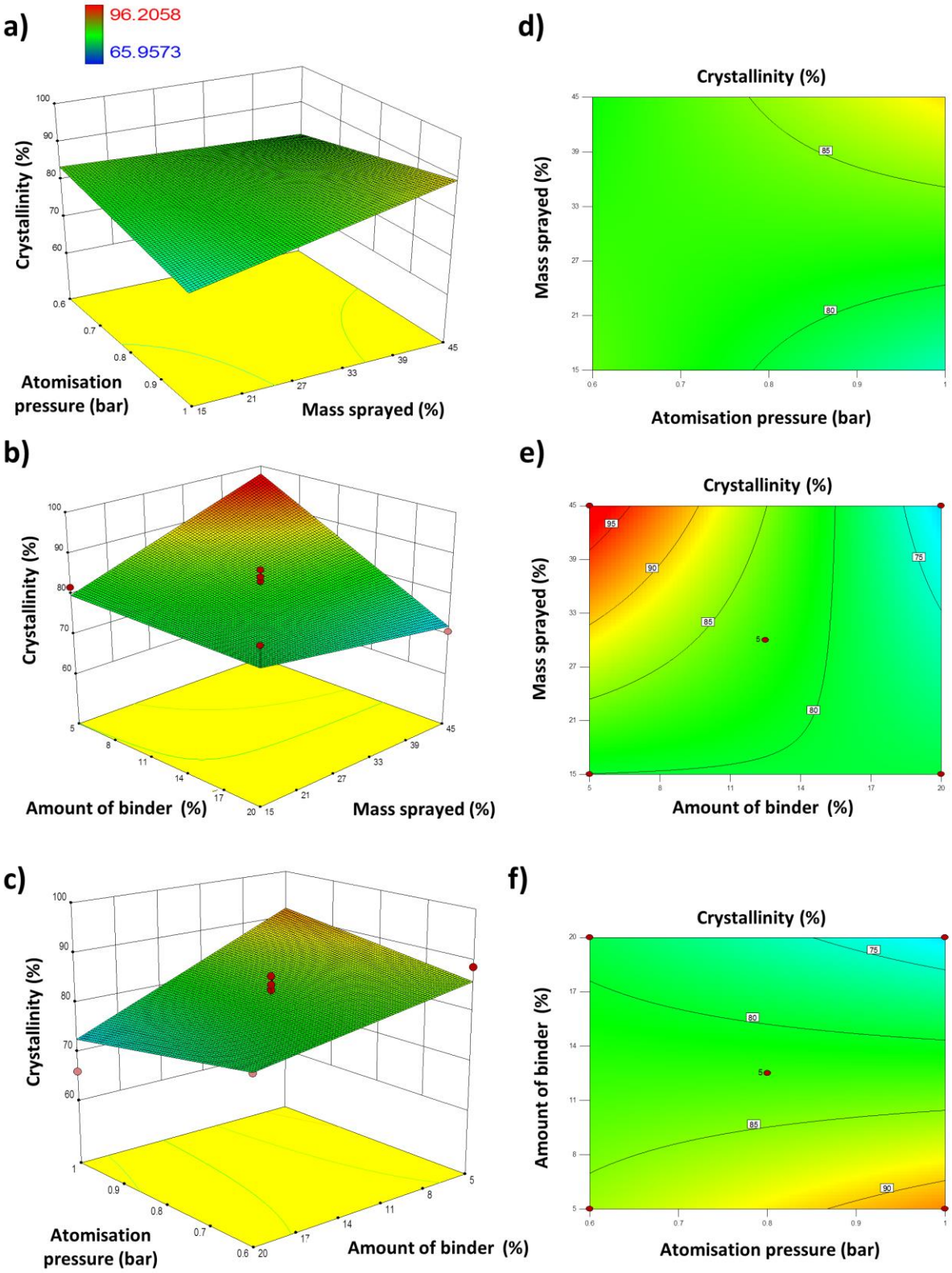

Figure 6.13. 3D response surface (a, b, c) and 2D contour plots (d, e, f) showing the influence of atomisation pressure, the amount of spray dried mass and the amount of binder on the degree of crystallinity of the spray coated cocrystal.

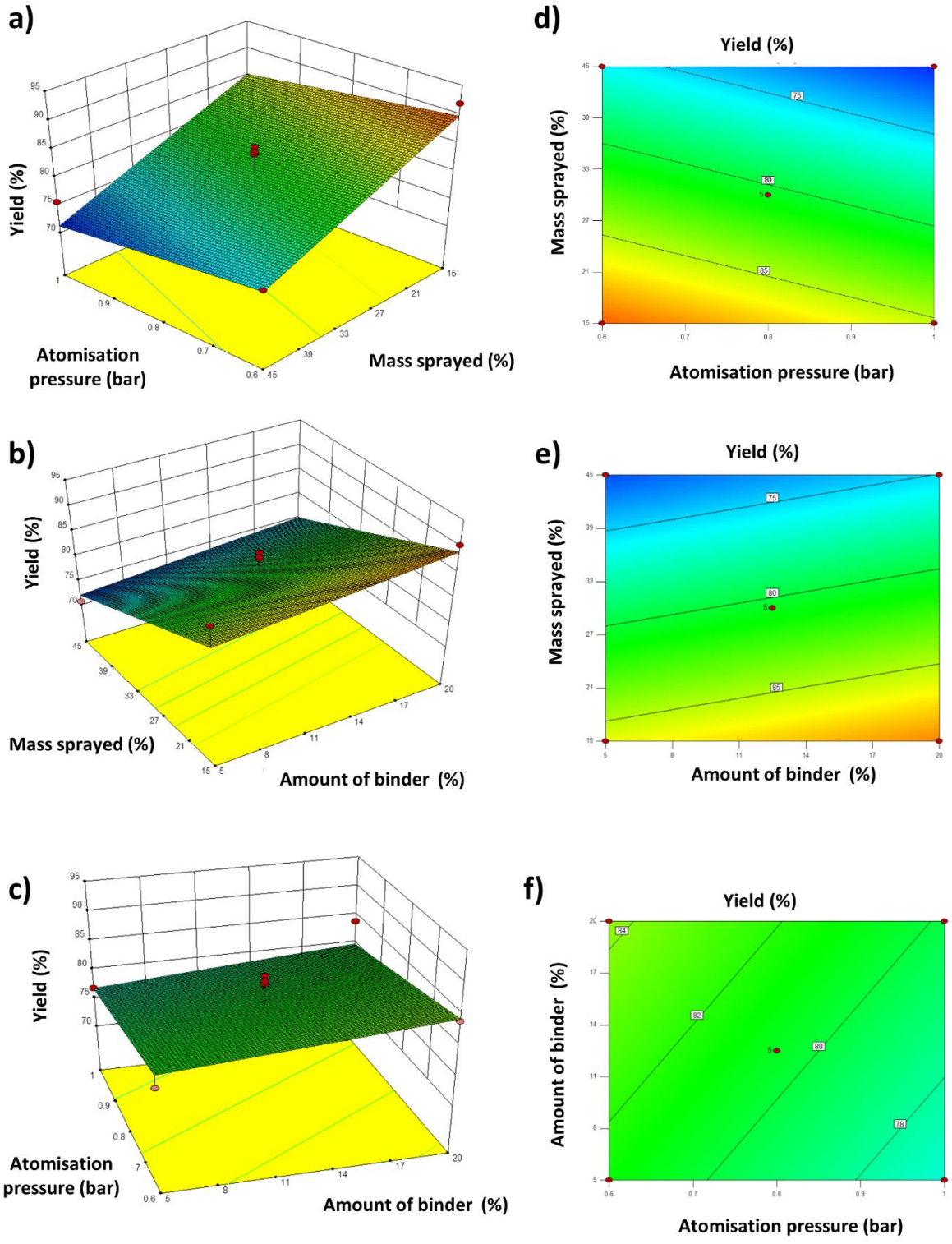

Figure 6.14. 3D response surface (a, b, c) and 2D contour plots (d, e, f) showing the influence of the atomisation pressure, the amount of sprayed mass and the amount of binder on the yield.

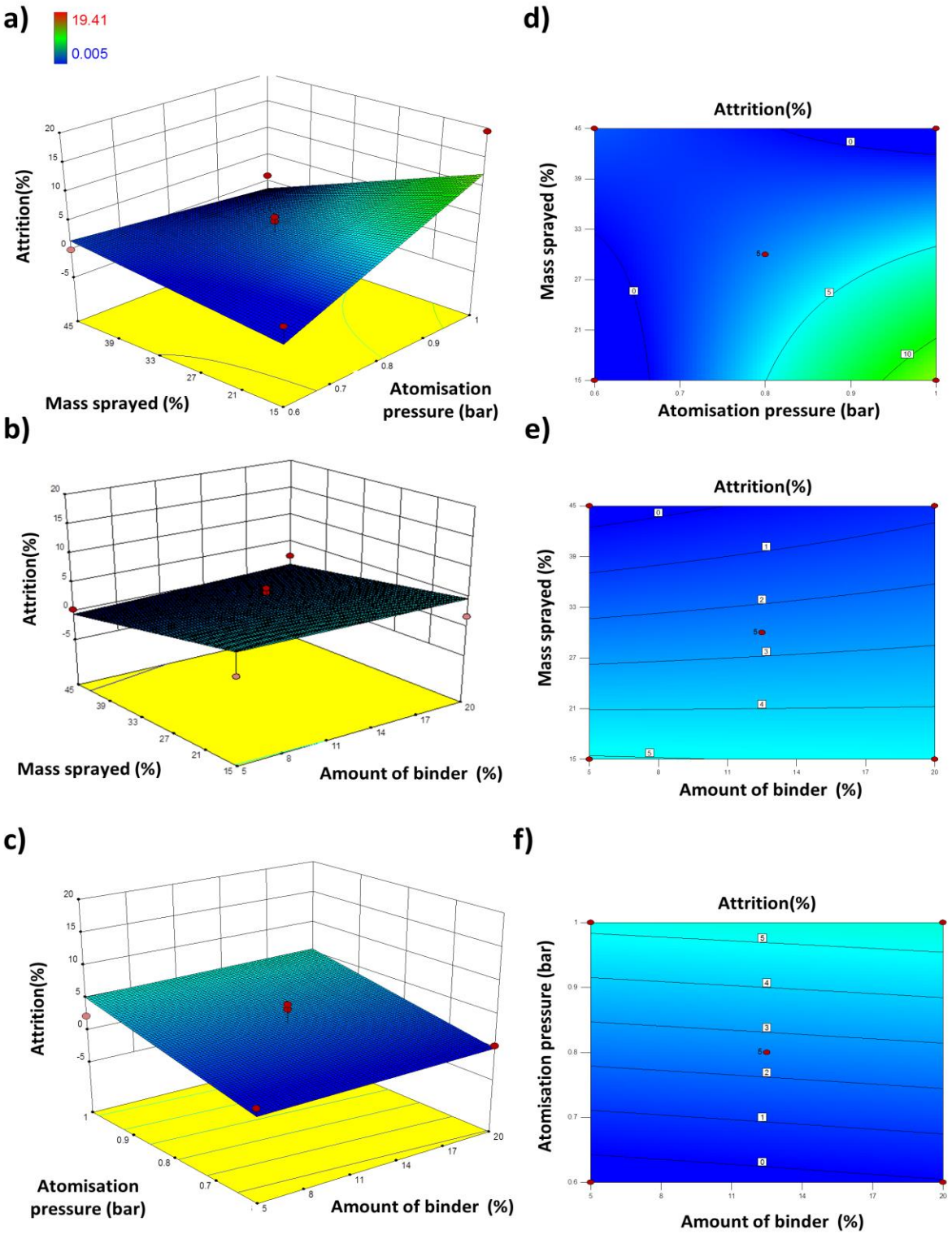

Figure 6.15. 3D response surface (a, b, c) and 2D contour plots (d, e, f) showing the influence of the atomisation pressure, the amount of sprayed mass and the amount of binder on the percentage of attrition.

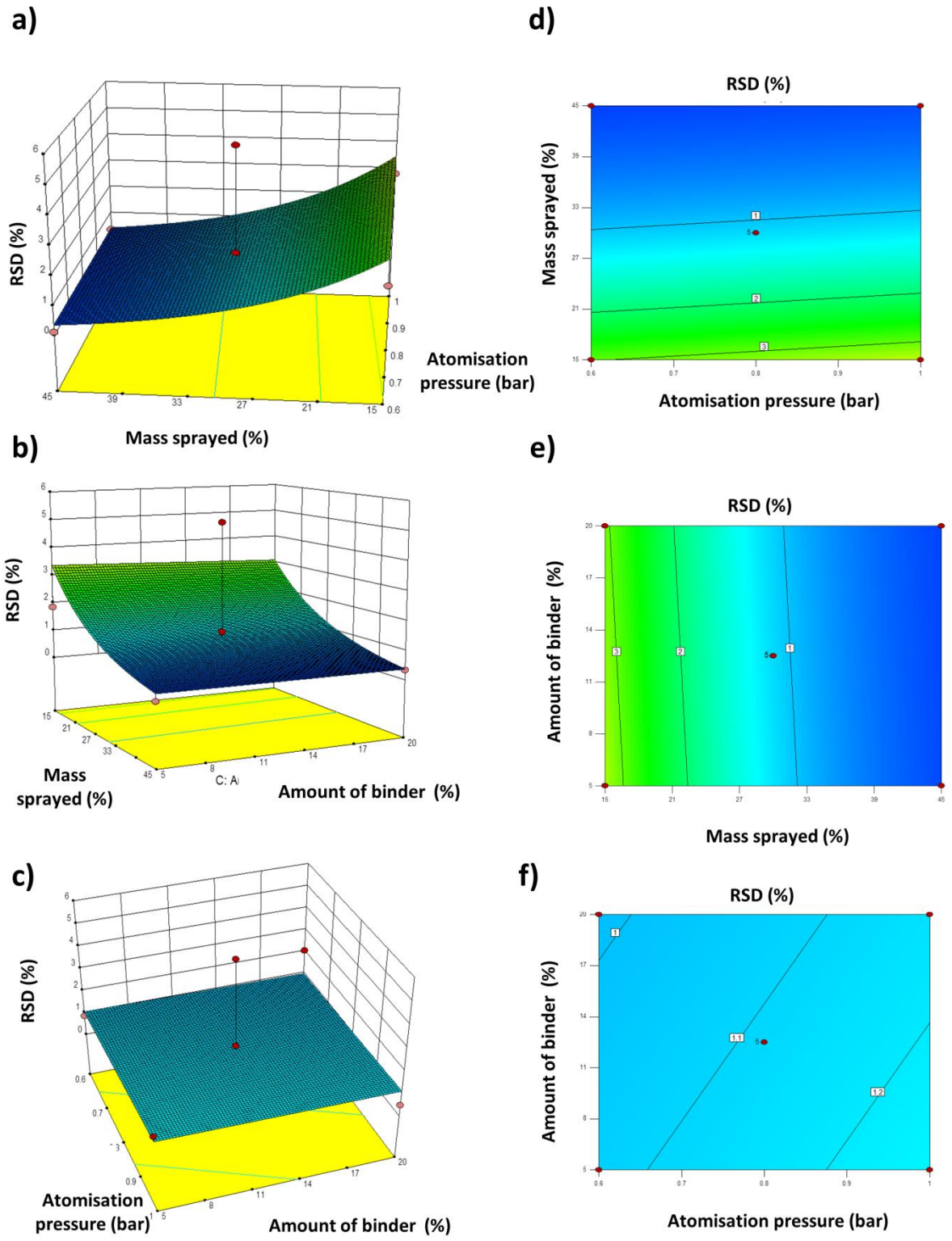

Figure 6.16. 3D response surface (a, b, c) and 2D contour plots (d, e, f) showing the influence of the atomisation pressure, the amount of sprayed mass and the amount of binder on content uniformity (% RSD).

6.2.4 Validation studies

The search for an optimum formulation was carried to attain the desired objectives, giving priority to maximisation of loading efficiency and degree of crystallinity. Based on the aforementioned objectives, the optimised process and formulation parameters were: **5:95** binder:cocrystal weight ratio, **45 %** sprayed mass and **0.75 bar** as atomisation pressure, resulting in **22.1 %** loading efficiency and **96.2 %** crystallinity (Table 6.4). Validation of the optimised parameters revealed close proximity between the predicted values of the responses with observed ones for prepared check-point formulations (Table 6.5). The percent prediction error for the validated runs varied between 1.10 % and 1.63 % for loading efficiency and degree of crystallinity respectively, ratifying excellent goodness of fit. Attempts to maximise the yield resulted in a decrease in the loading efficiency and degree of crystallinity, so it was decided to set a target of 'in range' for the yield. As these experiments are performed at a small scale, yield may become more important when the process is subjected to scale up.

	Aims	Lower limit	Upper limit
Factors			
Amount of binder (%)	In range	-1	+1
Amount of sprayed mass (%)	In range	-1	+1
Atomisation pressure (Bar)	In range	-1	+1
Response			
Loading efficiency (%)	Maximisation	4.9	24.7
Degree of crystallisation (%)	Maximisation	65.9	96.0
Yield (%)	In range	70.5	91.9
Attrition (%)	In range	0.01	19.41
RSD of content uniformity (%)	In range	0.03	5.09
Optimised formulation			
Amount of binder (%)	5	-	-
Amount of sprayed mass (%)	45	-	-
Atomisation pressure (Bar)	0.75	-	-

Table 6.4. Results of numeric optimisation of cocrystal-coated beads.

Response	Experimental Results					Predicted results			
	Run 1	Run 2	Run 3	Mean	StD	Predicted	Percent Error	95% CI low	95% CI high
Loading efficiency (%)	22.51	22.11	20.50	21.71	1.06	22.07	1.63	19.54	24.61
Degree of crystallinity (%)	93.48	97.47	94.49	95.15	2.07	96.21	1.10	87.99	104.41

Table 6.5. Comparison of experimental results with predicted responses. Key: CI, Confidence intervals.

6.2.5 Further investigation of the effect of PVP K90 loading, bead size and batch size

The effect of other factors was investigated while keeping constant the optimised parameters from the second DoE. In these studies, the % of mass sprayed and the mass of beads was kept constant. The only parameter which was altered was the ratio of cocrystal:binder. The PVP K90 concentration played a key role in the spray coating process, significantly affecting both the loading efficiency and the degree of crystallinity. A minimum percentage of the binder was required to ensure that the sprayed solution appropriately coated the beads within the fluidised bed. When no binder was used, the loading efficiency was considerably reduced. However, very high percentages of PVP K90 did not result in greater loading efficiencies (Figure 6.17), as the spray solution was extremely sticky hampering the coating process, resulting in twinning of the beads. Also, the larger the percentage of binder, the higher the depression of the melting point of the cocrystal and the lower the degree of crystallinity due to the formation of an amorphous solid dispersion (Figure 5.18). The glass transitions for amorphous SDM and PVP K90 were reported to be 78 ˚C and 173 ˚C, respectively (Caron et al., 2011, Knopp et al.,

2015). No experimental glass transition has been reported for 4ASA due to its high tendency for crystallisation. Attempts to amorphise 4ASA by spray drying and melt quenching did not prove successful. After spray coating, an amorphous system could be formed due to the interaction between SDM and PVP rather than with 4ASA. At higher percentages of PVP (≥20%), evidence of a glass transition was observed in some of the systems. Spray coating a solution of SDM and PVP on to beads using the optimal conditions resulted in an amorphous system with a T_g of 98.23 ^oC (Figure A.4.3, Appendix 4).

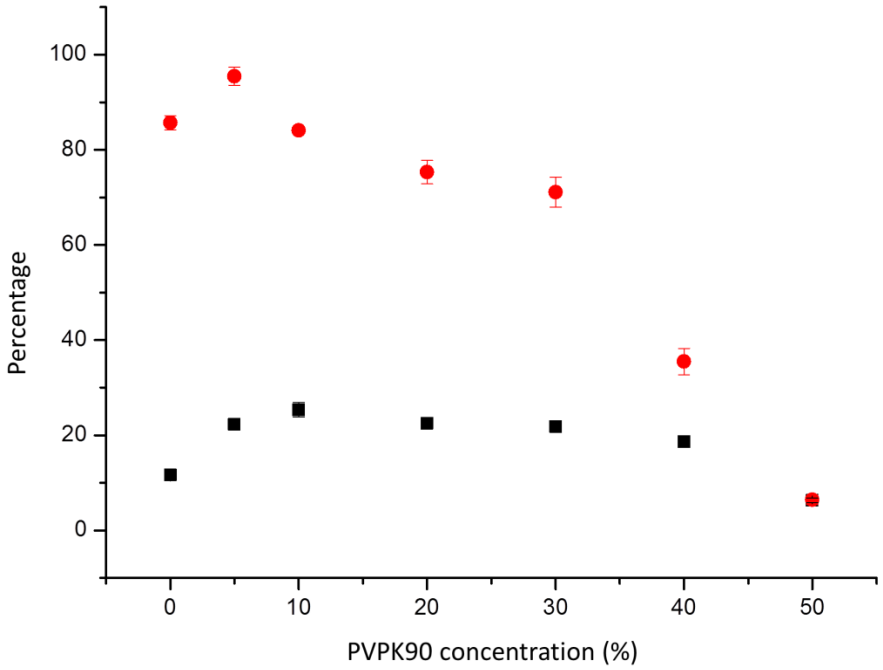

Figure 6.17. Effect of PVP K90 concentration on cocrystal formation during spray coating. Key: The percentage of the degree of crystallinity and loading efficiency are represented in red (●) and black (■) respectively.

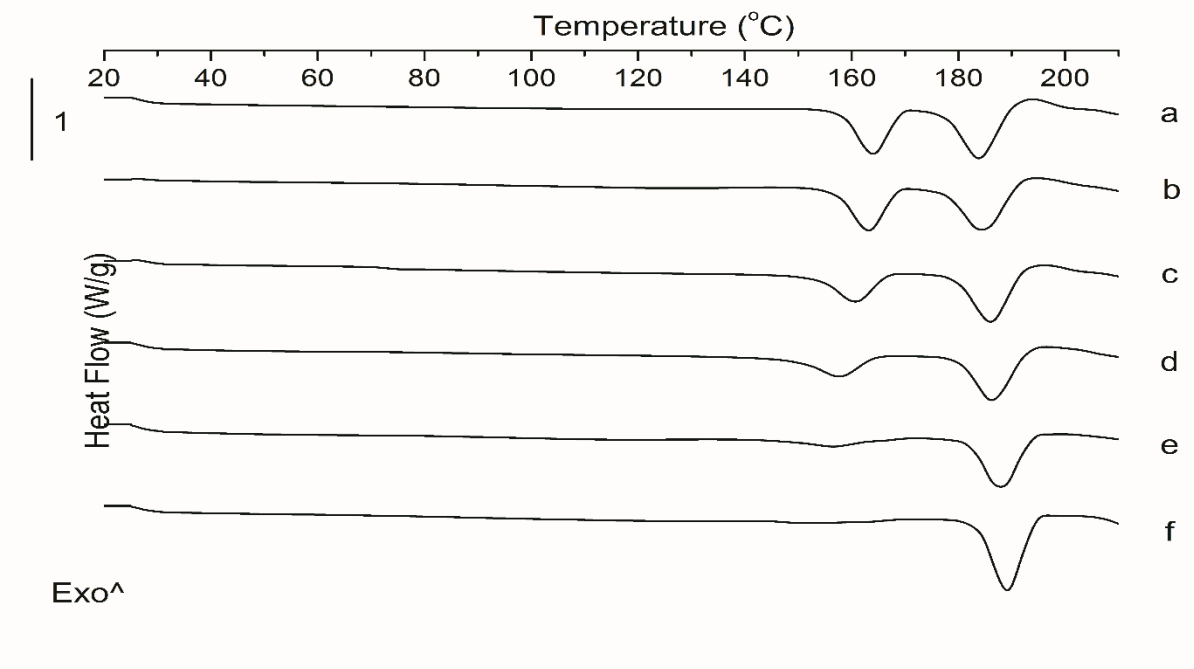

Figure 6.18. DSC curves of the runs performed with the optimized conditions with varying PVP K90 loadings. a) 5 % PVP, v) 10 % PVP, c) 20 % PVP, d) 30 % PVP, e) 40 % PVP, f) 50 % PVP.

The bead size had a significant impact on the loading efficiency and degree of crystallinity. 500 µm beads were found to be the optimal size to ensure high loading and high crystallinity. When a larger bead size was used, the surface area available for coating was reduced and then the loading efficiency was lower. The greater mass of the beads resulted in a higher kinetic energy of the beads during the spray coating process, resulting in higher levels of attrition. However, a smaller bead size did not improve the loading as the starter cores exhibited poor flow within the fluidised bed, resulting in lower coating efficiency. When the batch size was increased from 5 to 25 g, the coating efficiency was higher (1.7-2.2-fold) but the degree of crystallinity was 7-8 % lower, probably indicating that less binder is required in the manufacture of larger batches (Figure 6.19).

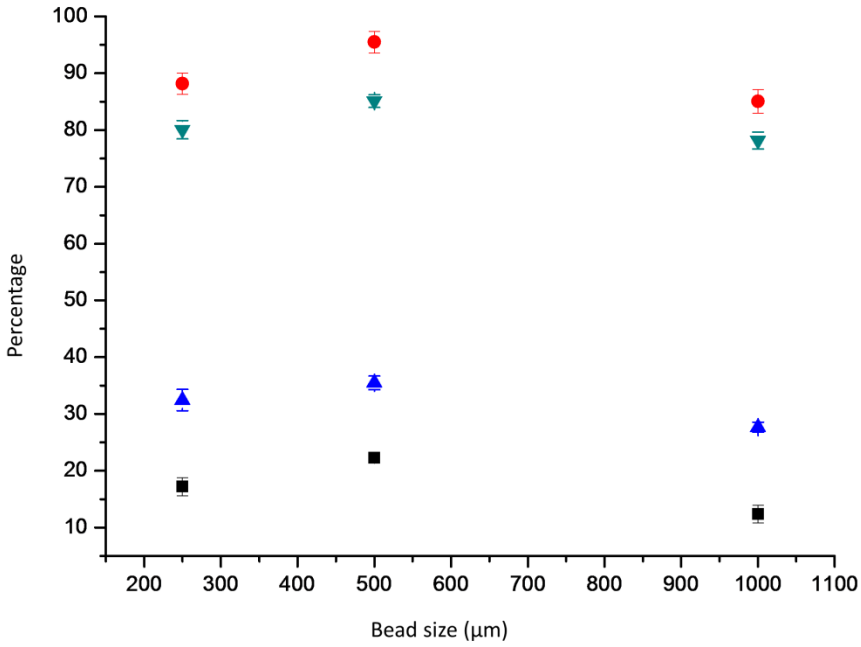

Figure 6.19. Effect of bead and batch size on cocrystal formation during spray coating. Key: The percentage of the degree of crystallinity and loading efficiency for the 5 g batch size are represented in red (●) and black (■) respectively and for the 25 g batch size in green (▼) and blue (▲).

6.2.6 Physicochemical characterisation

The SEM micrographs showed that the morphology of the coated beads was quasi spherical (Figure 6.20, 6.21). At higher magnifications, the deposition of small crystals was observed. However, it can be seen that the loading efficiency of the cocrystal on to the surface of the bead is low when no binder is used (Figure 6.20, a1-a2) A larger amount of cocrystal was coated on to the surface of the beads when binder was used. Also, at larger magnifications, it was observed that cocrystals were embedded within a smoother matrix corresponding to the PVP (Figure 6.21, b1-c2). Higher loads of PVP also resulted in the formation of an amorphous phase as opposed to cocrystal formation. The higher amounts of PVP led to a lower surface area and at the same time higher residual water content which can be a disadvantage in terms of chemical stability (Figure A.3.4) Twinning of the beads can also be seen at high PVP loads (Figure 6.21, c1).

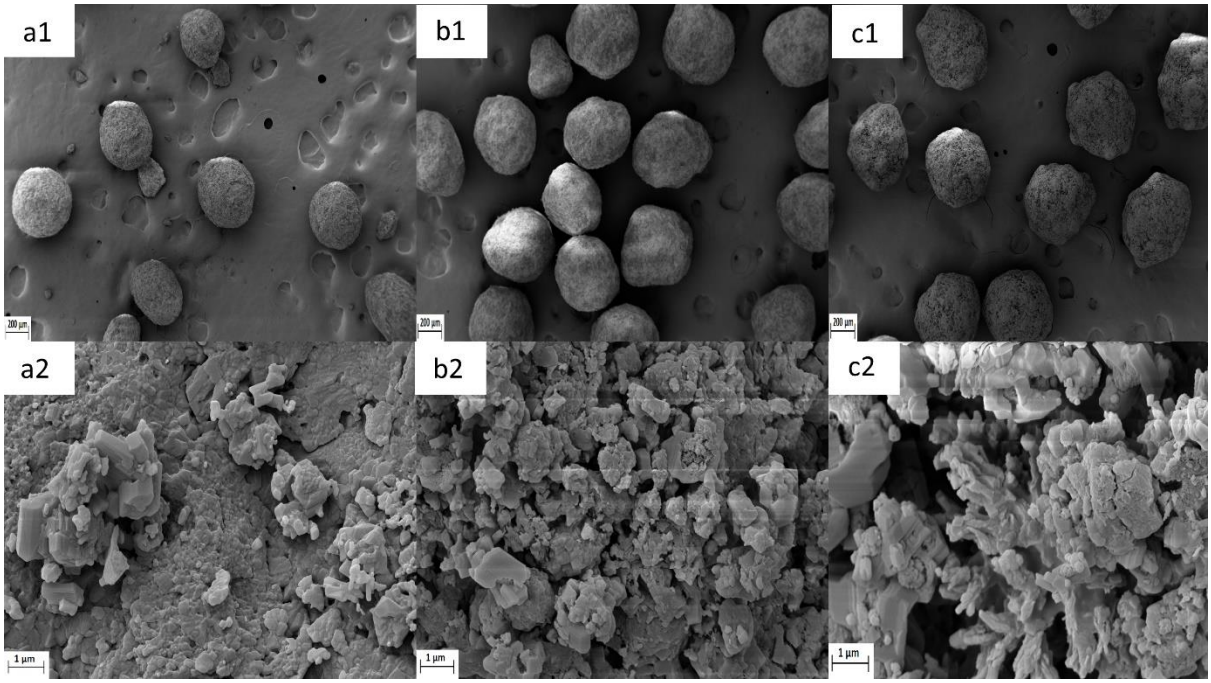

Figure 6.20. SEM micrographs of cocrystal coated 500 μm beads. a) 100 % cocrystal, 0 % PVP, b) 95 % cocrystal, 5 % PVP, c) 90 % cocrystal, 10 % PVP.

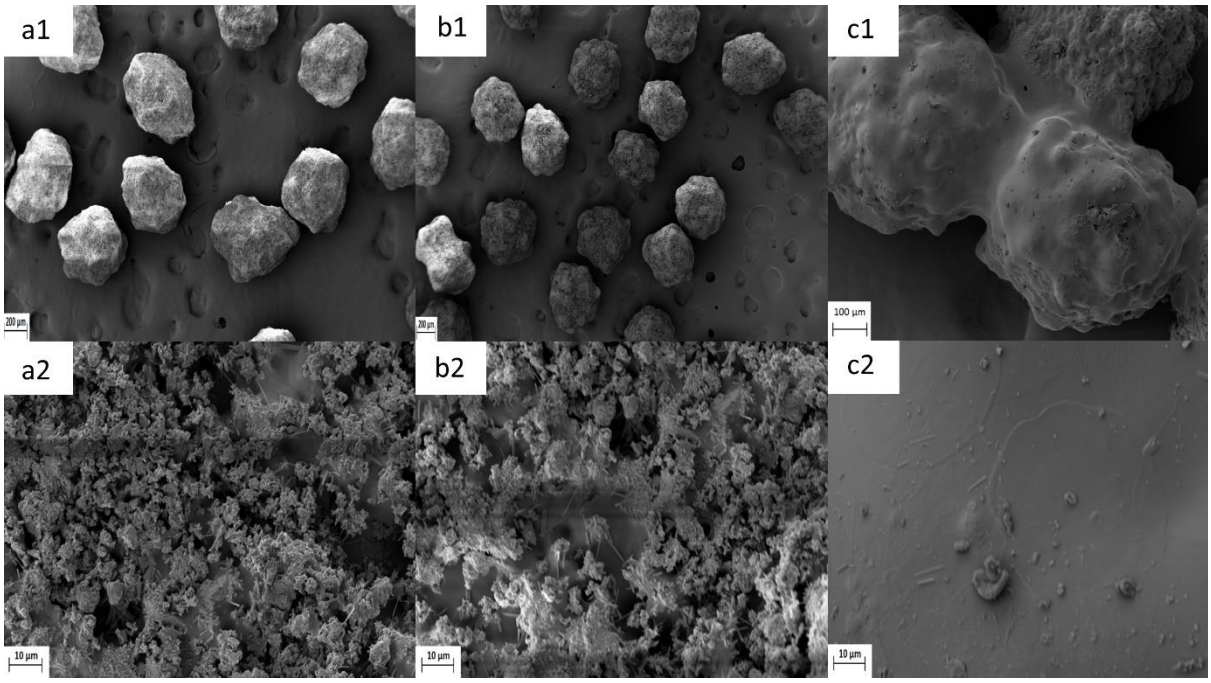

Figure 6.21. SEM micrographs of cocrystal coated 500 μm beads. a) 80 % cocrystal, 20 % PVP, b) 70 % cocrystal, 30 % PVP, c) 50 % cocrystal, 50 % PVP.

The DVS sorption profiles showed a large uptake of water between 60 to 90 % relative humidity for uncoated beads due to their hydrophilic nature. In contrast, the cocrystal coated beads exhibited a lower water uptake at these relative humidity values. The decreased uptake for the cocrystal coated beads can be attributed to the lower uptake of moisture by the cocrystal (Figure 6.22). Both batches were performed using the optimized parameters from the Box-Behnken DoE, which are 45 % mass sprayed, 95:5 cocrystal:binder and 0.75 bar atomisation pressure.

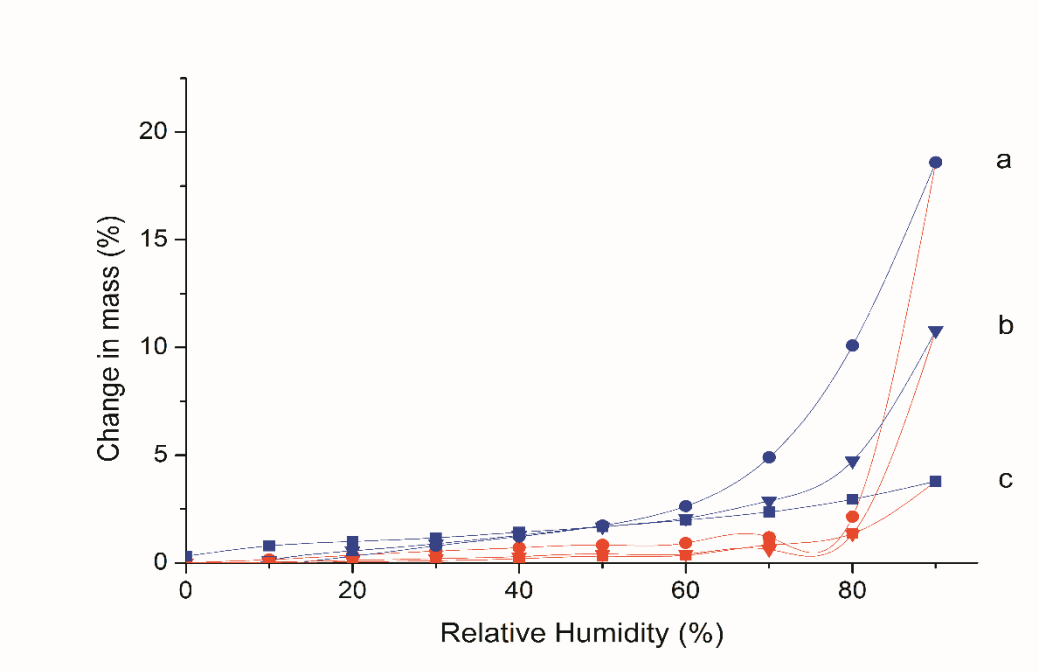

Figure 6.22. DVS sorption (blue) and desorption (red) profiles of a) uncoated beads, b) 5g batch of cocrystal coated beads, c) 25g batch of cocrystal coated beads. All beads were 500 µm.

The flow properties of the coated and uncoated beads were also investigated (Figure 6.23). Considering that the beads are intended for capsule filling, good flow is recommended in order to avoid weight, and therefore dose variability. Cocrystal coated on non-pareil sugar beads exhibited lower SE compared to the uncoated beads, indicating that the spray coating process led to less cohesive particles than the starting beads, except for those of 1000 µm, for which a higher SE was obtained after the coating. A value of SE less than 5 mJ/g was observed in all the coated systems (except for those of 1000 µm) which is associated with less cohesive solid particles, indicating that they are suitable for acceptable capsule filling. Overall the coated beads exhibit a less cohesive behaviour with

stable flow properties, indicated by SI values which were closer to unity than uncoated beads (Freeman, 2007).

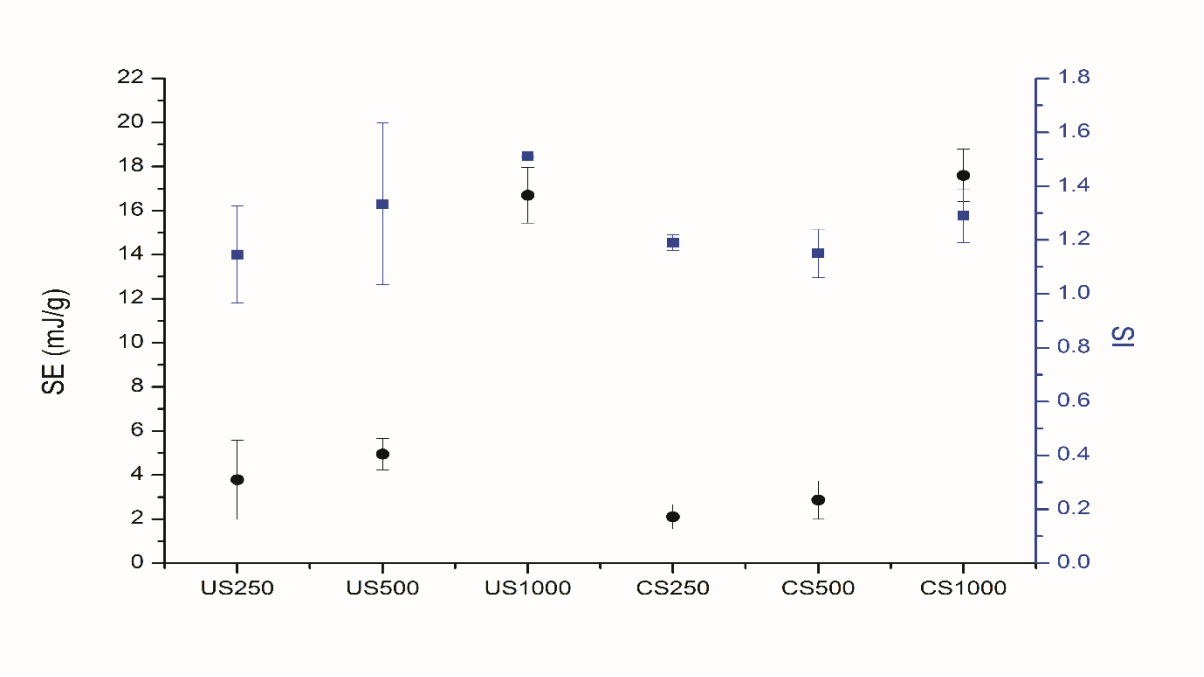

Figure 6.23. SE and SI values for coated and uncoated beads. Key: US-uncoated sugar beads, CS-coated sugar beads.

6.2.7 Dissolution studies

Dissolution studies were performed on the optimized spray coated cocrystal beads with varying amounts of PVP and on the beads coated with SDM using the optimized parameters, as well as the cocrystal produced by spray drying. For all formulations, a lag time of 10 minutes was observed due to the initial dissolution of the capsule shell. In terms of dissolution, the presence of PVP controlled the release of SDM over time. The batch without binder exhibited the highest release (92.3 %) at 15 min. In all the cases, 100 % release was achieved after 60 min. Dissolution of the cocrystal produced by spray drying was slower than the spray coated cocrystal beads with 0, 5 and 10 % binder. This is likely due to aggregation of the spray dried cocrystal in solution. The system with the slowest dissolution rate was the SDM:PVP coated beads. The dissolution profiles are presented in Figure 6.24.

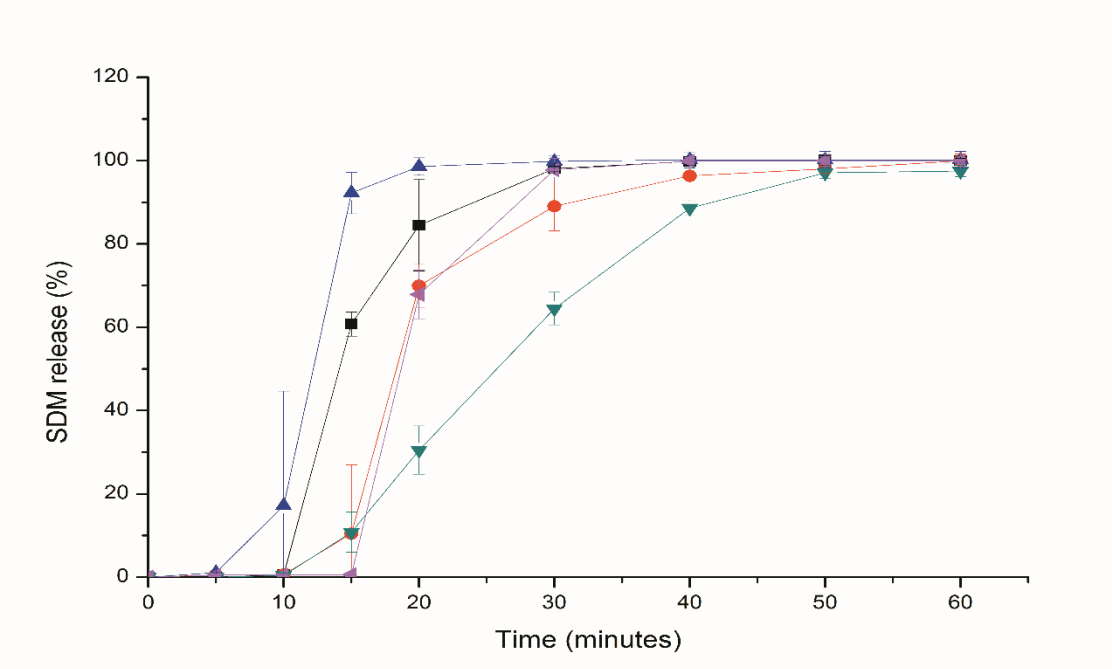

Figure 6.24. Dissolution profiles of spray dried cocrystal (●), spray coated beads with no binder (▲), spray coated beads with 5 % binder (■), spray coated beads with 10 % binder (◀) and SDM coated beads (▼).

6.3 Conclusions

Spray coating has been successfully employed to produce cocrystals deposited as a coating layer on to inert beads. While this method has previously been used to deposit an amorphous layer of API on to inert beads, as in the case of Sporanox^{TM}, and to coat pellets of an API with ethyl cellulose in the case of Efexor^{TM}, coating of beads with cocrystals has not been demonstrated previously. Two Design of Experiments were performed to identify the optimum process and formulation parameters to produce cocrystal coated beads. The balance between high loading efficiencies and high degree of crystallinity was achieved when 5 % of binder was used. However, these parameters may not be amenable to scale up, as the production of larger sized batches may require less binder to produce an acceptable product. The cocrystal coated beads also demonstrated favourable dissolution properties compared to the cocrystal produced by spray drying. The coated beads are large enough to inhibit agglomeration in solution, therefore demonstrating a favourable dissolution rate.

CHAPTER 7

General Discussion

This thesis has investigated processing an API and coformer in the presence of a range of excipients by spray drying, hot melt extrusion and spray coating. In all cases, generation of a cocrystal in the presence of an excipient was possible. However, the ratios of cocrystal components to excipient varied according to each method used. This was especially highlighted when generating a model cocrystal both by spray drying and hot melt extrusion.

7.1 Spray drying

Chapter 3 has demonstrated the feasibility of cocrystal formation and inclusion within an excipient matrix, through the process of co-spray drying. PXRD and DSC analyses for the cocrystal-in-excipient systems were consistent with those of the cocrystal produced by solvent evaporation, indicating that cocrystal formation still occurred when the cocrystal was co-spray dried with some of the excipients included in this study. Differences in DSC results were noted between the cocrystal-in-excipient systems and the corresponding physical mixtures; it was found that the heat of fusion was lowered (and the melting temperature depressed when higher ratios of excipient were used) for the co-spray dried systems. PXRD and DSC results also revealed a loss of crystallinity, indicating that the spray drying process induced some level of amorphisation of the cocrystal, without fully impeding cocrystal formation. In some cases, subjecting an amorphous or partially amorphous system to humidity stress resulted in crystallisation of a co-amorphous system to the cocrystal without the generation of single component crystals attributable to the API or coformer. However, above a certain limit of excipient weight fraction, crystallisation of an amorphous system resulted in single component crystals, as well as the cocrystal. In this case, it is possible that a binary co-amorphous system was formed between the excipient and the API or coformer, leaving the free API or coformer to crystallize independently, or the metastable binary phase to crystallize.

Previously, it has been determined that a difference in HSP of less than 7 $MPa^{0.5}$ indicates that materials are miscible (Mohammad et al., 2011). This theory has been utilised previously to predict cocrystal formation, whereby drug and coformer with $\Delta HSP < 7$ $MPa^{0.5}$ were shown to be likely to form a cocrystal due to their miscibility. In Chapter 3, the same principle was applied to predict cocrystal formation in the presence of a carrier excipient. However, in this case it was anticipated that the closer the HSP value for the cocrystal and carrier excipient, the less likely cocrystal formation would be, because the carrier excipient would be miscible with the API and coformer and thus prevent cocrystal

formation. The findings from the study involving the SDM:4ASA cocrystal showed that a clear correlation exists between the HSP difference between the cocrystal and carrier excipient, and the likelihood of cocrystal formation occurring. It can be deduced that $\Delta HSP > 9.6\ MPa^{0.5}$ for the cocrystal and carrier excipient leads to formation of the cocrystal when it is co-spray dried with the carrier excipient. $\Delta HSP < 9.6\ MPa^{0.5}$ for the cocrystal and carrier excipient results in either a completely amorphous form following co-spray drying, or cocrystal with traces of the individual components (API, coformer) of the cocrystal.

However, it is important to acknowledge that HSPs do not include thermodynamic considerations. HSPs were originally designed for, and applied to inks, paints and polymers, where the thermodynamics cancel out. It has been suggested that corrections may need to be made for small molecular solutes, taking into account considerations such as the crystal lattice energy. Therefore, the HSP values for crystalline materials may need corrections according to the size of the solvent molecule, the lattice energy of the crystalline solute and the specificity of the hydrogen bonding interactions (Louwerse et al., 2017).

The experimental solubility of the cocrystal, API and coformer in the amorphous excipients was also determined. This was then compared to the difference in the calculated HSP value between the cocrystal and selected excipients. A high experimental solubility of the API/coformer in the excipient indicates miscibility of the API/coformer with the excipient. Miscibility between the API/coformer and excipient is unlikely to result in a cocrystal-in-excipient system when the three components are co-spray dried together.

The ratio of excipient: cocrystal had a major impact on cocrystal formation as well as the overall miscibility between the cocrystal and the excipient. In order to get a deeper insight into the process of producing a cocrystal-in-excipient system by spray drying, a parameter to predict cocrystal formation (CFP) was calculated using Equation 7.1:

$$CFP = \frac{\Delta HSP}{Fe * S} \qquad \text{(Eq. 7.1)}$$

Where ΔHSP is the difference in HSP between the cocrystal and the excipient, F_e is the excipient fraction and S is the measured solubility of the cocrystal within the excipient matrix. Based on the CFP calculated values and the experimental results (Table 7.1), it

can be concluded that for those systems with a CFP value > 10, there is a high probability of cocrystal formation, while values below 1 indicate that there is a high probability of co-amorphous systems forming. Some exceptions were found, such as chitosan, probably due to its basic behaviour and interaction in solution with the acidic coformer, which may decrease the H-bonding interaction between 4ASA and SDM.

Table 7.1. Prediction of SDM:4ASA cocrystal formation based on calculated CFP values (from Eq. 7.1). Darker areas (CFP < 1) indicate that the formation of a co-amorphous system is likely, while lighter areas (CFP>10) indicate that there is a high likelihood of cocrystal formation to occur in the co-spray dried system.

	Ratio of Excipient								
Excipient	0.1	0.2	0.3	0.4	0.5	0.6	0.7	0.8	0.9
Inulin	50.1	25.1	16.7	12.5	10	8.4	7.2	6.3	5.6
MCC	30.5	15.3	10.2	8	6.1	5.1	4.4	3.8	3.4
Chitosan	34.4	17.2	11.5	8.6	6.9	5.7	4.9	4.3	3.8
Dextran	24.8	12.4	8.3	6.2	5	4.1	3.5	3.1	2.8
PVA	3.5	1.7	1.2	0.9	0.7	0.6	0.5	0.4	0.4
PVP K15	1.6	0.8	0.5	0.4	0.3	0.3	0.2	0.2	0.2
Soluplus	1.5	0.8	0.5	0.4	0.3	0.3	0.2	0.2	0.2
HPMC	1	0.5	0.3	0.2	0.2	0.2	0.1	0.1	0.1

For those co-spray dried systems that allowed cocrystal formation, FTIR analyses revealed no interaction between the cocrystal and the excipient. Also, dissolution studies from constant surface area disks showed no differences in the SDM release rate among the different excipients, suggesting that the release of SDM was determined only by the cocrystal itself. Release of the API and coformer became congruent over time in all cases, as the molar excess of SDM which exists due to the sublimation of 4ASA crystallizes. Congruent dissolution of SDM and 4ASA, as measured by HPLC, indicates that the cocrystal is stable in solution.

For two of the excipients (inulin and dextran), recrystallisation of the cocrystal to the lower energy polymorph was not seen when the disks were analysed by PXRD after dissolution studies, suggesting that rational excipient selection may stabilise metastable cocrystal polymorphs during dissolution. However, only minor differences in dissolution between the two SDM:4ASA polymorphs have been reported (Grossjohann et al., 2015). As the predominant factor by which cocrystals of BCS Class II drugs exhibit increased dissolution and solubility in aqueous media is by enhanced solvation, differences in

dissolution between cocrystal polymorphs are likely to be minimal. No statistical differences were seen between the SDM:4ASA cocrystal-in-excipient systems based on ANOVA and f_2 analysis.

Preliminary studies on process intensification showed that co-spray dried systems had better compaction properties than physical mixtures, suggesting that a secondary excipient blending step might be avoided. These studies also revealed that the cocrystal was stable under the compaction pressures, as PXRD analyses revealed no process induced phase transformation.

Cocrystallisation in the presence of two excipients was also successful. In this case, two immiscible excipients were chosen and were co-spray dried with the API and coformer at ratios of up to 50 % w/w total excipient. It is important to note that, in this case, one excipient was in solution (inulin) and another in suspension (MCC). It would be expected that the suspended excipient would be phase separated from the API and coformer. Significant differences in the relative crystallinity and Carr's index were not observed with alteration of the assessed input factors, which were the total excipient percentage, ratio of inulin:MCC and the airflow. In Chapter 3, it was observed that a reduction was seen in the relative crystallinity for the co-spray dried cocrystal in MCC system with 50 % excipient. A much smaller reduction in crystallinity was seen when the API and coformer were co-spray dried with inulin at the same excipient loading (50 %). It is possible that in Chapter 4, significant decreases in crystallinity may not have been observed due to the narrow design space investigated. The percentage of each excipient may be a more important parameter than the combined percentage excipient. Significant differences in the Carr's index of the co-spray dried powders were also not observed. It might have been expected that a higher airflow would provide more energy for fluid dispersion, thus reducing the particle size. This may then be reflected in the Carr's index value, with a smaller particle size leading to more cohesive particles due to the higher surface area available for interaction between the particles. However, no statistical differences in Carr's index were observed between the samples.

However, statistical differences were observed between the samples with respect to the tensile strength of the tablets formed, indicating that the total excipient percentage had a significant positive impact on tensile strength. This may indicate that tablets with high cocrystal loadings form weaker tablets, and that high excipient loadings are required to

produce a tablet with a higher tensile strength, which may prevent tablet disintegration upon storage and transport. This study also shows that a separate blending step may be avoided when mixing the cocrystal and multiple excipients, and that a cocrystal-in-excipient system can be created using a one-step spray drying process. While differences in tensile strength were seen, and the crystallinity of the cocrystal was not adversely affected even with high (50 %) excipient loadings, the Carr's index of the co-processed powders was not acceptable in any case. A larger scale spray dryer may produce a product with a larger particle size, which may result in a less cohesive powder with a lower Carr's index. Powders with a Carr's index > 25 are considered to be cohesive, and therefore poorly flowable (De Villiers, 2005). It was therefore decided to investigate other processing methods, such as hot melt extrusion and spray coating, as methods to form cocrystals in the presence of an excipient which may result in a product which is more processible for downstream processing.

7.2 Spray drying versus hot melt extrusion

The comparison of spray drying versus HME in order to formulate amorphous solid dispersions has been widely studied. However, our initial work on spray drying did not consider HME as a method to produce a cocrystal-in-excipient system. Therefore, the impact of ΔHSP between the cocrystal and excipient during the HME process was unknown. For spray drying, the solubility of the drug in the solvent is crucial to ensure a readily scalable and viable process, whereas for HME, the solubility of the drug in the polymer is key to achieve a thermodynamically stable formulation. From an industrial point of view, the phase of development is also important in process selection. Bearing in mind that API availability is often limited at early stages, spray drying is preferable because preliminary formulation experiments can be performed with amounts as low as 50-100 mg (Dobry et al., 2009), whereas at least several grams of API are required for HME (Guns et al., 2012). In spite of the use of solvents, spray drying is often preferred over HME for several reasons such as thermally induced degradation of the drug (Hengsawas Surasarang et al., 2017), phase separation (Lenz et al., 2017) and high shear forces during the HME process (Guns et al., 2010).

To the best of our knowledge, the feasibility of employing both techniques to form cocrystals within a carrier excipient has not previously been compared. In order to ensure cocrystal formation, the H-bonding interaction between API and coformer has to be

stronger than the interaction of the individual components with the carrier excipient. Otherwise, cocrystal integrity will not be preserved. Differences in HSP between the cocrystal and excipient have previously been employed as a useful, reliable tool to predict cocrystal formation in the presence of a carrier excipient by spray drying, as demonstrated in Chapters 3 and 4. However, HSP differences should not be used as the only indicator for cocrystal formation, as the ratio of carrier excipient: cocrystal also has a major impact. When the difference in HSP between the cocrystal and the excipient is very small, cocrystal integrity can still be preserved at low excipient ratios (10 %).

The impact of HSP differences has been demonstrated again in Chapter 5 for the IBU:INA cocrystal: excipient systems produced by spray drying. When the difference in HSP between the cocrystal and the excipient was greater than 9.6 $MPa^{0.5}$, as in the case of mannitol (ΔHSP of 18.3 $MPa^{0.5}$), larger amounts of excipient, up to 50 %, could be incorporated during the spray drying process without altering the integrity of the cocrystal. For the other two tested excipients, Soluplus and PVP K15 where the difference in HSP between the cocrystal and excipient was much lower, at 2.1 and 1.6 $MPa^{0.5}$ respectively, the IBU:INA cocrystal was only formed when very low amounts of excipient (10 %) were used. Even with 10 % PVP K15, small traces of amorphous content were observed. However, traces of individual crystalline API or coformer were not detected by PXRD or DSC analysis. Remarkably different results were obtained when HME was employed for processing. In the case where xylitol was used as the carrier excipient, with a difference in HSP between the cocrystal and excipient of 20.7 $MPa^{0.5}$, a similar order of magnitude as that for mannitol, pure cocrystal (devoid of API or conformer contaminants) resulted on co-processing by HME. While it has been reported that cocrystal formation can occur even with high xylitol loads (50 %), this required alteration of the extrusion elements and processing temperature (Li et al., 2017). Spray drying may be seen as a more robust process, as alteration of spray drying parameters was not required to produce a cocrystal with high mannitol loads. In the case of Soluplus and PVP K15, a mixture of cocrystal with single components was obtained with 10 % excipient when processed by HME, while the equivalent spray dried systems showed cocrystal with no contaminating crystalline API or coformer starting materials could be prepared at the equivalent weight ratios.

The different results obtained for spray drying and HME are probably related to the speed of the processes and the energy (mechanical and thermal) imparted during mixing of the

cocrystal components and the excipient. The evaporation of the solvent during the spray drying process takes place in milliseconds and hence, there is less chance for the cocrystal to interact within the excipient molecules, whereas the mixing of the components in HME is a more energetic and longer process, potentially facilitating interactions between the cocrystal components and the excipients. For this reason, highly immiscible systems (cocrystal: excipient) are required to guarantee selective H-bond interactions between the drug and the coformer molecules and probably larger differences in HSP are necessary to ensure cocrystal formation in HME processes. The extent of mixing and homogeneity of the systems during the cocrystallisation process is also an important parameter to consider. Prior to spray drying, the API, coformer and excipient exists in a homogenous solution. When this system reaches the 'reactor' phase, a homogenous phase of API, coformer and excipient is present. For the purposes of spray drying, the 'reactor' is the droplet generated after atomisation prior to the drying phase. In the case of HME, a molten system of API, coformer and excipient exists. Complete cocrystallisation has previously been shown to occur via HME when processed above the eutectic temperature of the API and coformer. Similarly, cocrystal formation can occur in the DSC pan when heated above the eutectic temperature, previously confirmed by variable temperature XRD (VTXRD) (Lu et al., 2008). However, other studies have indicated that cocrystal formation between AMG-517 and sorbic acid does not appear to be mediated by eutectic formation, and instead appears to be mediated by the amorphous state (Daurio et al., 2014). It is important to note that the 'reactor' in this case is the extruder barrel, as this is where cocrystallisation occurs. The mixing between the components in this case is not as thorough as during spray drying, as the reduced molecular mobility through the molten phase may impede the interaction between the API and coformer. Molten xylitol rapidly solidifies upon cooling, which can trap the molten API/coformer. However, this can further reduce the molecular mobility, and can impede further the interaction between the API and coformer, resulting in single components, especially at higher excipient loads. When the API and coformer is processed with amorphous polymeric excipients by HME, the high viscosity of the excipient above the T_g can prevent crystallisation of the API and/or coformer upon cooling. However, processing with an excipient below its T_g did not result in a pure cocrystal, as was seen with PVP K15. It is important to note, however, that the process parameters were not altered to optimize the process. Therefore, it may be possible to produce a cocrystal in the presence of these excipients with varying excipient loads by altering process parameters such as screw speed, screw configuration and

processing temperatures. The impact of the solid state nature of the excipient does not appear to be as significant when co-spray drying. Instead, the differences in HSP between the excipient and coformer dominates.

7.3 Spray coating

Spray coating a solution of API, cocrystal and binder onto inert beads has also shown to be a viable method to produce cocrystals. The cocrystal in this case was the SDM:4ASA cocrystal. This method can serve to reduce agglomeration of cocrystals in solution (Serrano et al., 2015), and hence prevent a reduction in dissolution rate. The form II polymorph of the cocrystal was produced by both spray drying, as demonstrated in Chapters 3 and 4, and spray coating in Chapter 6. Similar to co-spray drying experiments with two excipients, the spray coating process involves the use of two excipients as well as the API and coformer. The binder in solution is required to ensure the cocrystal loading onto the surface of the beads is acceptable while maintaining a high level of crystallinity, while the inert beads exist as a solid. This is the first time that fluid bed coating has been used to deposit a layer of a multicomponent crystal on to an inert bead. Low levels of binder and a larger percentage of spray dried mass resulted in a high cocrystal loading without the generation of single component crystals or amorphous domains. While PVP K90 is miscible with the API and coformer, the low percentage of binder does not have a significant impact on cocrystal formation, as seen previously when spray drying in Chapters 3 and 5, where cocrystal formation can still occur when co-spray dried with low percentages (10 %) of miscible excipients. It is also important to note that spray coating was performed at lower temperatures than spray drying. This can prevent sublimation of thermolabile chemicals such as 4ASA. No differences between the molar ratios of SDM and 4ASA were seen after spray coating, whereas a 3.5 % excess of SDM was present after spray drying, as determined by HPLC analysis in Chapter 3.

Three process parameters (spray rate, nitrogen flow rate and atomisation pressure) and four formulation parameters (bead size, % sprayed mass, % binder and type of binder) were assessed and optimized during this study. Both the spray rate of the solution onto the beads and the percentage of sprayed mass had a positive effect on both the degree of crystallinity of the cocrystal and the loading efficiency of the cocrystal onto the substrate. When these parameters are set to the upper limits in this study, there is a larger amount of solution to be dried. When the airflow is unchanged, drying a smaller amount of

solution may result in a higher number of crystal defects, as the same amount of energy is input to dry a smaller amount of solution, which may negatively impact the degree of crystallinity of the cocrystal.

The nitrogen airflow and atomisation pressure both had a negative impact on the loading efficiency. Both of these factors may result in the cocrystal being stuck to the filters and the walls of the spray coater, due to the higher amount of energy being input to the process. The atomisation pressure also had a significant negative effect on the number of intact beads at the end of the process. The higher bead size promoted attrition, due to the greater kinetic energy of the larger beads. The larger beads also resulted in a lower loading efficiency, due to the smaller available surface area for the cocrystal to deposit.

The type and percentage of binder did not have a significant impact on the loading efficiency or degree of crystallisation. Due to the small amount of binder in the sprayed solution (max 5 % in initial studies), cocrystal formation was not impeded by PVP K90 when compared to inulin. Some attrition was seen when inulin was used as a binder. Therefore, PVP K90 was used in the Box-Behnken DoE.

Further studies performed during the Box-Behnken DoE revealed that higher concentrations of binder can result in the formation of amorphous domains, which results in a decrease in cocrystal crystallinity. The higher binder concentration can also result in an increased yield, likely due to decreased collisions between the beads.

Production of a 25 g batch of cocrystal coated beads was also trialed using the optimized parameters for a 5 g batch. While the loading efficiency was higher for the 25 g batch when compared to the 5 g batch, the degree of crystallinity was reduced. This suggests that scale-up of the process may require lower amounts of binder to produce an acceptable product.

This study also revealed that the cocrystal coated beads had favourable flow properties when compared to the uncoated beads. The coated 250 µm and 500 µm beads had improved flow properties when compared to the uncoated beads, while both the coated and uncoated 1000 µm beads have a high specific energy (SE) value. SE values below 5 mJ/g indicate a free-flowing material, while SE values above 10 mJ/g indicate a cohesive material (Leaper et al., 2017). Spray coating of cocrystals onto substrates can result in favourable flow properties compared to spray drying. Cohesive powders were produced

when co-spray drying excipients with the API and coformer, as all powders had a high Carr's index. However, it appears that the flow properties of the spray coated cocrystal beads is dominated mainly by the beads themselves. Only small differences exist between the coated and uncoated beads for all bead sizes. It is likely that the thin layer of cocrystal on the surface of the beads has only a small impact on the flow properties. Nonetheless, it appears that the cocrystal coated beads are suitable to downstream processing such as capsule filling due to their favourable flow properties. This contrasts with the co-spray dried cocrystal-in-excipient systems, all of which exhibited a Carr's index above 25 and can be defined as poorly flowable.

7.4 Mechanism of cocrystal formation in the presence of an excipient

In this thesis, cocrystals have been produced in the presence of an excipient by three different methods of manufacture: spray drying, hot melt extrusion and spray coating. It has previously been reported that the production of cocrystals by spray drying is likely to be mediated by the amorphous phase (Alhalaweh and Velaga, 2010). It has been suggested that during spray drying, droplets containing stoichiometric ratios of API and coformer dry, and a metastable co-amorphous system of API and coformer is formed. This system can then instantaneously crystallize to form the cocrystal. In the presence of an excipient, the same process can occur. When the excipient is immiscible with the API and coformer, as defined by the difference in HSP, the binary co-amorphous system of API and coformer can crystallize to form a cocrystal without interacting with the excipient. The resultant powder is a cocrystal-in-excipient system. When only small differences in HSP between the cocrystal and excipient exist, an amorphous dispersion was formed. It is likely that during the drying process, a ternary amorphous system is formed between the API, coformer and excipient due to the miscibility of all three components. All three excipients which were defined to be miscible with the cocrystal (PVP K15, Soluplus and HPMC) are amorphous polymeric excipients. These excipients are miscible with the API and coformer, and can prevent the crystallisation of the API and coformer, either as a cocrystal or as single component crystals. A mix of cocrystal and single component crystals was seen when chitosan, polyvinyl alcohol and glycine were co-spray dried with the API and coformer at excipient loadings of 50 %. In these systems, it is likely that partial miscibility of the excipient with the API and coformer may lead to the formation of a binary system of excipient and API or coformer. This can

leave a single component amorphous domain, which can quickly crystallize. Additionally, a metastable binary amorphous domain can also crystallize. As the excipient is only partially miscible, there may also be interactions only between the API and coformer, which can result in cocrystal formation. In this case, both single component crystals and cocrystals can be seen in the PXRD diffractogram.

It has previously been suggested that the production of cocrystals by hot melt extrusion is mediated by the amorphous state or a eutectic state. Studies by *Dhumal et. al.* demonstrated that cocrystals of ibuprofen and nicotinamide could by formed by HME. In this previous study, process parameters such as screw configurations, processing temperatures and screw speeds were investigated. Lower screw speeds, and screw configurations which promoted a high level of distributive and dispersive mixing, promoted cocrystal formation. Interestingly, cocrystal formation was assessed both above and below the eutectic temperature of the API and coformer. Cocrystal formation, without the presence of contaminating individual API and coformer, occurred above the eutectic temperature, and it has been suggested that cocrystal formation occurs from the eutectic phase (Dhumal et al., 2010). However, it is important to note that while complete cocrystal formation was not seen below the eutectic temperature, some Bragg peaks attributable to the cocrystal were observed in the PXRD diffractogram at this processing temperature. This suggests that cocrystal formation may occur via shear forces or may be mediated by the amorphous phase.

Cocrystals of AMG-517 and sorbic acid have also been produced by hot melt extrusion (Daurio et al., 2014). In this previous study, screw configuration, feed rate, screw speed and processing temperature were identified as the important experimental parameters which can affect cocrystal formation. However, alteration of the processing temperature revealed that cocrystal formation was still seen well below the eutectic temperature of the API and coformer. 57 % conversion of the API and coformer to the cocrystal was seen at temperatures as low at 10 ^{o}C. This suggests that cocrystallisation of this cocrystal does not occur from the eutectic melt, and instead may be amorphous mediated. It is likely that higher temperatures can facilitate greater mixing, and can improve the kinetics of cocrystal formation.

The mechanism of cocrystal formation of the IBU:INA cocrystal by HME has not previously been investigated. All extrusion experiments performed in Chapter 5 were

processed above the eutectic temperature of the API and coformer. *Li et. al.* found that temperatures that promote solubilisation of the API and coformer in the molten excipient during processing were preferred, and that decreasing the temperature after cocrystallisation was necessary to assist precipitation of the cocrystal from the carrier melt. The temperature in the final zone should be reduced further to solidify the carrier excipient. However, it is possible that cocrystallisation in this case is also mediated by the amorphous phase, similar to spray drying. The higher temperatures may serve to increase the mobility of the particles in the molten 'melt pool' during extrusion, thereby enhancing the kinetics of cocrystal formation. The molten excipient should have some miscibility with the API and coformer at the higher extrusion temperature, to allow the API and coformer to diffuse through this molten phase and enable cocrystallisation between the API and coformer. The temperature gradient may be important to reduce miscibility between the cocrystal and excipient after cocrystal formation, as the excipient and cocrystal should become less miscible at lower temperatures. However, cocrystal formation was seen only at low excipient loadings, while cocrystal formation was seen at higher excipient loadings with a similar excipient by spray drying. This suggests that the greater molecular mobility of the API and coformer in solution can allow for greater excipient loadings to be incorporated into the one-step process. The reduced molecular mobility of the API and coformer in the molten system relative to a solution can prevent interaction between the API and coformer. However, alteration of HME process parameters such as screw speed and screw configuration may increase the mixing in the extruder barrel, thereby allowing higher excipient loads to be incorporated.

While cocrystallisation in the presence of a low molecular weight excipient was possible, the production of cocrystals in the presence of Soluplus and PVP K15 was not successful. It is likely that processing the API and coformer with these excipients resulted in a binary or ternary amorphous dispersion. In both cases, Bragg peaks attributable to INA were present in the PXRD diffractogram. It is likely that a binary amorphous system of IBU and excipient was formed, resulting in crystallisation of INA. Diffusion of the API and coformer may also have been reduced by the polymers compared to the molten xylitol, thereby further decreasing the possibility of cocrystal formation.

Cocrystal formation by spray coating is likely to proceed by a similar mechanism to spray drying. In both cases, droplets containing API, coformer and excipient are dried by a heated air stream. However, when spray coating, deposition of the cocrystal on to the

solid substrate is critical. Like spray drying, spray coating is commonly used to produce an amorphous API. When spray coating, it is likely that a co-amorphous system of API and coformer is formed on the surface of the bead, which then rapidly crystallises to form a cocrystal. While a miscible excipient is also present in the sprayed solution, the low percentage of PVP K90 in the optimised formulation prevented the formation of an amorphous dispersion. The beads themselves were phase separated from the solution, and did not impede cocrystal formation. It has previously been reported that heterogenous crystallisation of an API can occur on an excipient surface (Arribas Bueno et al., 2017). However, due to the fast crystallisation of the co-amorphous system on the surface of the bead, heterogenous crystallisation of single component crystals promoted by the bead is unlikely.

Based on the studies conducted and presented in this thesis, it is likely that cocrystals of an API and coformer can form in the presence of an excipient when cocrystal formation occurs via an amorphous intermediate. Miscibility between the co-amorphous intermediate and excipient can then determine the type of system formed. The individual process and process parameters can impact on the excipient loadings that can be incorporated into the process while still maintaining cocrystal formation. Based on these results, it is hypothesized that a cocrystal-in-excipient system could be formed by a method such as freeze drying. It has previously been demonstrated that the production of cocrystals by this method occurs via an amorphous intermediate that is formed as solvent sublimes during the freeze drying process (Eddleston et al., 2013). Like spray drying, freeze drying is a commonly used method utilised in the pharmaceutical industry which is amenable to scale up. As this is also a solvent based method, there may be a higher molecular mobility which may allow higher excipient loads to be incorporated into the process without impacting on cocrystal formation.

Other processes such as dry grinding and liquid assisted grinding may also be amenable to produce a cocrystal in the presence of an excipient. However, no single pathway has been identified by which cocrystallisation occurs by dry grinding. It is thought that cocrystallisation can occur by dry grinding via molecular diffusion, eutectic formation or through an amorphous intermediate (Friščić and Jones, 2009). Liquid assisted grinding can improve the kinetics of cocrystal formation. Further to this, if a co-amorphous system between the API and coformer could form by this method in the presence of an immiscible excipient, the solvent could act as a plasticizer, lowering the glass transition

temperature and causing the co-amorphous system to crystallize quickly. Therefore, cocrystallisation in the presence of an excipient by freeze drying, dry grinding and liquid assisted grinding could be explored in future work. It is unlikely that cocrystallisation in the presence of an excipient would be successful by methods such as cooling crystallisation or solvent evaporation. The slow crystallisation rate may promote heterogenous crystallisation of single components onto the surface of an excipient.

Main findings

- Cocrystal formation in the presence of an excipient can occur via spray drying, hot melt extrusion and spray coating. In the case of spray drying and spray coating, studies were performed which confirmed that more than one excipient can be incorporated into a one-step process. These processes can be used to create powder which is directly compressible to a tablet, or cocrystal coated beads which are suitable for capsule filling.
- Cocrystal formation in the presence of an excipient can occur when the cocrystallisation is mediated by the amorphous state.
- The amount of excipient that can be incorporated into a one-step process can be process dependent. Higher loads of excipient could be incorporated in to the process by spray drying compared to hot melt extrusion without compromising cocrystal formation. Alteration of hot melt extrusion process parameters can facilitate higher excipient loadings.
- The difference in Hansen Solubility Parameter between the excipient and cocrystal can been used to predict cocrystal formation by spray drying. Cocrystal formation occurred at high excipient loads (50 %) when the difference in HSP was > 9.6 $MPa^{0.5}$.
- Cocrystal formation can still occur in the presence of miscible excipients when low excipient loads are incorporated.
- Excipients incorporated into the one-step process can serve to control the polymorphic form of the cocrystal during dissolution studies, as recrystallisation to the lower energy polymorph was not seen during dissolution experiments of the SDM:4ASA cocrystal in the presence of inulin and dextran.
- Polymeric excipients such as Soluplus and PVP K15 prevented recrystallisation of the IBU:INA cocrystal to their single component crystals during dissolution experiments. This can be advantageous for low solubility APIs, as the dissolution rate from the cocrystal is likely to be enhanced when compared to the crystalline API.
- Cocrystal coated beads can have improved flow properties when compared to the unprocessed beads. This can be advantageous for processes such as capsule filling.

- All processes explored to produce a cocrystal-in-excipient system are commonly employed processes used in the pharmaceutical industry and are amenable to scale up.

Future Work

- Investigate the formation of cocrystals in the presence of an excipient by methods such as freeze drying, dry grinding and liquid assisted grinding.
- Investigate the pH-solubility profile of the IBU:INA cocrystal, correlate the findings with the pH-solubility profile of IBU, and assess differences in the dissolution behaviour of IBU and the IBU:INA cocrystal.
- Scale up of the spray drying process to produce particles with a larger particles size to improve downstream processing.
- Optimisation of the spray drying process to produce cocrystal-in-excipient systems with two excipients and perform further flow and tabletting studies.
- Investigate if cocrystal formation can occur with different grades of the same excipient. The difference in viscosity of different grades of the same polymer in solution could result in kinetic trapping of the API and coformer and prevent cocrystal formation.
- Alteration of HME process parameters to incorporate higher excipient loadings without compromising cocrystal formation, and investigate if these changes can result cocrystal formation by this method in the presence of amorphous polymeric excipients.

References

AAKERÖY, C. B., FASULO, M., SCHULTHEISS, N., DESPER, J. & MOORE, C. 2007. Structural competition between hydrogen bonds and halogen bonds. *Journal of the American Chemical Society,* 129**,** 13772-13773.

AAKERÖY, C. B., FORBES, S. & DESPER, J. 2009. Using Cocrystals To Systematically Modulate Aqueous Solubility and Melting Behavior of an Anticancer Drug. *Journal of the American Chemical Society,* 131**,** 17048-17049.

AAKERÖY , C. B. & SALMON, D. J. 2005. Building co-crystals with molecular sense and supramolecular sensibility. *CrystEngComm,* 7**,** 439-448.

ABDULLAH, E. C. & GELDART, D. 1999. The use of bulk density measurements as flowability indicators. *Powder technology,* 102**,** 151-165.

AGNESE, T., CECH, T., GEISELHART, V. & WAGNER, E. 2010. Comparing the wet granulation properties of PVA-PEG graft copolymer and different PVP grades in fluid bed granulation processes applying different inlet air temperatures. *Aix en Provence: 2nd Conference on Innovation in Drug Deliver*.

AGUILLON, A. R., MASCARELLO, A., SEGRETTI, N. D., DE AZEVEDO, H. F. Z., GUIMARAES, C. R. W., MIRANDA, L. S. M. & DE SOUZA, R. O. M. A. 2018. Synthetic Strategies toward SGLT2 Inhibitors. *Organic Process Research & Development*.

AINOUZ, A., AUTHELIN, J.-R., BILLOT, P. & LIEBERMAN, H. 2009. Modeling and prediction of cocrystal phase diagrams. *International Journal of Pharmaceutics,* 374**,** 82-89.

AITIPAMULA, S., BANERJEE, R., BANSAL, A. K., BIRADHA, K., CHENEY, M. L., CHOUDHURY, A. R., DESIRAJU, G. R., DIKUNDWAR, A. G., DUBEY, R. & DUGGIRALA, N. 2012. Polymorphs, salts, and cocrystals: what's in a name? *Crystal growth & design,* 12**,** 2147-2152.

ALHALAWEH, A. & VELAGA, S. P. 2010. Formation of Cocrystals from Stoichiometric Solutions of Incongruently Saturating Systems by Spray Drying. *Crystal Growth & Design,* 10**,** 3302-3305.

ALMANSA, C., MERCÈ, R., TESSON, N., FARRAN, J., TOMÀS, J. & PLATA-SALAMÁN, C. R. 2017. Co-crystal of tramadol hydrochloride–celecoxib (ctc): a novel API–API co-crystal for the treatment of pain. *Crystal Growth & Design,* 17**,** 1884-1892.

ALSHAHATEET, S. F. 2010. Synthesis and supramolecularity of hydrogen-bonded cocrystals of pharmaceutical model rac-ibuprofen with pyridine derivatives. *Molecular Crystals and Liquid Crystals,* 533**,** 152-161.

ALSHAHATEET, S. F. 2011. Synthesis and X-ray Crystallographic Analysis of Pharmaceutical Model Rac-Ibuprofen Cocrystal. *Journal of Chemical Crystallography,* 41**,** 276-279.

ALVAREZ, C., NUNEZ, I., TORRADO, J. J., GORDON, J., POTTHAST, H. & GARCIA-ARIETA, A. 2011. Investigation on the possibility of biowaivers for ibuprofen. *J Pharm Sci,* 100**,** 2343-9.

AMBIKE, A. A., MAHADIK, K. R. & PARADKAR, A. 2005. Spray-dried amorphous solid dispersions of simvastatin, a low T g drug: in vitro and in vivo evaluations. *Pharmaceutical research,* 22**,** 990-998.

AMHARAR, Y., CURTIN, V., GALLAGHER, K. H. & HEALY, A. M. 2014. Solubility of crystalline organic compounds in high and low molecular weight amorphous matrices above and below the glass transition by zero enthalpy extrapolation. *International Journal of Pharmaceutics,* 472**,** 241-247.

AMIDON, G. L., LENNERNÄS, H., SHAH, V. P. & CRISON, J. R. 1995. A Theoretical Basis for a Biopharmaceutic Drug Classification: The Correlation of in Vitro Drug Product Dissolution and in Vivo Bioavailability. *Pharmaceutical Research,* 12**,** 413-420.

ANDRIENKO, D. 2018. Introduction to liquid crystals. *Journal of Molecular Liquids,* 267**,** 520-541.

ANTONIOU, E., THEMISTOU, E., SARKAR, B., TSIANOU, M. & ALEXANDRIDIS, P. 2010. Structure and dynamics of dextran in binary mixtures of a good and a bad solvent. *Colloid and Polymer Science,* 288**,** 1301-1312.

ARRIBAS BUENO, R., CROWLEY, C. M., HODNETT, B. K., HUDSON, S. & DAVERN, P. 2017. Influence of Process Parameters on the Heterogeneous Nucleation of Active Pharmaceutical Ingredients onto Excipients. *Organic Process Research & Development,* 21**,** 559-570.

BABU, N. J., CHERUKUVADA, S., THAKURIA, R. & NANGIA, A. 2010. Conformational and synthon polymorphism in furosemide (Lasix). *Crystal Growth & Design,* 10**,** 1979-1989.

BABU, N. J. & NANGIA, A. 2011. Solubility advantage of amorphous drugs and pharmaceutical cocrystals. *Crystal Growth & Design,* 11**,** 2662-2679.

BAG, P. P., PATNI, M. & REDDY, C. M. 2011. A kinetically controlled crystallization process for identifying new co-crystal forms: fast evaporation of solvent from solutions to dryness. *CrystEngComm,* 13**,** 5650-5652.

BAGHEL, S., CATHCART, H. & O'REILLY, N. J. 2016. Polymeric amorphous solid dispersions: a review of amorphization, crystallization, stabilization, solid-state characterization, and aqueous solubilization of biopharmaceutical classification system class II drugs. *Journal of pharmaceutical sciences,* 105**,** 2527-2544.

BAIRD, J. A. & TAYLOR, L. S. 2012. Evaluation of amorphous solid dispersion properties using thermal analysis techniques. *Advanced Drug Delivery Reviews,* 64**,** 396-421.

BAK, A., GORE, A., YANEZ, E., STANTON, M., TUFEKCIC, S., SYED, R., AKRAMI, A., ROSE, M., SURAPANENI, S., BOSTICK, T., KING, A., NEERVANNAN, S., OSTOVIC, D. & KOPARKAR, A. 2008. The co-crystal approach to improve the exposure of a water-insoluble compound: AMG 517 sorbic acid co-crystal characterization and pharmacokinetics. *Journal of Pharmaceutical Sciences,* 97**,** 3942-3956.

BAKILER, M., BOLUKBASI, O. & YILMAZ, A. 2007. An experimental and theoretical study of vibrational spectra of picolinamide, nicotinamide, and isonicotinamide. *Journal of Molecular Structure,* 826**,** 6-16.

BASAVOJU, S., BOSTRÖM, D. & VELAGA, S. P. 2008. Indomethacin–Saccharin Cocrystal: Design, Synthesis and Preliminary Pharmaceutical Characterization. *Pharmaceutical Research,* 25**,** 530-541.

BAUER, J., SPANTON, S., HENRY, R., QUICK, J., DZIKI, W., PORTER, W. & MORRIS, J. 2001. Ritonavir: An Extraordinary Example of Conformational Polymorphism. *Pharmaceutical Research,* 18**,** 859-866.

BECHT, S., FRANKE, R., GEIßELMANN, A. & HAHN, H. 2009. An industrial view of process intensification. *Chemical Engineering and Processing: Process Intensification,* 48**,** 329-332.

BERGE, S. M., BIGHLEY, L. D. & MONKHOUSE, D. C. 1977. Pharmaceutical salts. *Journal of pharmaceutical sciences,* 66**,** 1-19.

BERNHARDSON, D., BRANDT, T. A., HULFORD, C. A., LEHNER, R. S., PRESTON, B. R., PRICE, K., SAGAL, J. F., ST. PIERRE, M. J., THOMPSON, P. H. & THUMA, B. 2014. Development of an early-phase bulk enabling route to sodium-dependent glucose cotransporter 2 inhibitor ertugliflozin. *Organic Process Research & Development,* 18**,** 57-65.

BERNSTEIN, J. 2002. *Polymorphism in molecular crystals,* Oxford University Press.

BERRY, D. J., SEATON, C. C., CLEGG, W., HARRINGTON, R. W., COLES, S. J., HORTON, P. N., HURSTHOUSE, M. B., STOREY, R., JONES, W. & FRISCIC, T. 2008. Applying hot-stage microscopy to co-crystal screening: a study of nicotinamide with seven active pharmaceutical ingredients. *Crystal Growth and Design,* 8**,** 1697-1712.

BETHUNE, S. J., HUANG, N., JAYASANKAR, A. & RODRÍGUEZ-HORNEDO, N. R. 2009. Understanding and predicting the effect of cocrystal components and pH on cocrystal solubility. *Crystal Growth & Design,* 9**,** 3976-3988.

BHARATE, S. S., BHARATE, S. B. & BAJAJ, A. N. 2016. Interactions and incompatibilities of pharmaceutical excipients with active pharmaceutical ingredients: a comprehensive review. *Journal of Excipients and Food Chemicals,* 1**,** 3-26.

BHATT, P. M. & DESIRAJU, G. R. 2007. Tautomeric polymorphism in omeprazole. *Chemical communications***,** 2057-2059.

BHOGALA, B. R., BASAVOJU, S. & NANGIA, A. 2005. Tape and layer structures in cocrystals of some di-and tricarboxylic acids with 4, 4'-bipyridines and isonicotinamide. From binary to ternary cocrystals. *CrystEngComm,* 7**,** 551-562.

BHOGALA, B. R. & NANGIA, A. 2008. Ternary and quaternary co-crystals of 1, 3-cis, 5-cis-cyclohexanetricarboxylic acid and 4, 4′-bipyridines. *New Journal of Chemistry,* 32**,** 800-807.

BLAGDEN, N., DE MATAS, M., GAVAN, P. T. & YORK, P. 2007. Crystal engineering of active pharmaceutical ingredients to improve solubility and dissolution rates. *Advanced Drug Delivery Reviews,* 59**,** 617-630.

BLUNDELL, D. J. 1987. On the interpretation of multiple melting peaks in poly(ether ether ketone). *Polymer,* 28**,** 2248-2251.

BOLDYREV, V. V. 2004. Mechanochemical modification and synthesis of drugs. *Journal of materials science,* 39**,** 5117-5120.

BOSQUILLON, C., LOMBRY, C., PRÉAT, V. & VANBEVER, R. 2001. Influence of formulation excipients and physical characteristics of inhalation dry powders on their aerosolization performance. *Journal of Controlled Release,* 70**,** 329-339.

BOWLES, P., BRENEK, S. J., CARON, S. P., DO, N. M., DREXLER, M. T., DUAN, S., DUBÉ, P., HANSEN, E. C., JONES, B. P. & JONES, K. N. 2014. Commercial route research and development for SGLT2 inhibitor candidate ertugliflozin. *Organic Process Research & Development,* 18**,** 66-81.

BRAGA, D., GREPIONI, F., MAINI, L., PROSPERI, S., GOBETTO, R. & CHIEROTTI, M. R. 2010. From unexpected reactions to a new family of ionic co-crystals: the case of barbituric acid with alkali bromides and caesium iodide. *Chemical communications,* 46**,** 7715-7717.

BREITENBACH, J. 2002. Melt extrusion: from process to drug delivery technology. *European Journal of Pharmaceutics and Biopharmaceutics,* 54**,** 107-117.

BRITTAIN, H. G. 2013. Pharmaceutical Cocrystals: The Coming Wave of New Drug Substances. *Journal of Pharmaceutical Sciences,* 102**,** 311-317.

BRITTAIN, H. G., BYRN, S. R. & LEE, E. 1999. Structural aspects of polymorphism. *Polymorphism in pharmaceutical solids,* 95.

BROADHEAD, J., EDMOND ROUAN, S. K. & RHODES, C. T. 1992. The spray drying of pharmaceuticals. *Drug Development and Industrial Pharmacy,* 18**,** 1169-1206.

BRUKER 2014. APEX v2014.11-0, Bruker AXS Inc., Madison, Wisconsin, USA.

BRUKER 2014/5. SADABS, Bruker AXS Inc., Madison, Wisconsin, USA.

BRUNNER, E. 1904. Reaktionsgeschwindigkeit in heterogenen Systemen. *Zeitschrift für physikalische Chemie,* 47**,** 56-102.

BUCHHOLZ, S. 2010. Future manufacturing approaches in the chemical and pharmaceutical industry. *Chemical Engineering and Processing: Process Intensification,* 49**,** 993-995.

BUČAR, D. K., LANCASTER, R. W. & BERNSTEIN, J. 2015. Disappearing polymorphs revisited. *Angewandte Chemie International Edition,* 54**,** 6972-6993.

BYRN, S. R., PFEIFFER, R. R. & STOWELL, J. G. 1999. Solid-State Chemistry of Drugs, SSCI, West Lafayette, 1999;(b) Polymorphism in Pharmaceutical Solids. Marcel Dekker, New York.

CAL, K. & SOLLOHUB, K. 2009. Spray Drying Technique. I: Hardware and Process Parameters. *Journal of Pharmaceutical Sciences,* 99**,** 575-586.

CARON, V., TAJBER, L., CORRIGAN, O. I. & HEALY, A. M. 2011. A Comparison of Spray Drying and Milling in the Production of Amorphous Dispersions of

Sulfathiazole/Polyvinylpyrrolidone and Sulfadimidine/Polyvinylpyrrolidone. *Molecular Pharmaceutics,* 8**,** 532-542.

CARPENTER, J. F. & CROWE, J. H. 1989. An infrared spectroscopic study of the interactions of carbohydrates with dried proteins. *Biochemistry,* 28**,** 3916-3922.

CAVAZZUTI, M. 2013. Design of experiments. *Optimization Methods.* Springer.

CENSI, R. & DI MARTINO, P. 2015. Polymorph impact on the bioavailability and stability of poorly soluble drugs. *Molecules,* 20**,** 18759-18776.

CHADWICK, K., DAVEY, R. & CROSS, W. 2007. How does grinding produce co-crystals? Insights from the case of benzophenone and diphenylamine. *CrystEngComm,* 9**,** 732-734.

CHATTORAJ, S., SHI, L. & SUN, C. C. 2010. Understanding the relationship between crystal structure, plasticity and compaction behaviour of theophylline, methyl gallate, and their 1: 1 co-crystal. *CrystEngComm,* 12**,** 2466-2472.

CHAUDHARI, S. P. & DAVE, R. H. 2015. To prepare and characterize microcrystalline cellulose granules using water and isopropyl alcohol as granulating agents and determine its end-point by thermal and rheological tools. *Drug development and industrial pharmacy,* 41**,** 744-752.

CHAVAN, R. B., THIPPARABOINA, R., YADAV, B. & SHASTRI, N. R. 2018. Continuous manufacturing of co-crystals: challenges and prospects. *Drug Delivery and Translational Research,* 8**,** 1726-1739.

CHEN, H., KHEMTONG, C., YANG, X., CHANG, X. & GAO, J. 2011. Nanonization strategies for poorly water-soluble drugs. *Drug Discovery Today,* 16**,** 354-360.

CHEN, S., XI, H., HENRY, R. F., MARSDEN, I. & ZHANG, G. G. Z. 2010. Chiral co-crystal solid solution: structures, melting point phase diagram, and chiral enrichment of (ibuprofen) 2 (4, 4-dipyridyl). *CrystEngComm,* 12**,** 1485-1493.

CHIARELLA, R. A., DAVEY, R. J. & PETERSON, M. L. 2007. Making co-crystals the utility of ternary phase diagrams. *Crystal growth & design,* 7**,** 1223-1226.

CHILDS, S. L. 2009. Cocrystal design and packing analysis based on a family of crystal structures containing a common molecule. *ABSTRACTS OF PAPERS OF THE AMERICAN CHEMICAL SOCIETY,* 237.

CHILDS, S. L. & HARDCASTLE, K. I. 2007. Cocrystals of piroxicam with carboxylic acids. *Crystal Growth & Design,* 7**,** 1291-1304.

CHILDS, S. L., RODRÍGUEZ-HORNEDO, N., REDDY, L. S., JAYASANKAR, A., MAHESHWARI, C., MCCAUSLAND, L., SHIPPLETT, R. & STAHLY, B. C. 2008. Screening strategies based on solubility and solution composition generate pharmaceutically acceptable cocrystals of carbamazepine. *CrystEngComm,* 10**,** 856-864.

CHILDS, S. L., STAHLY, G. P. & PARK, A. 2007. The salt− cocrystal continuum: the influence of crystal structure on ionization state. *Molecular pharmaceutics,* 4**,** 323-338.

CHIN CHUNG, M., LONGHIN BOSQUESI, P. & LEANDRO DOS SANTOS, J. 2011. A prodrug approach to improve the physico-chemical properties and decrease the genotoxicity of nitro compounds. *Current pharmaceutical design,* 17**,** 3515-3526.

CHIOU, D. & LANGRISH, T. A. G. 2008. A comparison of crystallisation approaches in spray drying. *Journal of Food Engineering,* 88**,** 177-185.

CHIOU, D., LANGRISH, T. A. G. & BRAHAM, R. 2008. The effect of temperature on the crystallinity of lactose powders produced by spray drying. *Journal of Food Engineering,* 86**,** 288-293.

CHOW, S. F., CHEN, M., SHI, L., CHOW, A. H. L. & SUN, C. C. 2012. Simultaneously Improving the Mechanical Properties, Dissolution Performance, and Hygroscopicity of Ibuprofen and Flurbiprofen by Cocrystallization with Nicotinamide. *Pharmaceutical Research,* 29**,** 1854-1865.

CINČIĆ, D., FRIŠČIĆ, T. & JONES, W. 2008. Isostructural Materials Achieved by Using Structurally Equivalent Donors and Acceptors in Halogen-Bonded Cocrystals. *Chemistry-A European Journal,* 14**,** 747-753.

COOK, D., BROWN, D., ALEXANDER, R., MARCH, R., MORGAN, P., SATTERTHWAITE, G. & PANGALOS, M. N. 2014. Lessons learned from the fate of AstraZeneca's drug pipeline: a five-dimensional framework. *Nat Rev Drug Discov,* 13**,** 419-431.

CORRIGAN, O. I. 1995. Thermal analysis of spray dried products. *Thermochimica Acta,* 248**,** 245-258.

CRAIG, D. Q. M., ROYALL, P. G., KETT, V. L. & HOPTON, M. L. 1999. The relevance of the amorphous state to pharmaceutical dosage forms: glassy drugs and freeze dried systems. *International Journal of Pharmaceutics,* 179**,** 179-207.

CROWLEY, M. M., ZHANG, F., REPKA, M. A., THUMMA, S., UPADHYE, S. B., KUMAR BATTU, S., MCGINITY, J. W. & MARTIN, C. 2007. Pharmaceutical applications of hot-melt extrusion: part I. *Drug development and industrial pharmacy,* 33**,** 909-926.

CRUZ-CABEZA, A. J. 2012. Acid–base crystalline complexes and the p K a rule. *CrystEngComm,* 14**,** 6362-6365.

DAHAN, A., MILLER, J. M. & AMIDON, G. L. 2009. Prediction of solubility and permeability class membership: provisional BCS classification of the world's top oral drugs. *The AAPS journal,* 11**,** 740-746.

DAURIO, D., NAGAPUDI, K., LI, L., QUAN, P. & NUNEZ, F.-A. 2014. Application of twin screw extrusion to the manufacture of cocrystals: scale-up of AMG 517–sorbic acid cocrystal production. *Faraday discussions,* 170**,** 235-249.

DAVID, S. T. & AUGSBURGER, L. L. 1977. Plastic flow during compression of directly compressible fillers and its effect on tablet strength. *Journal of pharmaceutical sciences,* 66**,** 155-159.

DAVIS, M. T., POTTER, C. B. & WALKER, G. M. 2018. Downstream processing of a ternary amorphous solid dispersion: The impacts of spray drying and hot melt extrusion on powder flow, compression and dissolution. *International Journal of Pharmaceutics,* 544**,** 242-253.

DE VILLIERS, M. M. 2005. Powder flow and compressibility. *Theory and Practice of Contemporary Pharmaceutics, CRC Press, Boca Raton, Florida, USA***,** 298-299.

DESIRAJU, G. R. 1995. Supramolecular synthons in crystal engineering—a new organic synthesis. *Angewandte Chemie International Edition in English,* 34**,** 2311-2327.

DHANESHWAR, S. & VADNERKAR, G. 2011. Rational design and development of colon-specific prodrugs. *Current topics in medicinal chemistry,* 11**,** 2318-2345.

DHINGRA, G., SREELESH, B., NAGPAL, M., RAKHA, P. & NAGORI, B. P. 2010. In Vitro Dissolution Testing of Ibuprofen Using Compendial and Biorelevant Dissolution Media. *Research Journal of Pharmacy and Technology,* 3**,** 931-933.

DHUMAL, R. S., KELLY, A. L., YORK, P., COATES, P. D. & PARADKAR, A. 2010. Cocrystalization and simultaneous agglomeration using hot melt extrusion. *Pharmaceutical research,* 27**,** 2725-2733.

DI MARIA, F., FABIANO, E., GENTILI, D., BIASIUCCI, M., SALZILLO, T., BERGAMINI, G., GAZZANO, M., ZANELLI, A., BRILLANTE, A. & CAVALLINI, M. 2014. Polymorphism in Crystalline Microfibers of Achiral Octithiophene: The Effect on Charge Transport, Supramolecular Chirality and Optical Properties. *Advanced Functional Materials,* 24**,** 4943-4951.

DO AMARAL, L. H., DO CARMO, F. A., AMARO, M. I., DE SOUSA, V. P., DA SILVA, L. C. R. P., DE ALMEIDA, G. S., RODRIGUES, C. R., HEALY, A. M. & CABRAL, L. M. 2018. Development and Characterization of Dapsone Cocrystal Prepared by Scalable Production Methods. *AAPS PharmSciTech,* 19**,** 2687-2699.

DOBRY, D. E., SETTELL, D. M., BAUMANN, J. M., RAY, R. J., GRAHAM, L. J. & BEYERINCK, R. A. 2009. A Model-Based Methodology for Spray-Drying Process Development. *Journal of Pharmaceutical Innovation,* 4**,** 133-142.

DOMÍNGUEZ, L., FAGIOLINO, P., GORDON, S. & MANTA, E. 1995. Bioavailability comparison between albendazole and albendazole sulphoxide in rats and man. *Farmaco (Societa chimica italiana: 1989),* 50**,** 697-702.

DUBEY, R. & DESIRAJU, G. R. 2015. Combinatorial selection of molecular conformations and supramolecular synthons in quercetin cocrystal landscapes: a route to ternary solids. *IUCrJ,* 2**,** 402-408.

DUGGAN, D., HARE, L., DITZLER, C., LEI, B. & KWAN, K. 1977. The disposition of sulindac. *Clinical Pharmacology & Therapeutics,* 21**,** 326-335.

DUGGIRALA, N. K., SMITH, A. J., WOJTAS, Ł., SHYTLE, R. D. & ZAWOROTKO, M. J. 2014. Physical stability enhancement and pharmacokinetics of a lithium ionic cocrystal with glucose. *Crystal Growth & Design,* 14**,** 6135-6142.

ECCLES, K. S., DEASY, R. E., FABIAN, L., BRAUN, D. E., MAGUIRE, A. R. & LAWRENCE, S. E. 2011. Expanding the crystal landscape of isonicotinamide: concomitant polymorphism and co-crystallisation. *CrystEngComm,* 13**,** 6923-6925.

EDDLESTON, M. D., PATEL, B., DAY, G. M. & JONES, W. 2013. Cocrystallization by freeze-drying: preparation of novel multicomponent crystal forms. *Crystal Growth & Design,* 13**,** 4599-4606.

EMA 2010. Guideline on the investigation of bioequivalence. *London: European Medicines Agency*.

EMA 2015. Reflection paper on the use of cocrystals of active substances in medicinal products. *EMA/CHMP/CVMP/QWP/284008/2015*.

EMA 2018. Steglatro Public Assessment Report.

ENRIGHT, S. & DALTON, M. 2013. The impact of the patent cliff on pharma-chem output in Ireland. *Journal of the Statistical and Social Inquiry Society of Ireland,* 43**,** 91.

FDA 2016. Regulatory Classification of Pharmaceutical Co-Crystals Guidance for Industry. *US Dept. of Health and Human Services FDA Center for Drug Evaluation and Research (CDER)*.

FDA 2018. Regulatory Classification of Pharmaceutical Co-Crystals Guidance for Industry. *US Dept. of Health and Human Services FDA Center for Drug Evaluation and Research (CDER)*.

FEIL, H., BAE, Y. H., FEIJEN, J. & KIM, S. W. 1993. Effect of comonomer hydrophilicity and ionization on the lower critical solution temperature of N-isopropylacrylamide copolymers. *Macromolecules,* 26**,** 2496-2500.

FENG, L., KARPINSKI, P. H., SUTTON, P., LIU, Y., HOOK, D. F., HU, B., BLACKLOCK, T. J., FANWICK, P. E., PRASHAD, M., GODTFREDSEN, S. & ZILTENER, C. 2012. LCZ696: a dual-acting sodium supramolecular complex. *Tetrahedron Letters,* 53**,** 275-276.

FERNÁNDEZ-BERTRAN, J. F. 1999. Mechanochemistry: an overview. *Pure and applied chemistry,* 71**,** 581-586.

FILHO, O. T., PINHEIRO, J. C., COSTA, E. B. D., KONDO, R. T., SOUZA, R. A. D., NOGUEIRA, V. M. & MAURO, A. E. 2006. Theoretical and experimental study of the infrared spectrum of isonicotinamide. *Journal of Molecular Structure: THEOCHEM,* 763**,** 175-179.

FINI, A. 2016. Release Problems for Nifedipine in the Presence of Soluplus. *Ommega Internationals,* 3**,** 1-8.

FORSTER, A., HEMPENSTALL, J., TUCKER, I. & RADES, T. 2001. Selection of excipients for melt extrusion with two poorly water-soluble drugs by solubility parameter calculation and thermal analysis. *International Journal of Pharmaceutics,* 226**,** 147-161.

FREEMAN, R. 2007. Measuring the flow properties of consolidated, conditioned and aerated powders — A comparative study using a powder rheometer and a rotational shear cell. *Powder Technology,* 174**,** 25-33.

FREUNDLICH, H. 1909. Kolloidchemie. *Akademischer Verlagsgeselschaft, Leipzig*.

FRIŠČIĆ, T. & JONES, W. 2009. Recent advances in understanding the mechanism of cocrystal formation via grinding. *Crystal Growth and Design,* 9**,** 1621-1637.

FRIŠČIĆ, T. & JONES, W. 2007. Cocrystal architecture and properties: design and building of chiral and racemic structures by solid–solid reactions. *Faraday discussions,* 136**,** 167-178.

FUCKE, K., MYZ, S. A., SHAKHTSHNEIDER, T. P., BOLDYREVA, E. V. & GRIESSER, U. J. 2012. How good are the crystallisation methods for co-crystals? A comparative study of piroxicam. *New Journal of Chemistry,* 36**,** 1969-1977.

GAGNIÈRE, E., MANGIN, D., PUEL, F., RIVOIRE, A., MONNIER, O., GARCIA, E. & KLEIN, J.-P. 2009. Formation of co-crystals: kinetic and thermodynamic aspects. *Journal of Crystal Growth,* 311**,** 2689-2695.

GENINA, N., HADI, B. & LÖBMANN, K. 2017. Hot melt extrusion (HME) as solvent-free technique for a continuous manufacturing of drug-loaded mesoporous silica. *Journal of Pharmaceutical Sciences*.

GHADI, R. & DAND, N. 2017. BCS class IV drugs: Highly notorious candidates for formulation development. *Journal of Controlled Release,* 248**,** 71-95.

GOOD, D. J. & RODRÍGUEZ-HORNEDO, N. R. 2009. Solubility advantage of pharmaceutical cocrystals. *Crystal Growth and Design,* 9**,** 2252-2264.

GRANT, D. J. W. & YORK, P. 1986. Entropy of processing: a new quantity for comparing the solid state disorder of pharmaceutical materials. *International Journal of Pharmaceutics,* 30**,** 161-180.

GREENHALGH, D. J., WILLIAMS, A. C., TIMMINS, P. & YORK, P. 1999. Solubility parameters as predictors of miscibility in solid dispersions. *Journal of Pharmaceutical Sciences,* 88**,** 1182-1190.

GRIESSER, U. J. 2006. The importance of solvates. Wiley-VCH, Weinheim. p.

GROOM, C. R., BRUNO, I. J., LIGHTFOOT, M. P. & WARD, S. C. 2016. The Cambridge Structural Database. *Acta Crystallographica Section B,* 72**,** 171-179.

GROSSJOHANN, C., ECCLES, K. S., MAGUIRE, A. R., LAWRENCE, S. E., TAJBER, L., CORRIGAN, O. I. & HEALY, A. M. 2012. Characterisation, solubility and intrinsic dissolution behaviour of benzamide: dibenzyl sulfoxide cocrystal. *International Journal of Pharmaceutics,* 422**,** 24-32.

GROSSJOHANN, C., SERRANO, D. R., PALUCH, K. J., O'CONNELL, P., VELLA-ZARB, L., MANESIOTIS, P., MCCABE, T., TAJBER, L., CORRIGAN, O. I. & HEALY, A. M. 2015. Polymorphism in Sulfadimidine/4-Aminosalicylic Acid Cocrystals: Solid-State Characterization and Physicochemical Properties. *Journal of Pharmaceutical Sciences,* 104**,** 1385-1398.

GU, J., NOE, A., CHANDRA, P., AL-FAYOUMI, S., LIGUEROS-SAYLAN, M., SARANGAPANI, R., MAAHS, S., KSANDER, G., RIGEL, D. F. & JENG, A. Y. 2010. Pharmacokinetics and Pharmacodynamics of LCZ696, a Novel Dual-Acting Angiotensin Receptor—Neprilysin Inhibitor (ARNi). *The Journal of Clinical Pharmacology,* 50**,** 401-414.

GUNS, S., DEREYMAKER, A., KAYAERT, P., MATHOT, V., MARTENS, J. A. & VAN DEN MOOTER, G. 2010. Comparison Between Hot-Melt Extrusion and Spray-Drying for Manufacturing Solid Dispersions of the Graft Copolymer of Ethylene Glycol and Vinylalcohol. *Pharm Res,* 28**,** 673-82.

GUNS, S., MATHOT, V., MARTENS, J. A. & VAN DEN MOOTER, G. 2012. Upscaling of the hot-melt extrusion process: Comparison between laboratory scale and pilot scale production of solid dispersions with miconazole and Kollicoat® IR. *European Journal of Pharmaceutics and Biopharmaceutics,* 81**,** 674-682.

HAN, X., GHOROI, C., TO, D., CHEN, Y. & DAVÉ, R. 2011. Simultaneous micronization and surface modification for improvement of flow and dissolution of drug particles. *International Journal of Pharmaceutics,* 415**,** 185-195.

HANCOCK, B. C. 2002. Disordered drug delivery: destiny, dynamics and the Deborah number. *Journal of pharmacy and pharmacology,* 54**,** 737-746.

HANCOCK, B. C. & PARKS, M. 2000. What is the true solubility advantage for amorphous pharmaceuticals? *Pharmaceutical research,* 17**,** 397-404.

HANCOCK, B. C., SHAMBLIN, S. L. & ZOGRAFI, G. 1995. Molecular mobility of amorphous pharmaceutical solids below their glass transition temperatures. *Pharmaceutical research,* 12**,** 799-806.

HANCOCK, B. C., YORK, P. & ROWE, R. C. 1997. The use of solubility parameters in pharmaceutical dosage form design. *International Journal of Pharmaceutics,* 148**,** 1-21.

HANCOCK, B. C. & ZOGRAFI, G. 1997. Characteristics and significance of the amorphous state in pharmaceutical systems. *Journal of pharmaceutical sciences,* 86**,** 1-12.

HANSEN, C. M. 1969. The universality of the solubility parameter. *Industrial & engineering chemistry product research and development,* 8**,** 2-11.

HANSEN, C. M. 2002. *Hansen solubility parameters: a user's handbook*, CRC press.

HANSEN, C. M. 2004. 50 Years with solubility parameters—past and future. *Progress in Organic Coatings,* 51**,** 77-84.

HARRISON, W. T. A., YATHIRAJAN, H. S., BINDYA, S. & ANILKUMAR, H. G. 2007. Escitalopram oxalate: co-existence of oxalate dianions and oxalic acid molecules in the same crystal. *Acta Crystallographica Section C: Crystal Structure Communications,* 63**,** o129-o131.

HEALY, A. M., WORKU, Z. A., KUMAR, D. & MADI, A. M. 2017. Pharmaceutical solvates, hydrates and amorphous forms: A special emphasis on cocrystals. *Advanced Drug Delivery Reviews,* 117**,** 25-46.

HENGSAWAS SURASARANG, S., KEEN, J. M., HUANG, S., ZHANG, F., MCGINITY, J. W. & WILLIAMS, R. O., 3RD 2017. Hot melt extrusion versus spray drying: hot melt extrusion degrades albendazole. *Drug Dev Ind Pharm,* 43**,** 797-811.

HENRY, T. R. 2003. The history of valproate in clinical neuroscience. *Psychopharmacology bulletin,* 37**,** 5-16.

HIENDRAWAN, S., VERIANSYAH, B., WIDJOJOKUSUMO, E., SOEWANDHI, S. N., WIKARSA, S. & TJANDRAWINATA, R. R. 2016. Physicochemical and mechanical properties of paracetamol cocrystal with 5-nitroisophthalic acid. *International Journal of Pharmaceutics,* 497**,** 106-113.

HILDEBRAND, J. H. 1936. Solubility of Non-electrolytes.

HUGGER, E. D., NOVAK, B. L., BURTON, P. S., AUDUS, K. L. & BORCHARDT, R. T. 2002. A comparison of commonly used polyethoxylated pharmaceutical excipients on their ability to inhibit P-glycoprotein activity in vitro. *Journal of pharmaceutical sciences,* 91**,** 1991-2002.

HUGHEY, J. R., KEEN, J. M., MILLER, D. A., KOLTER, K., LANGLEY, N. & MCGINITY, J. W. 2013. The use of inorganic salts to improve the dissolution characteristics of tablets containing Soluplus®-based solid dispersions. *European Journal of Pharmaceutical Sciences,* 48**,** 758-766.

HULSE, W. L., FORBES, R. T., BONNER, M. C. & GETROST, M. 2009. Influence of protein on mannitol polymorphic form produced during co-spray drying. *International Journal of Pharmaceutics,* 382**,** 67-72.

HÖRTER, D. & DRESSMAN, J. B. 2001. Influence of physicochemical properties on dissolution of drugs in the gastrointestinal tract. *Advanced Drug Delivery Reviews,* 46**,** 75-87.

IOGANSEN, A. V., KURKCHI, G. A. & DEMENT'EVA, L. A. 1977. Infrared spectra of primary amides in thevNH range. *Journal of Structural Chemistry,* 18**,** 589-595.

JAMES, S. L., ADAMS, C. J., BOLM, C., BRAGA, D., COLLIER, P., FRIŠČIĆ, T., GREPIONI, F., HARRIS, K. D. M., HYETT, G. & JONES, W. 2012. Mechanochemistry: opportunities for new and cleaner synthesis. *Chemical Society Reviews,* 41**,** 413-447.

JINNO, J.-I., KAMADA, N., MIYAKE, M., YAMADA, K., MUKAI, T., ODOMI, M., TOGUCHI, H., LIVERSIDGE, G. G., HIGAKI, K. & KIMURA, T. 2006. Effect of particle size reduction on dissolution and oral absorption of a poorly water-soluble drug, cilostazol, in beagle dogs. *Journal of Controlled Release,* 111**,** 56-64.

JOHNSON, S. L. & RUMON, K. A. 1965. Infrared spectra of solid 1: 1 pyridine-benzoic acid complexes; the nature of the hydrogen bond as a function of the acid-base levels in the complex. *The Journal of Physical Chemistry,* 69**,** 74-86.

JONES, W., MOTHERWELL, W. D. S. & TRASK, A. V. 2006. Pharmaceutical cocrystals: an emerging approach to physical property enhancement. *MRS bulletin,* 31**,** 875-879.

KALEPU, S. & NEKKANTI, V. 2015. Insoluble drug delivery strategies: review of recent advances and business prospects. *Acta Pharmaceutica Sinica B,* 5**,** 442-453.

KAWABATA, Y., WADA, K., NAKATANI, M., YAMADA, S. & ONOUE, S. 2011. Formulation design for poorly water-soluble drugs based on biopharmaceutics classification system: Basic approaches and practical applications. *International Journal of Pharmaceutics,* 420**,** 1-10.

KECK, C. M. & MÜLLER, R. H. 2006. Drug nanocrystals of poorly soluble drugs produced by high pressure homogenisation. *European journal of pharmaceutics and biopharmaceutics,* 62**,** 3-16.

KELLEHER, J. F., GILVARY, G. C., MADI, A. M., JONES, D. S., LI, S., TIAN, Y., ALMAJAAN, A., SENTA-LOYS, Z., ANDREWS, G. P. & HEALY, A. M. 2018. A comparative study between hot-melt extrusion and spray-drying for the manufacture of anti-hypertension compatible monolithic fixed-dose combination products. *International Journal of Pharmaceutics,* 545**,** 183-196.

KELLY, A. L., GOUGH, T., DHUMAL, R. S., HALSEY, S. A. & PARADKAR, A. 2012. Monitoring ibuprofen–nicotinamide cocrystal formation during solvent free continuous cocrystallization (SFCC) using near infrared spectroscopy as a PAT tool. *International Journal of Pharmaceutics,* 426**,** 15-20.

KHADKA, P., RO, J., KIM, H., KIM, I., KIM, J. T., KIM, H., CHO, J. M., YUN, G. & LEE, J. 2014. Pharmaceutical particle technologies: An approach to improve drug solubility, dissolution and bioavailability. *Asian Journal of Pharmaceutical Sciences,* 9**,** 304-316.

KHANKARI, R. K. & GRANT, D. J. W. 1995. Pharmaceutical hydrates. *Thermochimica acta,* 248**,** 61-79.

KIPP, J. E. 2004. The role of solid nanoparticle technology in the parenteral delivery of poorly water-soluble drugs. *International journal of pharmaceutics,* 284**,** 109-122.

KNOPP, M. M., OLESEN, N. E., HOLM, P., LANGGUTH, P., HOLM, R. & RADES, T. 2015. Influence of polymer molecular weight on drug–polymer solubility: a comparison between experimentally determined solubility in PVP and prediction derived from solubility in monomer. *Journal of pharmaceutical sciences,* 104**,** 2905-2912.

KOLAŠINAC, N., KACHRIMANIS, K., DJURIŠ, J., HOMŠEK, I., GRUJIĆ, B. & IBRIĆ, S. 2013. Spray coating as a powerful technique in preparation of solid dispersions with enhanced desloratadine dissolution rate. *Drug development and industrial pharmacy,* 39**,** 1020-1027.

KU, M. S. & DULIN, W. 2012. A biopharmaceutical classification-based Right-First-Time formulation approach to reduce human pharmacokinetic variability and project cycle time from First-In-Human to clinical Proof-Of-Concept. *Pharmaceutical Development and Technology,* 17**,** 285-302.

KUMAR, L., AMIN, A. & BANSAL, A. K. 2007. An overview of automated systems relevant in pharmaceutical salt screening. *Drug Discovery Today,* 12**,** 1046-1053.

KUMAR, S., SHEN, J., ZOLNIK, B., SADRIEH, N. & BURGESS, D. J. 2015. Optimization and dissolution performance of spray-dried naproxen nano-crystals. *International Journal of Pharmaceutics,* 486**,** 159-166.

LAITINEN, R., PRIEMEL, P. A., SURWASE, S., GRAESER, K., STRACHAN, C. J., GROHGANZ, H. & RADES, T. 2014. Theoretical considerations in developing amorphous solid dispersions. *Amorphous Solid Dispersions.* Springer.

LATIF, S., ABBAS, N., HUSSAIN, A., ARSHAD, M. S., BUKHARI, N. I., AFZAL, H., RIFFAT, S. & AHMAD, Z. 2018. Development of paracetamol-caffeine co-crystals to improve compressional, formulation and in vivo performance. *Drug Development and Industrial Pharmacy,* 44**,** 1099-1108.

LAURENCE, C. & BERTHELOT, M. 2000. Observations on the strength of hydrogen bonding. *Perspectives in Drug Discovery and Design,* 18**,** 39-60.

LEAPER, M. C., ALI, K. & INGHAM, A. J. 2017. Comparing the Dynamic Flow Properties and Compaction Properties of Pharmaceutical Powder Mixtures. *Chemical Engineering & Technology,* 41**,** 102-107.

LECHUGA-BALLESTEROS, D., ABDUL-FATTAH, A., STEVENSON, C. L. & BENNETT, D. B. 2003. Properties and stability of a liquid crystal form of cyclosporine—the first reported naturally occurring peptide that exists as a thermotropic liquid crystal. *Journal of pharmaceutical sciences,* 92**,** 1821-1831.

LEE, A. Y., ERDEMIR, D. & MYERSON, A. S. 2011. Crystal polymorphism in chemical process development. *Annual review of chemical and biomolecular engineering,* 2**,** 259-280.

LENZ, E., LOBMANN, K., RADES, T., KNOP, K. & KLEINEBUDDE, P. 2017. Hot Melt Extrusion and Spray Drying of Co-amorphous Indomethacin-Arginine With Polymers. *J Pharm Sci,* 106**,** 302-312.

LETURIA, M., BENALI, M., LAGARDE, S., RONGA, I. & SALEH, K. 2014. Characterization of flow properties of cohesive powders: A comparative study of traditional and new testing methods. *Powder Technology,* 253**,** 406-423.

LEVINTHAL, M. L. 1978. Propellant made with cocrystals of cyclotetramethylenetetranitramine and ammonium perchlorate. U.S. Patent 4,086,110.

LI, M., QIU, S., LU, Y., WANG, K., LAI, X. & REHAN, M. 2014a. Investigation of the effect of hydroxypropyl methylcellulose on the phase transformation and release profiles of carbamazepine-nicotinamide cocrystal. *Pharmaceutical research,* 31**,** 2312-2325.

LI, S., CHEN, J.-M. & LU, T.-B. 2014b. Synthon polymorphs of 1: 1 co-crystal of 5-fluorouracil and 4-hydroxybenzoic acid: their relative stability and solvent polarity dependence of grinding outcomes. *CrystEngComm,* 16**,** 6450-6458.

LI, S., JONES DAVID, S. & ANDREWS GAVIN, P. 2013. Hot Melt Extrusion: A Process Overview and Use in Manufacturing Solid Dispersions of Poorly Water-Soluble Drugs. *Drug Delivery Strategies for Poorly Water-Soluble Drugs***,** 325-358.

LI, S., YU, T., TIAN, Y., LAGAN, C., JONES, D. S. & ANDREWS, G. P. 2017. Mechanochemical Synthesis of Pharmaceutical Cocrystal Suspensions via Hot Melt Extrusion: Enhancing Cocrystal Yield. *Molecular Pharmaceutics,* 15**,** 3741-3754.

LI, S., YU, T., TIAN, Y., MCCOY, C. P., JONES, D. S. & ANDREWS, G. P. 2016. Mechanochemical Synthesis of Pharmaceutical Cocrystal Suspensions via Hot Melt Extrusion: Feasibility Studies and Physicochemical Characterization. *Molecular Pharmaceutics,* 13**,** 3054-3068.

LIPINSKI, C. A., LOMBARDO, F., DOMINY, B. W. & FEENEY, P. J. 2012. Experimental and computational approaches to estimate solubility and permeability in drug discovery and development settings. *Advanced drug delivery reviews,* 64**,** 4-17.

LITTRINGER, E. M., MESCHER, A., MAAS, S. G., WALZEL, P. & URBANETZ, N. A. 2011. Influence of droplet size on the crystallization behaviour of aqueous D-mannitol solutions during spray drying. *Institute for Liquid Atomization and Spray Systems***,** 1-8.

LIU, C., CHEN, Z., CHEN, Y., LU, J., LI, Y., WANG, S., WU, G. & QIAN, F. 2016. Improving oral bioavailability of sorafenib by optimizing the "Spring" and "Parachute" based on molecular interaction mechanisms. *Molecular pharmaceutics,* 13**,** 599-608.

LLINÀS, A. & GOODMAN, J. M. 2008. Polymorph control: past, present and future. *Drug Discovery Today,* 13**,** 198-210.

LOUWERSE, M. J., MALDONADO, A., ROUSSEAU, S., MOREAU-MASSELON, C., ROUX, B. & ROTHENBERG, G. 2017. Revisiting Hansen solubility parameters by including thermodynamics. *ChemPhysChem,* 18**,** 2999-3006.

LU, E., RODRÍGUEZ-HORNEDO, N. & SURYANARAYANAN, R. 2008. A rapid thermal method for cocrystal screening. *CrystEngComm,* 10**,** 665-668.

MAA, Y.-F., COSTANTINO, H. R., NGUYEN, P.-A. & HSU, C. C. 1997. The Effect of Operating and Formulation Variables on the Morphology of Spray-Dried Protein Particles. *Pharmaceutical Development and Technology,* 2**,** 213-223.

MACHUI, F., LANGNER, S., ZHU, X., ABBOTT, S. & BRABEC, C. J. 2012. Determination of the P3HT:PCBM solubility parameters via a binary solvent gradient method: Impact of solubility on the photovoltaic performance. *Solar Energy Materials and Solar Cells,* 100**,** 138-146.

MAHESHWARI, M., KETKAR, A. R., CHAUHAN, B., PATIL, V. B. & PARADKAR, A. R. 2003. Preparation and characterization of ibuprofen–cetyl alcohol beads by melt solidification technique: effect of variables. *International Journal of Pharmaceutics,* 261**,** 57-67.

MANIRUZZAMAN, M., BOATENG, J. S., SNOWDEN, M. J. & DOUROUMIS, D. 2012. A review of hot-melt extrusion: process technology to pharmaceutical products. *ISRN pharmaceutics***,** 1-9.

MARSAC, P. J., LI, T. & TAYLOR, L. S. 2009. Estimation of drug–polymer miscibility and solubility in amorphous solid dispersions using experimentally determined interaction parameters. *Pharmaceutical research,* 26**,** 139-151.

MATSUDA, Y., KAWAGUCHI, S., KOBAYASHI, H. & NISHIJO, J. 1984. Physicochemical characterization of spray-dried phenylbutazone polymorphs. *Journal of pharmaceutical sciences,* 73**,** 173-179.

MIAO, Z., NUCCI, G., AMIN, N., SHARMA, R., MASCITTI, V., TUGNAIT, M., VAZ, A. D., CALLEGARI, E. & KALGUTKAR, A. S. 2013. Pharmacokinetics, metabolism, and excretion of the antidiabetic agent ertugliflozin (PF-04971729) in healthy male subjects. *Drug Metabolism and Disposition,* 41**,** 445-456.

MILLQVIST-FUREBY, A., MALMSTEN, M. & BERGENSTÅHL, B. 1999. Spray-drying of trypsin — surface characterisation and activity preservation. *International Journal of Pharmaceutics,* 188**,** 243-253.

MIROSHNYK, I., MIRZA, S. & SANDLER, N. 2009. Pharmaceutical co-crystals–an opportunity for drug product enhancement. *Expert opinion on drug delivery,* 6**,** 333-341.

MOHAMMAD, M. A., ALHALAWEH, A. & VELAGA, S. P. 2011. Hansen solubility parameter as a tool to predict cocrystal formation. *Int J Pharm,* 407**,** 63-71.

MORADIYA, H. G., ISLAM, M. T., HALSEY, S., MANIRUZZAMAN, M., CHOWDHRY, B. Z., SNOWDEN, M. J. & DOUROUMIS, D. 2014. Continuous cocrystallisation of carbamazepine and trans-cinnamic acid via melt extrusion processing. *CrystEngComm,* 16**,** 3573-3583.

MORRIS, K. R. 1999. Structural aspects of hydrates and solvates. *Drugs and the pharmaceutical sciences,* 95**,** 125-181.

MUGHEIRBI, N. A., FLEISCHER, K. & TAJBER, L. 2016. A Rare Case of Mesomorphic Behavior–Molecular Reorientation of Itraconazole Liquid Crystal Induced by a Hygrothermal Treatment. *Crystal Growth & Design,* 16**,** 1329-1336.

MULLER, R. H. & KECK, C. M. 2004. Challenges and solutions for the delivery of biotech drugs–a review of drug nanocrystal technology and lipid nanoparticles. *Journal of biotechnology,* 113**,** 151-170.

MURDANDE, S. B., PIKAL, M. J., SHANKER, R. M. & BOGNER, R. H. 2011. Aqueous solubility of crystalline and amorphous drugs: Challenges in measurement. *Pharmaceutical Development and Technology,* 16**,** 187-200.

MÜLLER, R. H. & PETERS, K. 1998. Nanosuspensions for the formulation of poorly soluble drugs: I. Preparation by a size-reduction technique. *International Journal of Pharmaceutics,* 160**,** 229-237.

NAMBURI, R. R. & KERR, J. E. 2003. Oral itraconazole formulations and methods of making the same. U.S. Patent 6,663,897.

NARANG, A. S., SHEVEREV, V., FREEMAN, T., BOTH, D., STEPANIUK, V., DELANCY, M., MILLINGTON-SMITH, D., MACIAS, K. & SUBRAMANIAN, G. 2016. Process Analytical Technology for High Shear Wet Granulation: Wet Mass Consistency Reported by In-Line Drag Flow Force Sensor Is Consistent With Powder Rheology Measured by At-Line FT4 Powder Rheometer®. *Journal of pharmaceutical sciences,* 105**,** 182-187.

NERNST, W. 1904. Theorie der Reaktionsgeschwindigkeit in heterogenen Systemen. *Zeitschrift für physikalische Chemie,* 47**,** 52-55.

NEWMAN, A., KNIPP, G. & ZOGRAFI, G. 2012. Assessing the performance of amorphous solid dispersions. *Journal of pharmaceutical sciences,* 101**,** 1355-1377.

NEWMAN, A. & WENSLOW, R. 2016. Solid form changes during drug development: good, bad, and ugly case studies. *AAPS Open,* 2**,** 2.

NOYES, A. A. & WHITNEY, W. R. 1897. The rate of solution of solid substances in their own solutions. *Journal of the American Chemical Society,* 19**,** 930-934.

OSTWALD, W. 1900. Über die vermeintliche Isomerie des roten und gelben Quecksilberoxyds und die Oberflächenspannung fester Körper. *Zeitschrift für physikalische Chemie,* 34**,** 495-503.

PADRELA, L., RODRIGUES, M. A., VELAGA, S. P., FERNANDES, A. C., MATOS, H. A. & DE AZEVEDO, E. G. 2010. Screening for pharmaceutical cocrystals using the supercritical fluid enhanced atomization process. *The Journal of Supercritical Fluids,* 53**,** 156-164.

PADRELA, L., RODRIGUES, M. A., VELAGA, S. P., MATOS, H. A. & DE AZEVEDO, E. G. 2009. Formation of indomethacin–saccharin cocrystals using supercritical fluid technology. *European Journal of Pharmaceutical Sciences,* 38**,** 9-17.

PATEL, R. P., PATEL, M. P. & SUTHAR, A. M. 2009. Spray drying technology: an overview. *Indian Journal of Science and Technology,* 2**,** 44-47.

PAUDEL, A., WORKU, Z. A., MEEUS, J., GUNS, S. & VAN DEN MOOTER, G. 2013. Manufacturing of solid dispersions of poorly water soluble drugs by spray drying: Formulation and process considerations. *International Journal of Pharmaceutics,* 453**,** 253-284.

PERLOVICH, G. L., KURKOV, S. V., HANSEN, L. K. & BAUER-BRANDL, A. 2004. Thermodynamics of sublimation, crystal lattice energies, and crystal structures of racemates and enantiomers:(+)-and (±)-ibuprofen. *Journal of pharmaceutical sciences,* 93**,** 654-666.

PETRUŠEVSKI, G., NAUMOV, P., JOVANOVSKI, G., BOGOEVA-GACEVA, G. & NG, S. W. 2008. Solid-state forms of sodium valproate, active component of the anticonvulsant drug epilim. *ChemMedChem,* 3**,** 1377-1386.

POOLE, R. M. & DUNGO, R. T. 2014. Ipragliflozin: first global approval. *Drugs,* 74**,** 611-617.

QIAO, N., LI, M., SCHLINDWEIN, W., MALEK, N., DAVIES, A. & TRAPPITT, G. 2011. Pharmaceutical cocrystals: An overview. *International Journal of Pharmaceutics,* 419**,** 1-11.

RASENACK, N. & MÜLLER, B. W. 2002. Crystal habit and tableting behavior. *International journal of pharmaceutics,* 244**,** 45-57.

RASENACK, N. & MÜLLER, B. W. 2004. Micron-Size Drug Particles: Common and Novel Micronization Techniques. *Pharmaceutical Development and Technology,* 9**,** 1-13.

RAUTIO, J., KUMPULAINEN, H., HEIMBACH, T., OLIYAI, R., OH, D., JÄRVINEN, T. & SAVOLAINEN, J. 2008. Prodrugs: design and clinical applications. *Nature Reviews Drug Discovery,* 7**,** 255.

RAVINDRA, R., KROVVIDI, K. R. & KHAN, A. A. 1998. Solubility parameter of chitin and chitosan. *Carbohydrate Polymers,* 36**,** 121-127.

REMENAR, J. F., PETERSON, M. L., STEPHENS, P. W., ZHANG, Z., ZIMENKOV, Y. & HICKEY, M. B. 2007. Celecoxib: nicotinamide dissociation: using excipients to capture the cocrystal's potential. *Molecular pharmaceutics,* 4**,** 386-400.

ROTICH, M., GLASS, B. & BROWN, M. 2001. Thermal studies on some substituted aminobenzoic acids. *Journal of thermal analysis and calorimetry,* 64**,** 681-688.

ROWE, R. C. 1988. Interaction of lubricants with microcrystalline cellulose and anhydrous lactose — a solubility parameter approach. *International Journal of Pharmaceutics,* 41**,** 223-226.

ROY, S., AITIPAMULA, S. & NANGIA, A. 2005. Thermochemical analysis of venlafaxine hydrochloride polymorphs 1− 5. *Crystal growth & design,* 5**,** 2268-2276.

RÉ, M.-I. 2006. Formulating drug delivery systems by spray drying. *Drying Technology,* 24**,** 433-446.

SACHAN, N., BHATTACHARYA, A., PUSHKAR, S. & MISHRA, A. 2009. Biopharmaceutical classification system: A strategic tool for oral drug delivery technology. *Asian Journal of Pharmaceutics,* 3**,** 76.

SAHA, B. K., NANGIA, A. & JASKÓLSKI, M. 2005. Crystal engineering with hydrogen bonds and halogen bonds. *CrystEngComm,* 7**,** 355-358.

SAHA, S. & DESIRAJU, G. R. 2018. Acid··· Amide Supramolecular Synthon in Cocrystals: From Spectroscopic Detection to Property Engineering. *Journal of the American Chemical Society,* 140**,** 6361-6373.

SANDERS, R. 1987. The Pareto principle: its use and abuse. *Journal of Services Marketing,* 1**,** 37-40.

SARODE, A. L., SANDHU, H., SHAH, N., MALICK, W. & ZIA, H. 2013. Hot melt extrusion (HME) for amorphous solid dispersions: predictive tools for processing and impact of drug–polymer interactions on supersaturation. *European Journal of Pharmaceutical Sciences,* 48**,** 371-384.

SATHIGARI, S. K., RADHAKRISHNAN, V. K., DAVIS, V. A., PARSONS, D. L. & BABU, R. J. 2012. Amorphous-state characterization of efavirenz—polymer hot-melt extrusion systems for dissolution enhancement. *Journal of pharmaceutical sciences,* 101**,** 3456-3464.

SAVJANI, K. T., GAJJAR, A. K. & SAVJANI, J. K. 2012. Drug solubility: importance and enhancement techniques. *ISRN pharmaceutics,* 2012.

SCHULTHEISS, N. & NEWMAN, A. 2009. Pharmaceutical cocrystals and their physicochemical properties. *Crystal growth and design,* 9**,** 2950-2967.

SCOTT, G. 1992. Properties of polymers. Their correlation with chemical structure; their numerical estimation and prediction from additive group contributions. *Endeavour,* 16**,** 97-98.

SERAJUDDIN, A. T. M. 2007. Salt formation to improve drug solubility. *Advanced drug delivery reviews,* 59**,** 603-616.

SERRANO, D. R., O'CONNELL, P., PALUCH, K. J., WALSH, D. & HEALY, A. M. 2015. Cocrystal habit engineering to improve drug dissolution and alter derived powder properties. *Journal of Pharmacy and Pharmacology,* 68**,** 665-677.

SHAHRIN, N. 2013. Solubility and dissolution of drug product: A review. *International Journal of Pharmaceutical and Life Sciences,* 2**,** 33-41.

SHAN, N., PERRY, M. L., WEYNA, D. R. & ZAWOROTKO, M. J. 2014. Impact of pharmaceutical cocrystals: the effects on drug pharmacokinetics. *Expert Opinion on Drug Metabolism & Toxicology,* 10**,** 1255-1271.

SHAN, N., TODA, F. & JONES, W. 2002. Mechanochemistry and co-crystal formation: effect of solvent on reaction kinetics. *Chemical Communications***,** 2372-2373.

SHAN, N. & ZAWOROTKO, M. J. 2008. The role of cocrystals in pharmaceutical science. *Drug discovery today,* 13**,** 440-446.

SHELDRICK, G. M. 2008. A short history of SHELX. *Acta Crystallographica Section A: Foundations of Crystallography,* 64**,** 112-122.

SHELDRICK, G. M. 2015. SHELXT–Integrated space-group and crystal-structure determination. *Acta Crystallographica Section A: Foundations and Advances,* 71**,** 3-8.

SHEN, S. C., NG, W. K., CHIA, L., DONG, Y. C. & TAN, R. B. H. 2010. Stabilized amorphous state of ibuprofen by co-spray drying with mesoporous SBA-15 to enhance dissolution properties. *Journal of pharmaceutical sciences,* 99**,** 1997-2007.

SHEN, T.-Y. & WINTER, C. A. 1977. Chemical and biological studies on indomethacin, sulindac and their analogs. *Advances in drug research,* 12**,** 89-245.

SINKA, I. C., MOTAZEDIAN, F., COCKS, A. C. F. & PITT, K. G. 2009. The effect of processing parameters on pharmaceutical tablet properties. *Powder Technology,* 189**,** 276-284.

STAHLY, G. P. 2007. Diversity in single-and multiple-component crystals. The search for and prevalence of polymorphs and cocrystals. *Crystal growth & design,* 7**,** 1007-1026.

STELLA, V. J. 2010. Prodrugs: Some thoughts and current issues. *Journal of pharmaceutical sciences,* 99**,** 4755-4765.

STELLA, V. J. & NTI-ADDAE, K. W. 2007. Prodrug strategies to overcome poor water solubility. *Advanced Drug Delivery Reviews,* 59**,** 677-694.

STEVENSON, C. L., BENNETT, D. B. & LECHUGA-BALLESTEROS, D. 2005. Pharmaceutical Liquid Crystals: The Relevance of Partially Ordered Systems. *Journal of Pharmaceutical Sciences,* 94**,** 1861-1880.

STONE, K. H., LAPIDUS, S. H. & STEPHENS, P. W. 2009. Implementation and use of robust refinement in powder diffraction in the presence of impurities. *Journal of Applied Crystallography,* 42**,** 385-391.

STRICKLEY, R. G. 2004. Solubilizing Excipients in Oral and Injectable Formulations. *Pharmaceutical Research,* 21**,** 201-230.

SULEIMAN, M. S. & NAJIB, N. M. 1989. Isolation and physicochemical characterization of solid forms of glibenclamide. *International Journal of Pharmaceutics,* 50**,** 103-109.

SUN, D. D. & LEE, P. I. 2013. Evolution of supersaturation of amorphous pharmaceuticals: the effect of rate of supersaturation generation. *Molecular pharmaceutics,* 10**,** 4330-4346.

TAKAGI, T., RAMACHANDRAN, C., BERMEJO, M., YAMASHITA, S., YU, L. X. & AMIDON, G. L. 2006. A provisional biopharmaceutical classification of the top 200 oral drug products in the United States, Great Britain, Spain, and Japan. *Molecular pharmaceutics,* 3**,** 631-643.

TASKNEN, J. 2007. In silico predictions of solubility. *ADME-Tox approach*.

THAKURIA, R., DELORI, A., JONES, W., LIPERT, M. P., ROY, L. & RODRÍGUEZ-HORNEDO, N. 2013. Pharmaceutical cocrystals and poorly soluble drugs. *International Journal of Pharmaceutics,* 453**,** 101-125.

THOORENS, G., KRIER, F., ROZET, E., CARLIN, B. & EVRARD, B. 2015. Understanding the impact of microcrystalline cellulose physicochemical properties on tabletability. *International Journal of Pharmaceutics,* 490**,** 47-54.

TIAN, Y., CARON, V., JONES, D. S., HEALY, A. M. & ANDREWS, G. P. 2014. Using Flory–Huggins phase diagrams as a pre-formulation tool for the production of amorphous solid dispersions: a comparison between hot-melt extrusion and spray drying. *Journal of Pharmacy and Pharmacology,* 66**,** 256-274.

TOZIOPOULOU, F., MALAMATARI, M., NIKOLAKAKIS, I. & KACHRIMANIS, K. 2017. Production of aprepitant nanocrystals by wet media milling and subsequent solidification. *International Journal of Pharmaceutics,* 533**,** 324-334.

TRASK, A. V., MOTHERWELL, W. D. S. & JONES, W. 2004. Solvent-drop grinding: green polymorph control of cocrystallisation. *Chemical Communications***,** 890-891.

TRASK, A. V., MOTHERWELL, W. D. S. & JONES, W. 2006. Physical stability enhancement of theophylline via cocrystallization. *International Journal of Pharmaceutics,* 320**,** 114-123.

TUNG, H.-H., WATERSON, S. & REYNOLDS, S. D. 1991. Formation and resolution of ibuprofen lysinate. U.S. Patent 4,994,604.

ULLAH, M., ULLAH, H., MURTAZA, G., MAHMOOD, Q. & HUSSAIN, I. 2015. Evaluation of influence of various polymers on dissolution and phase behavior of carbamazepine-succinic acid cocrystal in matrix tablets. *BioMed research international,* 2015**,** 1-10.

VAN DEN MOOTER, G. 2012. The use of amorphous solid dispersions: A formulation strategy to overcome poor solubility and dissolution rate. *Drug Discovery Today: Technologies,* 9**,** e79-e85.

VAN DEN MOOTER, G., WUYTS, M., BLATON, N., BUSSON, R., GROBET, P., AUGUSTIJNS, P. & KINGET, R. 2001. Physical stabilisation of amorphous ketoconazole in solid dispersions with polyvinylpyrrolidone K25. *European Journal of Pharmaceutical Sciences,* 12**,** 261-269.

VAN KREVELEN, D. W. & TE NIJENHUIS, K. 2009. Chapter 7 - Cohesive Properties and Solubility. *Properties of Polymers (Fourth Edition).* Amsterdam: Elsevier.

VAN TONDER, E. C., MAHLATJI, M. D., MALAN, S. F., LIEBENBERG, W., CAIRA, M. R., SONG, M. & DE VILLIERS, M. M. 2004. Preparation and physicochemical characterization of 5 niclosamide solvates and 1 hemisolvate. *AAPS PharmSciTech,* 5**,** 86.

VARIANKAVAL, N., WENSLOW, R., MURRY, J., HARTMAN, R., HELMY, R., KWONG, E., CLAS, S.-D., DALTON, C. & SANTOS, I. 2006. Preparation and solid-state characterization of nonstoichiometric cocrystals of a phosphodiesterase-IV inhibitor and L-tartaric acid. *Crystal growth & design,* 6**,** 690-700.

VEHRING, R. 2008. Pharmaceutical particle engineering via spray drying. *Pharmaceutical research,* 25**,** 999-1022.

VEHRING, R., FOSS, W. R. & LECHUGA-BALLESTEROS, D. 2007. Particle formation in spray drying. *Journal of Aerosol Science,* 38**,** 728-746.

VERMA, S., KUMAR, S., GOKHALE, R. & BURGESS, D. J. 2011. Physical stability of nanosuspensions: Investigation of the role of stabilizers on Ostwald ripening. *International Journal of Pharmaceutics,* 406**,** 145-152.

VIDELA, S., LAHJOU, M., VAQUÉ, A., SUST, M., ENCABO, M., SOLER, L., SANS, A., SICARD, E., GASCÓN, N. & ENCINA, G. 2017. Single-dose pharmacokinetics of co-

crystal of tramadol–celecoxib: Results of a four-way randomized open-label phase I clinical trial in healthy subjects. *British journal of clinical pharmacology,* 83**,** 2718-2728.

VIPPAGUNTA, S. R., BRITTAIN, H. G. & GRANT, D. J. W. 2001. Crystalline solids. *Advanced Drug Delivery Reviews,* 48**,** 3-26.

VOORHEES, P. W. 1985. The theory of Ostwald ripening. *Journal of Statistical Physics,* 38**,** 231-252.

VUEBA, M. L., PINA, M. E. & BATISTA DE CARVALHO, L. A. E. 2008. Conformational stability of ibuprofen: assessed by DFT calculations and optical vibrational spectroscopy. *Journal of pharmaceutical sciences,* 97**,** 845-859.

VÖLGYI, G., BAKA, E., BOX, K. J., COMER, J. E. A. & TAKÁCS-NOVÁK, K. 2010. Study of pH-dependent solubility of organic bases. Revisit of Henderson-Hasselbalch relationship. *Analytica Chimica Acta,* 673**,** 40-46.

WALSH, R. D. B., BRADNER, M. W., FLEISCHMAN, S., MORALES, L. A., MOULTON, B., RODRIGUEZ-HORNEDO, N. & ZAWOROTKO, M. J. 2003. Crystal engineering of the composition of pharmaceutical phases. *Chemical Communications***,** 186-187.

WALTON, D. E. 2000. The morphology of spray-dried particles a qualitative view. *Drying Technology,* 18**,** 1943-1986.

WANG, Q., WONG, C.-H., CHAN, H. Y. E., LEE, W.-Y. & ZUO, Z. 2018. Statistical Design of Experiment (DoE) based development and optimization of DB213 in situ thermosensitive gel for intranasal delivery. *International Journal of Pharmaceutics,* 539**,** 50-57.

WEYNA, D. R., CHENEY, M. L., SHAN, N., HANNA, M., ZAWOROTKO, M. J., SAVA, V., SONG, S. & SANCHEZ-RAMOS, J. R. 2012. Improving solubility and pharmacokinetics of meloxicam via multiple-component crystal formation. *Molecular pharmaceutics,* 9**,** 2094-2102.

WEYNA, D. R., SHATTOCK, T., VISHWESHWAR, P. & ZAWOROTKO, M. J. 2009. Synthesis and structural characterization of cocrystals and pharmaceutical cocrystals: mechanochemistry vs slow evaporation from solution. *Crystal Growth and Design,* 9**,** 1106-1123.

WILLIAMS, H. D., TREVASKIS, N. L., CHARMAN, S. A., SHANKER, R. M., CHARMAN, W. N., POUTON, C. W. & PORTER, C. J. H. 2013. Strategies to Address Low Drug Solubility in Discovery and Development. *Pharmacological Reviews,* 65**,** 315.

WITTERING, K. E., AGNEW, L. R., KLAPWIJK, A. R., ROBERTSON, K., COUSEN, A. J. P., CRUICKSHANK, D. L. & WILSON, C. C. 2015. Crystallisation and physicochemical property characterisation of conformationally-locked co-crystals of fenamic acid derivatives. *CrystEngComm,* 17**,** 3610-3618.

WOUTERS, J. & QUÉRÉ, L. 2011. *Pharmaceutical salts and co-crystals,* Royal Society of Chemistry.

WU, C.-Y. & BENET, L. Z. 2005. Predicting drug disposition via application of BCS: transport/absorption/elimination interplay and development of a biopharmaceutics drug disposition classification system. *Pharmaceutical research,* 22**,** 11-23.

WU, L., ZHANG, J. & WATANABE, W. 2011. Physical and chemical stability of drug nanoparticles. *Advanced Drug Delivery Reviews,* 63**,** 456-469.

YAO, J., CHEN, J.-M., XU, Y.-B. & LU, T.-B. 2014. Enhancing the solubility of 6-mercaptopurine by formation of ionic cocrystal with zinc trifluoromethanesulfonate: single-crystal-to-single-crystal transformation. *Crystal Growth & Design,* 14**,** 5019-5025.

YOSHIOKA, S. & ASO, Y. 2007. Correlations between molecular mobility and chemical stability during storage of amorphous pharmaceuticals. *Journal of pharmaceutical sciences,* 96**,** 960-981.

YU, L. 2001. Amorphous pharmaceutical solids: preparation, characterization and stabilization. *Advanced Drug Delivery Reviews,* 48**,** 27-42.

YUKSEL, N., KANIK, A. E. & BAYKARA, T. 2000. Comparison of in vitro dissolution profiles by ANOVA-based, model-dependent and -independent methods. *Int J Pharm,* 209**,** 57-67.

ZHANG, G. G. Z. & ZHOU, D. 2017. Chapter 2 - Crystalline and Amorphous Solids. *Developing Solid Oral Dosage Forms (Second Edition).* Boston: Academic Press.

ZHANG, S. & RASMUSON, Å. C. 2012. The theophylline–oxalic acid co-crystal system: solid phases, thermodynamics and crystallisation. *CrystEngComm,* 14**,** 4644-4655.

ZHANG, Y., HUO, M., ZHOU, J., ZOU, A., LI, W., YAO, C. & XIE, S. 2010. DDSolver: an add-in program for modeling and comparison of drug dissolution profiles. *AAPS J,* 12**,** 263-71.

ZHAO, M., BARKER, S. A., BELTON, P. S., MCGREGOR, C. & CRAIG, D. Q. M. 2012. Development of fully amorphous dispersions of a low Tg drug via co-spray drying with hydrophilic polymers. *European Journal of Pharmaceutics and Biopharmaceutics,* 82**,** 572-579.

ZIMMERMANN, A., MILLQVIST-FUREBY, A., ELEMA, M. R., HANSEN, T., MÜLLERTZ, A. & HOVGAARD, L. 2009. Adsorption of pharmaceutical excipients onto microcrystals of siramesine hydrochloride: effects on physicochemical properties. *European Journal of Pharmaceutics and Biopharmaceutics,* 71**,** 109-116.

ÓGÁIN, O. N., LI, J., TAJBER, L., CORRIGAN, O. I. & HEALY, A. M. 2011. Particle engineering of materials for oral inhalation by dry powder inhalers. I—Particles of sugar excipients (trehalose and raffinose) for protein delivery. *International journal of pharmaceutics,* 405**,** 23-35.

Appendices

Appendix 1

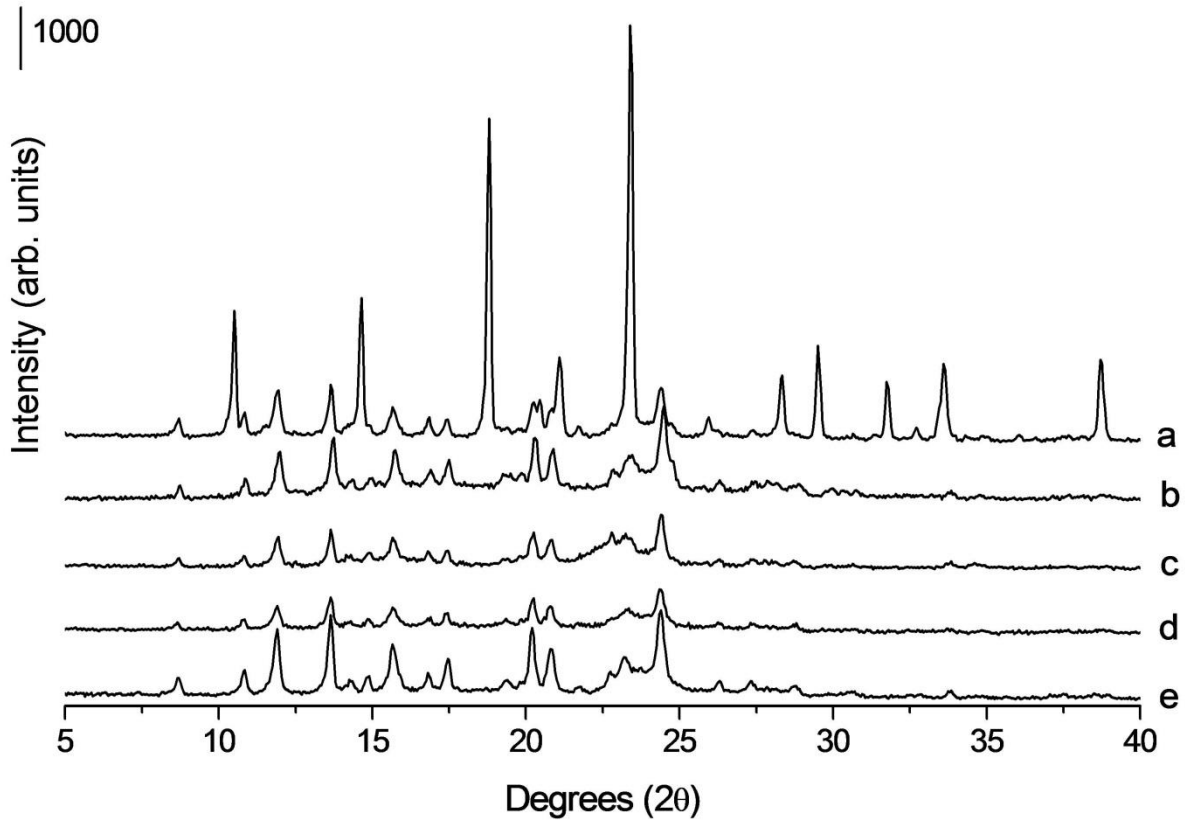

Figure A.1.1. PXRD analyses of physical mixtures of spray dried cocrystal and excipient at 50:50 % w/w ratios. a) Physical mixture of cocrystal and mannitol, b) Physical mixture of cocrystal and dextran, c) Physical mixture of cocrystal and MCC, d) Physical mixture of cocrystal and inulin, e) Spray dried cocrystal.

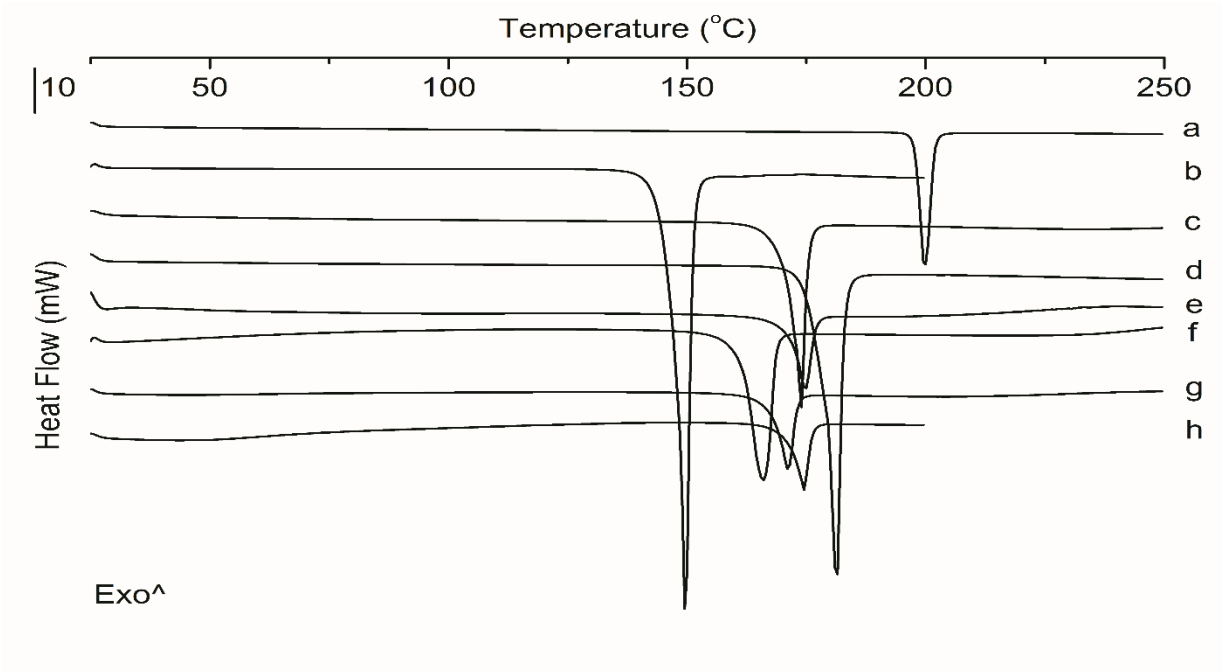

Figure A.1.2. DSC analyses of physical mixtures of cocrystal and excipients at 50:50 % w/w ratio. a) Unprocessed SDM, b) Unprocessed 4ASA, c) Cocrystal produced by spray drying, d) Cocrystal produced by solvent evaporation, e) Physical mixture of cocrystal and inulin, f) Physical mixture of cocrystal and mannitol, g) Physical mixture of cocrystal and MCC, h) Physical mixture of cocrystal and dextran.

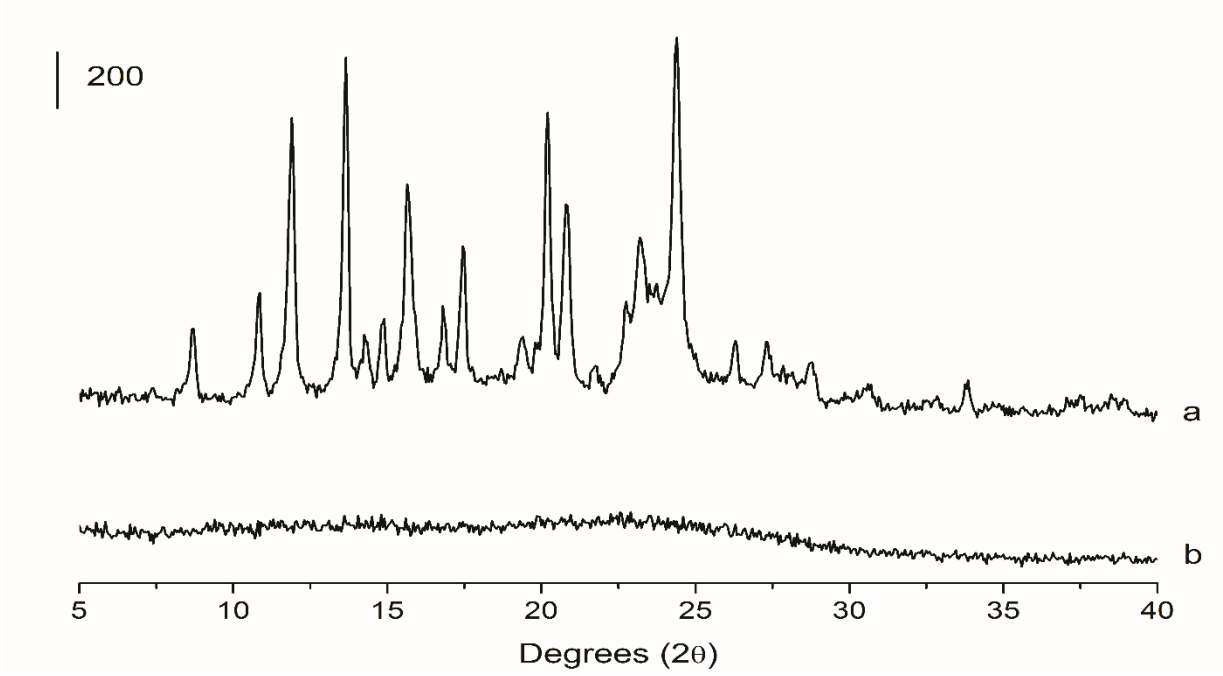

Figure A.1.3. PXRD patterns of a) Spray dried cocrystal, b) Co-spray dried system with HPMC (90:10 % w/w).

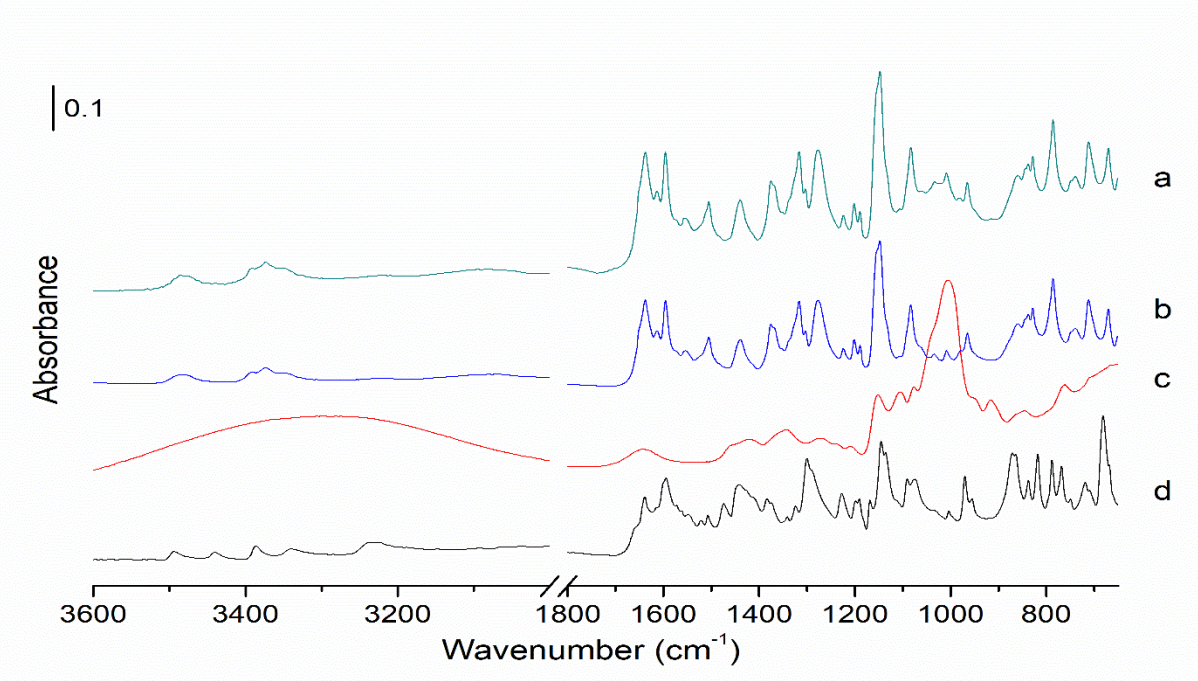

Figure A.1.4. FTIR analyses of a) co-spray dried cocrystal in dextran (50:50 % w/w ratio), b) spray dried cocrystal, c) dextran, d) physical mixture of SDM and 4ASA (1:1 molar ratio).

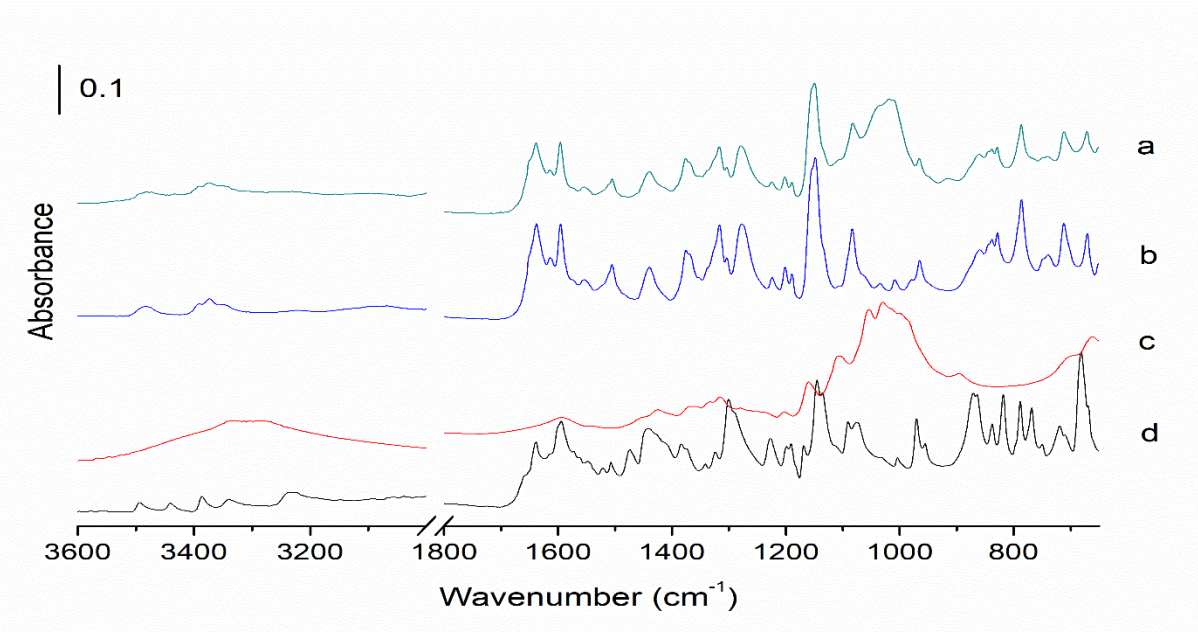

Figure A.1.5. FTIR analyses of a) co-spray dried cocrystal in MCC (50:50 % w/w ratio), b) spray dried cocrystal, c) MCC, d) physical mixture of SDM and 4ASA (1:1 molar ratio).

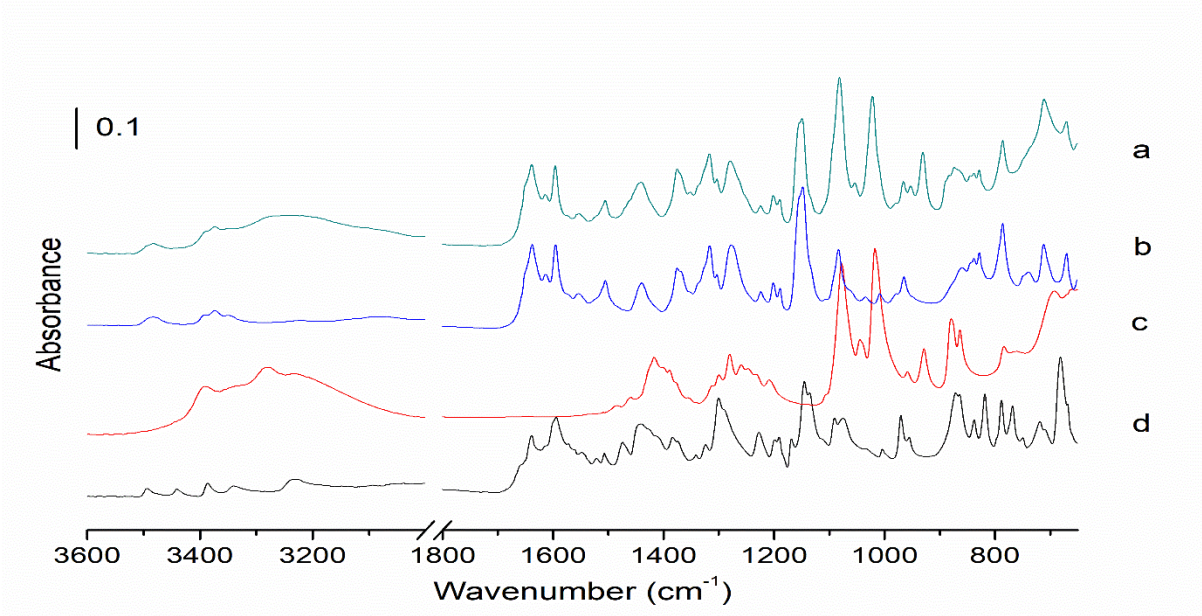

Figure A.1.6. FTIR analyses of a) co-spray dried cocrystal in mannitol (50:50 % w/w ratio), b) spray dried cocrystal, c) mannitol, d) physical mixture of SDM and 4ASA (1:1 molar ratio).

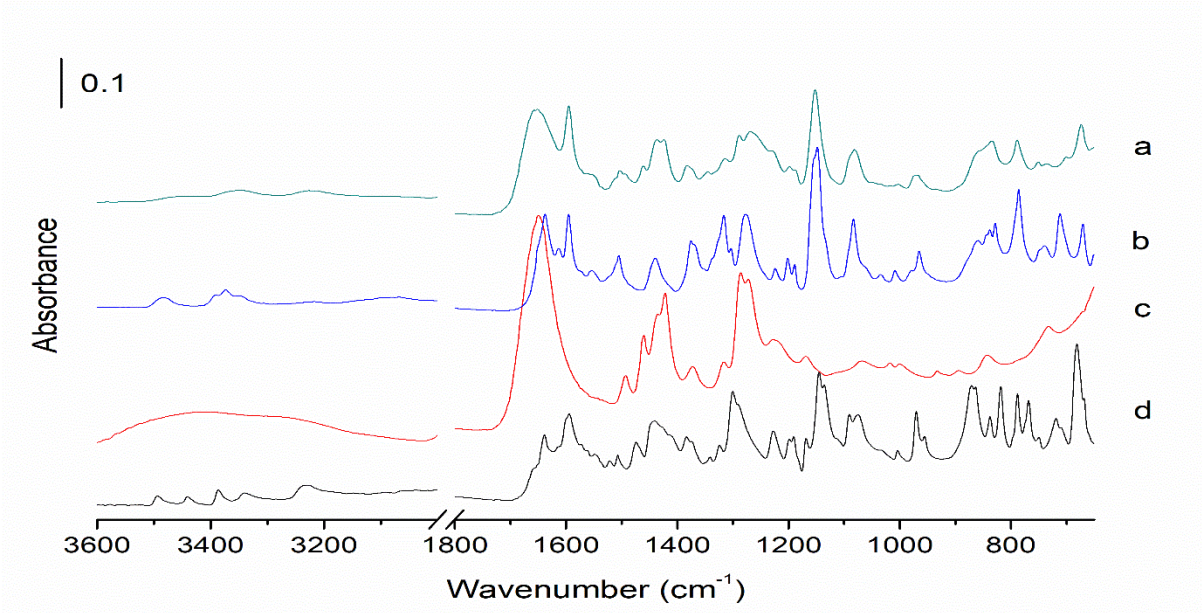

Figure A.1.7. FTIR analyses of a) co-spray dried cocrystal in PVP K15 (50:50 % w/w ratio), b) spray dried cocrystal, c) PVP K15, d) physical mixture of SDM and 4ASA (1:1 molar ratio).

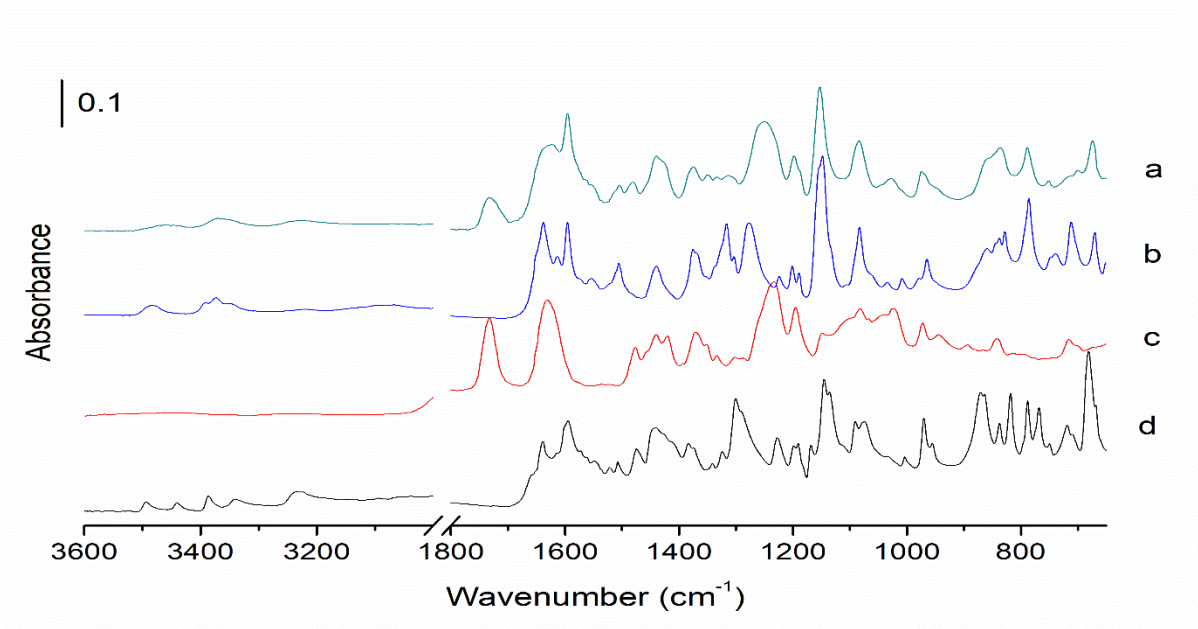

Figure A.1.8. FTIR analyses of a) co-spray dried cocrystal in Soluplus (50:50 % w/w ratio), b) spray dried cocrystal, c) Soluplus, d) physical mixture of SDM and 4ASA (1:1 molar ratio).

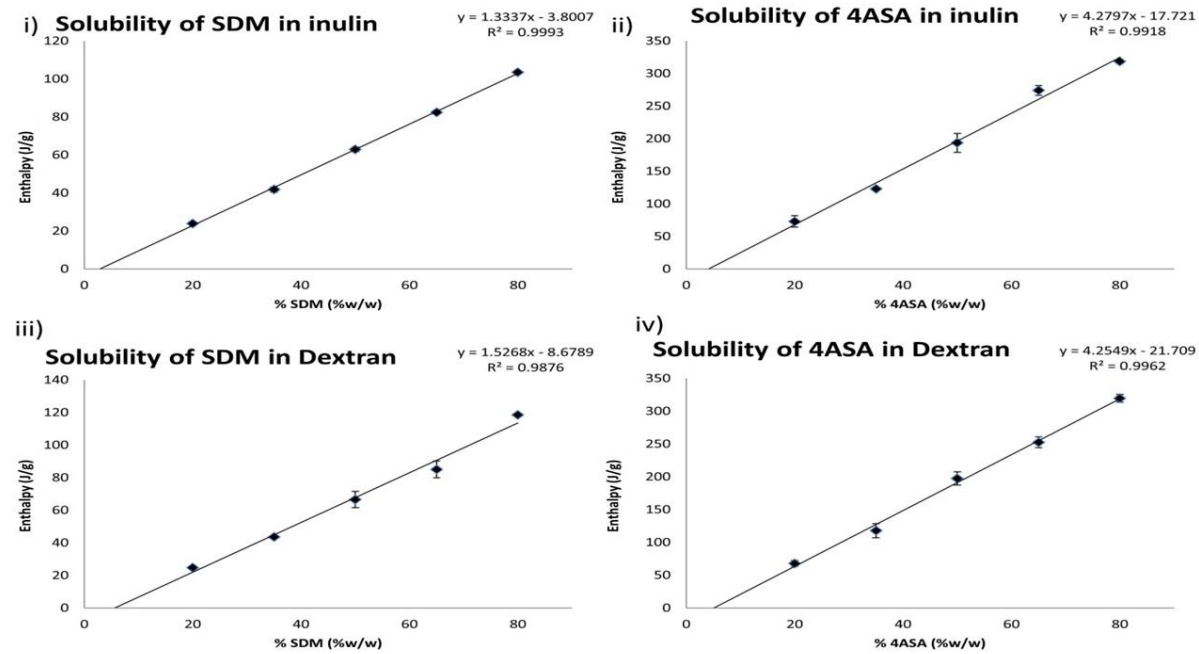

Figure A.1.9. Solubility of i) SDM in inulin, ii) 4ASA in inulin, iii) SDM in dextran, iv) 4ASA in dextran.

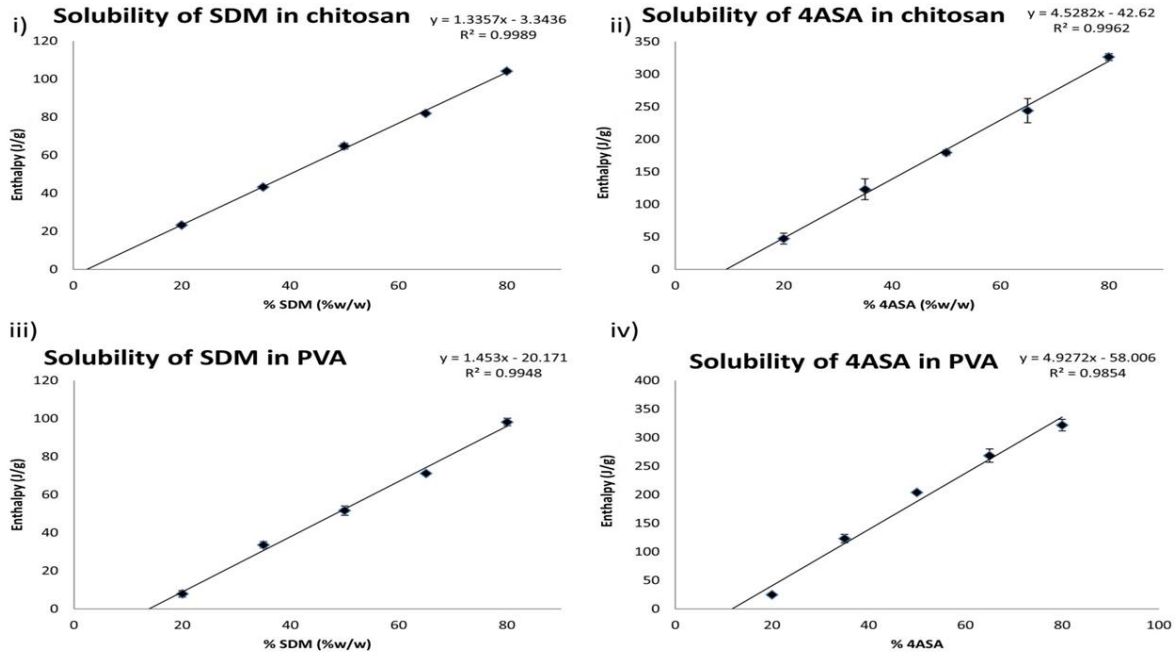

Figure A.1.10. Solubility of i) SDM in chitosan, ii) 4ASA in chitosan, iii) SDM in PVA, iv) 4ASA in PVA.

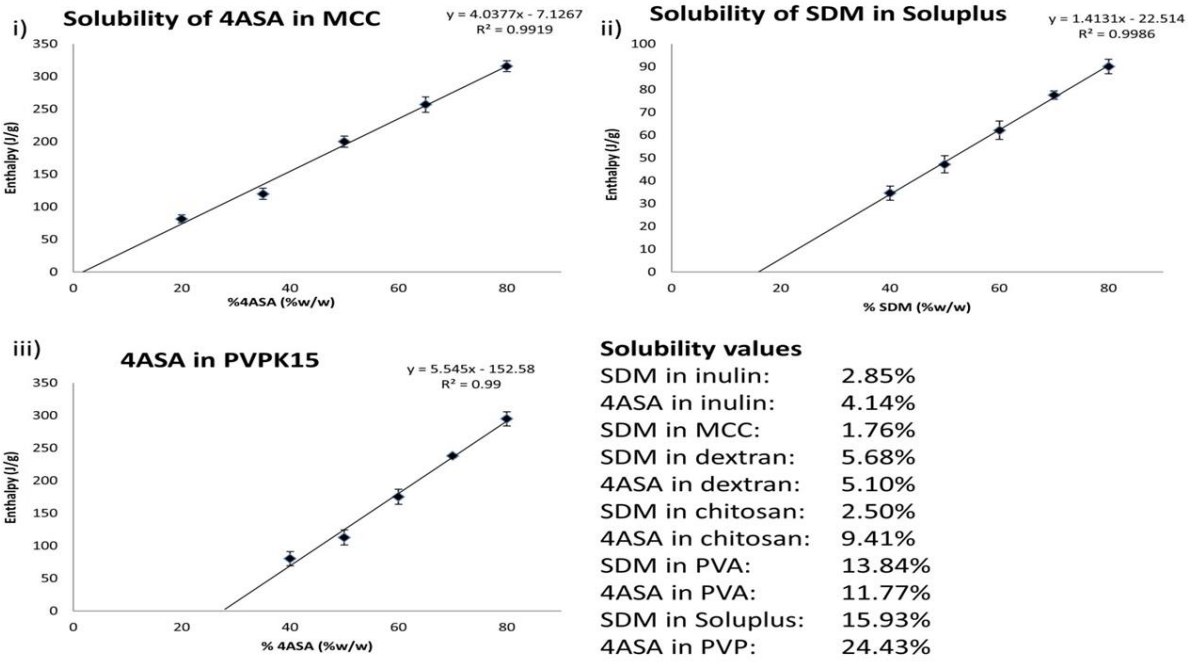

Figure A.1.11. Solubility of i) 4ASA in MCC, SDM in Soluplus, iii) 4ASA in PVP K15. Solubility values (expressed at % w/w) are also shown.

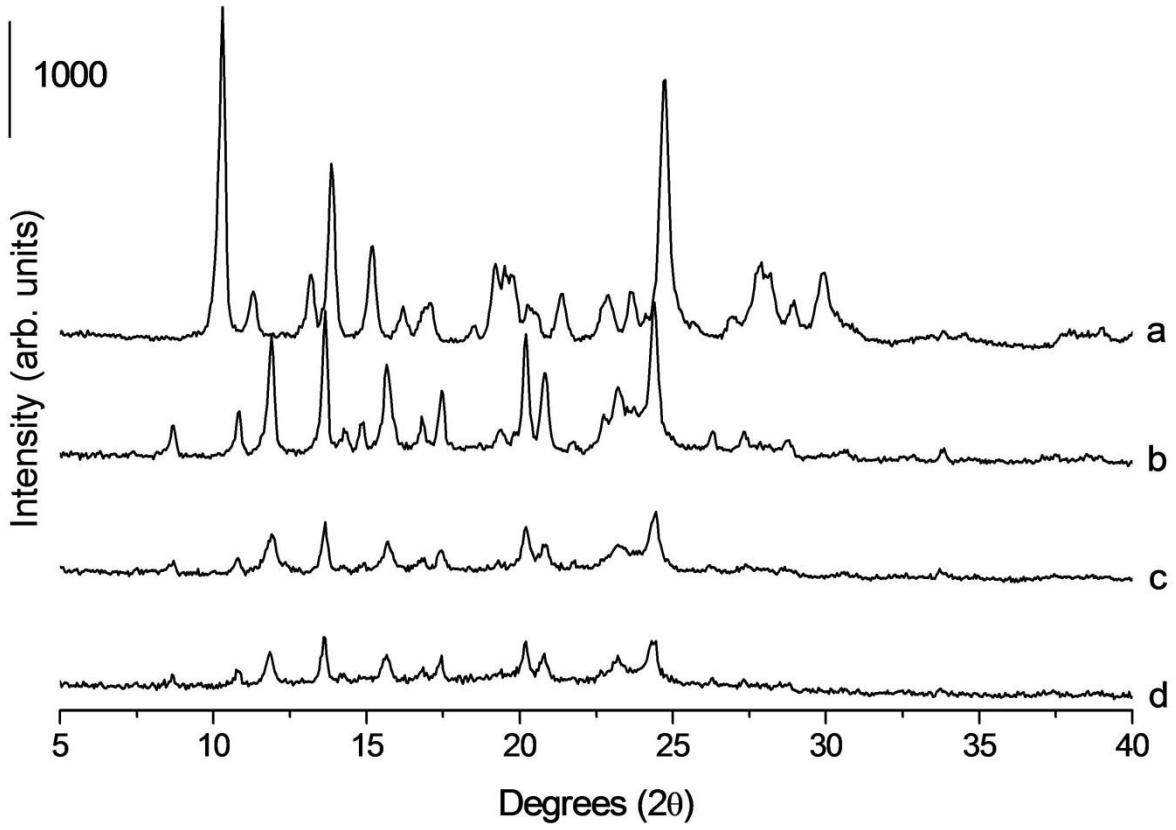

Figure A.1.12. PXRD analyses of co-spray dried system with inulin at 50:50 % w/w ratio after dissolution. a) Form I cocrystal, b) Form II cocrystal, c) Cocrystal components co-spray dried with inulin after dissolution, d) Cocrystal components co-spray dried with inulin.

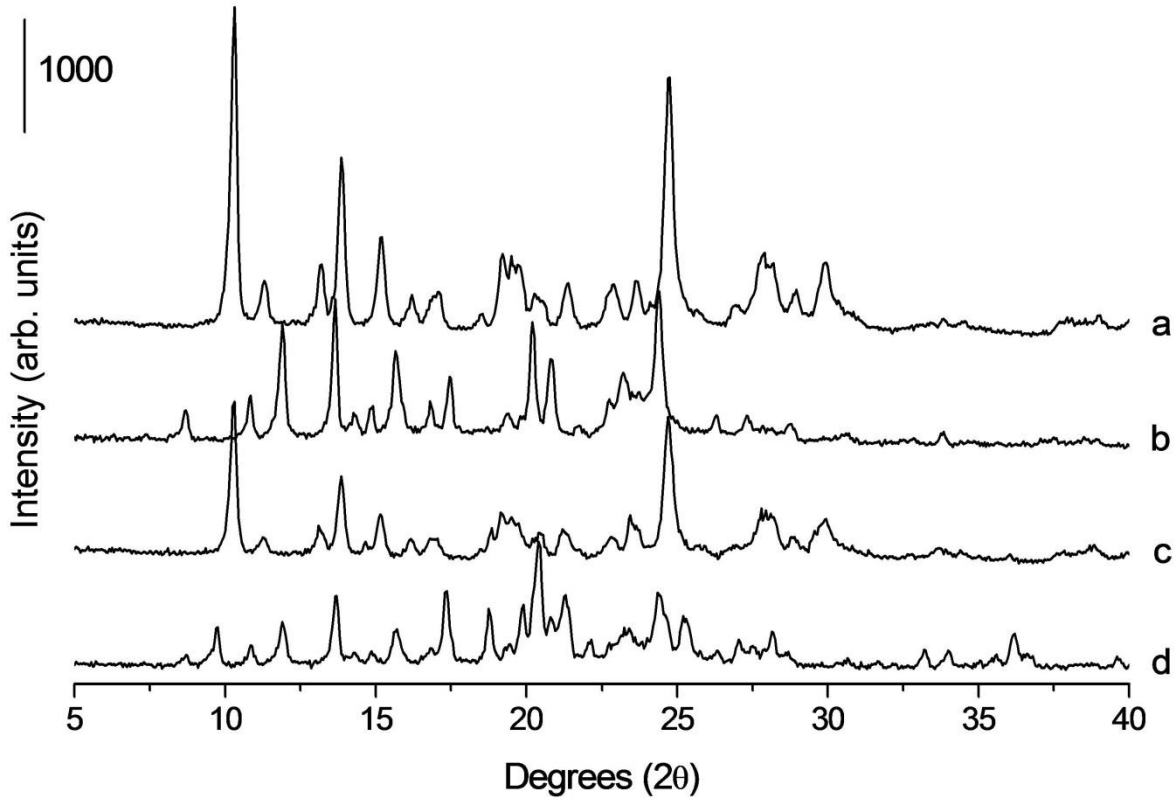

Figure A.1.13. PXRD analyses of co-spray dried system with mannitol at 50:50 % w/w ratio after dissolution. a) Form I cocrystal, b) Form II cocrystal, c) Cocrystal components co-spray dried with mannitol after dissolution, d) Cocrystal components co-spray dried with mannitol.

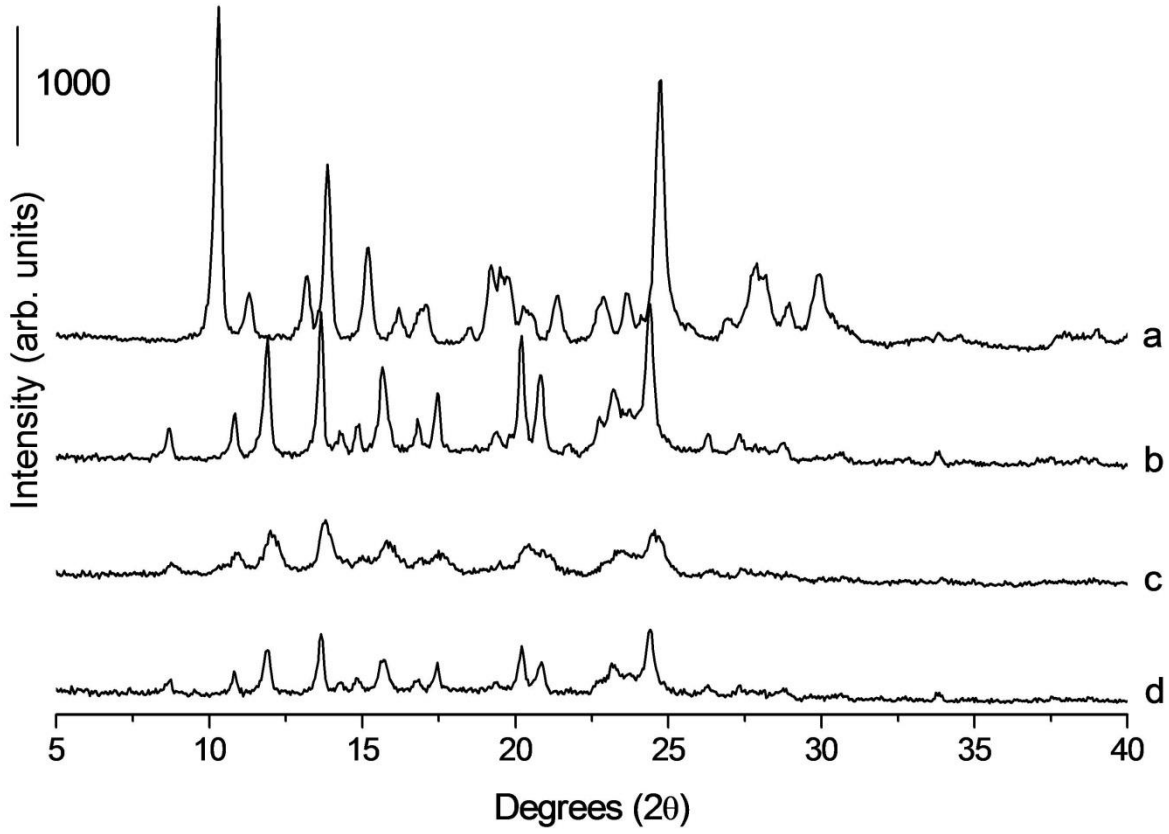

Figure A.1.14. PXRD analyses of co-spray dried system with dextran at 50:50 % w/w ratio after dissolution. a) Form I cocrystal, b) Form II cocrystal, c) Cocrystal components co-spray dried with dextran after dissolution, d) Cocrystal components co-spray dried with dextran.

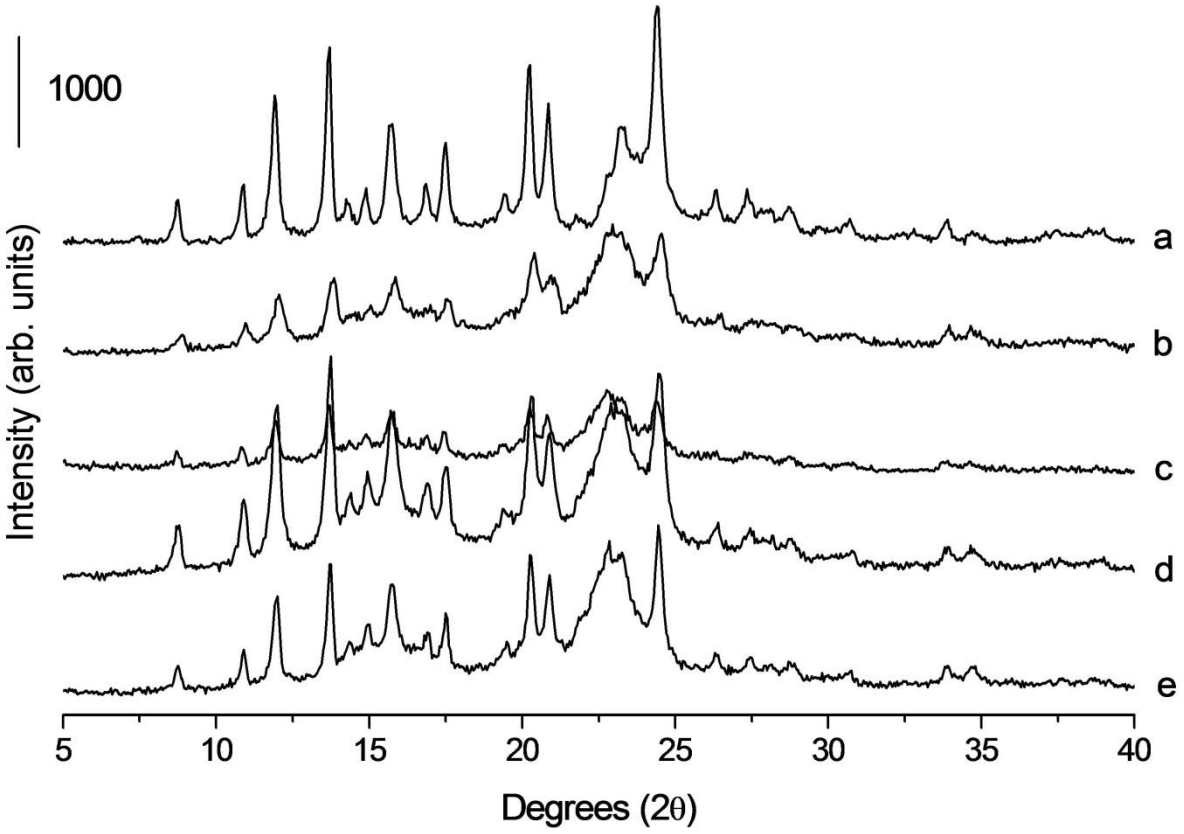

Figure A.1.15. PXRD analyses of co-spray dried system with MCC, a) Spray dried cocrystal, b) Co-spray dried system (50 % w/w cocrystal components, 50 % w/w MCC) after tabletting, c) Co-spray dried system (50 % w/w cocrystal components, 50 % w/w MCC), d) Physical mixture of cocrystal 50 % w/w, MCC 50 % w/w after tabletting, e) Physical mixture of cocrystal 50 % w/w, MCC 50 % w/w.

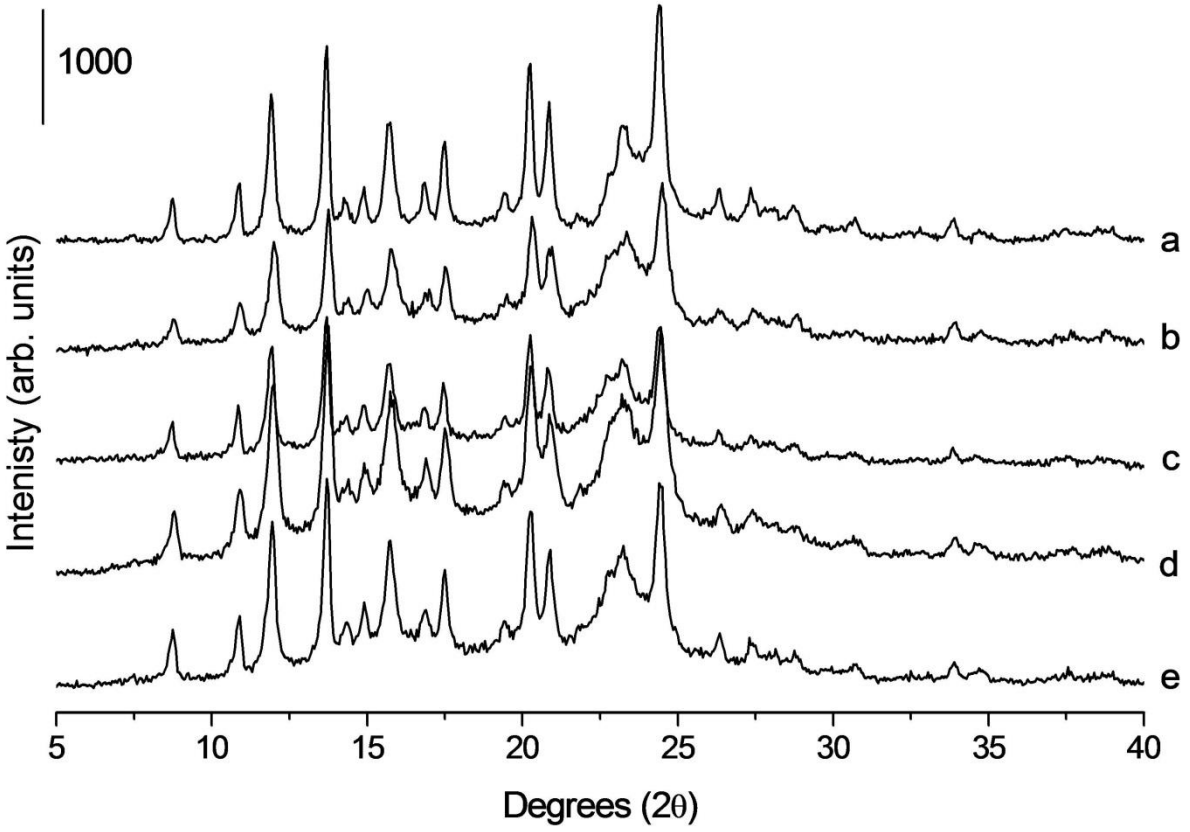

Figure A.1.16. PXRD analyses of co-spray dried system with inulin and MCC, a) Spray dried cocrystal, b) Co-spray dried system (60 % w/w cocrystal components, 20 % w/w inulin, 20 % w/w MCC) after tabletting, c) Co-spray dried system (60 % w/w cocrystal components, 20 % w/w inulin, 20 % w/w MCC), d) Physical mixture of cocrystal 60 % w/w, inulin 20 % w/w, MCC 20 % w/w after tabletting, e) Physical mixture of cocrystal 60 % w/w, inulin 20 % w/w, MCC 20 % w/w.

Appendix 2

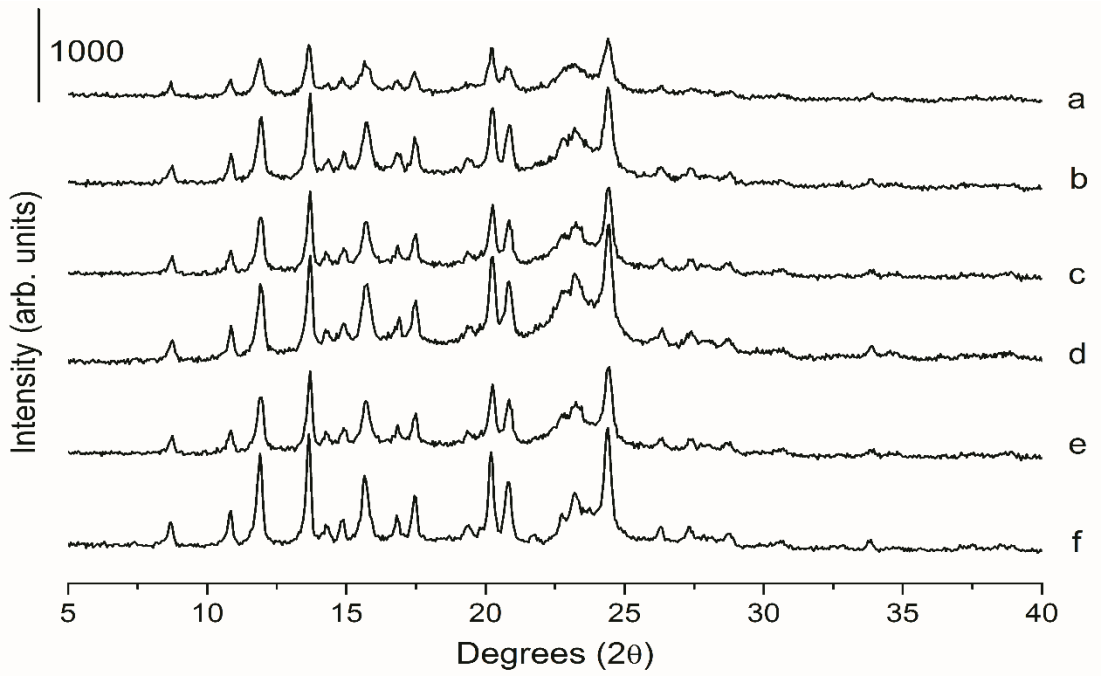

Figure A.4.1. PXRD patterns of centre point DoE runs. a) Run 16, b) Run 12, c) Run 11, d) Run 7, e) Run 1, f) Cocrystal produced by spray drying.

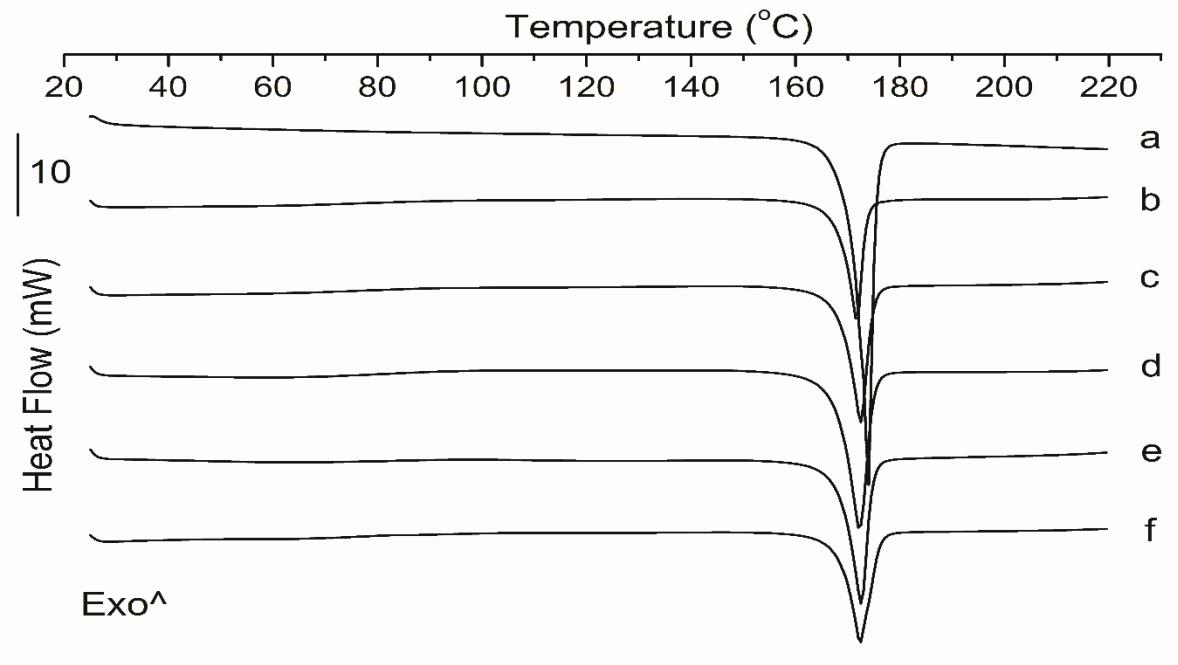

Figure A.4.2. DSC curves of centre point DoE runs. a) Cocrystal produced by spray drying, b) Run 1, c) Run 7, d) Run 11, e) Run 12, f) Run 16.

Appendix 3

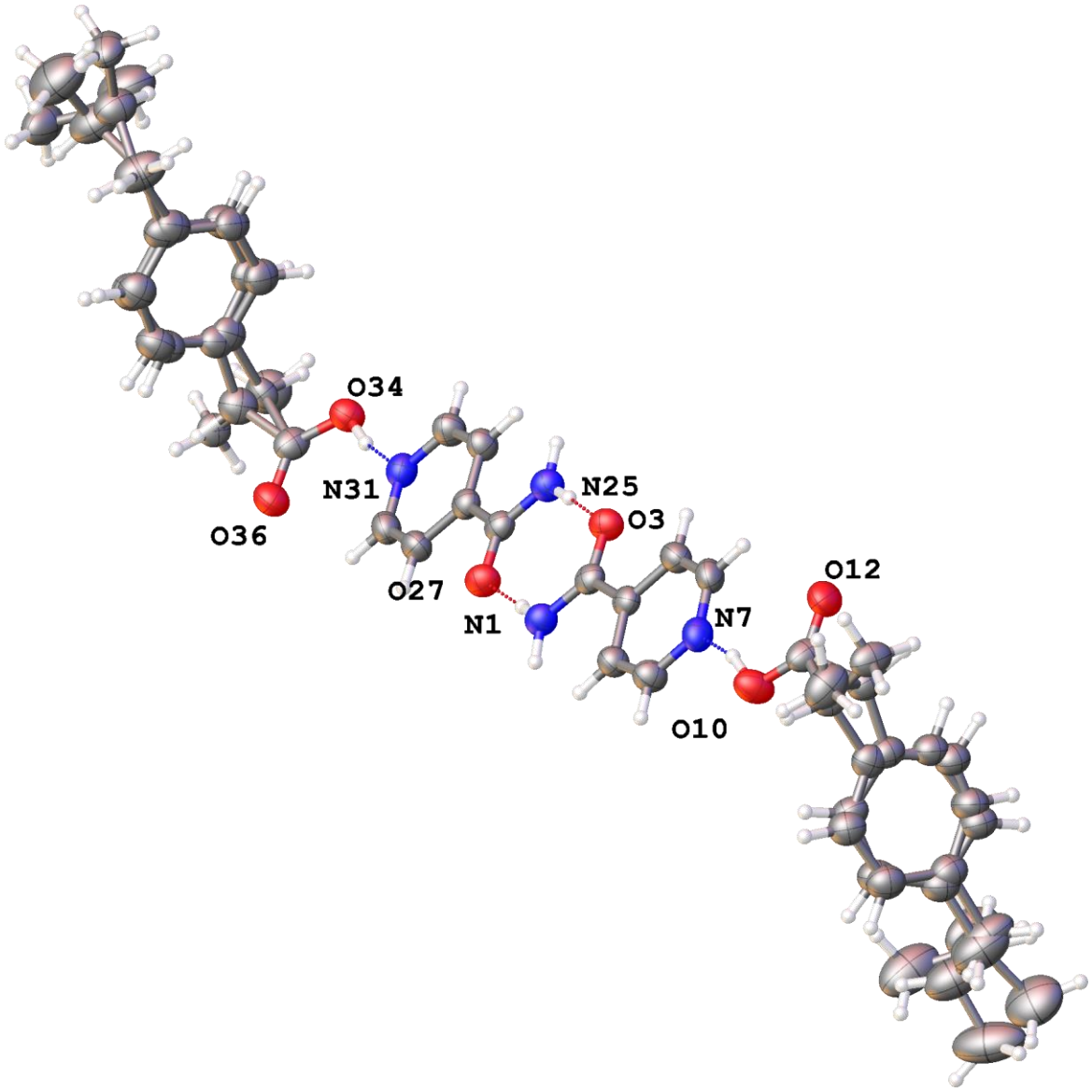

Figure A.3.1. Disordered tetrameric cocrystal of $C_{13}H_{18}O_2$:$C_6H_6N_2O$, IBU:INA. Each IBU is fully disordered except for the acid moiety and was modelled in two positions with O10/O12 64:36 % and O34/O36 53:47 % occupancy using restraints.

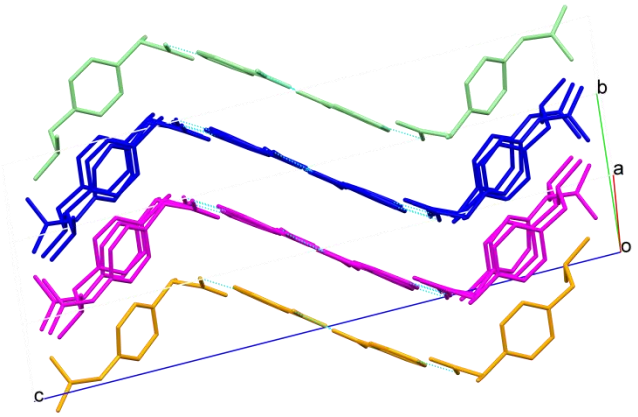

Figure A.3.2. Alternate layers of the IBU:INA cocrystal shown in different colours to highlight the packing.

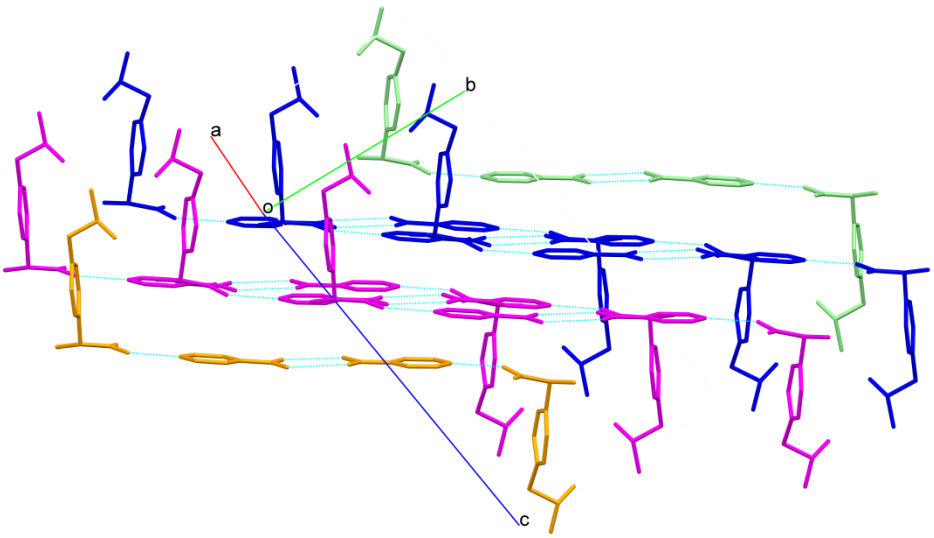

Figure A.3.3. Aligned layers showing the edge arrangement of IBU to facilitate packing between layers.

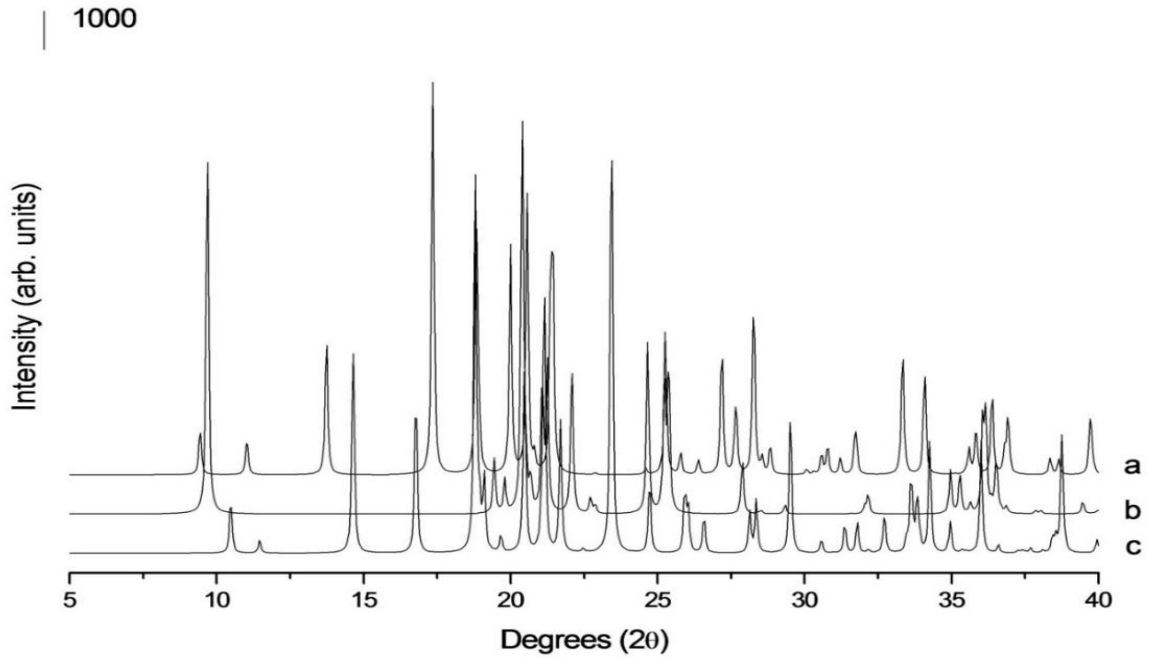

Figure A.3.4. PXRD data of mannitol polymorphs generated from single crystal data (in the Cambridge Crystallographic Data Centre) using Mercury software. a) Alpha, b) Delta, c) Beta.

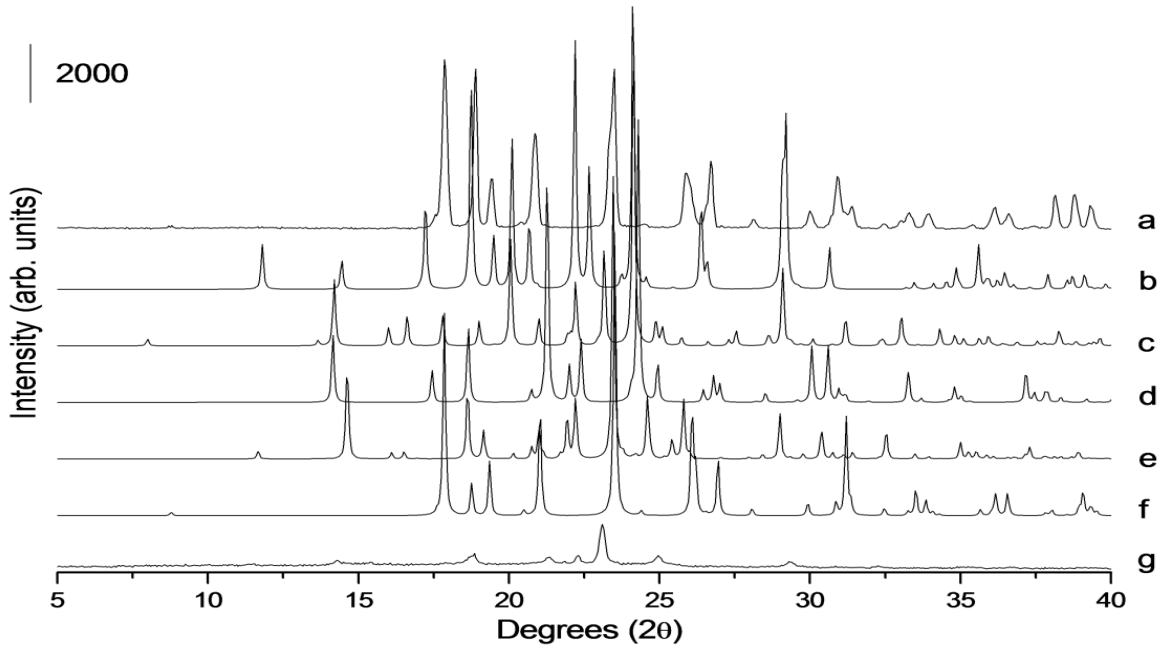

Figure A.3.5. PXRD data of INA polymorphs: a) Unprocessed INA, b) EHOWIH05, c) EHOWIH04, d) EHOWIH03, e) EHOWIH02, f) EHOWIH01, g) Co-spray dried INA with Soluplus (50:50 % w/w ratio). b-f are Mercury software-calculated PXRD patterns of INA polymorphs based on single crystal data (in the Cambridge Crystallographic Data Centre).

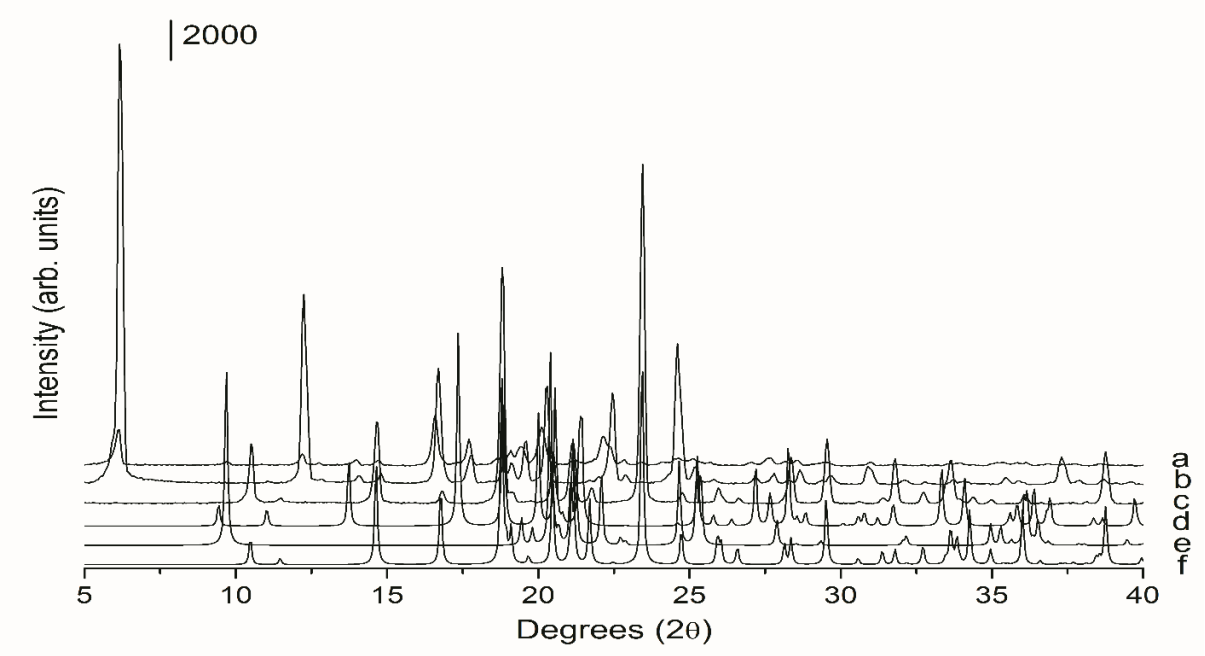

Figure A.3.6. PXRD patterns of a) IBU:mannitol prepared by spray drying, b) Unprocessed IBU, c) Unprocessed mannitol, d) Alpha mannitol, e) Beta mannitol, f) Delta mannitol. d-f are Mercury software-calculated PXRD patterns of mannitol polymorphs based on single crystal data (in the Cambridge Crystallographic Data Centre).

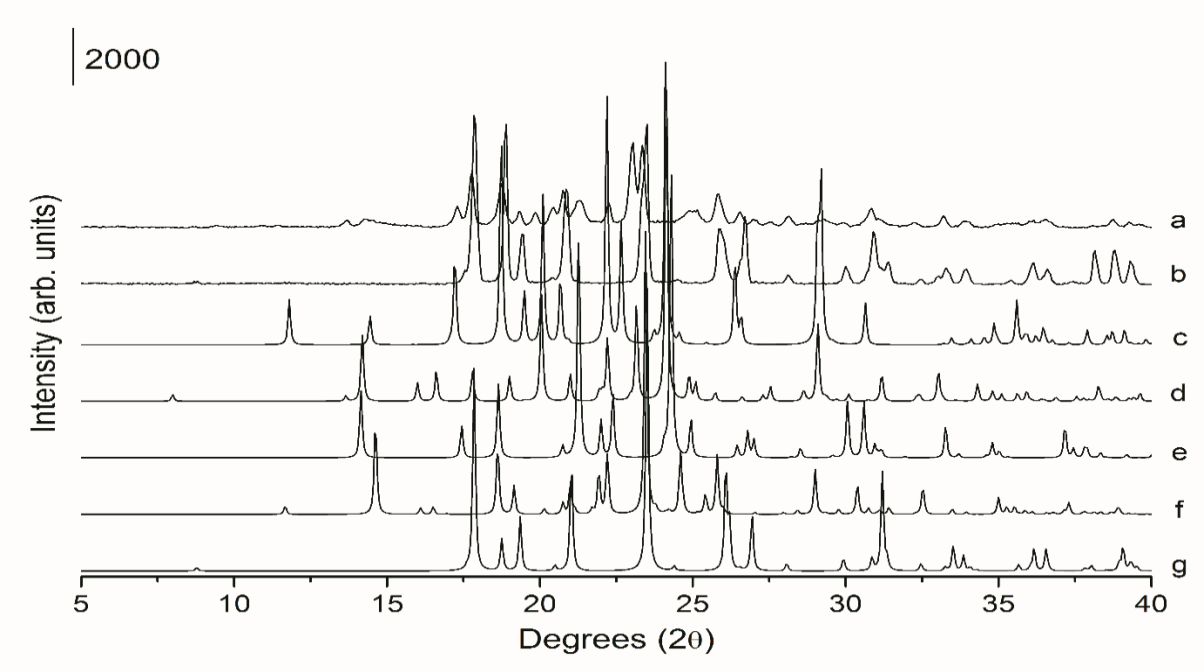

Figure A.3.7. PXRD patterns of a) INA:mannitol prepared by spray drying, b) Unprocessed INA, c) EHOWIH05, d) EHOWIH04, e) EHOWIH03, f) EHOWIH02, g) EHOWIH01. Patterns c-g are Mercury software-calculated PXRD patterns of INA polymorphs based on single crystal data (in the Cambridge Crystallographic Data Centre).

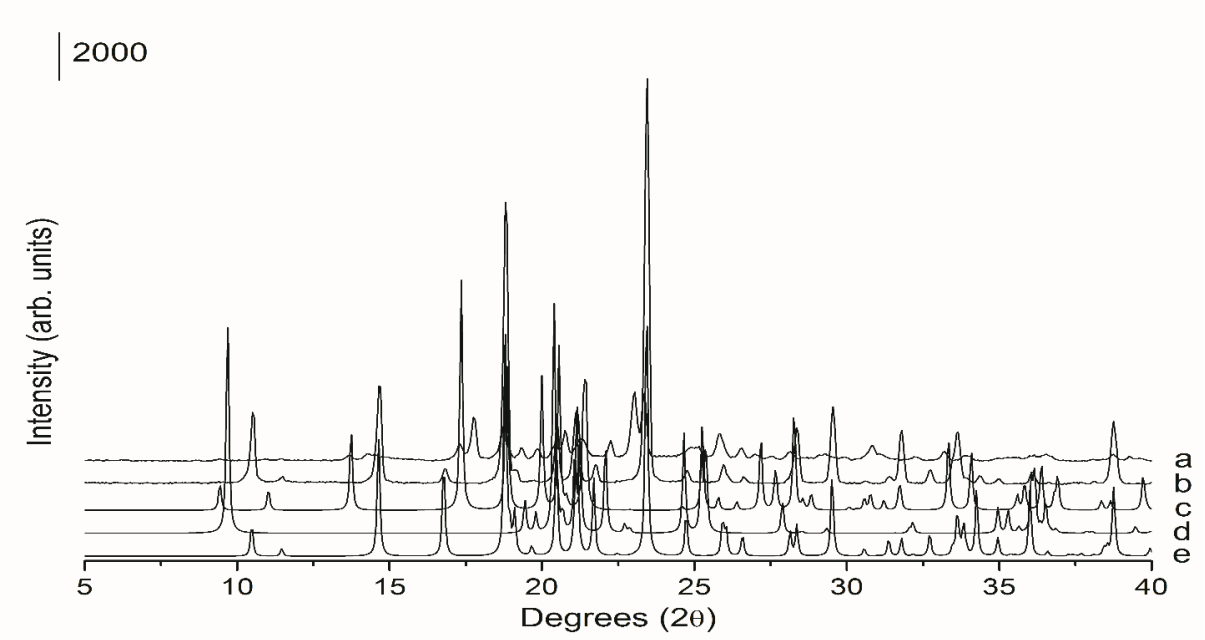

Figure A.3.8. PXRD patterns of a) INA:mannitol prepared by spray drying, b) Unprocessed mannitol, c) Alpha mannitol, d) Beta mannitol, e) Delta mannitol. c-e are Mercury software-calculated PXRD patterns of mannitol polymorphs based on single crystal data (in the Cambridge Crystallographic Data Centre).

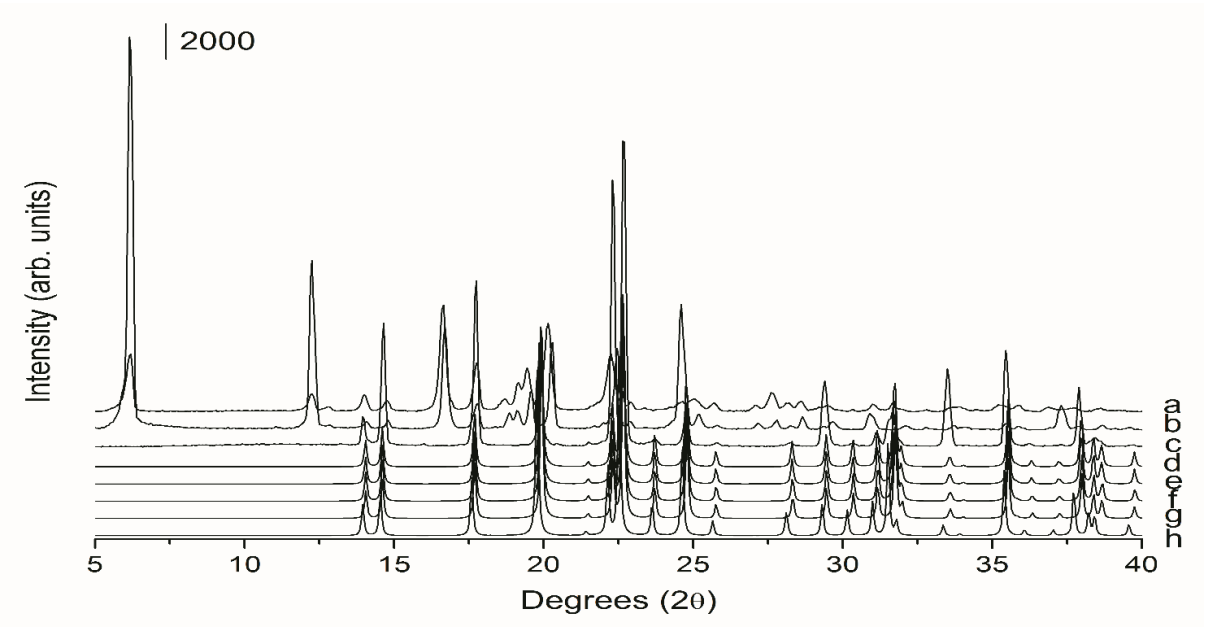

Figure A.3.9. PXRD patterns of a) IBU:xylitol prepared by HME, b) Unprocessed IBU, c) Unprocessed xylitol, d) Xyltol04, e) Xyltol03, f) Xyltol02, g) Xyltol01, h) Xyltol. d-h are Mercury software-calculated PXRD patterns of xylitol polymorphs based on single crystal data (in the Cambridge Crystallographic Data Centre).

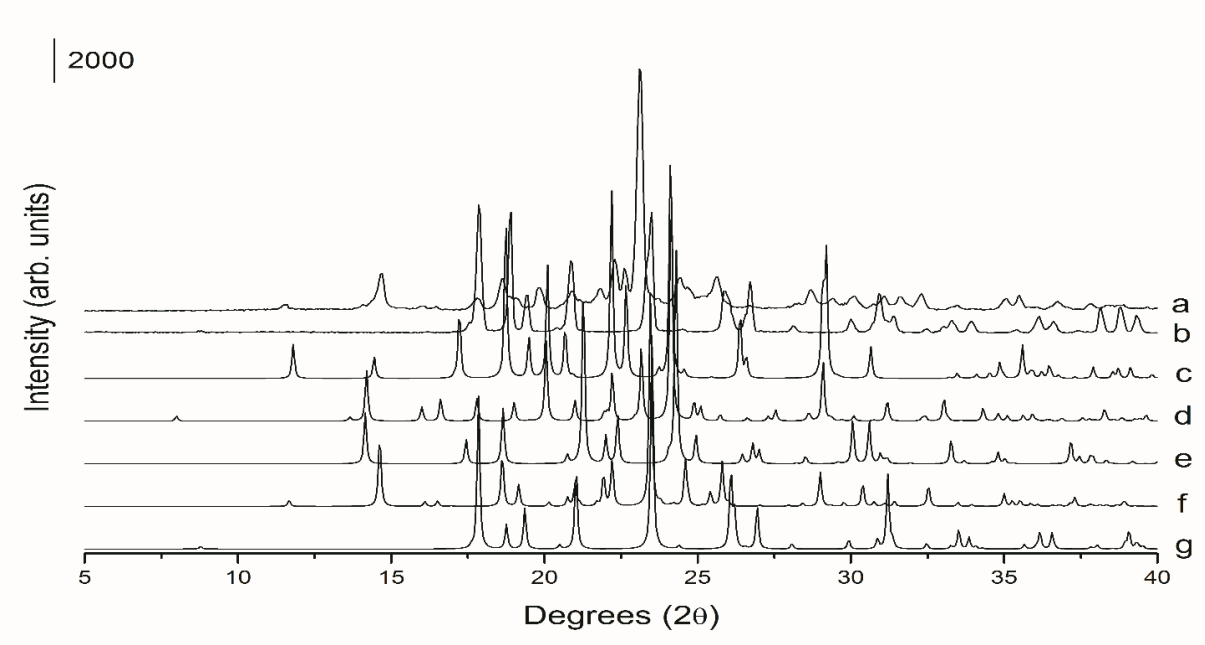

Figure A.3.10. PXRD patterns of a) INA:xylitol prepared by HME, b) Unprocessed INA, c) EHOWIH05, d) EHOWIH04, e) EHOWIH03, f) EHOWIH02, g) EHOWIH01. c-g are Mercury software-calculated PXRD patterns of INA polymorphs based on single crystal data (in the Cambridge Crystallographic Data Centre).

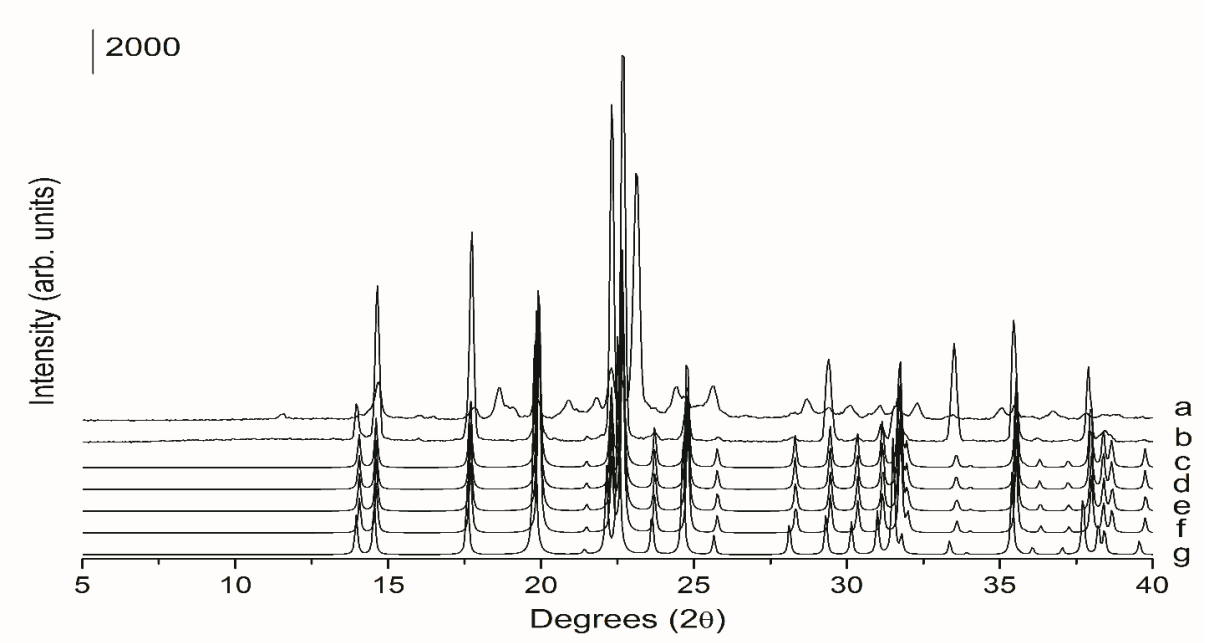

Figure A.3.11. PXRD patterns of a) INA: xylitol prepared by HME, b) Unprocessed xylitol, c) Xyltol04, d) Xyltol03, e) Xyltol02, f) Xyltol01, g) Xyltol. c-g are Mercury software-calculated PXRD patterns of xylitol polymorphs based on single crystal data (in the Cambridge Crystallographic Data Centre).

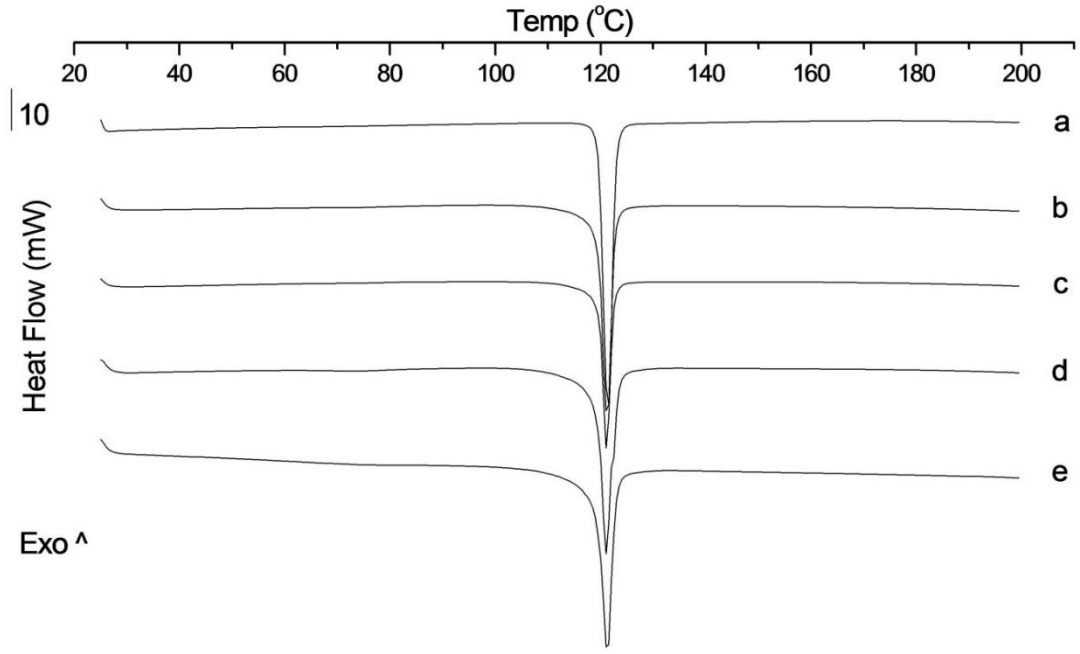

Figure A.3.12. DSC curves of physical mixtures of spray dried cocrystal and Soluplus. a) Spray dried cocrystal, b) Physical mixture of cocrystal and Soluplus (90:10 % w/w), c) Physical mixture of cocrystal and Soluplus (85:15 % w/w), d) Physical mixture of cocrystal and Soluplus (80:20 % w/w), e) Physical mixture of cocrystal and Soluplus (70:30 % w/w).

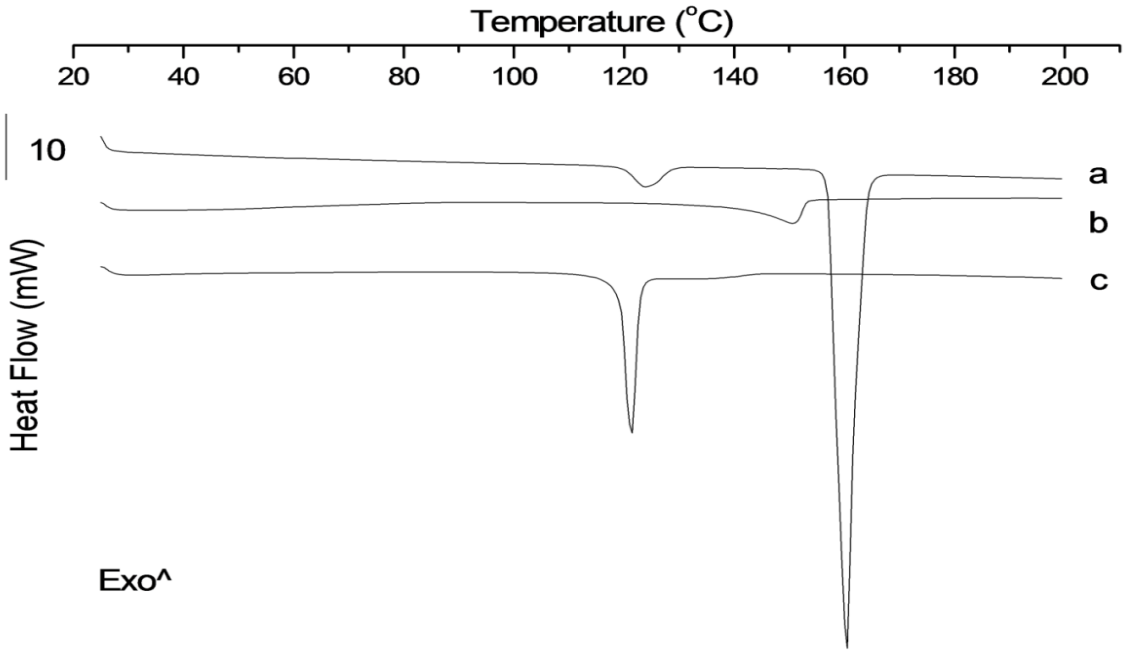

Figure A.3.13. DSC curves of a) Unprocessed INA, b) Co-spray dried INA with Soluplus (50:50 % w/w ratio), c) Physical mixture of cocrystal and (b) 80:20 (% w/w).

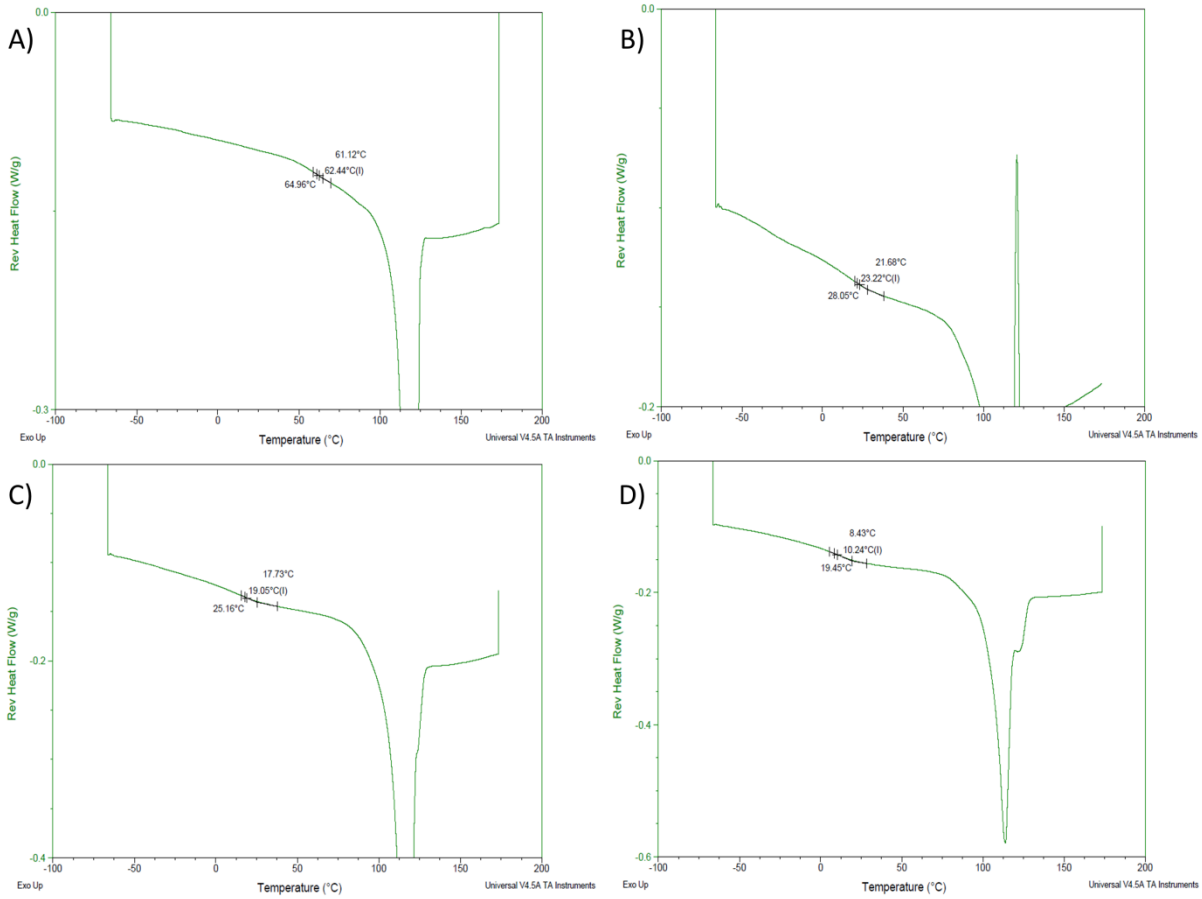

Figure A.3.14. MTDSC curves of a) SD-S-10, b) SD-S-15, c) SD-S-20. d) SD-S-30.

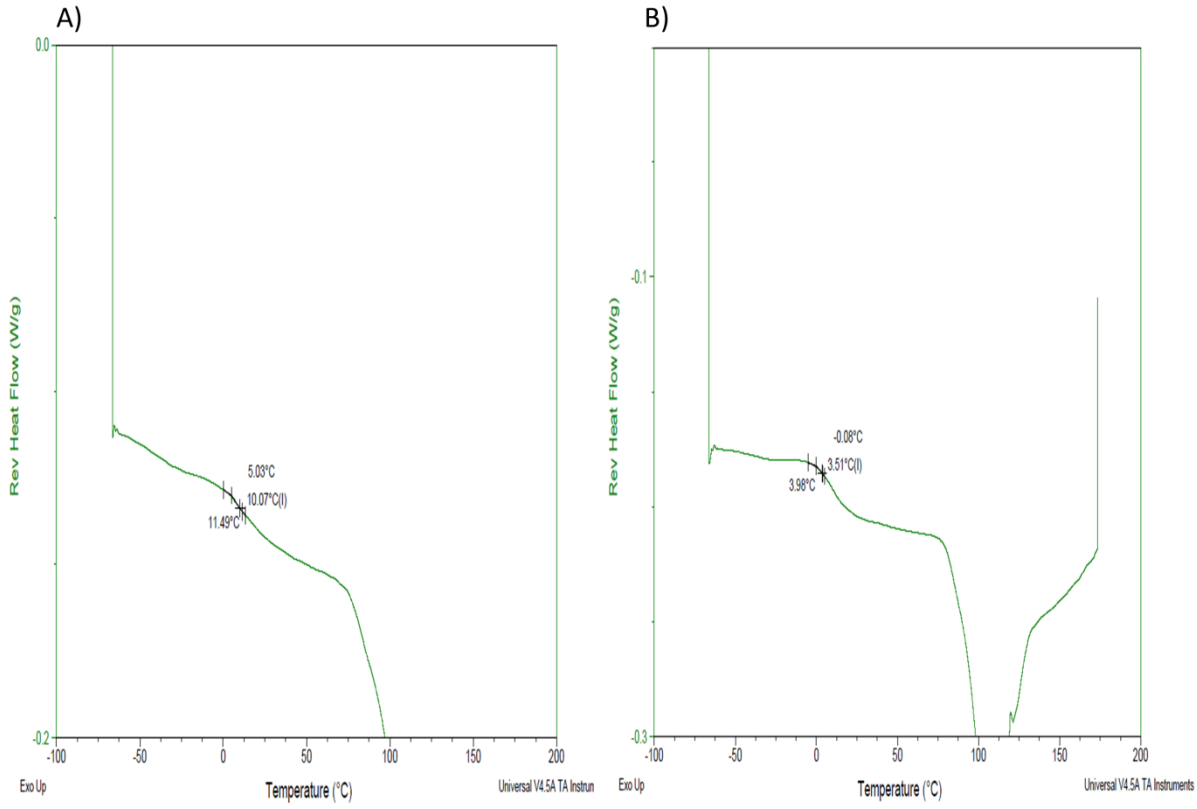

Figure A.3.15. MTDSC curves of a) SD-P-10, b) SD-P-20.

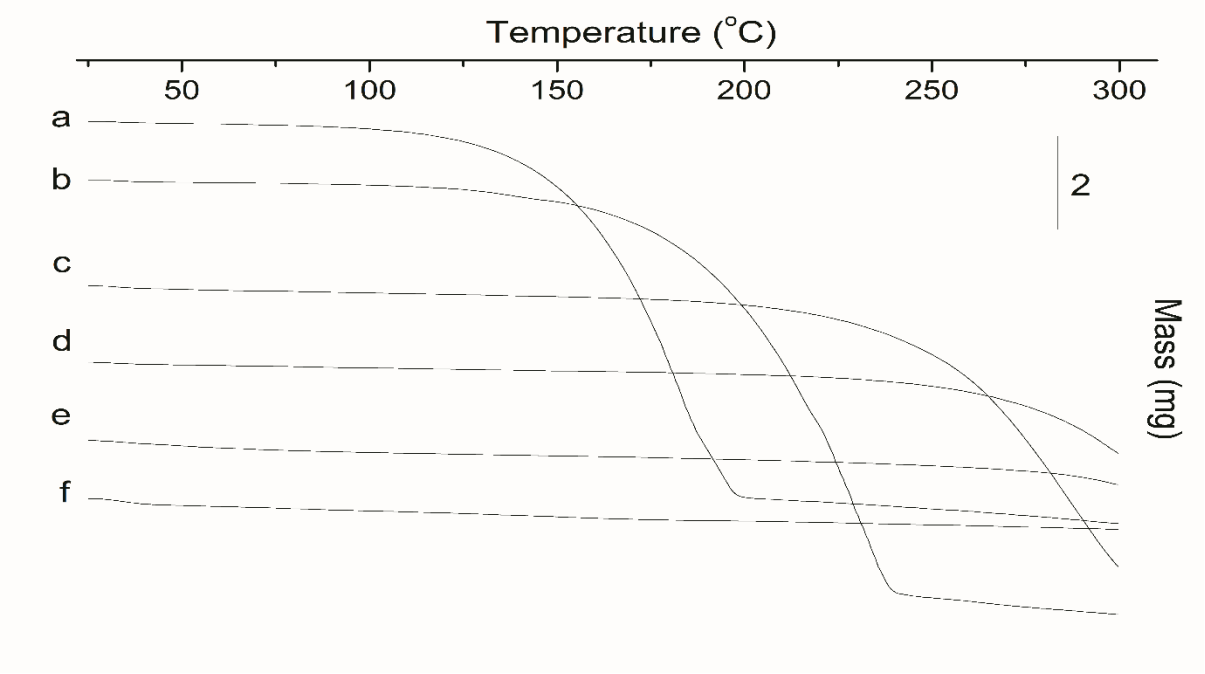

Figure A.3.16. TGA curves of raw materials. a) IBU, b) INA, c) xylitol, d) mannitol, e) Soluplus and f) PVP K15.

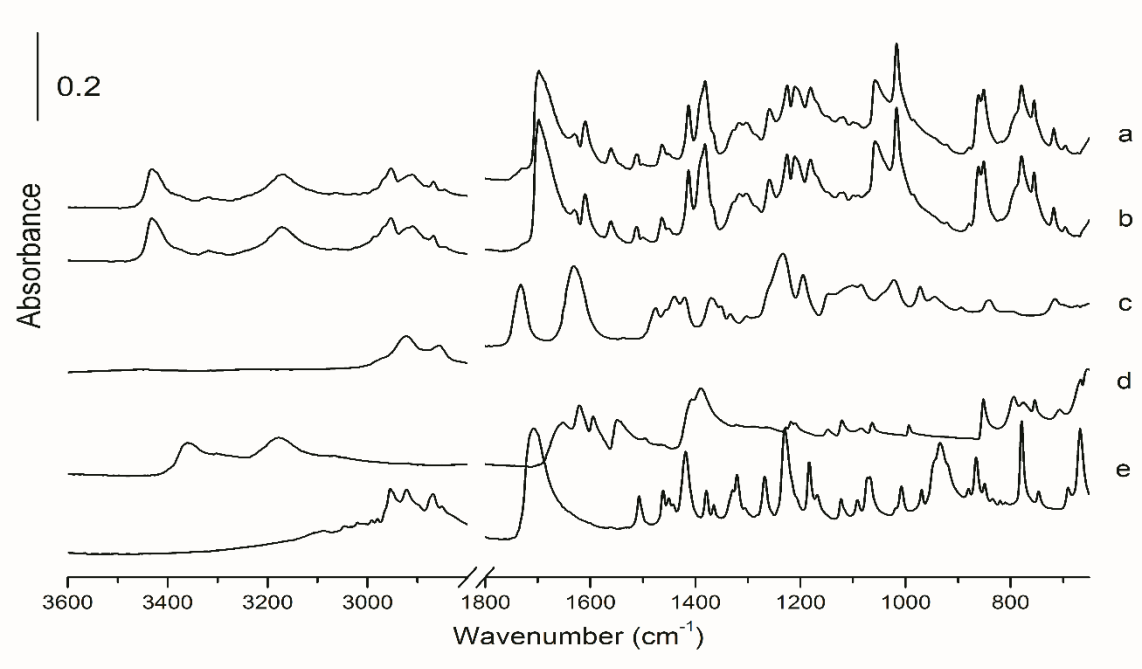

Figure A.3.17. Investigation of H-bonding by FTIR. Cocrystal co-spray dried with Soluplus; a) Co-spray dried IBU:INA 90 %, Soluplus 10 %, b) Cocrystal, c) Soluplus, d) INA, e) IBU.

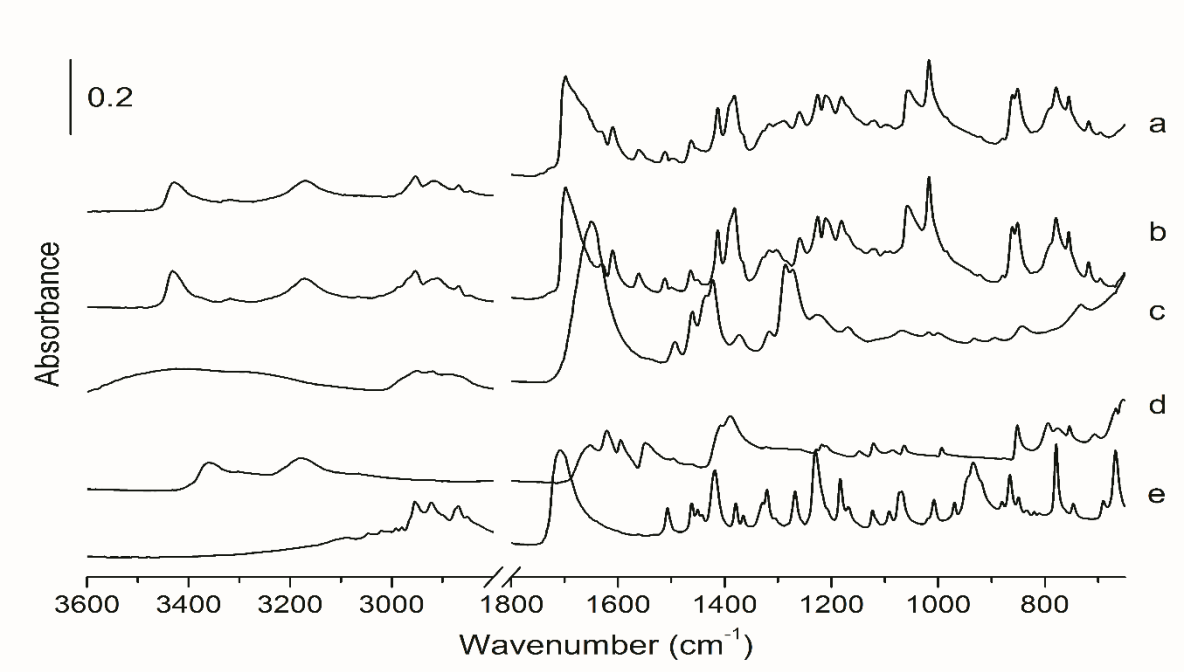

Figure A.3.18. Investigation of H-bonding by FTIR. Cocrystal co-spray dried with PVP K15; a) Co-spray dried IBU:INA 90 %, PVP K15 10 %, b) Cocrystal, c) PVP K15, d) INA, e) IBU.

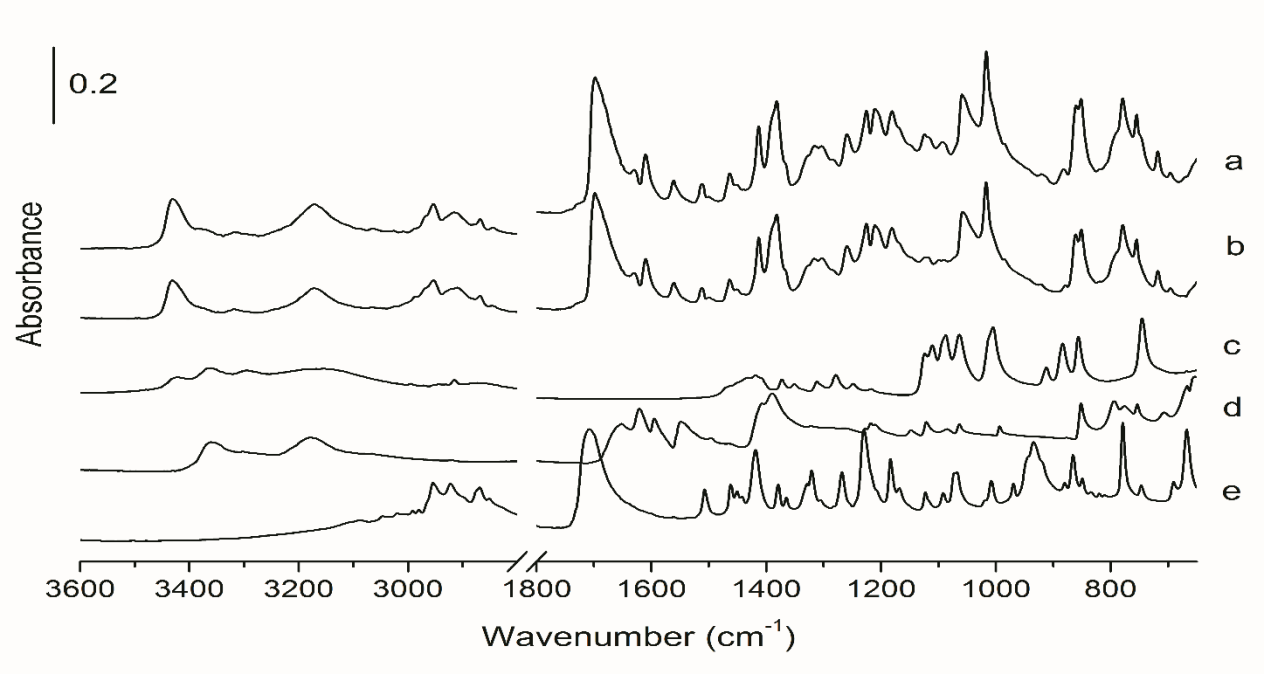

Figure A.3.19. Investigation of H-bonding by FTIR. Extruded cocrystal with xylitol; a) IBU:INA 90 % hot melt extruded with xylitol 10 %, b) Cocrystal, c) Xylitol, d) INA, e) IBU.

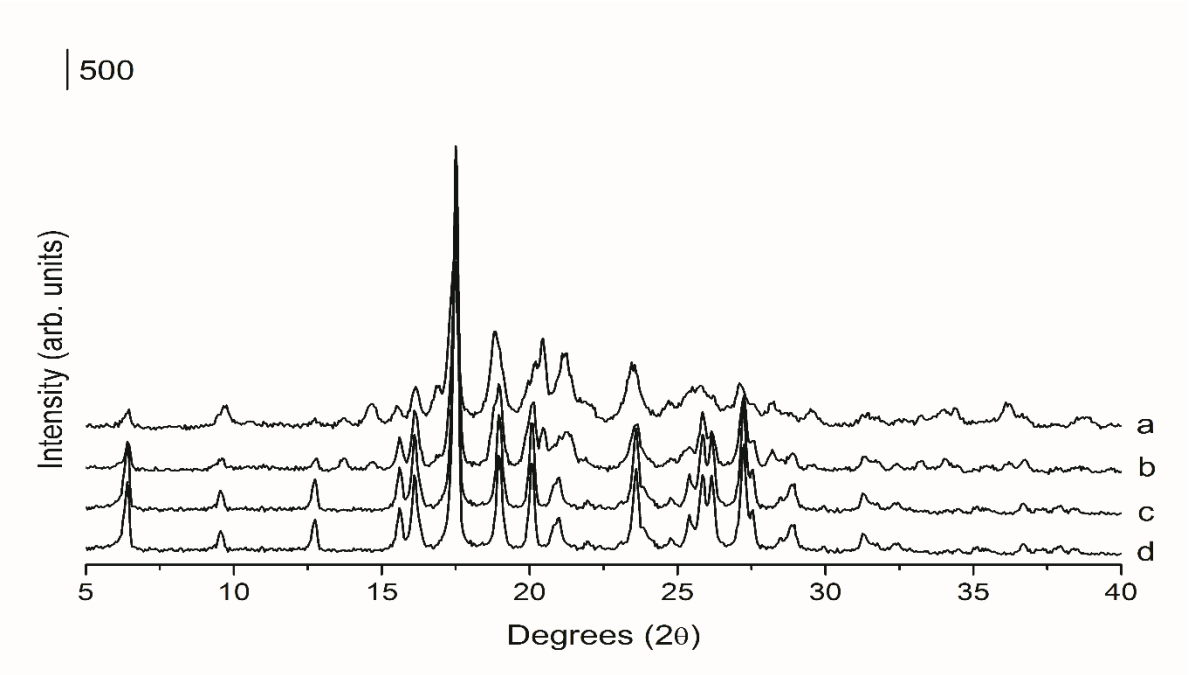

Figure A.3.20. PXRD analyses of co-spray dried systems with mannitol after DVS; a) IBU:INA 50 %, Mannitol 50 %, b) IBU:INA 70 %, Mannitol 30 %, c) IBU:INA 90 %, Mannitol 10 %, d) Spray Dried cocrystal.

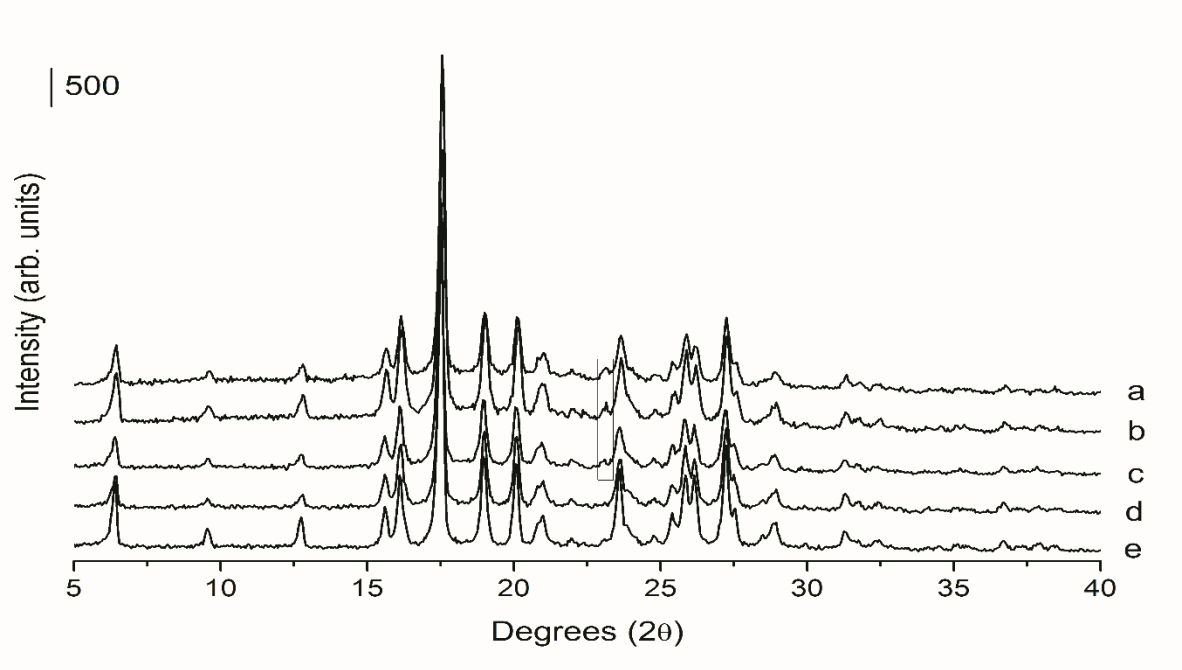

Figure A.3.21. PXRD analyses of co-spray dried systems with Soluplus after DVS; a) IBU:INA 70 %, Soluplus 30 %, b) IBU:INA 80 %, Soluplus 20 %, c) IBU:INA 85 %, Soluplus 15 %, d) IBU:INA 90 %, Soluplus 10 %, e) Spray Dried cocrystal.

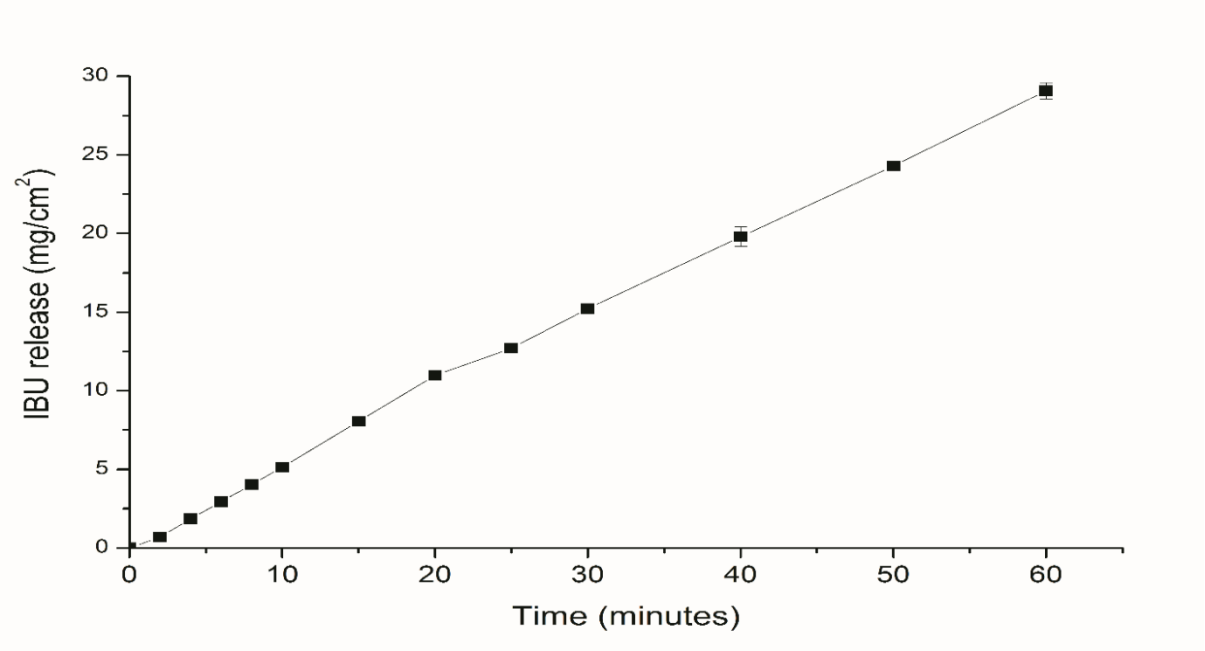

Figure A.3.22. Intrinsic dissolution profile of unprocessed IBU at 37 ^{o}C.

Appendix 4

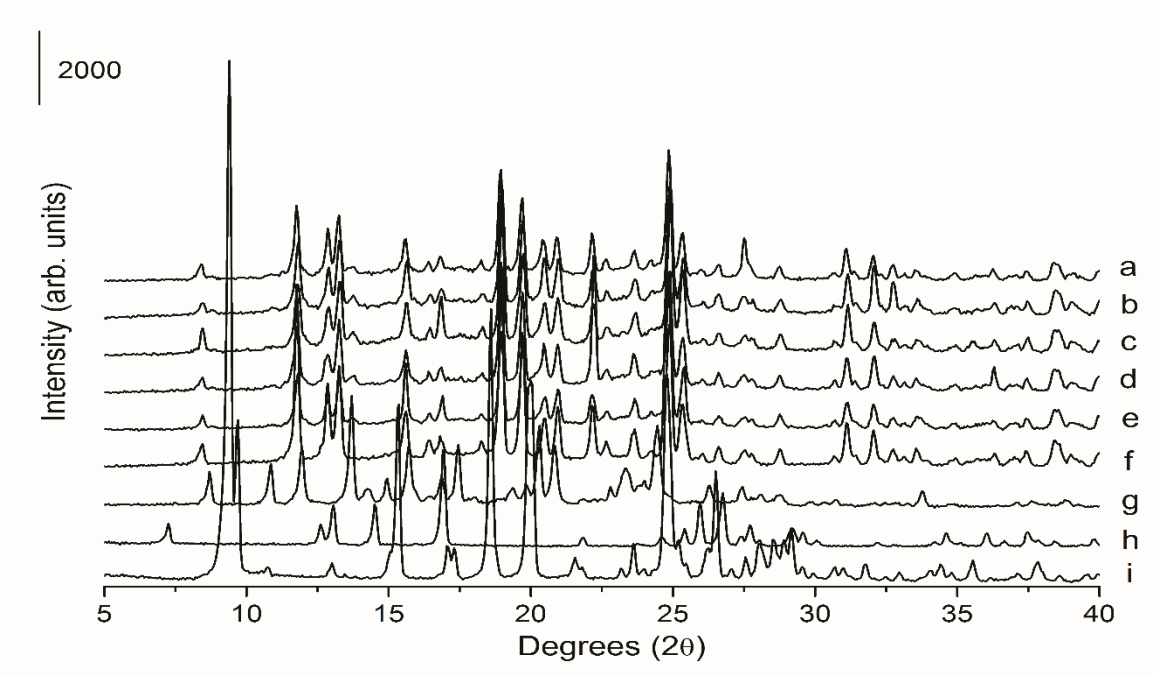

Figure A.4.1. PXRD analyses of centre point experiments performed as part of the Box-Behnken DoE. a) Run 17, b) Run 16, c) Run 13, d) Run 8, e) Run 5, f) Blank beads, g) Cocrystal produced by solvent evaporation, h) 4ASA, i) SDM.

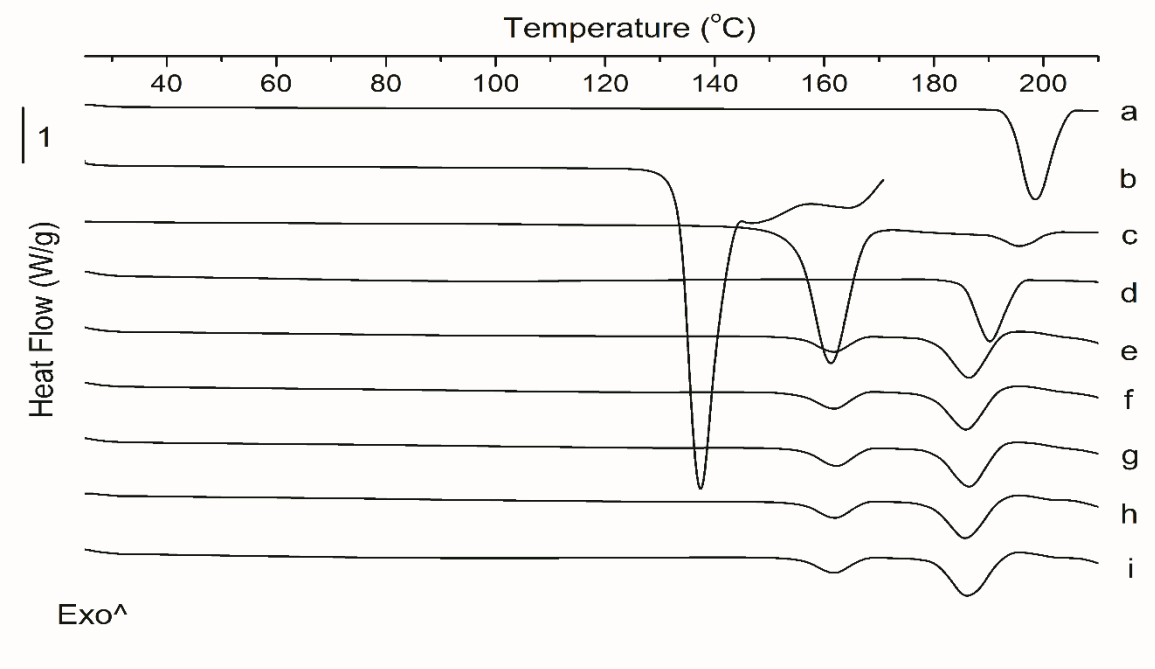

Fig A.4.2. DSC curves of centre point experiments performed as part of the Box-Behnken. a) SDM, b) 4ASA, c) Cocrystal produced by spray drying, d) Non-pareil beads, e) Run 5, f) Run 8, g) Run 13, h) Run 16, i) Run 17.

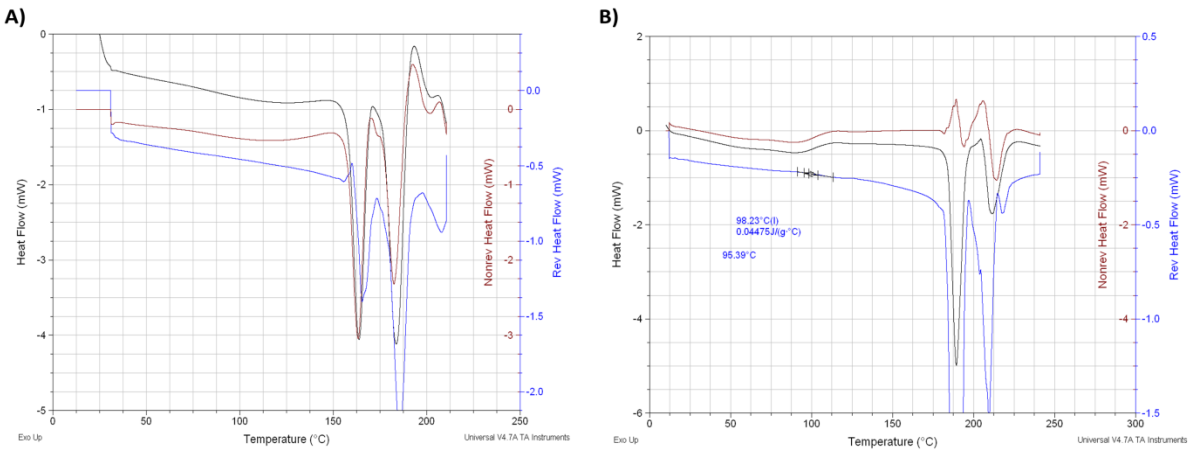

Figure A.3.3. MDSC thermograms of SDM:4ASA cocrystal coated beads (A) and SDM-PVP coated beads (B). The glass transition can be observed in the reversing heat flow signal (blue line).

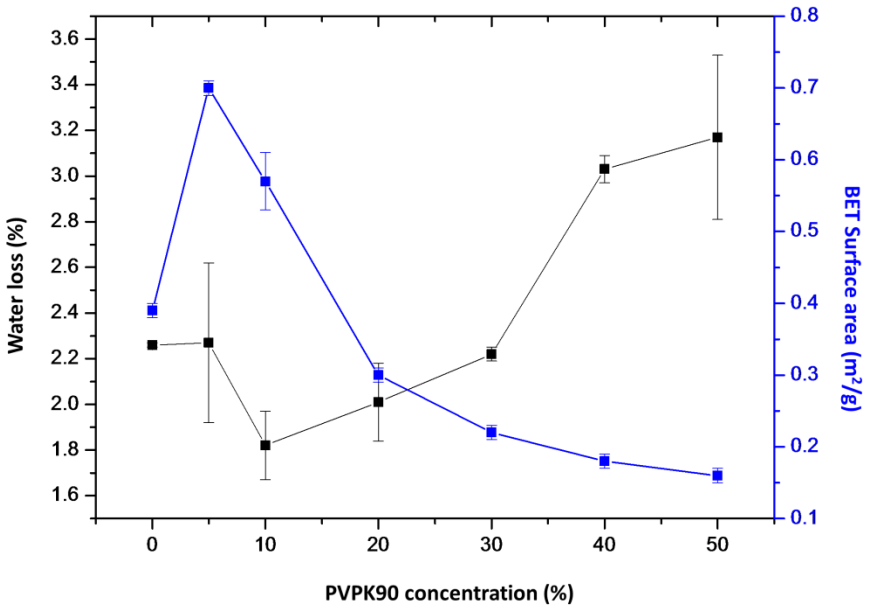

Figure A.4.4. Effect of PVP K90 concentration on water content (black ■) and surface area (blue ■) during spray coating.